Rope Hadronization, Geometry and Particle Production in pp and pA Collisions

Bierlich, Christian

Published: 2016-12-01

Document Version
Publisher's PDF, also known as Version of record

[Link to publication](#)

Citation for published version (APA):
Bierlich, C. (2016). Rope Hadronization, Geometry and Particle Production in pp and pA Collisions Lund: Lund University, Faculty of Science, Department of Astronomy and Theoretical Physics

Rope Hadronization, Geometry and Particle Production in pp and p*A* Collisions

Rope Hadronization, Geometry and Particle Production in pp and p*A* Collisions

by Christian Bierlich

LUND
UNIVERSITY

Thesis for the degree of Doctor of Philosophy
Thesis advisors: Prof. Leif Lönnblad
Faculty opponent: Prof. Klaus Werner

Organization	Document name	
LUND UNIVERSITY Department of Astronomy and Theoretical Physics Sölvegatan 14A SE–223 62 Lund Sweden	**DOCTORAL DISSERTATION**	
	Date of disputation 2017-01-27	
	Sponsoring organization	
Author(s) Christian Bierlich		
Title and subtitle Rope Hadronization, Geometry and Particle Production in pp and pA Collisions		

Abstract

This thesis concerns models of high energy collisions of sub-atomic particles, and the models' implementation in numerical simulations; so–called Monte Carlo event generators. The models put forth in the thesis improves the description of soft collisions of protons, and takes the first steps towards a new, microscopic description of collectivity in proton collisions and collisions of heavy nuclei such as lead.

Paper I. The Lund string hadronization model is reviewed, and a model for corrections in busy environments, such as pp minimum bias, are introduced, and its implementation in the event generator DIPSY is described. The model affects the hadrochemistry of the underlying event, and improves description of existing pp data from LHC and RHIC.

Paper II. A series of new observables sensitive to effects from rope hadronization is introduced, and predictions of the rope hadronization model is compared to predictions from a similar model based on junction formation.

Paper III. The Glauber formalism for collisions of nuclei is reviewed, and contributions from diffraction are considered. The Glauber–Gribov formalism for colour fluctuations is compared to the DIPSY model. On the basis of this comparision, corrections to the Glauber–Gribov parametrization of the pp cross section are suggested. This corrected formalism is then coupled to a particle production model, and preliminary descriptions of particle production in pA is given.

Paper IV. A model for string–shoving, expanding on the model from Paper I, is introduced at the proof–of–concept level. It is shown that the model qualitatively produces a rise of mean-$p_\perp$ with hadron mass and long range azimuthal correlations in pp collisions.

Key words		
QCD, Phenomenology, Hadronization, Heavy Ion Collisions		

Classification system and/or index terms (if any)		

Supplementary bibliographical information	Language English
ISSN and key title	ISBN 978-91-7753-148-7 (print) 978-91-7753-149-4 (pdf)

Recipient's notes	Number of pages 209	Price
	Security classification	

Signature _____   Date _____2016-12-16_____

DOKUMENTDATABLAD enl SIS 61 41 21

Rope Hadronization, Geometry and Particle Production in pp and p*A* Collisions

by Christian Bierlich

LUND
UNIVERSITY

A doctoral thesis at a university in Sweden takes either the form of a single, cohesive research study (monograph) or a summary of research papers (compilation thesis), which the doctoral student has written alone or together with one or several other author(s).

In the latter case the thesis consists of two parts. An introductory text puts the research work into context and summarizes the main points of the papers. Then, the research publications themselves are reproduced, together with a description of the individual contributions of the authors. The research papers may either have been already published or are manuscripts at various stages (in press, submitted, or in draft).

Populær sammenfatning på dansk

Et af de mest interessante spørgsmål en fysiker kan forsøge at svare på er *hvad består tingene af?*. Et hus kan skilles ad i mursten, og murstenen kan også skilles ad i sine bestanddele. Sådan kan man fortsætte indtil man bare har *atomer* tilbage. Atomerne kan skilles ad i elektroner og en atomkerne der består af neutroner og protoner. Elektronen er, så vidt vi ved, fundamental, og kan ikke skilles ad. Neutroner og protoner består af kvarker, holdt sammen af *den stærke kernekraft*, der overføres ved at gluoner sendes mellem kvarkerne. Den stærke kernekraft er både meget stærk og meget speciel. Hvis man havde en snor så stærk som den stærke kernekraft, den kunne holde en elefant oppe uden at knække. Den er speciel fordi kvarker og gluoner ikke opfører sig som andre partikler vi kender. Man kan for eksempel ikke fjerne en kvark eller en gluon fra protonen og inspicere den alene. Hiver man hårdt nok i protonen for at skille den ad, vil den skilles ad i flere protoner, og ikke flere kvarker. Her er billedet med elefanten i snoren godt som forklaring. Hvis vores elefant var for tung, og snoren knækkede, ville vi heller ikke stå med to snor-ender i hånden – vi ville slet og ret stå med to (mindre) snore.

Der findes en teori der beskriver den stærke kernekraft. Den hedder kvantekromodynamik, og med den i hånden kan man regne på hvad der sker når man støder atomkerner sammen med hastigheder tæt på lysets. Dette gør man blandt andet ved det store eksperiment LHC ved CERN i Frankrig og Schweiz, hvor både de mindste atomkerner stødes sammen – det er brintkerner, der bare består af en enkelt proton – såvel som bly, der består af 208 protoner og neutroner. Vi mener i dag at vide, at kvantekromodynamik er den korrekte teori for den stærke kernekraft. Vores metoder til at regne på teorien er udviklet gennem sidste halvdel af det 20. århundrede, men er stadig ikke så gode som vi kunne ønske os. Vi kan regne på teorien i flere forskellige *tilnærmelser*. Nogle tilnærmelser er effektive når man skal regne ud hvad protoner eller neutroners masse er, andre er effektive når man skal regne ud hvor sandsynligt det er at få en higgspartikel fra et sammenstød ved en bestemt energi. I denne afhandling anvendes og udvikles der tilnærmelser der er effektive til at beskrive sammenstød mellem protoner der involverer mange kvarker og gluoner. En "beskrivelse" af sammenstødet betyder i denne sammenhæng at kunne regne ud hvilke partikler man efterfølgende kan se hvor i detektoren.

I denne afhandling benyttes især tilnærmelser baseret på den snor-analogi for protoner, der blev introduceret i eksemplet med elefanten. Det viser sig at man opnår en god beskrivelse af sammenstød med få kvarker og gluoner ved at regne på dem som om en snor forbinder alle kvarkerne og gluonerne i sammenstødet. I sammenstød med mange kvarker og gluoner vil snorene blive "filtret sammen" og danne tykke reb. Det viser sig at have store konsekvenser for hvilke partikler man ser i detektoren. I sammenstød hvor der dannes tykke reb, får man for eksempel væsentligt flere partikler med kvarker af typen *strange* i sig.

Modellerne er ikke nogle man kan regne særligt langt på med papir og blyant. Efter mod-

ellerne er skrevet ned, er de implementeret i computerprogrammer der så bruges til at simulere sammenstød. Programmerne anvendt og udviklet i denne afhandling er udviklet i Lund og hedder DIPSY, ARIADNE, PYTHIA8 og FritiofP8. Programmerne finder anvendelse for fysikere verden over, der ønsker præcis viden om partikelsammenstød.

Contents

Introduction

One of the most interesting and fundamental questions of physics, is also one that is very easy to ask: *what are things made of?* It is seemingly easy to answer. Any macroscopic object can be taken apart into its constituents, and they can be examined individually. It turns out that every time we go down another level in size, we encounter a new type of substructure, and physics on a more fundamental level. It is crucial for our understanding of the world that we can always explain the physics of larger structures in terms of the physics of smaller structures – at least in principle. The smallest structures we can see with the naked eye, are some *molecular* structures, such as DNA or polymers. Other, less complex, molecules may measure down to about 1 Å (10^{-10} m), and can only be seen through a microscope. Molecules consists of *atoms*. In school they are taught as "The Elements", but even though they are very small, they are not elemental. We can sensibly ask and answer the question *what are the elements made of?* The modern starting point to the answer to this question, was provided by Rutherford in the beginning of the twentieth century, with the discovery that atoms have very small nucleus. We are now well beyond what can be seen with microscopes, and must rely on other types of experiments. We know today that even this nucleus has a substructure. It consists of protons and neutrons, which can, for example, be kicked out of the nucleus in radioactive processes, and examined individually.

At the scale of protons and neutrons, measuring about 1 fm (10^{-15} m) across, the preceding logic comes to a screeching halt. The question *what is a proton made of?* is not so easily answered. The easiest answer is that a proton consists of quarks and gluons. One could say that the quarks making up the proton are of the types *u* and *d*, which are the lightest of the six quark types. That would be a true statement. But it is not true in the sense we normally think about building blocks. You can cut a cell out of a piece of human skin, and put it in a petri dish. It may be very hard to do, and require a very skillful scientist, but in principle it

is possible. After the removal, the piece of skin will now lack the cells that are sitting in the petri dish. One cannot do the same thing with protons and its constituent quarks! It is not possible to remove a quark from a proton and have the quark sitting in one place, and the proton without the quark in another. Not because scientists are not skillful enough, but because the laws of nature *forbid* us to do so. This is known as the principle of *confinement*, saying that quarks cannot appear alone, but must be confined inside a *hadron*, which is the umbrella term for protons, neutrons and all other bound states of quarks and gluons.

A good analogy to a hadron is a piece of rubber band or string. In this analogy the quarks are the ends of the string[1], and the gluons are responsible for the force with which the string pulls back, when we try to pull its ends apart. How much force a given type of string can pull back with, is known as the string tension. The hadronic string is not just any old piece of string. It can carry a staggering 15 tonnes before it breaks, so the force mediated by the gluons is very *strong*. It is in fact so strong, that it is known as *the strong nuclear force*. The question of removing a quark from a hadron is now equivalent to the question of removing a string end from the string, and that does not make sense. If you pull hard enough that the string breaks, you will not sit with a free string end, you will rather sit with two pieces of string, equivalent to two hadrons.

Analogies like this are often used in physics. In spite of its simplicity, the string analogy is very useful when one wants to describe real physics – in fact much of this thesis is built upon this very analogy. But like analogies often do, also this analogy breaks down. It turns out that quarks and gluons can be freed from hadrons, and interact with *e.g.* quarks from another hadron, if only the collision energy is large enough, or similarly the length scales are small enough. This principle is known as *asymptotic freedom*. This does not mean that the quarks and gluons will *remain* free, they will only be free as long as the high energy interaction takes place. When the energy decreases again, all quarks and gluons must again be bound together.

1 The Quark Gluon Plasma

Knowing now that quarks and gluons will behave like free particles when the energy is large enough, let us imagine that we take a bunch of protons and put them under very stressful conditions. We enclose them in a sealed chamber and start to increase the temperature of the chamber. This could be achieved in two ways. Either by heating the system with an external source, say a Bunsen burner, or by decreasing the size of the chamber with the protons still in there. At some point the temperature – and thus the energy density – of

---

[1]A proton consists of three quarks, not two. But we can imagine a piece of string with three ends if we wish, think about a hadron consisting of a quark and an anti-quark, or simply make believe that a proton only consists of 2 quarks, without invalidating the analogy.

the chamber will be so high, that the quarks and gluons will behave as free particles inside. At this point we keep the temperature constant and wait until equilibrium is established. This means that the temperature is the same everywhere in the chamber. What do we now expect about the behavior of the contents of the chamber?

Some calculations in the theory of the strong force indicates that if the contents of the chamber is hot and compressed enough, the free quarks and gluons will behave like an almost perfect fluid, named the Quark Gluon Plasma (QGP). We would like to confirm that the box actually contains such a plasma, and not just the protons we had to begin with, but this is a hard task. We cannot just open the chamber. If we did, we would no longer have a hot, compressed state, and the quarks and gluons would form hadrons and escape our investigation. We sometimes say that the hadrons freeze out, or that the material inside the chamber *hadronizes*. We must think of some measurement to carry out on the resulting hadrons, which will reveal if a QGP was formed inside the box. Two ideas, which are followed in this thesis, are:

1. Since the temperature of the plasma is high, the production rate of hadrons requiring more relatively energy will be higher than normally. This includes hadrons containing a heavier type of quark, the so–called *s*-quark. If we measure the produced hadrons, after the chamber is opened, we should find an abundance of hadrons with *s*-quarks inside them, as compared to a chamber where no QGP is formed.

2. If the chamber contains a QGP, we know that contents of one end of the chamber should be affected by a disturbance in the other end of the chamber, since the contents would behave like a liquid. If, on the other hand, no QGP is formed, the disturbance would be localized. When we then open the chamber, we can measure whether the whole content is affected by small disturbances by measuring how the emerging hadrons are distributed.

Unfortunately it turns out that we cannot just put protons in a chamber and heat them up to obtain a QGP. The temperature required is simply way too large – more than 10^{12} K! For comparison, the core temperature of the Sun is colder by a factor of a million. The only point in time where we imagine the temperature was so large, was fractions of a second after the Big Bang. If we could find another way of obtaining the QGP, we would therefore get a source to obtain fundamental knowledge about the conditions of the very early Universe, which is believed to have been dominated by QGP. Instead of heating protons up in a chamber, we instead create "small bangs" in the laboratory, by colliding nuclei with each other, near the speed of light. It is imagined that the very hot and dense state created in such collisions, will be a QGP. The laboratory needed for such collisions is huge. Accelerators several kilometers in length are necessary to accelerate the beams of heavy nuclei, and detectors weighing several thousand tonnes are used to measure the results.

The abundance of hadrons with *s*-quarks was first observed at the Center for European Nuclear Research, CERN. In results [1] from collisions of sulfur, recorded with the NA35 experiment, a rise, with respect to proton–proton collisions where no rise was expected, of a factor 2 were shown. The measured hadrons are the so-called K_s^0, consisting of *s* - and *d*-quarks, and Λ or $\bar{\Lambda}$ which contains a *u*-, *d*- and an *s*-quark or their anti-particles respectively.

Measurements of disturbances were carried out around the same time. Such measurements are a bit more tricky to understand, as one must define both a disturbance and a way to measure them. What one often does, is to define the disturbance as the anisotropy in the initial stage of the collision. This anisotropy is due to the fact that the particles are not collided head on, but with varying degrees of overlap. If the QGP assumption is right, one should be able to measure varying degrees of anisotropy in the final state of the collision as well. In the final state we only have access to the momentum space anisotropy, quantified by so-called "flow" coefficients, so this is what is measured. Measurements of collisions of gold nuclei carried out at the Relativistic Heavy Ion Collider (RHIC) [2] by the STAR collaboration, showing large elliptic flow, are among the most important results pointing in the direction of the QGP.

Even though we have observed results which can be explained by the formation of a QGP, we cannot manifestly conclude that a QGP was in fact formed. To do so, we must also exclude the possibility that such results could be obtained *without* formation of a QGP, simply by the introduction of subtle, but normal, effects which are present in all types of collisions, but only visible when the colliding systems becomes of a certain size and temperature. This can seem a silly task. One can use the data mentioned above to either confirm or falsify a given model, but it seldomly works the other way around – one cannot disprove that introduction of new effects could lead to a given explanation. We therefore take on the opposite task: To actually construct the necessary corrections to existing models, which will explain QGP effects. If the measured effects can be explained by the corrections, one would need a strong argument to postulate a QGP. If the measured effects on the other hand cannot be explained by the corrections, the QGP postulate will gain additional weight.

If we are to take seriously an analogy where two quarks are connected by a string-like object, we need to also consider whether or not two quark pairs can interact through interaction of the strings. It turns out that the two QGP effects mentioned above can be at least qualitatively understood in terms of string interactions. To understand how, we need a somewhat deeper understanding of the strings. They are to be understood not as literal strings, but as fields confined to a cylindrical volume, measuring roughly 1 fm across, connecting the quarks. When these cylindrical tubes overlaps with each other, the overlap region will have different properties than individual, solitary strings. This will give rise to effects similar to the QGP effects.

The primary contribution of this thesis is the development of these corrections, and their implementation into a Monte Carlo event generator, which allows for direct comparison to data.

2 Monte Carlo event generators

Comparison to data is very important for development of physical theories. It is quite possible to build theories of physics which can be celebrated for their theoretical beauty, but if they cannot describe the real world around us, their utility as a theory of physics is limited. Since the 1980'ies, Monte Carlo event generators have gained enormous popularity in the particle physics community. The idea behind such generators is to generate computer simulated individual collisions (called "events"), which resemble the physics of the measurement as closely as possible. The sub-atomic world is governed by quantum mechanics, which is a probabilistic theory, meaning that one can only calculate the probability of a certain outcome. The event generator is therefore also probabilistic, hence the name "Monte Carlo".

The output from event generators has the large advantage that it can be processed in the same way as the measured data. This process is illustrated in the flowchart in figure 1.1. To the left we start, on one hand, with nature as it can be measured, and on the other hand our idealised ideas about the world – physics theory. Nature is probed by collider experiments such as those at the Large Hadron Collider (LHC), a large accelerator complex in France and Switzerland, and the physics theory is used as input for the Monte Carlo event generators. The event generator output is often called a "particle level" prediction. This means that the simulation provides results in terms of particles and their momenta. If we imagine a *perfect detector*, a thought-experiment detector, which has no restrictions in terms of measurement precision or coverage, that would provide a result similar to the one provided by the generator. The real–world experiment can not provide that type of result, as it is limited by constraints of the real world. A particle can escape detection, equipment for tracking or calorimetry is not infinitely fine grained, but limited by technology and so on. Before a physical result at particle level can be delivered, the responses from all the equipment need to be analysed and corrected to particle level. This is indicated in the box where the two paths meet. This is a highly non-trivial procedure, which involves both subjecting the Monte Carlo particle level result to simulations of detector geometry, thus correcting the Monte Carlo to detector level, but also the reverse process of detector unfolding where detector effects are removed from data, leaving only particle level results.

The unfolded data are to a large degree fed back into the Monte Carlo generators, in order to "tune" models – that is, determining model parameters. This is often necessary in order to understand also the parts of the collision one is not interested in for a particular analysis,
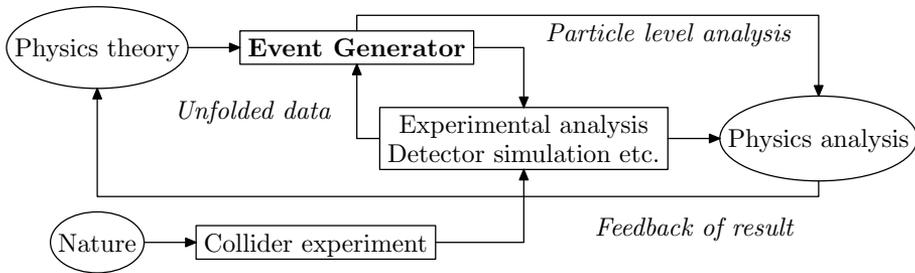
Figure 1.1: Flowchart sketch of the work flow of a high energy physics analysis involving both experimental data and comparison to theory.

i.e. the analysis' *background*. Once this iteration is done, the physics analysis is ready, which hopefully provides a new result about the world of fundamental particles. This result is then fed back into the underlying physics theory. This could for example be as a measurement of the *t*-quark mass, or the Higgs boson mass, which can put further constraints on models for new physics. In the case of the physics models developed in this thesis, future results and development will hopefully help understanding the nature of the strong force in a more quantitative way.

The Monte Carlo event generator thus serves a double purpose. On one hand it is a theoretical tool, which can be used to explore an abstract physics model, and see what its consequences are. On the other hand it is a very practical tool used in experiments as a part of simulating how the response from a certain signal looks in the detector.

3   Foundations and phenomenology

Before going into the very detailed models making up modern Monte Carlo event generators, it is useful to take a step back. We have outlined the phenomenon of the strong force and its physical theory "Quantum Chromodynamics" (QCD). Some of the underlying concepts of QCD, such as asymptotic freedom, were already mentioned in the introduction, as well as the string analogy which tries to provide a physical description – or a phenomenology – of confined quarks and gluons. The problem is that although there is little doubt that QCD is in fact the correct theory for strong dynamics, the theory is not fully understood. A place where the theory is quite well understood, is in the so-called perturbative approximation. In perturbation theory one writes out results in a series expansion in a sufficiently small parameter, and therefore only needs to calculate the first (or the few first) terms of the expansion. The usual choice of expansion parameter is the strong coupling α_s (one can think about it as the QCD analogue to the electron charge squared in electromagnetism), which depends strongly on the energy scale one is probing at. At high energies – producing *e.g.* Higgs bosons or Z^0-bosons, this is a good approximation. At low

energies the approximation breaks down, and one has to rely on phenomenological models such as the string model.

One cannot derive the phenomenological models directly from first principles, and often they are built from principles predating QCD. We will therefore begin by introducing some parts of the pre-QCD theory which provides inspiration for the models developed in the papers making up the bulk of this thesis.

3.1 Quark model phenomenology

Throughout the 1950'ies -and 60'ies, improvements in the design and implementation of particle accelerators and detectors, led to experiments with collision energies on the order of several hundreds of MeV. This is enough to produce many of the particles we today classify together as "hadrons". At that time the existence of a large number of "fundamental particles" was puzzling, and physicists sought to construct models which could reduce this vast amount of observations into fewer fundamental degrees of freedom. This was achieved by the theoretical physicists Murray Gell-Mann and Yuval Ne'eman in 1961, and extended by Gell-Mann and George Zweig in what is now known as "The Eightfold Way", "Flavour SU(3)" or simply "The Quark Model".

In the quark model, hadrons are built up by the three building blocks already mentioned in the introduction – the *quarks* named u (up), d (down) and s (strange)[2]. The quarks are fermions, having spin-$\frac{1}{2}$, and electric charge $\frac{2}{3}$, $-\frac{1}{3}$ and $-\frac{1}{3}$ respectively, all in fractions of the fundamental charge e. Remarkably, this simple picture allows for a full phenomenology of hadron species.

Besides categorizing the hadrons, the quark model itself does not do much. We are interested in learning the properties of hadron–hadron *scattering*, and for that we require a theory where scattering amplitudes, and thus cross sections, can be calculated.

3.2 S-matrix theory

Consider now the $2 \rightarrow n$ scattering of such hadrons. We use the *S*-matrix approach, following the presentation in ref. [3]. This approach examines the analytic properties of the *S*-matrix, rather than calculate matrix elements using quantum field theory. The *S*-matrix is a *scattering matrix*, defined such that the probability for taking an initial state $|i\rangle$ to a final

---

[2]There exist three more quark flavours, the c (charm), b (bottom/beauty) and t (top/truth). These are all heavy compared to the three light quarks considered here, and their production in soft processes are thus heavily suppressed.

state $\langle f|$ is:

$$P_{fi} = |\langle f|S|i\rangle|^2 = \langle i|S^\dagger|f\rangle\langle f|S|i\rangle. \tag{1.1}$$

Summing over all possible final states yields:

$$1 = \sum_f |\langle f|S|i\rangle|^2 = \sum_f \langle i|S^\dagger|f\rangle\langle f|S|i\rangle = \langle i|SS^\dagger|i\rangle = \langle i|i\rangle, \tag{1.2}$$

for any $|i\rangle$. Thus $S^\dagger S = 1$. Similarly $SS^\dagger = 1$, and S is therefore a unitary matrix. The unitarity of the S-matrix connects the elastic amplitude and the total cross section in the optical theorem. We begin with defining the *transition matrix* (T) through its relation to the S-matrix

$$S = 1 - i(2\pi)^4\delta^4(p_f - p_i)T. \tag{1.3}$$

The introduction of T signifies a distinction between an interaction (the unit operator) and the actual scattering process. Rewriting equation (1.2) in terms of the T matrix for any orthonormal states $\langle j|$ and $|i\rangle$ gives:

$$1 = \langle j|SS^\dagger|i\rangle = \sum_f \langle j|S|f\rangle\langle f|S^\dagger|i\rangle. \tag{1.4}$$

Inserting equation (1.3) and writing out just the matrix element for elastic scattering ($j = i$) we get:

$$2\Im\left(\langle i|T|i\rangle\right) = \sum_f (2\pi)^4\delta^4(p_f - p_i)|\langle f|T|i\rangle|^2. \tag{1.5}$$

We can rewrite eq. (1.5) as the optical theorem, since the right hand side is the total cross section modulo a kinematic factor, and the left hand side is the forward scattering (*i.e.* elastic) amplitude. In the large-s limit[3] the result reads:

$$\Im(A_{el}) = 2s\sigma_{tot}. \tag{1.7}$$

Up until this point we have worked in momentum space where the S-matrix is characterized by the Mandelstam variables. This thesis deals largely with the effects of multiple scatterings. Multiple scatterings corresponds to convolution in momentum space, but simplifies to multiplication in impact parameter space. Thus we will move to impact parameter space, making the amplitudes dependent on the impact parameter b (impact parameter is really a two-component vector, $\vec{b}$. But since we work with the simplification that all targets and projectiles are symmetric, we can remove the angular part, and write only the magnitude).

---

[3]The usual Mandelstam variables for the process $a + b \to c + d$ are:

$$s = (p_a + p_b)^2 = (p_c + p_d)^2, t = (p_a - p_c)^2 = (p_b - p_d)^2, u = (p_a - p_d)^2 = (p_b - p_c)^2. \tag{1.6}$$

At high energies the real part of the elastic amplitude becomes small enough that we will approximate it by zero. Assuming further that no diffractive excitation takes place, we write the absorption probability as $P_{abs}(b) = \sum_j |A_j(b)|^2$, where the sum runs over all inelastic (meaning absorptive in the absence of diffraction) channels. The elastic amplitude is then given by:

$$A_{el}(b) = i \left(1 - \sqrt{1 - P_{abs}(b)} \right). \tag{1.8}$$

Analogously to the T matrix, we now define the real amplitude (or profile function) $T(b)$ as well as $S(b)$ analogously to the S-matrix:

$$T(b) \equiv -iA_{el}(b) = 1 - S(b), \tag{1.9}$$

and for the remainder of this thesis T and S denotes these quantities (and not their momentum space counterparts), unless otherwise stated.

The fact that situations with multiple scatterings are easily dealt with in impact parameter space, is best illustrated with an example (with inspiration from ref. [4]). Consider the situation sketched in figure 1.2. We have here a projectile (p) scattering off three constituents each with profile function f_1, f_2 and f_3 respectively[4]. In the eikonal approximation the total probability for absorption at fixed b becomes:

$$P_{abs} = \frac{d\sigma_{abs}}{d^2 b} = f_1 + f_2 + f_3 - \text{double counting.} \tag{1.10}$$

The double counting terms are terms we need to insert in order to avoid counting the same probability twice, when hitting *e.g.* both target 1 and target 2. When those terms are subtracted we need however to add the term for hitting all three. The full probability then becomes:

$$P_{abs} = f_1 + f_2 + f_3 - f_1 f_2 - f_2 f_3 - f_1 f_3 + f_1 f_2 f_3 = 1 - (1 - f_1)(1 - f_2)(1 - f_3). \tag{1.11}$$

If each f_i is small, this exponentiates and thus:

$$P_{abs} \approx 1 - \Pi_i \exp(f_i) = 1 - \exp\left(\sum_i f_i \right) = 1 - \exp(-2F), \tag{1.12}$$

where F is introduced as a shorthand notation in the last equality. The above argument easily extends to an arbitrary amount of particles.

---

[4]Due to the optical theorem we can treat scattering amplitudes as probabilities, provided that the real part is approximately zero.
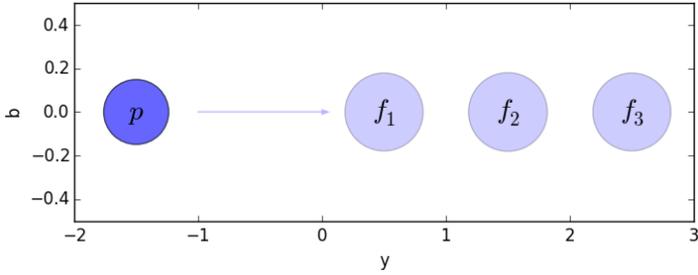
Figure 1.2: Scattering of a projectile (p) on a three-constituent target (f_1, f_2, f_3). This situation is conveniently described in impact parameter space.

3.3 Cross sections

We have now separated the cross section into two parts – the elastic and the inelastic. From equations (1.8), (1.9) and (1.12) we can write $T(b) = 1 - \exp(-F(b))$ and:

$$\frac{d\sigma_{el}}{d^2b} = T^2 \text{ and } \frac{d\sigma_{tot}}{d^2b} = 2T. \tag{1.13}$$

The total inelastic or *absorptive* cross section is then simply:

$$\frac{d\sigma_{abs}}{d^2b} = \frac{d\sigma_{tot}}{d^2b} - \frac{d\sigma_{el}}{d^2b} = T(2 - T). \tag{1.14}$$

Thus, if we can calculate the individual f_i, we can go on to calculate T and cross sections. Bare in mind that the above argument concerning multiple interactions holds true both for multiple partonic interactions in, say, a proton–proton collision, or multiple nucleus collisions in, say, a proton–lead collision. The f_i will of course be different in the two cases, as the fundamental degrees of freedom in the two calculations (partons vs. nucleons) are quite different.

Let us limit ourselves to proton–proton collisions. Here we want to further identify diffractive and non-diffractive contributions. According to the quantum mechanical Good–Walker formalism (see box 1 for details), diffraction can be included by taking into account fluctuations in projectile and target. To recover the cross sections from equation (1.13), one must average over the fluctuations, and thus:

$$\frac{d\sigma_{tot}}{d^2b} = 2 \langle T \rangle_{t,p}, \frac{d\sigma_{el}}{d^2b} = \langle T \rangle_{t,p}^2, \tag{1.15}$$

where subscripts t and p indicate an average over target and projectile respectively.
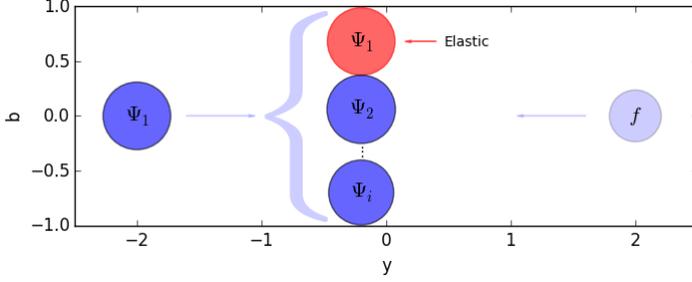
Figure 1.3: Illustration of projectile fluctuation which, in the Good-Walker formalism, leads to diffraction. See box 1 for further explanation.

Box 1: The Good–Walker formalism

In the Good–Walker formalism [5], diffraction is associated to fluctuations. Consider the situation sketched in figure 1.3. Here a projectile comes in from the left, to scatter on the target on the right. We denote its diffractive eigenstate Φ_k with corresponding eigenvalues (*i.e.* elastic scattering amplitudes) T_k. Its mass eigenstates Ψ_i will then be a linear combination of the diffractive eigenstates:

$$\Psi_i = \sum_k c_{ik}\Phi_k, \qquad (1.16)$$

where the mass eigenstate of the incoming projectile is labelled Ψ_1. We can write the transition amplitude to go from the incoming state to the i'th mass eigenstate as:

$$\langle \Psi_i | T | \Psi_1 \rangle = \sum_k c_{ik} T_k c_{1k}. \qquad (1.17)$$

The elastic cross section – where the incoming state is also the outgoing state – is then:

$$\frac{d\sigma_{el}}{d^2 b} = \langle \Psi_1 | T | \Psi_1 \rangle^2 = \langle T \rangle^2. \qquad (1.18)$$

The total diffractive contribution is:

$$\sum_i \langle \Psi_1 | T | \Psi_i \rangle \langle \Psi_i | T | \Psi_1 \rangle = \langle T^2 \rangle, \qquad (1.19)$$

and the diffractive *excitation* is then the total diffractive minus the elastic:

$$\frac{d\sigma_{diff,p}}{d^2 b} = \langle T^2 \rangle - \langle T \rangle^2. \quad (1.20)$$

The single diffractive cross sections involves averaging over only one side at a time (*c.f.* equation 1.20 in box 1):

$$\frac{d\sigma_{SD,(p|t)}}{d^2 b} = \left\langle \langle T \rangle_{(t|p)}^2 \right\rangle_{(p|t)} - \langle T \rangle_{p,t}^2. \qquad (1.21)$$

The double diffractive cross section is then obtained by subtracting both contributions from single diffractive excitation from the total diffractive cross section. Since the elastic

contribution is already subtracted, this needs to be added again, in order to avoid double subtraction:

$$\frac{d\sigma_{DD}}{d^2 b} = \left\langle T^2 \right\rangle_{p,t} - \left\langle \left\langle T \right\rangle_t^2 \right\rangle_p - \left\langle \left\langle T \right\rangle_p^2 \right\rangle_t + \left\langle T \right\rangle_{p,t}^2 \tag{1.22}$$

In section 5.2 we will introduce a QCD based model (the DIPSY model) for calculating f_i, and thus $T(b)$, which is obviously necessary to calculate cross sections. But here we will instead take an aside to the pre-QCD theory by Tulio Regge. Besides being a theory for calculating cross sections, this also inspired the string model for mesons, which will play a large role in the thesis.

3.4 Regge theory

We now go back to the momentum space picture, and look at the amplitude of $2 \to n$ processes, exemplified by the $p\bar{p}$ total cross section. We know the result from experiments, in figure 1.4 the total cross section as function of $\sqrt{s}$ is shown. We will now argue that exchanges of mesons in the t-channel are particularly important, inspired by the discussion in ref. [3]. Consider the processes $p\bar{p} \to \bar{\Sigma}^+\Sigma^-$ and $p\bar{p} \to \bar{\Sigma}^-\Sigma^+$. Though the processes are seemingly similar, we know that the cross sections are not, as $\sigma(p\bar{p} \to \bar{\Sigma}^-\Sigma^+) \gg \sigma(p\bar{p} \to \bar{\Sigma}^+\Sigma^-)$. We know [6], however, that the quantum numbers charge (q) and isospin (I_3) are different among the final state particles. For a t-channel meson exchange to be allowed for the process $\sigma(p\bar{p} \to \bar{\Sigma}^+\Sigma^-)$, the exchanged particle should have $I_3 = \frac{3}{2}$ and $q = 2$. No such meson exists. However, for the process $\sigma(p\bar{p} \to \bar{\Sigma}^-\Sigma^+)$, the exchanged meson in the t-channel should have $I_3 = \frac{1}{2}$ or $\frac{3}{2}$ and no charge. Such mesons do exist, and the fact that the mesonic t-channel is open for this process, explains why the cross section is much larger. The exchange of resonances in the t-channel is thus argued to be an important contribution to the cross section at high energies.

We therefore wish to examine the t-channel exchange a bit further. From quantum mechanics we know that a scattering amplitude can be expanded in partial waves:

$$A(k, \cos(\theta)) = \sum_{l=0}^{\infty} (2l + 1)a_l(k)P_l(\cos(\theta)), \tag{1.23}$$

where P_l are the Legendre polynomials of first kind, order l. The partial wave amplitudes are denoted a_l and θ is the scattering angle. For $2 \to 2$ processes and equal masses, $\cos(\theta) = 1 + \frac{2s}{t - 4m^2}$ and:

$$A(s, t) = \sum_{l=0}^{\infty} (2l + 1)a_l(t)P_l(1 + \frac{2s}{t - 4m^2}). \tag{1.24}$$
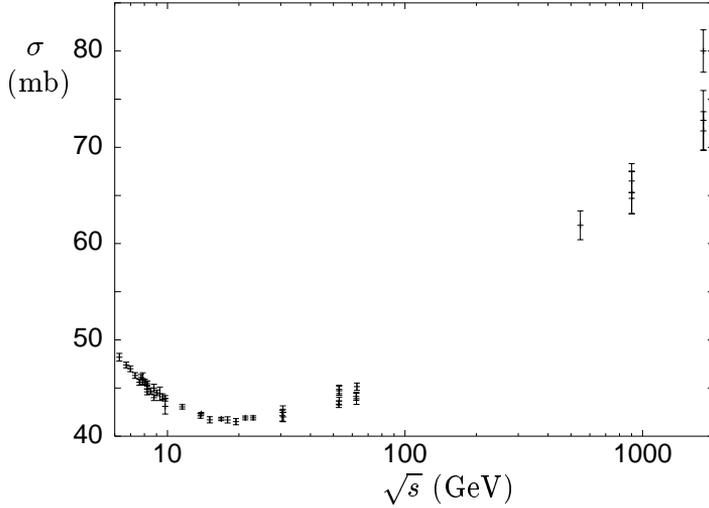
Figure 1.4: The total $p\bar{p}$ cross section as function of center–of–mass energy. Reproduced with permission from ref. [3].

When s becomes large, $P_l \approx s^l$, which obviously makes the series diverge. We shall not unfold the full analytical apparatus here, but rather exemplify based on ref. [3], where also the full derivation can be found.

Consider the exchange of just a single resonance of a given spin l_0 in the large-s limit. Equation (1.24) then reduces to $A(s,t) \propto s^{l_0}$. Using the optical theorem in the large-s limit (equation (1.7), remembering that the real part of the amplitude is ≈ 0), we get $\sigma_{tot} \propto s^{l_0-1}$. Having an integer value of l_0 does not correspond well to the picture observed in figure 1.4, and we must imagine that several particles are exchanged, and we must consider them all at once. The formalism for doing this, is called Regge theory. It involves making an analytical continuation of a_l to the complex l-plane. Equation (1.24) becomes an integral in the complex l-plane, with poles traced out by *Regge trajectories*:

$$l = \alpha(t). \tag{1.25}$$

We can readily associate such poles with particles. Values of t for which l corresponds to an integer is then the squared mass of a resonance with that spin. One then finds the following asymptotic s-dependence of the amplitude:

$$A(s,t) \to \beta(t)s^{\alpha(t)} \text{ as } s \to \infty. \tag{1.26}$$

3.5 String picture of mesons

Plotting meson spins against their squared mass, reveals a very simple form of the Regge trajectories (equation 1.25). In figure 1.5, an example of such a trajectory is shown. It is seen

that they are (almost) linear in t:

$$\alpha(t) = \alpha(0) + \alpha' t. \tag{1.27}$$

We can now ask ourselves what kind of internal meson dynamics could give such simple trajectories. In other words: What is the nature of the potential binding the two quarks together? We consider the "leading" trajectory, which is the one that maximises l at given t. Let the two quarks be connected by a force field with the property that the potential rises linearly with the distance between the quarks, like a classical string. We physically think of this string as a narrow flux tube, which carries all the energy, and thus neglect the quark masses. Since we want to maximize l, we let the flux tube rotate around its center. As the quarks are massless, the ends move with the speed of light. If the string length is called r, and the string tension in rest is κ, then:

$$\sqrt{t} = \int_{-r/2}^{r/2} dx \frac{\kappa}{\sqrt{1 - v_\perp^2}} = \frac{r\kappa}{2} \int_{-1}^{1} \frac{dy}{\sqrt{1 - y^2}} = \frac{\pi r \kappa}{2}, \tag{1.28}$$

with $v_\perp(x) = 2x/r$ being the transverse velocity. Similarly the angular momentum is:

$$l = \int_{-r/2}^{r/2} dx \frac{\kappa v_\perp x}{\sqrt{1 - v_\perp^2}} = \frac{r^2 \pi \kappa}{8}. \tag{1.29}$$

This model fulfills that:

$$\frac{l}{t} = \frac{1}{2\pi\kappa} = \alpha' = \text{const.} \tag{1.30}$$

and given the value of α' extracted from fits to the experimentally obtained trajectories, we get a string tension $\kappa \approx 0.180 \text{ GeV}^2 = 0.91 \text{ GeV/fm}$.

3.6 The Pomeron

We can now insert equation (1.26) with a trajectory as given by equation (1.27) into the optical theorem. Since we are considering only the elastic amplitude ($t = 0$), the total cross section is only dependent on the intercept $\alpha(0)$ and not the slope:

$$\sigma_{tot} \propto s^{\alpha(0)-1}. \tag{1.31}$$

From figure 1.5, $\alpha(0) \approx 0.5$. This corresponds to exchange of the mesons shown in the figure. As the energy rises, it becomes necessary to exchange a family of particles with $\alpha(0) > 1$, if the cross section should rise as data shows. In a theorem known as *the Pomeranchuk theorem* it is stated that a process with non-vanishing cross section as s increases
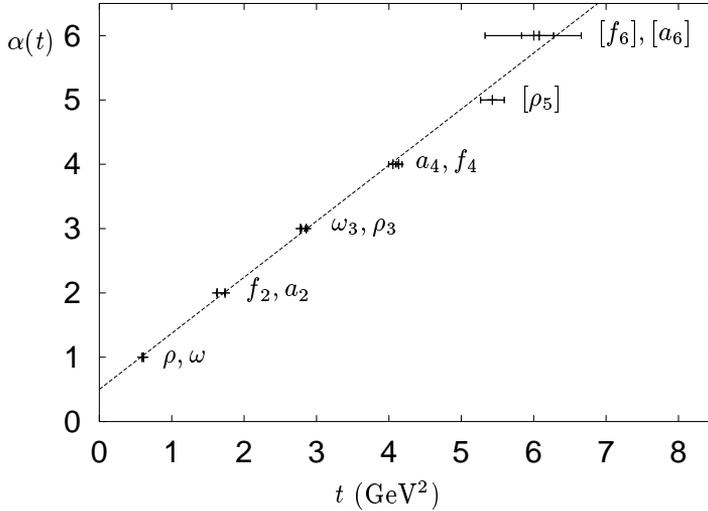
Figure 1.5: Regge trajectories, particle spins plotted against their squared masses. Reproduced with permission from ref. [3].

must be dominated by exchange of vacuum quantum numbers. Such an exchange is called a Pomeron, and the trajectory in question is called the *Pomeron trajectory*.

The $p\bar{p}$ cross-section in figure 1.4 can thus be described by a two-term parametrization, where both terms are proportional to $s^{\alpha(0)-1}$. One for low energies with an intercept similar to the one in figure 1.5, and one for higher energies with the Pomeron intercept. A good fit was found by Donnachie and Landshoff [7]:

$$\sigma_{tot}^{p\bar{p}} = (21.7s^{0.08} + 98.4s^{-0.45})\text{mb}. \tag{1.32}$$

Similarly for pp collisions:

$$\sigma_{tot}^{pp} = (21.7s^{0.08} + 56.1s^{-0.45})\text{mb}. \tag{1.33}$$

4   Electron–positron collisions

We have now reviewed a lot of basic principles and ideas which will be useful for a modern description of high energy proton collisions, based on QCD. We can now go on to explain the more concrete building blocks of a modern Monte Carlo event generator. We start with the simplest possible system, namely an e^+e^- annihilation. We will focus on a hadronic final state arising from the production of a $q\bar{q}$ pair and it properties, using a parton cascade and hadronization. When we later move on to proton–proton collisions, parts of the calculation are already fixed from e^+e^-, and one can concentrate on complications arising from having a QCD initial state.
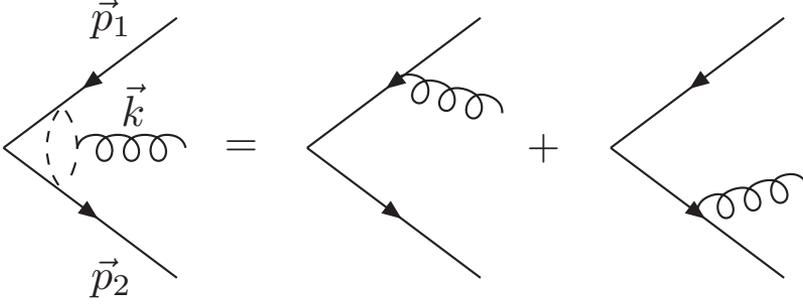
Figure 1.6: Relevant diagrams for the dipole parton shower. To the left the dipole along with some notation, to the right, the two relevant diagrams.

4.1 Dipole radiation in the final state

We will here deal with the gluon radiation from a $q\bar{q}$ pair coming from an off-shell photon or Z^0. This is the basis of a dipole parton shower such as ARIADNE [8], used in this thesis. We consider the $Z/\gamma^* \rightarrow q\bar{q}g$ amplitude, as a correction to the $Z/\gamma^* \rightarrow q\bar{q}$ amplitude, which we denote as $\mathcal{M}_{q\bar{q}}$. The "dipole" in a dipole parton shower denotes such colour dipoles as formed by a colourless $q\bar{q}$ pair. In figure 1.6 the two relevant diagrams are shown. The idea behind the dipole parton shower (or cascade) is to calculate the gluon emission probability from a dipole, once and for all. When a gluon has been emitted, we say that the dipole has been split up into two new dipoles, which in turn can emit individually, using the same emission probability as the first, initial dipole.

The squared matrix element, averaged over spins, polarizations and colours is:

$$\left|\mathcal{M}_{q\bar{q}g}\right|^2 = \left|\mathcal{M}_{q\bar{q}}\right|^2 C_F g_s \frac{2\vec{p}_1 \cdot \vec{p}_2}{(\vec{p}_1 \cdot \vec{k})(\vec{p}_2 \cdot \vec{k})}, \tag{1.34}$$

where $\vec{p}_1$, $\vec{p}_2$ and $\vec{k}$ are the momenta of the quark, anti quark and gluon respectively. The spectrum is then:

$$\omega \frac{dN}{d\omega d^2 k_\perp} = \frac{\alpha_s C_F}{2\pi^2} \frac{\vec{p}_1 \cdot \vec{p}_2}{(\vec{p}_1 \cdot \vec{k})(\vec{p}_2 \cdot \vec{k})}, \tag{1.35}$$

The last term can be rewritten in terms of the angles between the quarks $\theta_{q\bar{q}}$ and between the gluon and the (anti-)quark θ_{qg} ($\theta_{\bar{q}g}$), such that:

$$dN \propto \frac{1 - \cos(\theta_{q\bar{q}})}{(1 - \cos(\theta_{qg}))(1 - \cos(\theta_{\bar{q}g}))}. \tag{1.36}$$

This result can be rewritten as the sum of two terms $W_{(q|\bar{q})} = \frac{1}{\cos(\theta_{(q|\bar{q})})}$, minus a slightly more complicated mixed term we call $2R$. We can split it up:

$$dN \propto \left((W_q - R) + (W_{\bar{q}} - R) \right) = X_q + X_{\bar{q}}. \qquad (1.37)$$

We interpret X_q as radiation from the quark and $X_{\bar{q}}$ as radiation from the anti-quark. Integrating over azimuthal angle gives:

$$\int_0^{2\pi} \frac{d\phi}{2\pi} X_q = \frac{1}{1 - \cos(\theta_{qg})} \Theta(\theta_{q\bar{q}} - \theta_q), \qquad (1.38)$$

and similar for $X_{\bar{q}}$; Θ is the step-function. This means that radiation is forbidden outside the cone initially defined by the $q\bar{q}$ dipole, but inside the cone the two quarks emit independently – a result known as angular ordering.

To make a heuristic interpretation of this result in transverse space, we interpret the transverse size of the emitted gluon as: $\lambda_\perp \approx \frac{1}{k_\perp} = \frac{1}{\omega\theta}$. The formation time is $\tau \approx \frac{\omega}{k_\perp^2}$, so the transverse size of the dipole while the gluon is being formed is $r_\perp \approx \theta_{q\bar{q}}\tau = \frac{\theta_{q\bar{q}}}{\omega\theta}$. We see now that emissions in the forbidden region (outside the cone) would correspond to emissions of gluons larger than its mother dipole ($\lambda_\perp > r_\perp$), and our interpretation is that the dipole is simply too small to be resolved by such gluons. The production of such gluons is thus suppressed. For $\lambda_\perp < r_\perp$ we have independent emissions from the two quarks. The emission of more gluons becomes more complicated, as the number of diagrams grows exponentially in the number of gluons. Instead we can iterate the above procedure, as the result factorizes when the emissions are strongly ordered [9]. Going to the $N_c = \infty$ limit[5], the emission of the first gluon splits the dipole into two new ones, which can in turn emit more gluons and thus continue the process.

Ordered emissions

When doing multiple emissions, we order the emissions such that emissions of higher $k_\perp$ are realized first. This is conveniently achieved by introducing a Sudakov form factor (see box 2), describing the no-emission probability from a starting scale down to the current emission scale. Once we have emitted down to a scale $\approx \Lambda_{QCD}$, we can no longer rely on the perturbative expressions going into the parton shower. Furthermore we need to transform the fundamental degrees of freedom from quarks and gluons to hadrons. The inherently non-perturbative framework for this, will be described next.

---

[5]N_c denotes the number of colours in QCD. This, as well as many other calculations simplify in this approximation.

For the purpose of Monte Carlo event generation, the "Sudakov form factor" provides a very useful calculational tool (see *e.g.* [10]). Consider (in somewhat generalized terms) the case of the dipole shower. We have an emission probability $\frac{d\sigma}{dp_\perp^2 \, dy}$, and we wish to generate a number of emissions, each with a fixed value of $p_\perp$. We could in principle just throw random numbers and accept or reject them using the cross section, but that would be highly inefficient. Consider instead the integral of the emission probability over all allowed values of y at one fixed value of $p_\perp$:

$$\mathcal{I}(p_\perp^2) = \int_{y_{min}(p_\perp^2)}^{y_{max}(p_\perp^2)} dy' \, \frac{d\sigma}{dp_\perp^2 \, dy'}. \tag{1.39}$$

If we now divide $p_\perp^2$ into small intervals $\delta p_\perp^2$ from the maximally allowed $p_\perp^2$ down to zero, then the probability *not* to have an emission between $p_\perp^2$ and $p_\perp^2 - \delta p_\perp^2$ is $1 - \mathcal{I}(p_\perp^2)\delta p_\perp^2$. For $\delta p_\perp^2 \to 0$, we can now start at $p_{\perp max}$, and the no-emission probability down to a given $p_\perp^2$ will exponentiate:

$$\mathcal{P}(p_{\perp max}, p_\perp) = \tag{1.40}$$

$$\exp\left(-\int_{p_\perp}^{p_{\perp max}} dp_\perp^2 \mathcal{I}(p_\perp^2)\right).$$

The probability to actually make an emission at this scale, will then be given by the product of the emission probability here, times the no emission probability from the scale of the last emission, down to this scale.

4.2   Hadronization

The quarks and gluons produced by the parton shower are, due to confinement, not measurable by experiments. Experiments measure hadrons, and in order for the formalism to be complete, we need a procedure to construct hadrons from the dipole chains produced by the shower. The string picture of mesons introduced in section 3.5 provides a good starting point for such a formalism which, in the end, becomes the Lund string hadronization model. We will here present some of the main features of this model.

The yo-yo

We shall no longer work with the circular motion of a flux tube, but employ a simpler picture known as the *yo-yo* [11]. We consider a single $q\bar{q}$ dipole with ends moving back and forth in 1D-space (x) and forward in time (t), under the influence of the string tension κ. As the motion is purely one-dimensional, there is now no angular momentum. In figure 1.7
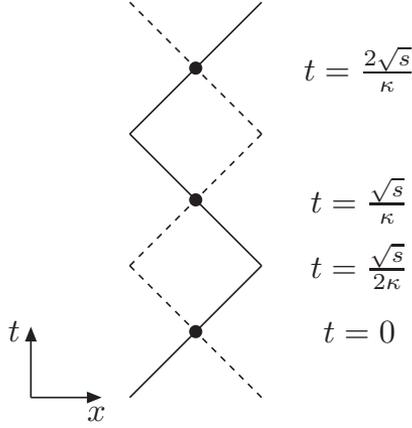
Figure 1.7: The *yo-yo* in its rest system with demarcations of its characteristic times, (1) when a period starts, (2) first point of maximal extension, (3) after half a period, the positions are back to start, while the momenta are swapped, (4) after a full period.

we show the motion of such a yo-yo in an (x, t)-coordinate system. We start time at the beginning of a period. Here all the energy is in the motion of the quarks, and no energy is stored in the string:

$$(E, p_x)_{(q|\bar{q})} = \frac{1}{2}(\sqrt{s}, \pm\sqrt{s}), E_{\text{string}} = 0. \tag{1.41}$$

At time $t = \frac{\sqrt{s}}{2\kappa}$, the string is maximally extended, and all energy is stored in the string:

$$(E, p_x)_{(q|\bar{q})} = (0, 0), E_{\text{string}} = \sqrt{s}. \tag{1.42}$$

At time $t = \frac{\sqrt{s}}{\kappa}$ the yo-yo has been through half a period. The quarks are back to their original positions, but the momenta are swapped:

$$(E, p_x)_{(q|\bar{q})} = \frac{1}{2}(\sqrt{s}, \mp\sqrt{s}), E_{\text{string}} = 0. \tag{1.43}$$

At time $t = \frac{\sqrt{s}}{\kappa}$, the string has been through a full period.

String breaking

We now consider the breaking of a long string into hadrons. In equation (1.42) we saw that when the string is maximally extended, all the energy is stored in the string, *i.e.* as potential energy in the field. If it is energetically favorable for a hadron to tunnel out of the field, we would like to allow this through a string breaking. We would like each hadron to be represented by a yo-yo mode, and describe the breaking process in space coordinates where
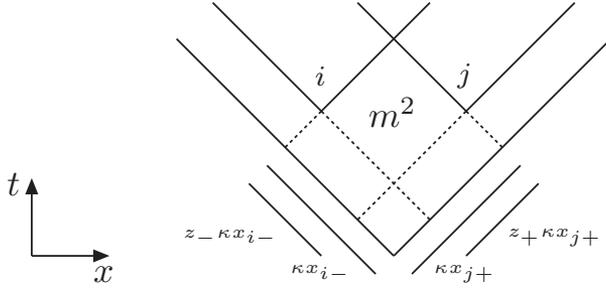
Figure 1.8: Sketch of string breaking, inspired by ref. [12]. The string breaks in vertices i and j, which has lightcone coordinates as indicated. The fraction of remaining lightcone momentum taken away by hadron production is denoted $z_\pm$.

the string axis is the x-axis. The breaking itself is sketched in figure 1.8. The string breaks in the two vertices labelled i and j, following the derivation in ref. [12]. The total energy stored in the string is, given in lightcone coordinates[6] of the breaking vertices:

$$E_{\text{string}} = \kappa^2 x_{i-} x_{j+}. \tag{1.44}$$

After the two breakups, we are left with three string segments. One from the initial $\bar{q}$ to the q coming from vertex i, one from the initial q to the $\bar{q}$ from vertex j, and finally a segment from i to j, which we will consider to be the produced hadron.

We now wish to assign properties to the string breaking at the vertices. This is done in an iterative way, such that the properties of each breaking are to be selected from a probability density function. In the following we will discuss the properties of this function.

We write up the vertices in coordinates given by:

$$\Gamma = \kappa^2 x_+ x_- \text{ and } y = \frac{1}{2} \ln\left(\frac{x_+}{x_-}\right). \tag{1.45}$$

We assume that the vertex i can be reached from the left, or j from the right, by taking many steps, even when the energy is large. The fraction of remaining (positive or negative) lightcone momentum taken away by the production of the hadron is denoted $z_\pm$, and has the range $0 < z_\pm < 1$ with this definition. Looking at figure 1.8, we can therefore establish that the hadron mass is:

$$m^2 = \kappa^2 z_- x_{i-} z_+ x_{j-}, \tag{1.46}$$

as also indicated on the figure.

The probability to go on the positive lightcone (from right to left in figure 1.8) and arrive at vertex j is $H(\Gamma_j) d\Gamma_j dy_j$, where H is an unknown probability distribution we wish to determine. Producing a hadron with a given momentum fraction, *i.e.* the one which takes you to

---

[6]The spatial lightcone coordinates are given by the transformation $x_\pm = t \pm x$.

vertex i, is $f(z_+)dz_+$, where f is another unknown probability distribution. The combined probability is the product of the two, and we can trivially write up the probability to go from left to right instead, this time producing the hadron by going from i to j. Physically these two probabilities must be the same, and we write:

$$H(\Gamma_j)d\Gamma_j dy_j f(z_+)dz_+ = H(\Gamma_i)d\Gamma_i dy_i f(z_-)dz_-. \tag{1.47}$$

From figure 1.8 we can obtain relations between the variables in equation (1.47). We already have one in equation (1.46), and we can also write directly:

$$\Gamma_i = \kappa^2 x_{i+}x_{i-} = \kappa^2(1-z_+)x_{j+}x_{i-} \text{ and } \Gamma_j = \kappa^2 x_{j+}x_{j-} = \kappa^2 x_{j+}(1-z_-)x_{i-}. \tag{1.48}$$

Treating m^2 as fixed, and $dy_i = dy_j$, there are only two independent variables left in equation (1.47), which we take to be $z_\pm$. We can thus write the equation as:

$$h(\Gamma_j(z_\pm)) + g(z_+) = h(\Gamma_i(z_\pm)) + g(z_-), \tag{1.49}$$

where $h(\Gamma) = \ln(\Gamma)$ and $g(z) = \ln(zf(z))$. With a bit of algebra (see ref. [12]), this can be turned into a differential equation for h only in Γ (b is a constant, not to be confused with impact parameter):

$$\frac{d}{d\Gamma}\left(\Gamma\frac{dh}{d\Gamma}\right) = -b \Rightarrow H(\Gamma) = C\Gamma^a \exp(-b\Gamma), \tag{1.50}$$

where C and a are constants of integration; C normalizes the distribution. Inserting in eq. (1.47), one obtains for $f(z)$:

$$f(z) = N\frac{(1-z)^a}{z}\exp\left(-\frac{bm^2}{z}\right), \tag{1.51}$$

where N is a normalization constant and m is to be replaced with $m_\perp$ for a particle with transverse momentum. Before moving on to production of different hadron species, we will discuss the result in eq. (1.51) (often referred to as the Lund symmetric fragmentation function), and its consequences.

First and foremost, the fragmentation function decides the hardness in mainly the longitudinal direction. From inspection of the distribution we directly see that large a suppress the $z \to 1$ region, while large b suppress the $z \to 0$ region. The $p_\perp$ is decided separately (see section 4.2), but enters $f(z)$ indirectly through $m_\perp$.

Since eq. (1.51) determines the amount of momentum taken away by a hadron, and the system will stop producing hadrons when it runs out of available momentum, also the amount of hadrons produced per string (and thus largely the event multiplicity) is decided by the parameters a and b by the relation [13]:

$$\frac{dN}{dy} \sim \frac{\sqrt{\langle\tau^2\rangle}\kappa}{m} = \sqrt{\frac{1+a}{bm^2}}, \tag{1.52}$$

where y is rapidity and $\langle\tau^2\rangle$ is the typical proper production time squared of a hadron.

Transverse momentum and hadron flavours

Until now, we have only considered a one dimensional process where the produced $q\bar{q}$ pair is massless with no transverse momentum. If we allow an $m_\perp > 0$, we can no longer produce the pair in a vertex, but it needs to tunnel a distance $m_\perp/\kappa$ away to be produced. Using the WKB approximation to calculate the probability [14], one obtains for the quark flavour q:

$$\frac{1}{\kappa}\frac{d\mathcal{P}_q}{d^2p_\perp} \propto \exp(-\pi m^2_{\perp q}/\kappa) = \exp(-\pi p^2_\perp/\kappa)\exp(-\pi m^2_q/\kappa). \qquad (1.53)$$

This factorization allows for a very convenient separation of the treatment of $p_\perp$ generation from flavour generation. The two are essentially only connected through the string tension κ. Taking a closer look at the latter part, it is clear that heavier quarks will be suppressed relative to light ones, as *e.g.* a strange quark will be suppressed relative to a u -or d-type by a factor of:

$$\rho = \exp\left(-\frac{\pi(m^2_s - m^2_u)}{\kappa}\right). \qquad (1.54)$$

Since the question of which quark masses to use cannot be unambiguously answered, ρ is essentially a free parameter, to be tuned to data from e^+e^- collisions, current tunes to LEP data [15] places $\rho = 0.217$. Even though quark masses are not unambiguously known, one can say directly from equation (1.54) that production of c-quarks from hadronization should not be considered, as it is suppressed by a factor $\approx 10^{-4}$, and thus negligible compared to perturbative production.

Box 3: Hadronization parameters

The implementation of the hadronization model in Pythia 8 [16] contains in total about 20 tunable parameters, most relating to hadron flavour. The parameters mostly relevant to this thesis, beyond ρ, concern baryon production. Similarly to strange quarks being produced in a breakup, one can also consider a diquark pair being produced. The suppression factor for diquark production is denoted ξ. We can have additional suppression (or enhancement) of diquarks containing s-quarks (parameter named x) or diquarks with spin (parameter named y). Current fits [15] place:

$$\xi = 0.081, x = 0.915, y = 0.0275. \qquad (1.55)$$

---

5 Proton–proton collisions

Hadronic collisions are more complicated than e^+e^- collisions, as we now have to worry about a confined QCD initial state. As a first approximation, we can ask what the cross section of a proton–proton collision is, and given that, a given partonic sub-collision. The partonic sub-collision can then be subjected to the same final state model as for e^+e^-, adding radiation in the initial state, which is now coloured. This approach will work fine for collisions with just a single partonic sub-collision of interest (*e.g.* production of a Higgs boson), which is easily separable from other partonic interactions in the same collision. If we, however, are looking at a situation with multiple partonic interactions (MPIs) which are not easily separable, the situation is different. Since the MPIs are not separable, they can and will interfere with each other, giving visible effects in the final state. So besides having corrections from a QCD initial state, the parton shower and hadronization formalisms will also receive corrections. Since we would like the models to still provide a good description of e^+e^-, the corrections should be of a nature that they vanish when taken to an environment without MPIs.

We can give a rough sketch of the work flow going from the final state model og e^+e^- to the final state model of pp as follows:

1. Take the full model from e^+e^- collisions.

2. Add corrections arising from protons in the initial state.

3. Add corrections arising from multi parton interactions.

4. Tune the new model(s) to proton data.

5. Go back to e^+e^- and retune the old model, given the new corrections – effects should be minimal.

6. Steps 4 and 5 can be repeated until parameter values converge.

5.1 Proton structure

The most important contribution entering when going from collisions of electrons to collisions of protons, is the proton structure. A new quantity enters the discussion; a parton distribution function. For a parton of species a, it is a distribution function $f_a(x, Q^2)$, giving the probability to extract this type of parton, given x and Q^2, where x is the fraction of energy taken away from the proton by the parton, and Q^2 is the collision scale.
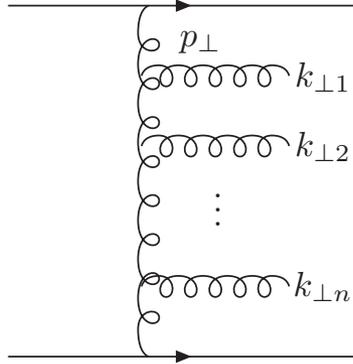
Figure 1.9: Sketch of an exchange ladder. The straight, horizontal lines at top and bottom are the protons, the curly lines are the radiated gluons.

The DGLAP approximation

The most common approach to such calculations, follows a picture outlined by collinear factorization, where the cross section for a scattering sub-process $a + b \rightarrow n$ is a convolution with parton densities [17]:

$$\sigma = \sum_{a,b} \int_0^1 dx_a dx_b \int f_a(x_a, Q^2) f_b(x_b, Q^2) d\hat{\sigma}_{a,b \rightarrow n}. \tag{1.56}$$

The partonic cross section is – just as in $e^+ e^-$ – calculable from Feynman diagrams, and the factorization theorem thus ensures that the physics related to the protons is absorbed into the parton densities f_a and f_b. We will now look closer at the parton densities. In equation (1.56) we essentially describe a situation where the parton densities has been measured at a certain Q^2, as a distribution in x – this can be done in DIS experiments. We would then like to evolve f_a to another virtuality. When Q^2 is large and x is not too small, this amounts to exchange of a ladder of the type sketched in figure 1.9.

The ladder sketched is essentially a Feynman diagram. Normally when one deals with Feynman diagrams, it is enough to truncate the series at a given order in[7] α_s. In the high energy limit of QCD one needs to take care, as each factor of α_s comes with a factor of $\ln(Q^2)$. As this factor can be large, we can have the product $\alpha_s \ln(Q^2|) \approx 1$. The expansion in α_s can therefore not be truncated after a few terms, and one needs in principle to calculate to all orders in α_s. This is, however, not possible at present day, and one needs to rely on approximations. One popular approximation is to keep only *leading logarithms*. At a given order in α_s, this means keeping only the terms carrying the largest power in $\log(Q^2)$. This is called the leading logarithmic approximation (LLA).

---

[7]Where α_s is the strong coupling, not to be confused with the Regge slope α'.

At large Q^2 and x not to small, the resulting evolution equation is called DGLAP evolution (Dokshitzer, Gribov, Lipatov, Altarelli and Parisi [18, 19, 20]). This has the property of being an ordered evolution. Denoting the total virtuality as $p_\perp + \sum_i k_{\perp i}$ (see figure 1.9 for notation), we have that $p_\perp \gg k_{\perp 1} \gg ... \gg k_{\perp n}$. We can give a heuristic explanation of what this means for the proton structure in transverse space. The distance in momentum space between emissions is large, giving the individual emission a large range in $k_\perp$ to potentially occupy. It follows that the transverse size of partons must be confined to a small $r_\perp$.

The BFKL approximation

We now want to lower x while keeping Q^2 large. We no longer have emissions strongly ordered in $k_\perp$, but instead in x. For the emissions we rather have $p_\perp \approx k_{\perp 1} \approx ... \approx k_{\perp n}$. This means that the emissions are now very constrained in momentum space, and in our heuristic explanation, they are now free to occupy large $r_\perp$, while all being roughly the same size.

In figure 1.10, the transverse structure of the proton is drawn as a cartoon, subjected to the two evolution schemes. At not too small x, using DGLAP, we evolve to a proton consisting of more partons, taking up only a small fraction of transverse space. If we instead use BFKL to evolve to smaller x, we fill up the proton with partons. At some point the partons starts to overlap, and we enter into a region where the number of partons are not only determined by splittings, but also recombination, *i.e.* a saturation region.

5.2   The DIPSY formalism

We will now describe a different, convenient formalism for small-x evolution. It is based on a model initially developed by Mueller and coworkers [21], and later generalized to the DIPSY model [22] and implemented in a Monte Carlo which takes a central part in this thesis. The idea behind the model is to evolve an initial proton consisting of three valence dipoles, to the initial state one wants to collide, on an event by event basis. The evolution is – in contrast to the formalisms described above – done in transverse space and rapidity. In this way one can model fluctuations in the proton transverse structure event by event. This turns out to be particularly useful when one wants to model final state interactions. The evolution is built on the following equation giving the probability for a dipole spanned between two partons at transverse positions $\vec{r}_1$ and $\vec{r}_2$ to emit a gluon at $\vec{r}_g$, thus splitting the dipole into two new dipoles.

$$\frac{dP_g}{dY} = \frac{\bar{\alpha}}{2\pi} d^2\vec{r}_g \frac{(\vec{r}_1 - \vec{r}_2)^2}{(\vec{r}_1 - \vec{r}_g)^2(\vec{r}_g - \vec{r}_2)^2}\,, \quad \text{with } \bar{\alpha} = \frac{N_c \alpha_s}{\pi}. \quad (1.57)$$
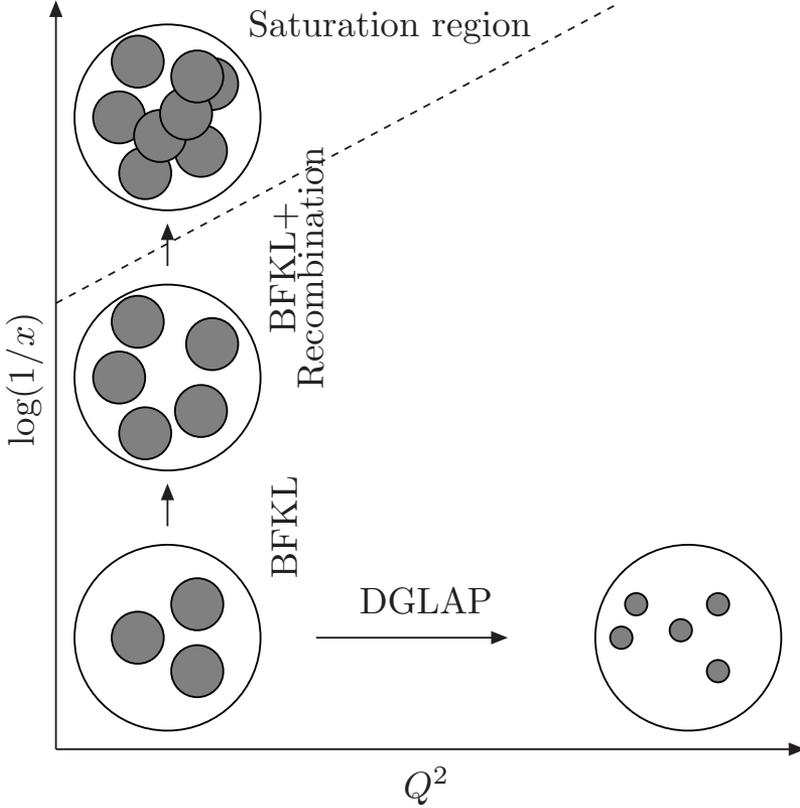
Figure 1.10: Cartoon of DGLAP evolution and BFKL/BFKL+saturation respectively.

In the large-N_c limit we can again treat further emissions as independent. The interaction probability between two dipoles i and j, each consisting of particles labelled 1 and 2:

$$f_{ij} = \frac{\alpha_s^2}{4} \left[\ln \left(\frac{(\vec{r}_{i1} - \vec{r}_{j1})^2 (\vec{r}_{i2} - \vec{r}_{j2})^2}{(\vec{r}_{i1} - \vec{r}_{j2})^2 (\vec{r}_{i2} - \vec{r}_{j1})^2} \right) \right]^2 . \tag{1.58}$$

In DIPSY we correct for finite N_c by assigning randomly each dipole one of N_c^2 possible colors. In figure 1.11 the evolution from the initial three-dipole states to a state ready for collision is shown. In section 5.3 we continue to the final state of pp collisions, but first we take a small aside to saturation.
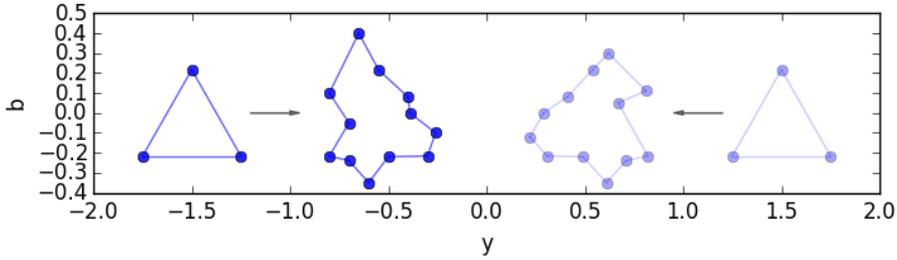
Figure 1.11: A cartoon picture of the DIPSY evolution of two protons from an initial state with three dipoles, to a frame where they are ready for collision.

Box 4: The *pp* cross section

In section 3.3 we discussed collisions between particles with a substructure in general terms. We notice therefore that equation (1.58) can be used directly in the equation (1.12) to obtain the total and semi-inclusive cross-sections.

With the dipole formalism one can calculate cross sections, following section 3.3. The dipole cascades introduce fluctuations on both sides, and it is thus possible to calculate single -and double diffractive cross sections from the model as well as total and elastic cross sections.

Multiple interactions and saturation

In figure 1.11 we clearly see that the collision between two protons in the DIPSY formalism is not limited to one dipole–dipole interaction. Should we, however, limit ourselves to one interaction per event, we obtain the equivalent of the gluon ladder diagram giving the BFKL equation. It can in fact be shown [4] that the DIPSY formalism reproduces LLA BFKL if we limit ourselves to one interaction. Going beyond one interaction, we thus introduce corrections beyond BFKL in the interaction, but not in the cascade. This introduces an inconsistency. Consider scattering of onia[8] in the center of mass frame as depicted in figure 1.12. The two onia are evolved to dipole chains, and each pair of dipoles can interact through color exchange as depicted. This gives rise to the formation of dipole "loops". Considering the same situation in the rest frame of one of the two onia, the situation has changed drastically, as depicted in figure 1.13. As the onium on the right is now not evolved before the collision, it is still just a single dipole, while the onium on the right is now evolved further. Since interactions are modeled as dipole–dipole interactions, changing the color flow, there is now no room for loop formation. We are thus unable to obtain the loop configurations from figure 1.12.

---

[8]Onium is a particle and its anti-particle, *i.e.* just a single dipole or a meson.
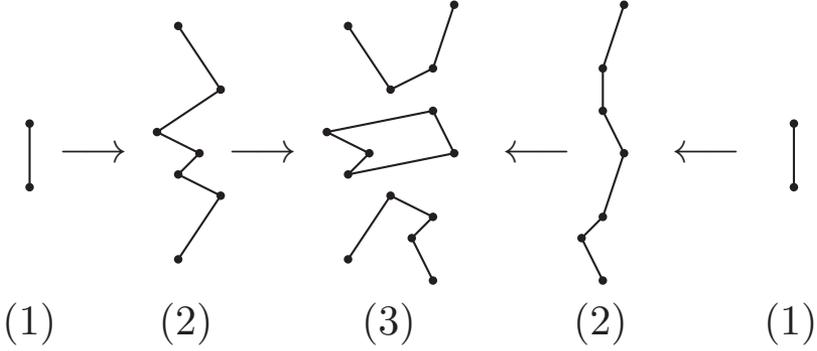
Figure 1.12: Cartoon of onium scattering in the center of mass frame. Multiple scatterings allows for loop configurations.

The loop configurations should be formed inside the cascade on the left. This would be a saturation effect, which would limit the exponential growth in the number of dipoles with rapidity, by allowing dipoles inside the cascade to interact. Following the logic from the collision of cascades, the saturation should happen by exchange of a gluon, changing the color flow. In DIPSY this is done through a "dipole swing" mechanism. Two dipoles, i and j, of the same color, within the same cascade can recouple (or "swing") with the probability:

$$p_{ij} = \frac{(\vec{r}_{i1} - \vec{r}_{i2})^2 (\vec{r}_{j1} - \vec{r}_{j2})^2}{(\vec{r}_{i1} - \vec{r}_{j2})^2 (\vec{r}_{j1} - \vec{r}_{i2})^2}. \tag{1.59}$$

In this way, multiple interactions in one frame becomes saturation in another. In DIPSY the swing is treated as a competing process to the emissions. At a given step a dipole can thus either swing or emit, but not both.

We can give the swing a heuristic interpretation in terms of the proton transverse structure, similar to the interpretations of DGLAP and BFKL in section 5.1. First of all we see that the effect of the swing is to replace large dipoles with smaller ones. If we again see each parton taking up $r_\perp \approx 1/k_\perp$ then keeping $k_\perp$ fixed and evolving to higher energies will meet a natural boundary when gluon occupation saturates because of mutual interactions. At this point we have no choice but to increase $k_\perp$, thus making the gluons smaller. This is exactly the mechanism of the swing. When the dipole overlap is small, the probability to swing is small, but as occupation grows, so does the probability to swing. The number of dipoles will keep increasing, but as it grows larger, the dipoles will become smaller.
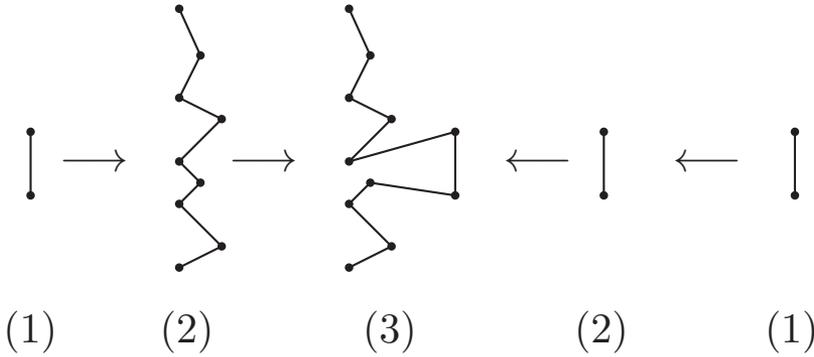
Figure 1.13: Cartoon of onium scattering the rest frame of the right onium. No multiple scatterings can occur, and thus no loop formations are allowed.

Box 5: The Pythia MPI model

Another model for multiple interactions used for pA collisions in ref. [23], is the Pythia MPI model [24]. In this model, multiple interactions are generated in decreasing order of $p_\perp$, using a Sudakov like expression (see box 2), with the perturbative $2 \to 2$ cross section. Since that cross section diverges at low $p_\perp$, it is regulated using a tunable parameter $p_{\perp 0}$:

$$\frac{d\sigma_{2\to 2}}{dp_\perp^2} \propto \frac{\alpha_s^2(p_\perp^2)}{p_\perp^4} \to \frac{\alpha_s^2(p_\perp^2 + p_{\perp,0}^2)}{(p_\perp^2 + p_{\perp,0}^2)^2}.$$
(1.60)

Since this model is built on parton distribution functions (PDFs), and not a dynamical model, the PDF of the parton species taken out during an MPI, is rescaled by the momentum fraction.

5.3 Corrections in dense environment

The major contribution of the articles in this thesis is about corrections to the dipole parton shower and hadronization model, presented in sections 4.1 and 4.2, arising from the fact that we can have many strings on top of each other, when multiple partons interact in a pp collision. In figure 1.14 a typical e^+e^- event is shown to the left, and a pp event with many overlapping strings to the right. The colored tubes depicts Lund strings, the kinks on the strings are gluons. The axes on the figures are transverse space and rapidity, and it seems reasonable to think that:

- More than one possible configuration of strings is possible – *i.e.* which gluons are connected to which by strings – and the formalism should account for this.
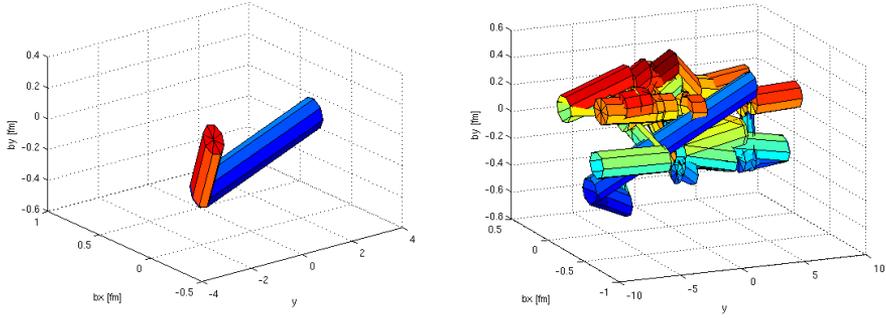
Figure 1.14: Picture in impact parameter space and rapidity of a $Z^0/\gamma^* \to q g \bar{q}$ (left) and a $\sqrt{s} = 7$ TeV pp collision (right). The event activity – and thus the string overlap – is much larger in the pp event.

- If strings can somehow interact, any measurable effect should be more pronounced in the figure to the right than to the left.

- If strings can interact, the string sitting in the center of figure 1.14 (right) should receive a larger contribution than a string sitting in the periphery.

The final state swing

The final state swing tries to address the first of the three points given above. The effect can be considered already in $e^+ e^- \to Z^0/\gamma*$, which provides also a pedagogical introduction.

Consider the situation in figure 1.15. Here we have a Z^0/γ^* going to a $q\bar{q}$ pair. The dipole emits two gluons using the dipole shower formalism introduced in section 4.1. As seen on the right side of the figure, two different string structures are possible, though the association of each emitted dipole in the shower with a new link of the string, only allows for the first one.

Using a semi-classical language, we can gain some intuition for the situation. As the partons move farther and farther apart, confinement effects kicks in. The resulting string ends will then assume colour charges r, g, b or conversely $\bar{r}, \bar{g}$ and $\bar{b}$. The initial dipole is always in a singlet configuration, here exemplified as $b\bar{b}$. The two emitted gluons are both given a colour and an anti-colour randomly, the probability for the two gluons to be able to form a new colour singlet is therefore $\frac{1}{N_c^2-1}$.

The final state swing provides a mechanism for generating both configurations, through a correction of the shower. Upon creation, each dipole is assigned colour state randomly. At each step in the evolution, colour compatible dipoles have the opportunity to swing, and thus connect with each other, instead of emitting. We now introduce as a competing
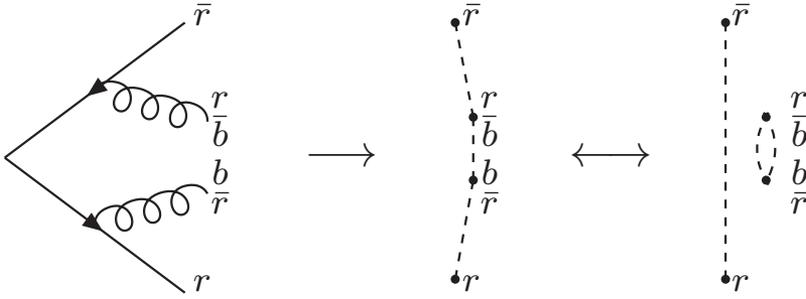
Figure 1.15: The final state swing in a situation where a $Z^0/\gamma^* \to q\bar{q}$ with two further gluon emissions. The parton shower can only deliver the first string configuration whereas the swing can transform it into the second, where the two gluons are in a singlet state.

process to emission, a reconnection probability between two compatible dipoles:

$$\frac{dP_r}{d\ln(p_\perp^2)} = \lambda \frac{(\vec{p_1} + \vec{p_2})^2 (\vec{p_3} + \vec{p_4})^2}{(\vec{p_1} + \vec{p_4})^2 (\vec{p_2} + \vec{p_3})^2}, \tag{1.61}$$

where $\vec{p_i}$ are the momenta of the four partons making up the dipoles, and λ is a parameter.

Enhancement of string tension

Enhancement of string tension is a way of accounting for the overlap of strings still existing after the final state swing has reconfigured the string topology. Physically, the idea is closely connected to the principle of superposition, well known from electrodynamics. Since the strings are really colour field flux tubes, the field strength can change when several strings overlap. Thinking in terms of the simple string introduced in section 3.5, it is clear that if the field strength, and thus the energy, grows, then so must the string tension.

The reality of QCD is, however, not as simple as electrodynamics. As with the final state swing, we must take into account the fact that there are three colour charges and three anti-colour charges. Consider the example sketched in figure 1.16.

Here two $q\bar{q}$ strings, with end colours $c_1, \bar{c}_1$ and $c_2, \bar{c}_2$ are sitting on top of each other, meaning that the quarks acts together coherently. We can be in two distinct situations:

$c_1 = c_2$ Both strings in the figure are $r\bar{r}$, and the endpoint charges should therefore be the resulting $r \oplus r$ and $\bar{r} \oplus \bar{r}$ charges.

$c_1 \neq c_2$ This case is in the figure exemplified with one string being $r\bar{r}$ and the other being $b\bar{b}$. The resulting string will be $\bar{g}g$, a simple dipole like the two initial dipoles, but with colour flow pointing in the opposite direction.
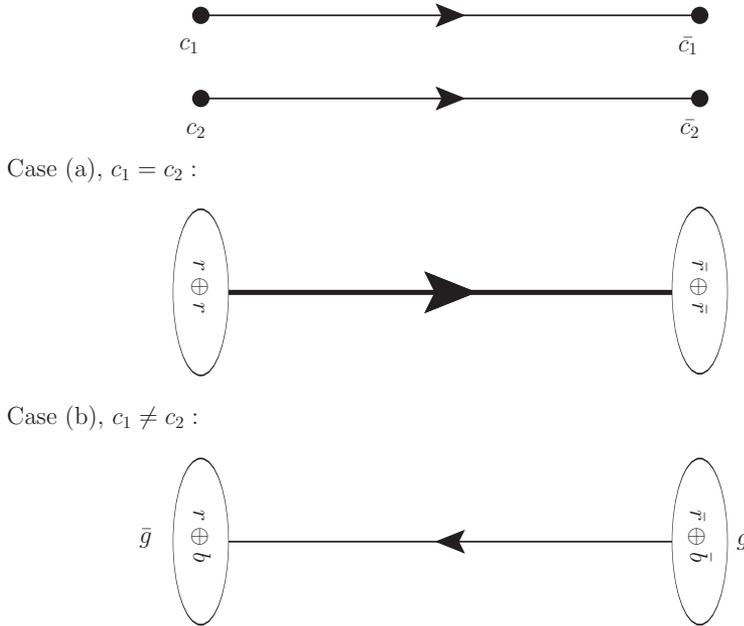
Figure 1.16: The simplest example of rope formation. Two $q\bar{q}$ triplet strings form a rope, as the endpoint quarks acts coherently as one colour charge. In case (a) the endpoint colours are equal, resulting in a sextet, in case (b) they are not, resulting in an anti-triplet.

The combined strings are called "ropes", and correspond to multiplets arising from combining triplets with anti-triplets. In ref. [13] recursion relations for combining any number of triplets and anti-triplets (*i.e.* dipoles pointing "left" vs. dipoles pointing "right") are derived. A multiplet is characterized by two quantum numbers $\{p, q\}$, a triplet is $\{1, 0\}$ and an anti-triplet is $\{0, 1\}$. The string tension of the rope is determined from these quantum numbers, as the ratio of the rope's string tension to the normal string tension is:

$$\frac{\tilde{\kappa}}{\kappa} = \frac{1}{4}\left(p^2 + q^2 + pq + 3(p+q)\right).\tag{1.62}$$

We now let the rope hadronize string by string. This means that a breakup takes us from $\{p, q\}$ to either $\{p-1, q\}$ or $\{p, q-1\}$. In case (a) of figure 1.16, we are in the multiplet $\{2, 0\}$ (a sextet). The first string of the rope breaks with a tension of $\frac{3}{2}\kappa$ and the second with κ.

The enhancement of string tension affects the flavour composition. Here we treat the strangeness suppression parameter ρ from equation (1.54). For a treatment of the other parameters, see ref. [13].

The $\tilde{\rho}$ parameter with some enhanced string tension $\tilde{\kappa}$ will have the same definition as the original ρ. We get directly that:

$$\tilde{\rho} = \exp\left(-\frac{\pi(m_s - m_u)}{\tilde{\kappa}}\right) = \exp\left(-\frac{\pi(m_s - m_u)}{\tilde{\kappa}\frac{\kappa}{\kappa}}\right) = \rho^{\frac{\kappa}{\tilde{\kappa}}}. \qquad (1.63)$$

As the string tension increases, so does $\tilde{\rho}$, which means that increased string tension should lead to more hadrons with strange quarks being produced. Notice the limiting behaviour of the expression: $\tilde{\rho} \to 1$ as $\tilde{\kappa} \to \infty$, meaning that no matter how strong a rope we get, it will never be more likely to produce an s-quark pair than the lightest quarks.

6 Collisions of nuclei

We now take the final step, and move to collisions of nuclei. The idea is to follow the same modus as described for proton collisions such that the same model, with the same parameter values, can be used for everything from e^+e^- collisions, to collisions of protons with lead.

6.1 Particle production and wounded nucleons

The so-called "wounded nucleon" model describes a way of extrapolating particle production from pp to pA collisions. The idea is built on arguments of particle formation time, the Landau-Pomeranchuk formation time (see *e.g.* ref. [25]). Consider a particle produced in a collision between a proton and a nucleus. If we look at the produced particle in a frame where it only has transverse velocity, the Landau-Pomeranchuk formation time – which signifies the minimal possible production time – is $\tau_0 \approx \frac{1}{m_\perp}$. A boost to the laboratory frame is carried out by multiplying with a Lorentz factor:

$$\tau = \gamma\tau_0 = \frac{E}{m_\perp^2} = \frac{\cosh(y)}{m_\perp}, \qquad (1.64)$$

where E is the energy of the particle, and y is its rapidity. The particle is moving with a speed v, which means that it can resolve the nucleus at a length scale no smaller than:

$$v\tau = \frac{\sinh(y)}{m_\perp}. \qquad (1.65)$$

If we look in the central rapidity bin, at not too large $p_\perp$, this resolution scale becomes so large that individual nucleon collisions cannot be resolved. In this region it is therefore reasonable to suggest that the total multiplicity scales with just the number of wounded nucleons. We denote this number $N_w^t + 1$, the number of wounded nucleons in the target, plus one for the projectile. The multiplicity for the pA collision divided by the multiplicity

for a pp collision then becomes $\frac{N_w^t+1}{2}$, since each individual wounded nucleon contributes roughly as half a pp collision.

If $p_\perp$ is high, the resolution scale becomes small enough that every collision is resolved. Now we scale with the number of sub-collisions, and the multiplicity divided by the pp multiplicity becomes just N_w^t.

6.2 Glauber models

From the above arguments, it is clearly important to calculate the number of wounded nucleons if one wants to describe final state multiplicity. For that purpose, Glauber models have served as a workhorse since first introduced in the 1950'ies. We can follow the logic from section 3.2, where now the scattering matrix $S^{(pA)}(b)$ describes the total scattering matrix. In impact parameter space the matrices describing the interactions with individual nucleons will – just as in the example in section 3.2 – factorize, and we get for the profile function:

$$T^{(pA)}(b) = 1 - \exp\left(-\sum_i F^{(pN_i)}(b_i)\right), \tag{1.66}$$

where the sum runs over all nucleons. F can now be understood as the probability for the proton to interact with the individual nucleons *i.e.* some inclusive or semi-inclusive pp cross section.

In figure 1.17 a collision in impact parameter space is sketched. The proton (black) hits a number of nucleons which are then labelled as "participating" or "wounded" nucleons, whereas the rest are spectators.

It is worth noting that different choices of profile functions can lead to very different behaviour. In figure 1.17, the choice is a simple cylindric one, and the projectile hits the target nucleons with which it has direct geometric overlap. In ref. [23] we explored various choices for both semi-inclusive cross sections and profile functions. If one considers projectile and nucleons not as black disks which will always hit when they overlap geometrically, but rather as semi-transparent clouds described by a distribution and an opacity, one can easily imagine a projectile centered one place, also wounding nuclei centered in a different geometric location. This of course has large consequences when one considers corrections to hadronization with the rope formalism presented in section 5.3.

6.3 String shoving

We have already described in section 5.3 how rope formation can enhance the production of hadrons with strange content. Since the overlap region is more energetic than an isolated
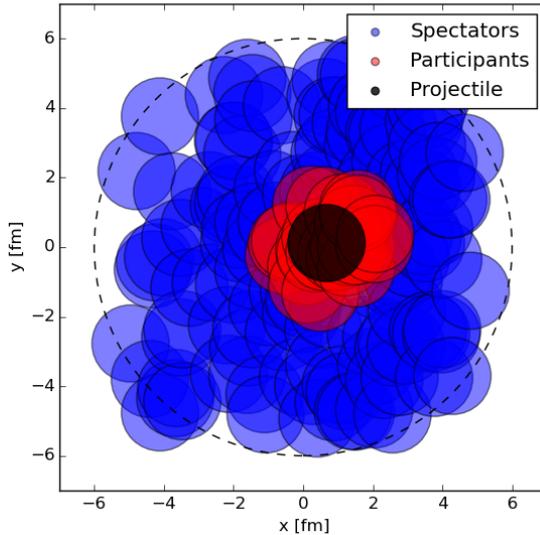
Figure 1.17: Cartoon of a pPb collision, in impact parameter space, in a simple Glauber picture. The projectile is the black circle, and all nuclei with which it overlaps, are "wounded" or "participating" in the collision. The rest are just spectating.

string, string segments will acquire a transverse "push" [26], as indicated in figure 1.18.

The idea that strings may push each other in the transverse direction, is an attempt to microscopically construct flow patterns, which are quite well reproduced by macroscopic, thermodynamic models imposing a hydrodynamic pressure.

Consider the overlap in impact parameter space of two string segments in a small slice of rapidity. The segments are overlapping, and will thus push each other apart. In the figure, the strings are drawn as cylinders, but we model them with a Gaussian profile and get a momentum push:

$$dp_\perp \propto \exp\left(-\frac{d^2}{2R^2}\right),\tag{1.67}$$

where d is the distance between the segment centers and R is a characteristic transverse size of the string. The direction of the push is simply the vector between the two centers. By construction, the push so far conserves transverse momentum.

The push is implemented as an excitation on the string, *i.e.* a gluon, placed on each string, in each rapidity slice. When a gluon gets a kick in the transverse direction, we let the other dipole recoil, to also conserve lightcone momentum.

At the time of writing, the full consequences of this shoving model is still unknown. Similar models were suggested as early as 1988 [27], and recently a toy implementation of a
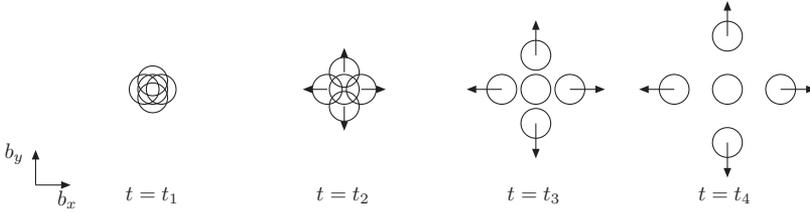
Figure 1.18: Cartoon of five strings shoving each other in impact parameter space. At time $t = t_1$ they overlap a lot, and as they are shoved away from each other, they acquire $p_\perp$. Figure reprinted from ref. [26].

similar model [28] showed promising results, event though the push implementation and the hadronization procedure are somewhat more simple than in a full event generator.

7 Outlook

The papers of this thesis have the overarching goal of constructing a framework to efficiently and realistically extrapolate the microscopic models used for modelling of pp and e^+e^--collision to collisions of heavy ions. This is still very much in its infancy. Thus, there are many places where a reader of this thesis, who would like to pick up where this thesis ends, could proceed this work.

7.1 Precise predictions of collectivity

The modelling of collectivity carried out with the "shoving" model in ref. [26], is clearly still only at a proof–of–concept level. Before it can be taken seriously, it must be able to correctly reproduce flow coefficents with the same definition as experiments. Since flow coefficents are best measured in collisions of heavy ions, this type of study is two–fold. First of all, the DIPSY model must be validated for heavy ion final states as well. Since the centrality measure, which is crucial for flow measurements, depends on total multiplicity, often in the forward region, this observable needs to be under good control in heavy ion collisions. Second, the comparison to experiments should be a proper "apples to apples" comparison. This means that the prediction needs to be processed through the same kind of analysis as data. This type of analysis is fairly evolved for pp collisions, less so for heavy ions.

7.2 The baryon problem

The rope hadronization model developed in ref. [13] predicts correctly a rise of strange hadrons to non-strange hadrons with multiplicity, but also a rise of baryons to mesons as shown in ref. [29]. Since this rise of baryons to mesons is not observed in data [30], the model should accommodate this. Other authors implementing a rope model [31], have previously suggested a mechanism similar to the popcorn mechanism to accommodate this, but this is a corner which needs further studies.

7.3 Heavy ions with FritiofP8

The FritiofP8 model for particle production introduced in ref. [23] is potentially a new path for extrapolation of pp collisions to heavy ions. Until now, only a model for pA collisions is implemented, this should be extended to full AA. If effects from rope hadronization should be taken into account, a model for string overlaps in impact parameter space needs to be developed, as the initial state model in FritiofP8 carries no impact parameter space information (below nucleon level), as opposed to DIPSY. Furthermore, uncertainties from using Pomeron PDFs in place of proper proton PDFs needs to be under better control, or better yet, removed entirely.

7.4 Comparison to hydrodynamics

We know that a very good macroscopic description of flow phenomena can be obtained by various hydrodynamical treatments. It would be very instructive to study whether a model like the shoving model, produces a pressure similar to the one obtained by hydrodynamics. In order for such a comparison to work, a translation from parton level Monte Carlo to a continuous stress–energy tensor for hydrodynamics needs to be worked out first.

7.5 Jet quenching

Imagine that one of the multiple parton interactions in DIPSY would produce a vector boson (Z^0 or $W^{\pm}$) in association with one or more jets. If the vector boson decays leptonically, the leptons can travel through the colour ropes unaffected, while the jets would be affected by rope shoving. It would be interesting to investigate whether rope shoving could give a dynamical explanation of the nuclear modification factor in such systems, or even nuclear modification factors in general.

7.6 Effects in e^+e^-

As indicated in ref. [13], corrections to shower and hadronization have effects in e^+e^-. Since these effects are quite rare, one cannot expect them to be very visible in existing LEP data. At a possible future e^+e^- collider with the goal of collecting $\mathcal{O}(10^{12})$ Z^0 particles, effects will be more pronounced. This will serve as a very good laboratory to gauge these effects, and as such, it is an obvious arena for future work.

References

[1] **NA35** Collaboration, J. Baechler *et al.*, "Strangeness enhancement in central S + S collisions at 200-GeV/nucleon," *Nucl. Phys.* **A525** (1991) 221C–226C.

[2] **STAR** Collaboration, K. H. Ackermann *et al.*, "Elliptic flow in Au + Au collisions at (S(NN))**(1/2) = 130 GeV," *Phys. Rev. Lett.* **86** (2001) 402–407, `arXiv:nucl-ex/0009011 [nucl-ex]`.

[3] S. Donnachie, H. G. Dosch, O. Nachtmann, and P. Landshoff, "Pomeron physics and QCD," *Camb. Monogr. Part. Phys. Nucl. Phys. Cosmol.* **19** (2002) 1–347.

[4] E. Avsar, *Non-linear evolution in High Energy QCD.* PhD thesis, Lund University, 2007.

[5] M. L. Good and W. D. Walker, "Diffraction disssociation of beam particles," *Phys. Rev.* **120** (1960) 1857–1860.

[6] **Particle Data Group** Collaboration, C. Patrignani *et al.*, "Review of Particle Physics," *Chin. Phys.* **C40** no. 10, (2016) 100001.

[7] A. Donnachie and P. V. Landshoff, "Total cross-sections," *Phys. Lett.* **B296** (1992) 227–232, `arXiv:hep-ph/9209205 [hep-ph]`.

[8] L. Lönnblad, "ARIADNE version 4: A Program for simulation of QCD cascades implementing the color dipole model," *Comput. Phys. Commun.* **71** (1992) 15–31.

[9] G. Gustafson, "Parton cascades, small x, multiple interactions, and saturation," *Acta Phys. Polon.* **B42** (2011) 2581–2606.

[10] A. Buckley *et al.*, "General-purpose event generators for LHC physics," *Phys. Rept.* **504** (2011) 145–233, `arXiv:1101.2599 [hep-ph]`.

[11] X. Artru, "Classical String Phenomenology. 1. How Strings Work," *Phys. Rept.* **97** (1983) 147.

[12] B. Andersson, "The Lund model," *Camb. Monogr. Part. Phys. Nucl. Phys. Cosmol.* **7** (1997) 1–471.

[13] C. Bierlich, G. Gustafson, L. Lönnblad, and A. Tarasov, "Effects of Overlapping Strings in pp Collisions," *JHEP* **03** (2015) 148, arXiv:1412.6259 [hep-ph].

[14] B. Andersson, G. Gustafson, G. Ingelman, and T. Sjöstrand, "Parton Fragmentation and String Dynamics," *Phys. Rept.* **97** (1983) 31–145.

[15] P. Skands, S. Carrazza, and J. Rojo, "Tuning PYTHIA 8.1: the Monash 2013 Tune," *Eur. Phys. J.* **C74** no. 8, (2014) 3024, arXiv:1404.5630 [hep-ph].

[16] T. Sjöstrand, S. Ask, J. R. Christiansen, R. Corke, N. Desai, P. Ilten, S. Mrenna, S. Prestel, C. O. Rasmussen, and P. Z. Skands, "An Introduction to PYTHIA 8.2," *Comput. Phys. Commun.* **191** (2015) 159–177, arXiv:1410.3012 [hep-ph].

[17] R. K. Ellis, W. J. Stirling, and B. R. Webber, "QCD and collider physics," *Camb. Monogr. Part. Phys. Nucl. Phys. Cosmol.* **8** (1996) 1–435.

[18] V. N. Gribov and L. N. Lipatov, "Deep inelastic e p scattering in perturbation theory," *Sov. J. Nucl. Phys.* **15** (1972) 438–450. [Yad. Fiz.15,781(1972)].

[19] Y. L. Dokshitzer, "Calculation of the Structure Functions for Deep Inelastic Scattering and e+ e- Annihilation by Perturbation Theory in Quantum Chromodynamics.," *Sov. Phys. JETP* **46** (1977) 641–653. [Zh. Eksp. Teor. Fiz.73,1216(1977)].

[20] G. Altarelli and G. Parisi, "Asymptotic Freedom in Parton Language," *Nucl. Phys.* **B126** (1977) 298–318.

[21] A. H. Mueller and B. Patel, "Single and double BFKL pomeron exchange and a dipole picture of high-energy hard processes," *Nucl. Phys.* **B425** (1994) 471–488, arXiv:hep-ph/9403256 [hep-ph].

[22] C. Flensburg, G. Gustafson, and L. Lönnblad, "Inclusive and Exclusive Observables from Dipoles in High Energy Collisions," *JHEP* **08** (2011) 103, arXiv:1103.4321 [hep-ph].

[23] C. Bierlich, G. Gustafson, and L. Lönnblad, "Diffractive and non-diffractive wounded nucleons and final states in pA collisions," *JHEP* **10** (2016) 139, arXiv:1607.04434 [hep-ph].

[24] T. Sjöstrand and M. van Zijl, "A Multiple Interaction Model for the Event Structure in Hadron Collisions," *Phys. Rev.* **D36** (1987) 2019.

[25] A. Białas, "Wounded nucleons, wounded quarks: An update," *J. Phys.* **G35** (2008) 044053.

[26] C. Bierlich, G. Gustafson, and L. Lönnblad, "A shoving model for collectivity in hadronic collisions," `arXiv:1612.05132 [hep-ph]`.

[27] V. A. Abramovsky, E. V. Gedalin, E. G. Gurvich, and O. V. Kancheli, "Long Range Azimuthal Correlations in Multiple Production Processes at High-energies," *JETP Lett.* **47** (1988) 337–339. [Pisma Zh. Eksp. Teor. Fiz.47,281(1988)].

[28] I. Altsybeev, "Mean transverse momenta correlations in hadron-hadron collisions in MC toy model with repulsing strings," *AIP Conf. Proc.* **1701** (2016) 100002, `arXiv:1502.03608 [hep-ph]`.

[29] C. Bierlich and J. R. Christiansen, "Effects of color reconnection on hadron flavor observables," *Phys. Rev.* **D92** no. 9, (2015) 094010, `arXiv:1507.02091 [hep-ph]`.

[30] **ALICE** Collaboration, J. Adam *et al.*, "Multiplicity-dependent enhancement of strange and multi-strange hadron production in proton-proton collisions at $\sqrt{s} = 7$ TeV," `arXiv:1606.07424 [nucl-ex]`.

[31] H. Sorge, M. Berenguer, H. Stoecker, and W. Greiner, "Color rope formation and strange baryon production in ultrarelativistic heavy ion collisions," *Phys. Lett.* **B289** (1992) 6–11.

8 Publications

Paper I

Christian Bierlich, Gösta Gustafson, Leif Lönnblad, Andrey Tarasov: *Effects of Overlapping Strings in pp Collisions*, e-print: arXiv:1412.6259 [hep-ph]. JHEP **03** (2015) 148.

The ideas behind this publication were developed by Gösta Gustafson and Leif Lönnblad, and initial studies were carried out by Andrey Tarasov. The main part of the further theoretical development were carried out in collaboration between Leif Lönnblad, Gösta Gustafson and myself. I did the implementation of the 'pipe' model while Leif Lönnblad did the implementation of the 'dipole' model. The interfacing to Pythia was based on previous work by Leif Lönnblad and extended by me.

The review part and model development part of the article was written primarily by Gösta Gustafson, the implementation part primarily by Leif Lönnblad, while I wrote the result part and appendix b.

Paper II

Christian Bierlich, Jesper Roy Christiansen: *Effects of color reconnection on hadron flavor observables*, e-print: arXiv:1507.02091 [hep-ph]. Phys.Rev. **D92** (2015), 9, 094010.

The idea for the paper was conceived by Jesper R. Christiansen (another Ph.D. student at Lund university) and myself. He contributed with the Pythia CR model and I contributed with the rope hadronization model. We both contributed to the common phenomenological studies. I wrote the parts related to the rope hadronization model and we both contributed equally to the common sections.

Paper III

Christian Bierlich, Gösta Gustafson, Leif Lönnblad: *Diffractive and non-diffractive wounded nucleons and final states in pA collisions*, e-print: arXiv:1607.04434 [hep-ph]. JHEP **10** (2016) 139.

The idea for this paper was mostly conceived by Gösta Gustafson, who also developed the notion of the wounded cross section. The idea for particle production in FritiofP8 was built on previous work by Gösta Gustafson, and extended to this paper by Leif Lönnblad. Leif Lönnblad and I did most of the implementation in parallel, in the end my implementation

was used to create all numerical results and plots for the paper. I wrote parts of section 4 and 5 and drafted the conclusion.

Paper IV

Christian Bierlich, Gösta Gustafson, Leif Lönnblad: *A shoving model for collectivity in hadronic collisions*, e-print arXiv:1612.05132 [hep-ph].

This letter gives proof–of–concept of an extension to the model introduced in Paper I, and is still in preprint form. Most of the theoretical development so far has been carried out in collaboration between Leif Lönnblad, Gösta Gustafson and myself. I have done most of the implementation of the model, as well as produced the figures of the articles. I drafted major parts of the letter.

9   Further published work

During my Ph.D. I have also published the following proceedings which are not included in the thesis, but listed here for the sake of completeness.

Paper V

Christian Bierlich: *Finite N_c effects in pp and AA Monte Carlo event generation with DIPSY*, in R. Astalos *et al.*: *Proceedings of the Sixth International Workshop on Multiple Partonic Interactions at the Large Hadron Collider,* e-print: arXiv:1506.05829 [hep-ph].

This paper is a conference proceedings based on a preliminary version of Paper I. I made the figures and wrote the paper.

Paper VI

Christian Bierlich: *Hadronisation Models and Colour Reconnection*, e-print: arXiv:1606.09456 [hep-ph]. PoS **DIS2016** (2016).

This paper is a conference proceedings giving some results from Paper I and II, plus results from a toy implementation of the rope hadronization model in Pythia 8, which is otherwise unpublished. I did the theoretical work behind the toy model, the implementation, the results and wrote the paper.

Paper VII

Christian Bierlich: *Multiparton interactions: From pp to pA*, e-print: arXiv:1610.09955 [nucl-th], to appear in: *Proceedings of the 8th International Conference on Hard and Electromagnetic Probes of High–Energy Nuclear Collisions*.

This paper is a conference proceedings based on Paper III. I made the figures and wrote the paper.

10 Acknowledgements

I

Effects of Overlapping Strings in *pp* Collisions

Christian Bierlich[1], Leif Lönnblad[1], Gösta Gustafson[1], and Andrey Tarasov[2].

[1] Dept. of Astronomy and Theoretical Physics, Lund University, Sölvegatan 14A, SE-223 62 Lund, Sweden.
[2] Theory Group, Jefferson Lab, Newport News, Virginia, USA.

ABSTRACT: In models for hadron collisions based on string hadronization, the strings are usually treated as independent, allowing no interaction between the confined colour fields. In studies of nucleus collisions it has been suggested that strings close in space can fuse to form "colour ropes". Such ropes are expected to give more strange particles and baryons, which also has been suggested as a signal for plasma formation. Overlapping strings can also be expected in *pp* collisions, where usually no phase transition is expected. In particular at the high LHC energies the expected density of strings is quite high. To investigate possible effects of rope formation, we present a model in which strings are allowed to combine into higher multiplets, giving rise to increased production of baryons and strangeness, or recombine into singlet structures and vanish. Also a crude model for strings recombining into junction structures is considered, again giving rise to increased baryon production. The models are implemented in the DIPSY MC event generator, using PYTHIA8 for hadronization, and comparison to *pp* minimum bias data, reveals improvement in the description of identified particle spectra.

1   Introduction

In most models for high energy collisions, like the popular PYTHIA [1] or HERWIG [2] models, the hadronization mechanism is described via strings or cluster chains. The strings are often treated as independent, but in connection with nucleus collisions it was early suggested that the many strings produced within a limited space may interact and form "colour ropes" [3, 4]. Such ropes have subsequently been studied by many authors with applications to high energy nucleus collisions [5, 6, 7, 8, 9, 10, 11]. The stronger field in a rope is expected to give larger rates for strangeness and baryons. The effect on the multiplicity is more difficult to predict, and here the results depend on simplified assumptions, often without a real motivation. Usually the result is either a decreased or an unmodified particle multiplicity.

As rope formation is expected to give increased rates of strange particles and baryons, which may mimic effects of plasma formation, it makes signals for a phase transition more difficult to interpret. It has also been suggested that ropes may initiate the formation of a quark–gluon plasma [12, 6, 13, 14]. At LHC energies many overlapping strings are also expected in pp scattering, where plasma formation normally is not expected. In this paper we want to study string interference effects in pp scattering, with the aim to get a better understanding of the dynamics in pp collisions, and simultaneously get a tool to estimate possible rope effects in nucleus collisions.

For a quantitative estimate of interaction between neighbouring strings, we believe it is essential to have a description formulated in transverse coordinate space. Such a formulation is also suitable for including effects of saturation for small x and high gluon densities. Here we will use the Lund dipole cascade model implemented in the event generator DIPSY [15, 16]. This model is based on a formulation of BFKL dynamics in transverse coordinate space, including non-leading-log and saturation effects, and also taking fluctuations and correlations into account.[1]

The Lund string hadronization model [22, 23][2], which has been particularly successful in describing data from e^+e^- annihilation at LEP [26, 27], is based on the assumption that a confined colour field between a quark and an antiquark is compressed to a linear flux tube, similar to a vortex line in a superconductor. When the string is stretched between separated colour charges, it can break by the production of $q\bar{q}$ pairs [28, 29, 30, 31] in a process similar to the production of e^+e^- pairs in a homogeneous electric field [32]. As demonstrated in ref. [33], this can be interpreted as the effect of a quantum-mechanical tunneling process.

---

[1]String interaction effects in pp collisions have also earlier been included in the event generator DTUJET [17], formulated in momentum space. This was generalized to nucleus collisions, including a geometric distribution of nucleons within a nucleus [18]. Rope effects are also included, together with hadron rescattering, in the RQMD model, with applications in the SPS fixed target and RHIC energy ranges [19, 20, 21].

[2]For a review of the Lund hadronization model see ref. [24], or a more recent summary in ref. [25].

In the Lund model the dynamical motion of the flux tube is approximated by an infinitely thin *massless relativistic string*, and gluons are identified with transverse excitations on such a string [23], which also has the effect that the model is infrared stable, *i.e.* insensitive to soft or collinear gluons.

It was early observed that when the string hadronization model is tuned to LEP data, it slightly underestimates the production of strange particles in hadronic collisions [34]. Similarly in DIS, the LEP tune works well in the current fragmentation region (in the Breit frame), while in the proton fragmentation end, one again observes an enhanced strange quark fraction [35]. This effect is enhanced in data from LHC, where a rather dramatic increase is observed in the fractions of strange particles and baryons, most notably that of strange baryons [36]. These observations should not be surprising. The colour flux tubes are expected to have a transverse width determined by the confinement scale, of ~ 1 fm. In *pp* collisions there can be several strings close to each other, and it should actually be rather surprising that models neglecting mutual string interaction are working as well as they do.

Biro *et al.* noted in ref. [3], that the colour charge at the endpoint of a rope formed by strings with random colour charges, is given by a random walk in colour space. The rope can break up in a stepwise manner by repeated production of $q\bar{q}$ pairs, as expected from a local interaction $\propto j_\mu A_\mu \sim \bar{\psi}\gamma_\mu\psi A_\mu$. This process is analogous to the production of e^+e^- pairs in an electric field. It was pointed out in ref. [3] that for a rope formed by random charges, the number of pairs produced before a total breakup of the rope is in general smaller than the number of initial strings, and also that the total time for this successive split is approximately the same as for a single string.

Although such a stepwise breakup of a rope is assumed in most studies, also an immediate breakup by production of multi-quark–antiquark systems has been advocated by Amelin, Braun, and Pajares [10] (also mentioned as a possibility in ref. [3]), and a breakup by the production of gluon pairs has been studied by Gyulassy and Iwazaki [6]. It has also been suggested that a rapid decay of the ropes into elementary partons is facilitating the formation of a quark–gluon plasma [6, 13, 14].

It was early suggested that, if the charges correspond to a specific SU(3) multiplet, the tension (or energy density) in the rope is given by the second Casimir operator [37]. For an isolated rope this conjecture has later been supported by lattice calculations [38]. However, if the rope is surrounded by other strings or ropes, we expect that the transverse area, and thus the rope tension, will be affected by the presence of the neighbouring ropes, which exert a pressure keeping the radius small. Such a pressure might also cause a collective expansion contributing to extra transverse momentum for the hadrons. It ought to be kept in mind, that this feature contributes to the necessary uncertainties in estimating the effects of rope formation.

As mentioned above we will here use the event generator DIPSY to study the effects of string

interaction and rope formation in more detail, beyond qualitative results such as increased strangeness and baryon production. The DIPSY model is a generalization and extension of Mueller's dipole model [39, 40, 41], which describes BFKL evolution in transverse coordinate space. At high energies the high density of soft gluons effectively screens colour charges, thus suppressing gluons with $p_\perp$ below a saturation scale Q_s. As in the Color Glass Condensate formalism for nucleus collisions [42, 43], we argue that this is a motivation for a perturbative treatment of the initial phase in terms of quarks and gluons. (This is also assumed in other models for soft interactions, like PYTHIA and HERWIG.)

While Mueller's model reproduces leading log BFKL evolution, the DIPSY model includes essential non-leading corrections to BFKL, as well as saturation within the cascade evolution, and confinement. It reproduces total, elastic, and diffractive cross sections in pp collisions and DIS, and gives a good description of particle distributions in minimum-bias final states[16]. However, as parton distributions are generated within the model, and therefore not tuned to data, and are in addition limited to gluons, the model is naturally less accurate than *e.g.* the PYTHIA and HERWIG models. Our aim has instead been focused on understanding the dynamics of small-x evolution and saturation, including correlations and fluctuations, *e.g.* in connection with multiple parton interactions [44] and diffraction [45, 46]. The formulation in transverse coordinate space makes the DIPSY model particularly suited for studies of string interference and rope formation. Although it has also been applied to collisions with nuclei (see *e.g.* refs. [47, 48]), we will in this paper limit our study to proton–proton collisions.

We will here assume that colour ropes can form by coherent interaction between a group of strings confined within a limited transverse size. As in ref. [3] we assume random colour charges for the individual strings, leading to a random walk in colour space. We also assume that the rope breaks by successive production of new $q\bar{q}$ pairs. The nature of the tunneling process implies here that an "effective string tension" is determined by the *reduction* in rope tension in each individual breakup. As mentioned in ref. [3], and discussed in detail below, the result of the rope formation is then a smaller number of $q\bar{q}$ pairs needed to break the rope, but a larger effective string tension. As is generally expected, this implies larger strangeness and baryon fractions. In addition our model also gives nontrivial effects on the $p_\perp$-dependence for different particle ratios, which to some extent mimic effects of transverse flow. In this paper we present results where the model (with some approximations) is compared to LHC pp scattering data, with encouraging qualitative agreement. In the future we plan to also study effects of rope formation in collisions with nuclei. We begin this article with a recapitulation of the relevant ingredients of the Lund string fragmentation in section 2, before we describe the basic idea of the rope model in section 3. Then we describe the proposed "final-state swing mechanism" together with the implementation of our rope model in the interface between DIPSY and PYTHIA8 in section 4. In section 5 we present some first results, and finally in section 6 we summarize our findings and give an outlook.

For completeness, we end the article with a number of appendices. There we first summarize details in the DIPSY model (appendix 1.A) that are important for our rope implementation, and also summarize the relevant colour algebra needed (appendix 1.B). Most of this can be found in various different references, but we think it is valuable to have the relevant issues collected here. Furthermore, we have collected some of the more technical points in our implementation and in the tuning procedure in appendices 1.C and 1.D respectively. Although these are important for our results, they tend to hamper the readability of the main text, and are therefore presented separately.

2 String fragmentation

In this section we will discuss the fragmentation of a single string. We first discuss the basic tunneling process, then the space-time picture describing how the produced quarks and antiquarks combine to hadrons, followed by a discussion of baryon production and spin effects. We end by a discussion of the effects of a modified effective string tension.

2.1 Tunneling

A linear colour electric field stretched between a quark and an antiquark, moving in opposite directions, can break up by the production of new $q\bar{q}$ pairs, in a way similar to the production of e^+e^- pairs in a homogenous electric field. As discussed by Schwinger [32] the electric field is unstable, and the decay can be interpreted as the result of the production of new e^+e^- pairs with a rate per unit time and unit volume given by:

$$\mathcal{P} \propto (e\mathcal{E})^2 \exp\left(-\frac{\pi\mu^2}{e\mathcal{E}}\right). \tag{1.1}$$

Here μ is the electron mass and $\mathcal{E}$ the electric field strength. Thus $e\mathcal{E}$ is the force acting on the produced electron or positron. As pointed out in ref. [33], this result can be interpreted as the effect of a tunneling process. Classically the electron and the positron cannot be produced in a point, but only separated by a distance $2\mu/e\mathcal{E}$, such that the reduction in the electric field energy can be transferred into the mass of the pair. In quantum theory the particles are produced locally by an interaction Lagrangian $\sim e\bar{\psi}(x)\gamma_\mu\psi(x)A_\mu(x)$, and have to tunnel through the classically forbidden region, where the wavefunctions can be estimated by the WKB method.

When generalizing this result to $q\bar{q}$ pair production [28, 29, 30, 31] in a linear confined colour field, the tunneling mechanism implies that $e\mathcal{E}$ has to be replaced by the force acting

on a quark, *i.e.* by the string tension[3] $\kappa \sim 1$ GeV/fm. For the production of a pair with opposite transverse momenta $p_\perp$ in this process, the mass μ in eq. (1.1) will be replaced by the transverse mass $\sqrt{\mu^2 + p_\perp^2}$. This gives

$$\frac{d\mathcal{P}}{d^2 p_\perp} \propto \kappa \exp\left(-\frac{\pi}{\kappa}(\mu^2 + p_\perp^2)\right), \qquad (1.2)$$

which integrated over $p_\perp$ gives the result in eq. (1.1), with the replacement $e\mathcal{E} \to \kappa$.

The result in eq. (1.2) can be used to estimate the relative production of quarks with different flavour, and the distribution in $p_\perp$. As it is not possible to theoretically determine the effective quark masses to be used in eq. (1.2), it is in practice necessary to tune the s/u ratio to experimental data. Fits to LEP data give $s/u \approx 0.2$ [26, 27], which is not inconsistent with eq. (1.2) for reasonable quark masses. This mechanism also implies that charm and heavier quarks cannot be produced in the soft hadronization process; they can only be produced in an initial perturbative phase. For the transverse momenta it gives a Gaussian $p_\perp$-distribution with $\sqrt{\langle p_\perp^2 \rangle} \approx 0.25$ GeV. Phenomenological fits to data will, however, also include effects from soft gluons below a necessary $p_\perp$ cut in the perturbative parton shower. Tunes to data therefore give a somewhat wider distribution, with a width $\sigma_{p_\perp} \approx 0.32$ GeV.

2.2 Space-time picture and longitudinal momentum distribution

The strange quark fraction and the $p_\perp$-distribution are governed by the tunneling mechanism, but for the longitudinal momentum distribution it is essential to take into account how the produced quarks and antiquarks can fit into a mesonic wavefunction, and combine to form final-state hadrons. The Lund fragmentation model is here inspired by the area law for Wilson loop integrals for a confining theory [49], in analogy with the Nambu–Goto action for a massless relativistic string. The boost invariance of the relativistic string (and of a linear homogenous electric field) has to result in a boost-invariant distribution of hadrons, produced around a hyperbola in space-time.

Consider, for simplicity, a model in one space dimension with only one quark flavour and a single mesonic state with mass m. In the Lund hadronization model the probability, $\mathcal{P}$,

---

[3]In ref. [28] $e\mathcal{E}$ was (for a quark with charge $g/2$) replaced by $g\mathcal{E}/2 = 2\kappa$, where the string tension κ was estimated from the energy in the colour-electric field. However, ref. [31] noted that, although the force on the electron is given by $e\mathcal{E}$ in a classical (macroscopic) electric field, in case the flux corresponds to only a single charge quantum, an extra contribution comes from the decreased field between the created quark and antiquark, giving $e\mathcal{E} \mapsto g\mathcal{E}/4$, just corresponding to the energy in the colour-electric field. In ref. [31] it was also noted that if the flux tube is embedded in a vacuum condensate, a further contribution to the string tension is given by the response from the condensate. In the bag model (similar to a type I superconductor) this contribution equals the energy in the colour-electric field.

for the production of a specific state with n mesons with momenta p_i $(i = 1, ..., n)$ is given by the relation [22]:

$$\mathcal{P} \propto \left\{ \left[\prod_1^n N d^2 p_i \delta(p_i^2 - m^2) \right] \delta^{(2)} (\sum p_i - P_{tot}) \right\} \exp(-bA). \qquad (1.3)$$

Here the term in curly parenthesis is a phase space factor, where the dimensionless constant N determines the relative weight between states with different number of mesons. The term bA in the exponent corresponds to the imaginary part of the action for the massless string, which is responsible for the decay and finite lifetime of the string. A is a measure of the space-time area covered by the string before the breakup, and b is a constant. Conventionally the area A is scaled by the square of the string tension κ:

$$A \equiv \mathcal{A} \kappa^2, \qquad (1.4)$$

where $\mathcal{A}$ is the area in space and time. Consequently the dimension of b is $(energy)^{-2}$.

The result in eq. (1.3) can be generated in a Monte Carlo simulation by producing the mesons in an iterative way starting from one of the string ends, where each meson takes a fraction z of the remaining energy. In each step the relevant z-value is given by the probability distribution or splitting function:

$$f(z) = N \frac{(1 - z)^a}{z} e^{-bm^2/z}. \qquad (1.5)$$

Here the constant a is related to N and b through the normalization constraint $\int f(z) \, dz = 1$. The production points for the pairs will be located around a hyperbola in space-time, with a typical proper time determined by

$$\langle \tau^2 \rangle = \frac{1 + a}{b \, \kappa^2}. \qquad (1.6)$$

This timescale is also related to the particle multiplicity via the relation

$$dN/dy \sim \sqrt{\langle \tau^2 \rangle} \, \kappa/m = \sqrt{\frac{1 + a}{b \, m^2}}. \qquad (1.7)$$

We note that absorbing the string tension in the definition of b, via the scaling in eq. (1.4), implies that κ does not appear explicitly in this expression for the splitting function or the particle density.

In three dimensions the hadron mass m in eqs. (1.3), (1.5), and (1.7) has to be replaced by the transverse mass $m_\perp = \sqrt{m^2 + p_\perp^2}$, in accordance with eq. (1.2). The parameters a and b, determined by the hadronic phase space and (the imaginary part of) the string action, have been tuned to LEP data, which in our case gives $a = 0.42$ and $b = 0.4$.

2.3 Baryon production

Besides including different quark species, the relations in eqs. (1.3) and (1.5) must also be generalized to include baryon production and effects of spin interaction. A quark and an antiquark can combine to a total spin 1 or 0. Fits to data favour a $\pi : \rho$ ratio about $1 : 1$ (rather than the $1 : 3$ expected from naive spin counting), which also can be understood as a result of normalization of the wavefunction in the tunneling process [50, 24].

A baryon–antibaryon pair can be formed if the string can break by the production of a diquark–antidiquark pair forming an antitriplet and a triplet respectively [51]. Such a process would be suppressed by a larger effective diquark mass. In this case the $\bar{B}B$ pair will always have two quark flavours in common, in conflict with experimental data from e^+e^- annihilation. A modified model with a stepwise production mechanism (called the popcorn model) was presented in [52], and has since been incorporated in PYTHIA.[4] In a red–antired ($r\bar{r}$) string-field a $g\bar{g}$ quark pair can be produced as a vacuum fluctuation (see figures 1.1a and 1.1b). If the r and g charges form a $\bar{b}$ antitriplet, a $b\bar{b}$ field can be formed between the new quarks, which means that the net force on the green quark or antiquark is zero. During this fluctuation a $b\bar{b}$ pair produced in the string can split the system by an effective diquark–anti-diquark production (see figure 1.1c). In this way one (or more) mesons can be produced between the baryon and antibaryon.

As hadronization is a non-perturbative process, estimating all possible hadron species in an MC implementation necessarily implies a set of additional phenomenological parameters, which all have to be tuned to experimental data. Although PYTHIA has adopted the popcorn model, it is reformulated in terms of diquark breakups with an additional probability for having mesons produced in between baryon pairs as in figure 1.1d. Most important for the result is therefore the diquark/quark ratio in the splitting process, together with the extra suppression of strange diquarks beyond the s/u suppression. A detailed description of the parameters involved in baryon production within the Lund model is presented in appendix 1.C.

We here also want to point out that, besides the different parameters, it is also very important to take into account that a produced baryon must be symmetric in flavour and spin, in order to preserve SU(3) flavour symmetry (as is done in the PYTHIA generator).

2.4 Effects of a modified string tension

We will in this paper assume that a rope breaks up by the repeated production of $q\bar{q}$ pairs, as expected from an analogy with e^+e^- pair production in QED. As mentioned in the

---

[4]A stepwise production mechanism was suggested by Casher *et al.* in ref. [28].
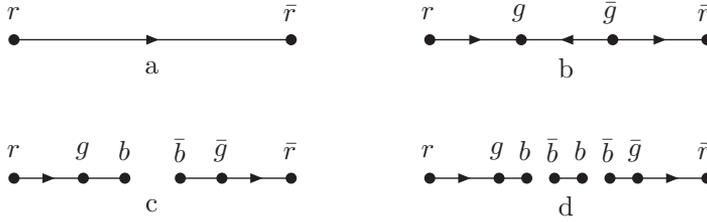
Figure 1.1: Illustration of popcorn production of a diquark pair. In frame a) no fluctuation has occurred, and a full string is spanned between a red–antired $q\bar{q}$ pair. In frame b) a green–antigreen pair has appeared on the string as a quantum fluctuation. If the red and green quarks form an antiblue triplet, this reverses the colour flow in this part of the string, and the net force acting on the green quark is zero. In frame c) the string breaks by the production of a $b\bar{b}$ pair, resulting in two string pieces with diquark ends. In frame d) another breakup in the blue triplet field results in an additional meson.

introduction, and discussed in detail in section 3, a rope formed by n elementary strings with random charges, can in general be fully extinguished by a number of $q\bar{q}$ pairs smaller than or equal to n. Here n breakups will be needed in case the colour charges combine to the highest possible multiplet. As can be understood from the tunneling mechanism, the "effective string tension", to be inserted in eqs. (1.1) and (1.2) for each step, is determined by the energy released in the step. This means the *reduction* in rope tension when the new $q\bar{q}$ pair is produced. We will therefore treat one step in the breakup of the rope, as the breakup of an individual string, with a modified effective string tension.

Effects on particle ratios

As discussed above, strangeness and baryon production is in the PYTHIA implementation determined by a set of phenomenological parameters, some of which represent the relative tunneling probabilities for different quarks and diquarks. Let the modification of the string tension be given by a simple scaling with an enhancement factor h, such that $\kappa \mapsto \tilde{\kappa} = h\kappa$. The result in eq. (1.1) or (1.2) then implies that the s/u ratio (called ρ), will be modified by the scaling relation

$$\rho \mapsto \tilde{\rho} = \rho^{1/h}. \tag{1.8}$$

Baryon production in the popcorn model is somewhat more complicated. Here we will assume that the production of the vacuum fluctuation giving the first new pair in figure 1.1b is insensitive to the string tension[5], while the production of the second pair shown in figure 1.1c, where the string breaks, is the result of a tunneling process. This means that we expect the same kind of scaling as for the s/u ratio in eq. (1.8) for the parameters which determine the extra suppression of diquarks with strange quark content relative to diquarks

---

[5]Also if the fluctuation probability does depend on the string tension, it turns out that this effect can be compensated by a change in the effective coherence radius for the rope formation, described in section 4.2.

without strange quarks, and the suppression of spin 1 diquarks relative to spin 0 diquarks. As these parameters go together with others that are not affected by string overlapping in defining the final diquark/quark ratio (called ξ), the resulting expression for the mapping becomes

$$\xi \mapsto \tilde{\xi} = \tilde{\alpha}\beta \left(\frac{\xi}{\alpha\beta} \right)^{1/h}. \tag{1.9}$$

The parameter α contains the parameters for all different types of diquark content, as mentioned above, and thus maps accordingly. The β-parameter is the popcorn fluctuation probability which in this work is assumed to be unaffected by changes in string tension. The complete mapping relation is derived in full in appendix 1.C.

The effect of a modified string tension on the s/u ratio and the net diquark/quark ratio is presented in figure 1.2. The range of h chosen in figure 1.2 is much larger than the range relevant for the pp collisions considered in this work (which generally have $h < 1.5$), but is chosen to show effects for large values of h relevant for heavy ion collisions[6].

The tunneling probability in eq. (1.2) will also give somewhat increased transverse momenta, but as the tunneling effect is a minor contribution to the $p_\perp$-distribution, this effect is rather small. A detailed description of the above modifications is presented in appendix 1.C.

Effects on multiplicity

One could assume, that the factor κ^2 in the production rate in eq. (1.1) should imply a change in the b-parameter in eqs. (1.3) and (1.5), and thus significantly modify hadron multiplicities. The quantity $\mathcal{P}$ in eq. (1.1) is the probability per unit volume and unit time. In a one-dimensional string, it should be interpreted as probability per unit length and unit time. Therefore the space-time distance between break-up points is expected to be proportional to $1/\kappa$. At the same time the "yo-yo" states representing mesons have extension and oscillation times proportional to $1/\kappa$. Thus the earlier production time is compensated by the smaller string length needed to form a meson. This is taken into account via the scaling factor κ^2 in eq. (1.4), with the effect that b is essentially unchanged. (For u and d quarks, with masses of the order 10 MeV, and a single string with tension $\kappa \approx 0.2 \, \text{GeV}^2$, the exponential factor in eq. (1.1) is very close to 1, and therefore not significantly changed by an increased string tension.) The second free parameter in the model (when flavours and spin are neglected) is the parameter N in eq. (1.3), which specifies the relative weights between hadron states with different multiplicities. As the density of hadronic states ought to be independent of the former colour configuration, we do not

---

[6]We note that the PYTHIA implementation currently limits all supression parameters from above at a value of one, corresponding to the situation where the supression is gone. The parameter $\tilde{\xi}$ can in principle take on larger values and will, with $\beta = 0.25$, saturate at $\tilde{\xi} = 1.75$.
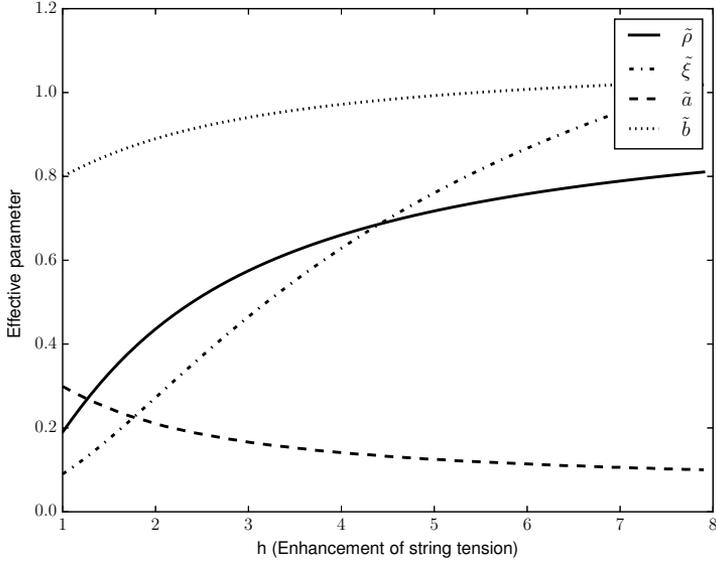
Figure 1.2: Effective parameters of the string model as a function of effective string tension. The parameters ρ and ξ control the strangeness content and baryonic content respectively, a and b are related to multiplicity. A modified string tension has a sizeable effect on ρ and ξ in particular. The range of h shown is much larger than relevant for pp collisions, which typically have $h < 1.5$. Larger values of h are, however, relevant for heavy ion collisions. The values of the parameters for $h = 1$ comes from a tune to LEP data.

expect any change in the N-parameter, although we admit that such modifications cannot be excluded when the mesons are produced in a stronger field.

Although the b-parameter would be unchanged if only light quarks were produced, it will increase slightly due to the enhanced production probability for strange quarks and diquarks, given by an increased exponential factor in eq. (1.1). This gives a shift

$$b \mapsto \tilde{b} = \frac{2 + \tilde{\rho}}{2 + \rho}\, b. \tag{1.10}$$

As the a-parameter is calculated from the normalization constraint for the splitting function in eq. (1.5), it will get a correspondingly moderate modification. The effect on the parameters a and b is also shown in figure 1.2, and we see that these parameters are less affected by an increased string tension than the parameters determining strangeness and baryon ratios. As it will be discussed in section 5.2, a typical value for the string tension enhancement factor h at LHC is around 1.2. Changes in a and b could therefore naively account for $\sim 5\%$ decrease in multiplicity in pp, as particle density is approximately proportional to $\sqrt{(1+a)/b}$ (see eq. (1.7)). Since some parameters must be retuned after implementation of the rope model, this effect will not appear in final state observables (note that the string hadronization parameters are still tuned to LEP data, see appendix 1.D for a detailed account of the tuning procedure.) The model should, however, not be further retuned when it is applied to nucleus collisions at LHC energies. Here h is expected to be so large, that a

decrease of the order $15 - 20\%$ in multiplicity, due to changes in $\tilde{a}$ and $\tilde{b}$, is a prediction of the model.

3 Ropes

In this section an ideal situation is considered, where separated colour charges within a limited area in transverse space act coherently to form a colour rope (assuming that the total system is a colour singlet.) As mentioned in the introduction, lattice calculations show that if the endpoint charges correspond to a specific SU(3) multiplet, the tension (or energy density) in the rope is given by the second Casimir operator [38]. This result is valid for an isolated rope, modifications must be expected in a situation where the rope is surrounded by other ropes or strings. Here we discuss the formation of a rope, its tension, and its eventual decay.

3.1 Rope formation

We study a situation, where a rope is formed by a group of ordinary triplet–antitriplet strings, where the net colour charge is obtained from the addition of m colour triplets and n antitriplets with random colours. As pointed out first in ref. [3], the result corresponds to a kind of random walk in colour space. A detailed discussion of this process can be found *e.g.* in ref. [53] or in appendix 1.B.1. Here we only present the main features essential for the later discussion.

While in SU(2) a multiplet is specified by the quantum number j, or its multiplicity $(2j+1)$, an SU(3) multiplet can be specified by two quantum numbers p and q. A specific state then corresponds to p coherent triplets (*e.g.* all red) and q coherent antitriplets (*e.g.* all antigreen). In addition the triplet and the antitriplet must be in an octet state (as is the case for red–antigreen), and not a singlet. The multiplicity, N, of the multiplet $\{p, q\}$ is then given by:

$$N = \frac{1}{2}(p + 1)(q + 1)(p + q + 2). \tag{1.11}$$

The result of adding a set of triplets and antitriplets can be calculated in an iterative way. Starting from a multiplet $\{p, q\}$ adding one more triplet, with random colour, one obtains the multiplets

$$\{p + 1, q\}, \quad \{p - 1, q + 1\}, \text{ and } \{p, q - 1\}, \tag{1.12}$$

with weights proportional to the corresponding multiplicities given by eq. (1.11). From symmetry, the addition of an antitriplet gives the multiplets $\{p, q+1\}$, $\{p+1, q-1\}$, and
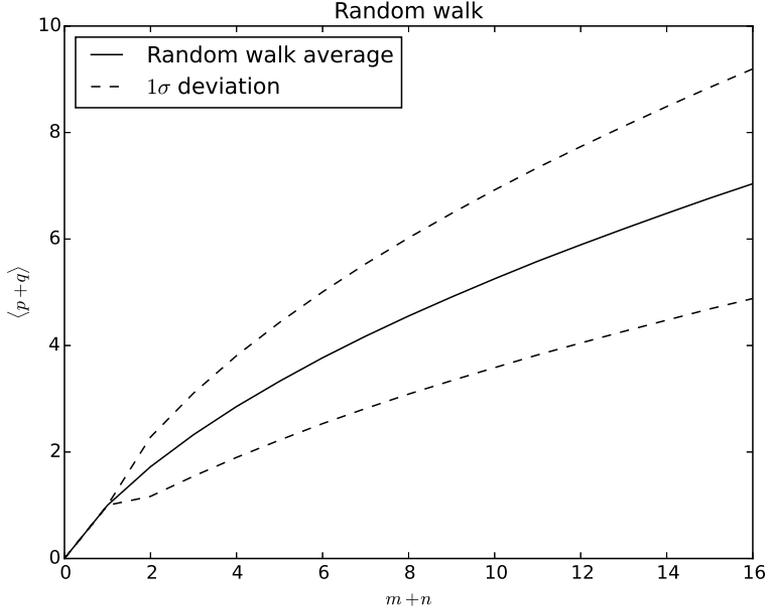
Figure 1.3: Relation between $\langle p+q \rangle$ and $m+n$ after a random walk in p, q-space. The shaded area corresponds to the standard deviation around the average $\langle p+q \rangle$.

$\{p-1, q\}$. Multiplets with negative values for p or q are not allowed. In appendix 1.B.1 the result for adding random colour octets (corresponding to gluons) is also described.

The average walk can be easily calculated numerically, and in figure 1.3 we show $\langle p+q \rangle$ obtained from randomly adding triplets and antitriplets, with a fixed number, $m+n$, of charges. (The individual numbers m and n are then given by a binomial distribution. The same result was also presented in ref. [3].) The width of the distribution is indicated by the band showing $1\,\sigma$ variations.

3.2 Rope tension

As mentioned in the introduction, lattice calculations show that the tension in an isolated static rope is proportional to the quadratic Casimir operator C_2 [38]. The Casimir operator is only defined up to a normalization constant, but for our purpose we only need the value of C_2 normalized to a triplet (antitriplet) $\{1, 0\}$ ($\{0, 1\}$), corresponding to the tension in a single string. This is given by

$$C_2(\{p, q\})/C_2(\{1, 0\}) = \frac{1}{4}\left(p^2 + pq + q^2 + 3p + 3q\right),\qquad (1.13)$$

which thus can be regarded as the relative strength of the "rope tension".

It is, however, possible that the energy is increased if the transverse area is constrained by neighbouring ropes and strings. This effect is very hard to estimate, and contributes to the uncertainties in the predictions from string interactions. To illustrate this problem we first look at the analogous situation in a normal superconductor. Here a longitudinal magnetic flux is confined by currents in the surrounding condensate. In an extreme type I superconductor the surface energy is small, and a tube with two flux quanta will have doubled cross section and doubled energy. If, however, the flux tube would be constrained within the same transverse area, the magnetic field energy will be multiplied by 4, but the energy to annihilate the condensate within the tube (originally equal to the field energy) will be unchanged. The net result is a change by a factor 2.5. In a type II superconductor the magnetic flux and the energy density are more concentrated close to the center of a flux tube or vortex line, and there is a repulsive (attractive) interaction between parallel (antiparallel) vortices, with a logarithmic dependence on the separation.

The simplest model for a colour flux tube is the bag model [54, 55], which is analogous to a type I superconductor. The tension in an unconstrained flux tube is here proportional to $\sqrt{C_2}$ [55], in contradiction to the lattice result. However, for a flux tube constrained to the width of an elementary string, the energy is indeed proportional to the lattice result C_2 [56].

Lattice calculations by Cardoso *et al.* [57] show that the energy in the longitudinal colour-electric field is dominating over the transverse colour-magnetic field, with other components small, and the result shows similarities with a type II superconductor. However, recent calculations by Cea *et al.* [58] indicate, that the best analogy with a dual superconductor is close to the transition between type I and type II, but with the Ginzburg–Landau parameter within the type I region.

We conclude that there are considerable uncertainties in the estimation of the tension in a rope. Fortunately it turns out that, for the results presented here, the effects of a modified effective rope tension can be compensated by a modified value for the effective rope width r_0. We will therefore in the following assume that the tension is proportional to the Casimir operator of the colour multiplet, in accordance with the lattice calculations for an isolated rope.

3.3   Fragmentation of a rope

Effective string tension and particle ratios

As in most studies of rope fragmentation, we will assume that the colour rope will break up in a stepwise manner, by the production of quark–antiquark pairs. This is the result for an interaction Lagrangian proportional to $\bar{\psi}\gamma_\mu\psi A_\mu$. In the region between the newly

produced quark and antiquark, the field corresponding to the $\{p, q\}$ multiplet can be reduced to either a $\{p-1, q\}$ or a $\{p, q-1\}$ multiplet. In the first case the antiquark is pulled towards the $\{p, q\}$ charge (and the quark towards the $\{q, p\}$ charge in the other end of the rope), and in the second case it is pulled in the opposite direction. As discussed in section 2.4, an essential point is that the energy released in the breakup is what enters in the tunneling process discussed in section 2.1, and thus determines the production probabilities in eqs. (1.1) and (1.2). This is given by the *difference* between the Casimir operators for the multiplets $\{p, q\}$ and $\{p-1, q\}$ or $\{p, q-1\}$ respectively. This difference thus represents an *effective string tension*, or $\tilde{\kappa}$, introduced in section 2.4.

For a breakup via the transition $\{p, q\} \to \{p-1, q\}$ we get from eq. (1.13) the effective string tension

$$\tilde{\kappa} = \frac{2p + q + 2}{4}\kappa. \tag{1.14}$$

We note that for large charges p this result grows $\sim (p/2)\kappa$, (*i.e.* more slowly than $\propto p\kappa$). As an example we have for a rope consisting of two parallel strings in a $\{2,0\}$-state the Casimir operator $C_2(\{2, 0\}) = 5/2 \times C_2(\{1, 0\})$. In the first breakup the effective string tension will then be $\tilde{\kappa} = (5/2 - 1)\kappa = (3/2)\kappa$, while for the second break-up we will have the normal tension $\tilde{\kappa} = \kappa$. A more complicated example is presented in appendix 1.B.2.

We want to emphasize that this result is significantly smaller than what is assumed in most studies of rope effects. Although the change in rope tension is used *e.g.* in ref. [7], it is quite common to use Schwinger's result in eq. (1.1), with a constant field $\mathcal{E}$ proportional to the charge Q. This would correspond to a situation where the field is confined within a tube with constant cross section A, and that the contribution from the bag pressure or confining currents is neglected [7]. The field energy per unit length is then given by $\frac{1}{2}A\mathcal{E}^2 = \frac{1}{2}Q\mathcal{E}$. We here used that the total flux, $A\mathcal{E}$, is determined by the charge Q spanning the rope. When a pair with elementary charge $g/2$ is produced, the field is reduced to $\mathcal{E} - \epsilon$, where $g/2 = A\epsilon$ is the flux from the elementary charge $g/2$. (The factor 1/2 is due to the conventional definition of g.) Neglecting the contribution to the tension from the bag pressure, and assuming that A is not modified, we obtain the "effective string tension" from the difference in field energy:

$$\tilde{\kappa} = \frac{1}{2}A\{\mathcal{E}^2 - (\mathcal{E} - \epsilon)^2\} = A\epsilon(\mathcal{E} - \epsilon/2) = \frac{1}{2}g(\mathcal{E} - \epsilon/2) \tag{1.15}$$

For a classical macroscopic field $\mathcal{E}$, the term $\epsilon/2$ can be neglected in the parenthesis $(\mathcal{E} - \epsilon/2)$, and the expression in eq. (1.15) therefore looks like eq. (1.1). A problem shows up, however, if this formula is used to relate the effective string tension to the tension in an elementary string. Here the term $-\epsilon/2$ can not be neglected, and it corresponds to the correction to the string tension due to the field produced by the new pair, as pointed out in

---

[7]In some cases the transverse area is taken as an undetermined parameter, *e.g.* in refs. [4, 7].

ref. [31]. Taking this into account we get for an elementary string, with $\mathcal{E} = \epsilon$, the tension $\kappa = g\epsilon/4$, and the result

$$\tilde{\kappa} = (2p - 1)\kappa. \tag{1.16}$$

We note that for strong ropes, *i.e.* large values of p, this result is a factor 4 larger than the result in eq. (1.14). Here a factor 2 comes from the correction term in the elementary string, and another factor 2 is due to the relatively slow increase of the rope tension in eq. (1.13) for large p.

Particle multiplicity

For a rope stretched by $(m + n)$ random colour charges, the rope can break up totally by only $(p + q)$ $q\bar{q}$ pairs. The random walk in colour space here gives $p + q \sim \sqrt{m + n}$ (see figure 1.3), and this effect therefore contributes to a reduction in the density of produced particles. In many references it is assumed that this is the dominant effect determining the multiplicity. Lacking a physical picture, it is often assumed that the hadrons are produced with the same separation in rapidity, see *e.g.* refs. [3, 5, 8].

Andersson and Henning [7] argue, however, that the early breakup can give a large energy to the leading particle(s), leaving less energy to produce softer particles. Amelin *et al.* [10] also argue that, as the breakups according to eq. (1.6) occur earlier for a stronger tension, the multiplicity should be lower. The arguments in refs. [7, 10] do, however not take into account that not only the space-time distance between breakup points becomes smaller for a higher effective string tension; also the size of the string pieces making up a hadron becomes smaller with the same scale factor. Therefore we argued in section 2.4 that the early breakup only gives a minor correction to the multiplicity, owing to the increased production of strange quarks (also admitting that unknown effects could influence the possibility for a $q\bar{q}$ pair to fit into a final state hadron in case of a stronger effective string tension). Thus in our approach, the dominant effect on the total multiplicity is due to the random walk in colour space discussed above.

4   Implementation of ropes in the DIPSY Generator

The rope model outlined above has been implemented in the DIPSY [15, 59, 60, 16] event generator. DIPSY is based on Mueller's dipole cascade model [39, 40, 41], which is a formulation of leading-log BFKL evolution [61, 62] in transverse coordinate space, making it very well suited for a study of coherence effects based on spatial overlap of strings.

The DIPSY model introduces many sub-leading effects to Mueller's dipole model (see appendix 1.A for an introduction to the DIPSY model). Important to emphasize here is the
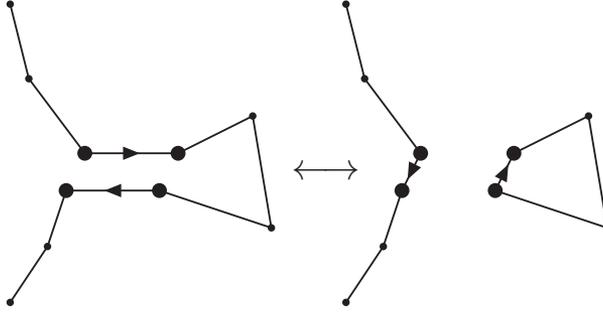
Figure 1.4: Sketch of how the initial state swing could reconnect colours between two dipoles in impact parameter space.

initial state "swing", which is a finite N_c effect. Two dipoles with the same colour form a colour quadrupole, where the colour field is better approximated by dipoles formed by the closest charge–anticharge pairs (*c.f.* figure 1.4). As smaller dipoles have smaller cross sections, this effect contributes to the saturation at small x.

By introducing saturation in the cascade using the colour swing, saturation directly becomes a finite-N_c effect, as the effect obviously vanishes in the large-N_c approximation. In section 4.1 we will argue how adding a similar reconnection effect in the final-state cascade, is a convenient way to introduce the singlet from the $3 \otimes \bar{3} = 8 \oplus 1$ decomposition.

The gluons produced in the initial state in DIPSY are in the end ordered in both positive and negative light-cone momenta, and are allowed to continue radiating final-state bremsstrahlung according to the time-like dipole radiation model in momentum space [63, 64] implemented in the ARIADNE program[65]. Before forming the ropes, which will be sent to PYTHIA8 [66] for hadronization as described in section 4.2, the strings may also reconnect via a "final state swing" between dipoles with identical colours. This is introduced to account for the singlet from the $3 \otimes \bar{3} = 8 \oplus 1$ decomposition of interacting string colours, and described in more details in section 4.1.

4.1 The Final-state Swing

The swing mechanism was inspired by the colour reconnection mechanism proposed in [67] for the time-like dipole shower in ARIADNE [65]. The need for colour reconnections in the final state had already been noted in the context of multiple interactions [68]. Several other investigations were performed in the eighties and nineties looking at recoupling effects both in e^+e^-, DIS and hadronic collisions, see *e.g.* [69, 70, 71, 72].

These reconnection models were based on the principle of minimizing "effective string lengths". This was inspired by the string fragmentation, where the string action is given by the area law for the Wilson loop [49]. For a simple $q\bar{q}$-string, which does not break,
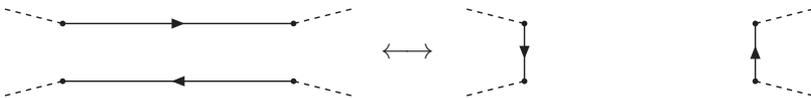
Figure 1.5: Sketch of how the final state-swing could reconnect colours between two dipoles in momentum space.

the action for one period is proportional to the total invariant squared mass s. For a string which breaks up into hadrons, the string area is instead proportional to $\ln(s/m_0^2)$, where the scale parameter m_0 is a typical hadronic scale, ~ 1 GeV. This area also determines the average hadron multiplicity. For a more complicated string configuration it is also possible to generalize this area to the so-called *lambda*-measure [73, 74]. The lambda-measure is infrared stable, but in cases without soft or collinear gluons, it can be approximated by

$$\lambda_s \propto \sum_{i=1}^{n-1} \ln \frac{(p_i + p_{i+1})^2}{m_0^2}. \tag{1.17}$$

Hence, when looking at the re-coupling of individual dipoles in a string it seems natural to try to minimise the sum of the logarithms of the dipole masses, or equivalently, the product of dipole masses.

In the original implementation in ARIADNE, only reconnections which decreased the total λ_s were allowed, but now we have reimplemented it in a way very similar to the swing in DIPSY. Between every final-state dipole radiation there is a possibility to recouple two dipoles, $(12)(34) \to (14)(32)$, if they are in the same colour state (using the same colour indices as in DIPSY). Again we treat emission and swing as competing processes, and while the emission of a gluon is simply given by the dipole formula

$$\frac{dP_g}{d\rho} \approx dy \frac{C_F \alpha_S}{2\pi} \tag{1.18}$$

(for a $q\bar{q}-$ dipole. For a gluon dipole $C_F \mapsto C_A/2$). Here $\rho = \ln(p_\perp^2)$ is the evolution parameter. We define the relative probability for the swing as

$$\frac{dP_s}{d\rho} = \lambda \frac{(p_1 + p_2)^2 (p_3 + p_4)^2}{(p_1 + p_4)^2 (p_3 + p_2)^2}, \tag{1.19}$$

with a free parameter λ governing the relative strength of the swing.

Dipoles spanning large distances in impact parameter space are heavily suppressed in DIPSY due to the confinement effects imposed by the introduction of a small gluon mass, m_g (see appendix 1.A). Even though the final-state swing in eq. (1.19) is formulated in momentum space and does not take into account any impact parameter dependence we still need to preserve these confinement effects. This is done by only considering dipoles which are closer in impact parameter space than a distance $\propto 1/m_g$ as candidates for a swing.
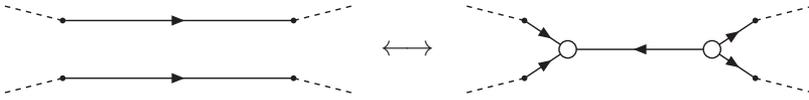
Figure 1.6: Sketch of how a antitriplet swing could reconnect colours between two dipoles by introducing two string junctions (denoted by circles).

It is interesting to note that if we have two completely anti-parallel dipoles, the probability of them having the same colour index is simply $1/N_c^2$, and if this is so, they will always reconnect, effectively breaking the "rope". This corresponds to the singlet term which arises when combining the triplet and anti-triplet string, $3 \otimes \bar{3} = 8 \oplus 1$ (see eq. (1.25)). This means that this effect in principle has already been taken care of before the formation of the rope, and when we later perform the random walk in colour space for overlapping strings, we need to constrain it to take this into account.

One could also imagine introducing another swing mechanism for the case of parallel strings, which would then imply that two (parallel) dipoles could swing into a single string according to the sketch in figure 1.6. This would involve the formation of two so-called *junctions* where three colour lines join. Although there is a mechanism for hadronizing junction strings in PYTHIA8, it has some technical limitations[8]. Also, the treatment of radiation from junction topologies in ARIADNE requires additional work, and we will thus defer the treatment of this new kind of swing to a future paper. Instead we will treat the corresponding multiplet configurations in the rope model below.

4.2 Estimates of overlap region

As discussed in more detail in appendix 1.A, the DIPSY Monte Carlo describes two colliding parton cascades, producing colour-connected partons located in transverse coordinate space and rapidity. This is followed by final-state radiation in momentum space from ARIADNE together with colour reconnection by the final-state swing. The location in the transverse plane is the basis for the interaction between the strings and the formation of ropes. As described in section 2.4, we expect that the dominant effect of rope formation is an enhanced production of strangeness and baryons, and in this paper we concentrate on these effects.

In section 3 we discussed an ideal situation with strings or colour flux tubes, which overlap completely in transverse space, and interfere constructively or destructively to form a coherent rope. A typical event, ready for hadronization, is shown in impact parameter space and rapidity in figure 1.7. The tubes in the figure represents colour connections between partons, and it is easy to see that real events are far from similar to the ideal situation, and

---

[8]While preparing this manuscript a slightly improved version of the junction fragmentation was implemented in PYTHIA together with a colour reconnection mechanism producing junctions in the way depicted in figure 1.6 [27].
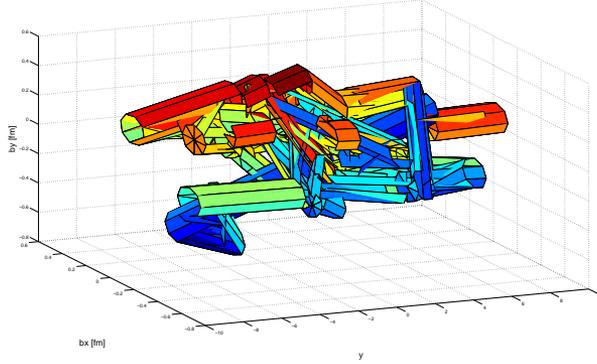
Figure 1.7: Illustration of strings from a *pp* event at $\sqrt{s} = 7$ TeV in $(\vec{b}_\perp, Y)$-space before hadronization. Notice that the string radius is set at 0.1 fm – an order of magnitude less than in the calculation – in order to improve readability of the figure.

we therefore need a way to estimate the amount of interaction. We naturally expect that strings close in transverse space should interfere more strongly than strings further away, with a typical interaction range of the order of the confinement scale. Our main assumption is therefore, that the degree of coherence between the strings is determined by the overlap between the corresponding flux tubes.

Since the DIPSY-generated events provide access to space-time information of strings, it is natural to alter the effect depending on the amount of overlap. Space-time information is usually not available in generators for *pp* collisions. It is, however, normally accesable in Molecular Dynamics Monte Carlo generators aimed for heavy ion collisions, where a similar approach (not including all fluctuations), has been studied in ref. [19]. We expect the coherence range (the radius of the flux tubes) to be of the order of the confinement scale, and put it to 1 fm. One could treat it as a completely free parameter, and tune it to data together with other free parameters, in order to give the most accurate description of data. Since neither the method of calculation of overlap between strings, nor the connection between this overlap and *m* and *n* (the number of uncorrelated colour and anticolour charges in one end of the rope) is obvious from first principles, we will present two different approaches for calculating the overlap. The first method is very crude, and approximates all strings as straight flux tubes ("pipes") parallel to the rapidity axis. In this pipe-based approach, a string will be given values for *m* and *n* that are averages over the whole string, in fact an average over the full area in transverse space covered by the string. The string is subsequently hadronized with a single average value for $\tilde{\kappa}$, determined from *m* and *n* by the random walk procedure.

The second method is more detailed and takes into account more fluctuations along the string. In this dipole-based approach, a string is viewed as a chain of dipoles, connected by

gluons, either with quarks at the endpoints, or as closed gluonic loops. Overlaps are then calculated and a random walk in colour space is performed for each dipole, at a specific rapidity value, in order to change the value for $\tilde{\kappa}$ at each breakup in the hadronization.

In both treatments the random walk is constrained to take into account that steps corresponding to $\{1,0\} \otimes \{0,1\} \mapsto \{0,0\}$ have already been treated in the final-state swing mechanism. Nevertheless it is clear that for $m + n$ overlapping strings or dipoles, may end up in multiplets $\{p, q\}$, where $p < m$ and/or $q < n$. This poses a problem, since for technical reasons, each of the $n + m$ strings are hadronized separately, so we cannot break them with only $p + q$ break-ups. Since the net effect is to reduce the multiplicity by a factor $\propto (p + q)/(m + n)$, we instead emulate this by simply randomly discarding strings in the pipe-based treatment with a probability $1 - (p + q)/(m + n)$. In the dipole-based treatment the approach is somewhat more sophisticated and we instead discard individual dipoles in a procedure inspired by the suggested *junction swing* in figure 1.6.

The details of the implementation of the two treatments are fairly technical and a full description is therefore deferred to appendices 1.C.1 and 1.C.2.

The aim of introducing two different approaches for calculating overlap, is to demonstrate that even the very crude pipe-based approach catches the gist of the model and improves the description of strangeness and baryon production, as described in section 5. Since further sophistication in the dipole-based approach can improve description of strange and baryonic content even further, we argue that a direct mapping from overlap in tranverse space to m and n is indeed sensible. Further sophistication of this calculation of overlap is left for future publications.

4.3 Exclusive observables with DIPSY

The DIPSY Monte Carlo is implemented in the event generator framework called THEPEG [75]. Also the ARIADNE program for final-state parton showers has been implemented in this framework and there we have now added the final-state swing mechanism described in section 4.1. In THEPEG we have also written an interface to the hadronization routines of the PYTHIA8 event generator, and it is here we have implemented our rope hadronization models described in the previous section. The whole code is available from the authors upon request.[9]

The full code can generate full, exclusive final states for *pp*, *pA* and *AA*. The goal driving event generators such as DIPSY is to be able to describe all collider physics with the same models, using the same parameters. As event generators in general have a quite large number of parameters, which parameterize the uncertainties in the models implemented, these

---

[9]See also `http://home.thep.lu.se/DIPSY` for installation instructions.

parameters need to be estimated from data in a "tuning" process. It is important to state that tuning does not mean fitting of individual spectra to data. It rather means that one set of parameter values are estimated such that the same models can describe anything from e^+e^- over pp to pA and AA collisions.

We have already discussed some of the parameters on the Lund string fragmentation level, but there are many others, such as the non-perturbative cutoff in the parton cascade and scale factors used in the running of α_S (to emulate untreated higher orders). The tuning of these parameters is quite a complicated task, and for each event generator there are typically several different tunes available (see *e.g.* `mcplots.cern.ch` [76] for comparisons between different tunes of different programs).

The most common strategy is to first tune parameters associated with the final-state showers and hadronization to data from e^+e^- colliders. Assuming jet universality these are then fixed when tuning further parameters related to initial-state showers and multiple parton interactions to data from hadron colliders.

As we have tried to argue in this paper, the concept of jet universality is not quite straightforward, and the hadronization may very well behave differently in hadronic and e^+e^- collisions. To see the effects of our new model it is therefore necessary to take some care and make sure that the description of the flavour-dependent observables we wish to study is not dominated by a general change of multiplicity distributions for all particles, as such global effects would normally be removed in a tuning procedure. Therefore we have made a careful tuning both for the cases with rope effects and without, as detailed in appendix 1.D.

Since the DIPSY event generator does not yet include a model for diffractive events, care also must be taken to only compare to observables that are not sensitive to diffraction. For that reason, we will primarily look at particle ratios. This point is also expanded upon in appendix 1.D.

5   Results

In this section we will present some results from applying the introduced rope model. We will concentrate on flavour observables in minimum bias events in hadronic collisions in the energy range where we believe the small-x approximation in the DIPSY model is valid, $\sqrt{s} \gtrsim 100$ GeV. After presenting comparisons to experimental data in section 5.1, we will look at the model's sensitivity to parameters and its behaviour at higher energies in section 5.2. In section 5.3 we discuss the flow-like effects shown in the results.
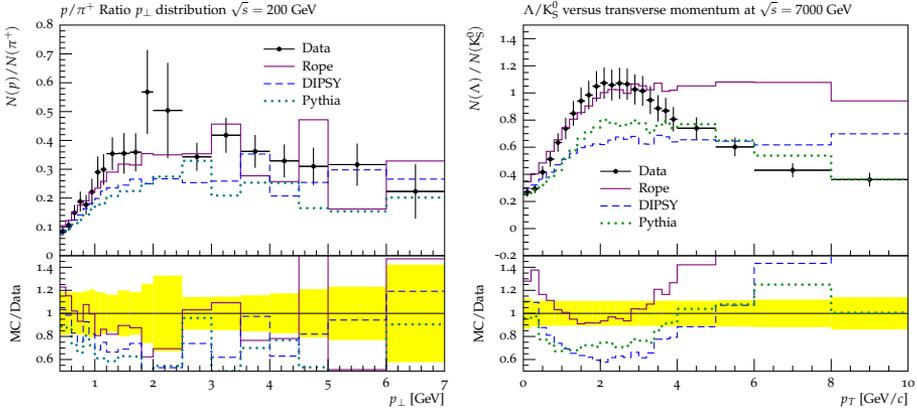
Figure 1.8: The proton to pion ratio in bins of $p_\perp$ as measured by STAR at $\sqrt{s} = 200$ GeV (left) and Λ/K_s^0 at 7000 GeV as measured by CMS (right). Both results are compared to DIPSY with and without rope, as well as with PYTHIA8.

5.1 Comparison to data

Results from DIPSY including the rope model in the dipole scheme (labelled 'Rope') are here compared to CMS data [36] at 900 and 7000 GeV as well as STAR data [77] at 200 GeV. We also show DIPSY with no rope effects on, labelled 'DIPSY', and finally a PYTHIA8 reference[10] labelled 'Pythia'. Comparison to data for more energies, and other kinematic variables *etc.* can be found on the project home page at `http://home.thep.lu.se/DIPSY/`. The parameters for rope hadronization used are $r_0 = 1$ fm, $\beta = 0.25$ and $m_0 = 0.135$ GeV. These choices will be further discussed in section 5.2.

In figure 1.8 (left) we see the proton/pion ratio in bins of $p_\perp$, as measured by STAR, compared to simulations. We clearly see that DIPSY with no added effects fails to describe this ratio, in the same way as PYTHIA8 does. The proton/pion ratio is a good measure of the relative amount of baryons with no strangeness, governed by the ξ-parameter, and we see that DIPSY with added rope effects indeed describes data better, both in terms of relative proton content and $p_\perp$.

In figure 1.8 (right) the Λ/K_s^0 ratio at $\sqrt{s} = 7$ TeV is shown in bins of $p_\perp$ as measured by CMS. As both the meson and the baryon has strangeness, this should also be a good measure of the influence of the ξ-parameter. We again see that including rope effects improves the description, especially in the low-$p_\perp$ end, where most of the multiplicity is concentrated. The high $p_\perp$-tail is poorly described, and we will discuss this further in section 5.3.

Figure 1.9 shows the Λ/K_s^0 ratio at $\sqrt{s} = 900$ GeV (left) and 7 TeV (right) in bins of rapidity as measured by CMS. We see here that the relatively weak dependence on energy is well described by the rope model, with the same values for r_0, β and m_0.

[10]Version 8.180, tune 4C.
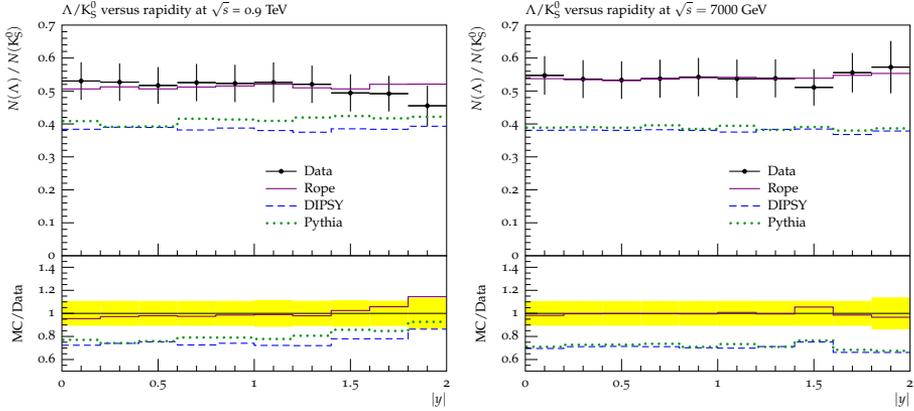
Figure 1.9: The Λ/K_s^0 ratio at 900 GeV (left) and 7000 GeV (right) as measured by CMS in bins of rapidity. The figure shows that the rope model captures the (albeit weak) energy dependence of this ratio, while DIPSY without ropes, as well as PYTHIA8, shows no energy dependence.

The Ξ^-/Λ ratio is an observable, that is particularly sensitive to the ρ parameter. Figure 1.10 shows this ratio in bins of rapidity at 900 GeV and 7000 GeV, and we see that the rope model also reproduces the behaviour of these data fairly well.

Although the energy dependence shown in figures 1.9 and 1.10 is fairly weak, the fact that it is well described by the rope model is a very important point. At higher energies more strings are confined within a small space, and with the amount of overlap as a measure of the size of the rope effect, one could expect a larger increase with energy. To further illustrate this point, and to serve as qualitative predictions for the integrated particle ratios, we show in figure 1.11 the total K/π, Λ/K_s^0 and Ξ^-/Λ ratios as a function of $\sqrt{s}$. We note here that the combined effect of strangeness and baryon suppression is not factorizing in a simple way. As discussed in appendix 1.C, the effects of an increased string tension is quite involved, especially for baryons. The fact that the relative abundances presented in figures 1.8-1.10 are well described, also for different energies, gives us confidence that our model has some physical relevance.

5.2 Model behaviour

The model introduces three new parameters. The string radius r_0, the popcorn-parameter β, and the parameter m_0 which is specific to the dipole approach. The parameters have not been tuned to data in the usual sense, but set to reasonable physical estimates. We believe that the model in its current state is not mature enough to warrant a tuning, but one should nevertheless get an intuition for the uncertainties associated with the choice of parameters. We will here motivate our choices, and show the sensitivity of the model to changes in the parameter values, and how the results vary with $\sqrt{s}$.
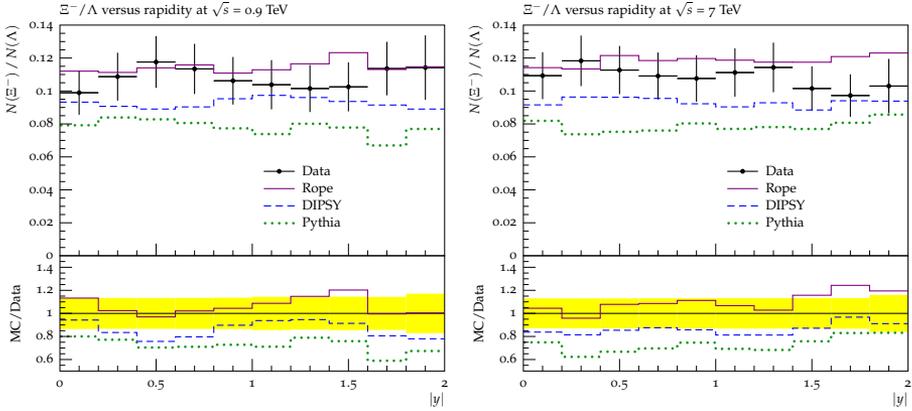
Figure 1.10: The ratio Ξ^-/Λ at 900 GeV (left) and 7000 GeV (right) as measured by CMS in bins of rapidity.

To gauge the sensitivity we look at two quantities: the average string tension and the number of junctions. Focusing on particle ratios, we normalize to the λ-measure, which is a measure for the hadronic multiplicity (see eq. (1.17)). Thus we study the event averaged string tension, defined by the relation

$$\langle \tilde{\kappa}/\kappa \rangle \equiv \frac{\sum_i \lambda_i \tilde{\kappa}_i/\kappa}{\sum_i \lambda_i} \tag{1.20}$$

(where i counts all dipoles and $\lambda_i = \ln(m_i^2/m_0^2)$), and the number of junctions per unit λ, $\langle n_j/\sum_i \lambda_i \rangle$. These quantities can act as indicators for the amount of string overlap, which grows with increasing energy, but is also sensitive to the tunable parameters r_0 and m_0.

Figure 1.12 (left) shows the average string tension as functions of $\sqrt{s}$, for $r_0 = 1$ fm and $m_0 = 0.135$ GeV. The dashed lines in figure 1.12 indicate the event-by-event fluctuations, showing one standard deviation. It is clearly visible that the enhancement effect rises logarithmically with $\sqrt{s}$. This is expected, as the number of gluons in the BFKL-based DIPSY cascade has the same energy dependence.

The average value of the string tension will thus increase with energy, and from figure 1.2 it is clear that this gives a larger amount of strange and baryonic activity as $\sqrt{s}$ goes up, as well as having a moderate effect on total multiplicity due to the effect on the parameters a and b in the splitting function in eq. (1.5). However, the multiplicity in pp collisions are heavily influenced by the parameters controlling the initial-state evolution in DIPSY, and as described in appendix 1.D, we tune these (while keeping the hadronization parameters tuned to LEP data fixed) to obtain the same multiplicity with and without rope effects. In this way the only effects from our rope model are the relative amounts of baryons and hadrons with a strange content; both are expected to increase.

The increase in the number of junctions per string length is also shown in figure 1.12 (right).
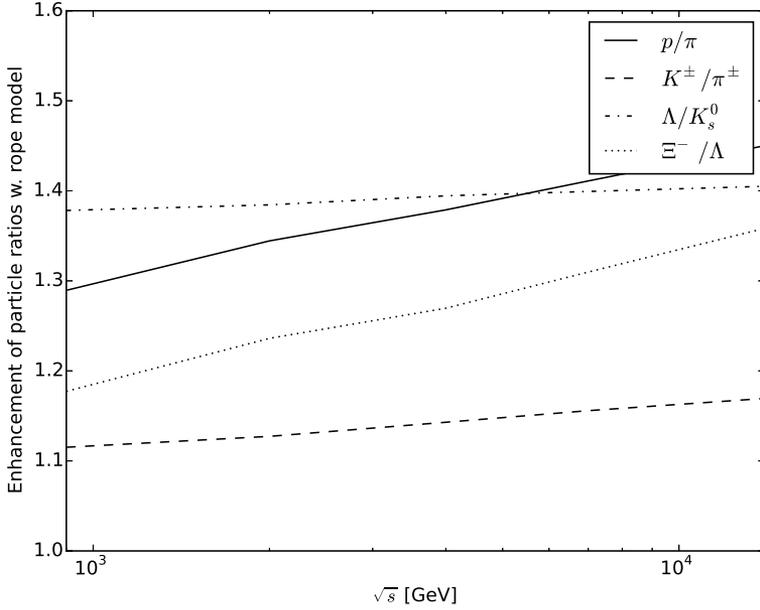
Figure 1.11: Enhancement of particle ratios of function of $\sqrt{s}$. Integrated ratios of $p^{\pm}$ and $K^{\pm}$ to $\pi^{\pm}$, $\Lambda\bar{\Lambda}$ to K_s^0 and Ξ^- to $\Lambda\bar{\Lambda}$ with the rope model (dipole approach) applied, normalized to the same ratio with ordinary string hadronization. All particles with $p_{\perp} > 200$ MeV are included.

The amount of baryons emerging from the produced junctions is, as explained in appendix 1.C.2, controlled by the popcorn strength parameter β (see eq. (1.33)). We note that while increasing β results in a stronger increase of baryons produced through diquark break-ups in the strings, it also decreases the probability that baryons are produced in junction structures, as explained in section 1.C.2. As our results thus have very little sensitivity to variations in β, it is fixed to 0.25 throughout the article, and we do not expect large theoretical uncertainty to be ascribed to this parameter should the model be thoroughly tuned.

The amount of overlap in an event will also increase by increasing r_0. In figure 1.13 (left) the average enhancement is shown as a function of r_0 at fixed energy $\sqrt{s} = 900$ GeV and $m_0 = 0.135$ GeV. It is interesting to note that the overlap saturates at $r_0 \sim 1.5$ fm, as the size of the strings becomes larger than the proton. This behaviour is almost independent of collision energy, as the cross section only increases logarithmically with energy, although the value at saturation is higher for higher energies. The same type of saturation effect is found in the number of junctions, shown in figure 1.13 (right). Throughout the article, r_0 is set to 1 fm, which is taken as a typical hadronic length scale. We expect variations in the parameter r_0 to be the largest source of theoretical uncertainty should the model be tuned. In the region around $r_0 \sim 1$ fm, small changes in r_0 can give up to 5 % change in average effective string tension, which will of course be reflected in the results.
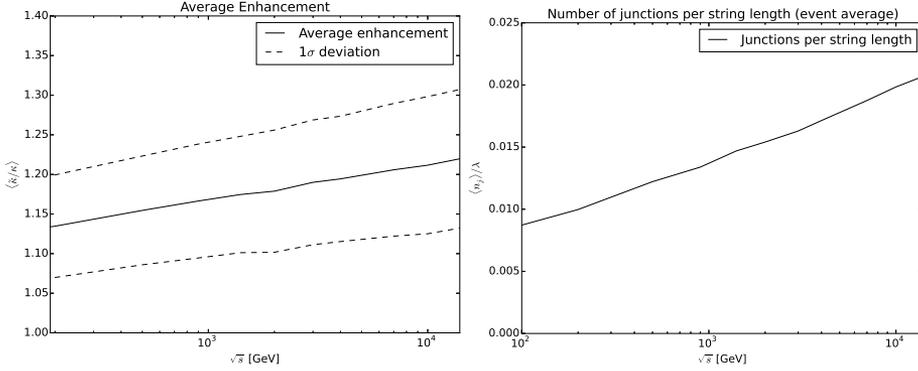
Figure 1.12: (left) Average enhancement $\langle h \rangle = \langle \tilde{\kappa}/\kappa \rangle$ as a function of $\sqrt{s}$ in pp collisions. The band indicates one standard deviation. (right) Number of junctions per string length as a function of $\sqrt{s}$.

Finally the parameter m_0 serves as a characteristic scale for the dipoles. This has both the effect of a cut-off in the rapidity span (gluons in a dipole at rest would otherwise give infinite rapidity), and as a propagation time ($1/m_0$), to let the gluons propagate a finite distance (determined by their $p_\perp$) before the overlap is calculated and hadronization takes place (see appendix 1.C.2 for further explanation). The average enhancement factor and the density of junctions as function of m_0, is shown in figure 1.14.

The model is not as sensitive to m_0 as to r_0, and we expect that the uncertainty after a tuning, which can be ascribed to m_0, will be only on the order of a few percent. In this article we have chosen to set the parameter m_0 to the pion mass, $m_0 = 0.135$ GeV, as no hadron can have a larger rapidity than the pion. The pion formation time will then be defining for the dipole propagation time. We believe that a tuning of this parameter will not give large deviations from the pion mass, as we have also tried hadronic scale $1/r_0 \approx 0.2$ GeV. This is numerically close to the pion mass, but does not give an equally good energy dependence.

5.3 Particle ratios and flow-like effects

As seen, rope effects introduce a $\sqrt{s}$-dependence of flavour ratios and baryon ratios in the fragmentation, and we note in particular that the rise at small $p_\perp$ is well described. This effect is often seen as an indication for the formation of a quark–gluon plasma phase, also in pp-collisions [78, 79], as the pressure in the hot plasma would push large mass particles to higher $p_\perp$ (compared to low mass ones). In our rope model it is mainly the result of the colour reconnections induced by the final state swing mechanism, which originate from the formation of lower colour multiplets. Ortiz *et al.* have previously noted that the colour reconnection model implemented in PYTHIA, gives rise to a flow-like effect in pp collisions at LHC [80].
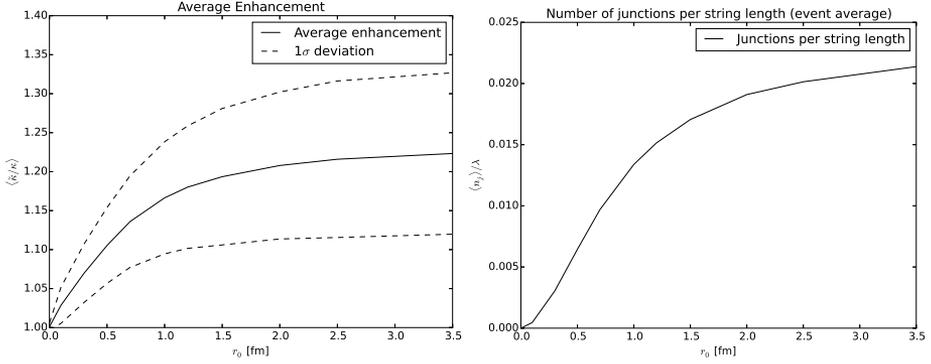
Figure 1.13: Average enhancement (left) $\langle h \rangle = \langle \tilde{\kappa}/\kappa \rangle$ as a function of r_0 at $\sqrt{s} = 900$ GeV in pp collisions. The band indicates one standard deviation. Number of junctions (right) per string length as a function of r_0.

It is also seen that, although the rise at small $p_\perp$ is well described, the experimentally observed fall at higher $p_\perp$, in *e.g.* Λ/K_s^0 shown in figure 1.8, is not reproduced by the present implementation of rope effects. In studies of plasma effects the hadrons with larger $p_\perp$ are expected to originate from high-$p_\perp$ jets fragmenting outside the plasma (see *e.g.* ref. [78]). Such an effect should also be expected in the rope picture, where high-$p_\perp$ gluons are expected to hadronize outside the region where strings interfere, illustrated in figure 1.7. This effect is, however, not taken into account in the present implementation.

As a means to approximately account for the reduced rope effect for high-$p_\perp$ jets, we have studied a modified version of the "pipe" implementation described in appendix 1.C.1. Here, in case any parton in the string, or any hadron arising from the string, obeys the criteria $|y| < 2.0$ and $p_\perp > 4$ GeV, the string will not feel any enhancement, but be hadronized with $\tilde{\kappa}/\kappa = 1$. As this happens in only a small fraction of the events, we believe that this crude measure gives a qualitatively correct estimate of the effect.

In figure 1.15 we show the $p^\pm/\pi^\pm$ rato at $\sqrt{s} = 200$ and 7000 GeV. The curve marked 'DIPSY' shows simulation with no rope effects, but as the final state swing (labelled 'Swing') is added, we already see how the high-$p_\perp$ tail of the ratio distribution (at both energies) falls off a bit. Adding all rope effects (labelled 'Rope'), we see how the integrated ratio increases (as shown before), but since the major effect on $p_\perp$, in the rope model, comes from the final state swing, the shape is not altered much. The curve labelled 'Pipe' shows the modified pipe-based approach to estimate the overlap, as discussed above. We see that in this version the high-$p_\perp$ tails are more suppressed, thus following the data better. The 'Pipe'-curves also show that the ratios for low to intermediate $p_\perp$ (where most of the multiplicity is) is affected roughly as expected, even with this very simple way of counting overlap[11]. The fact that even a simple treatment like the pipe based one can catch the gist of the rope model,

---

[11]We remind the reader that not even additional junctions are added in the 'Pipe'-approach, all is due to changes in the ξ parameter.
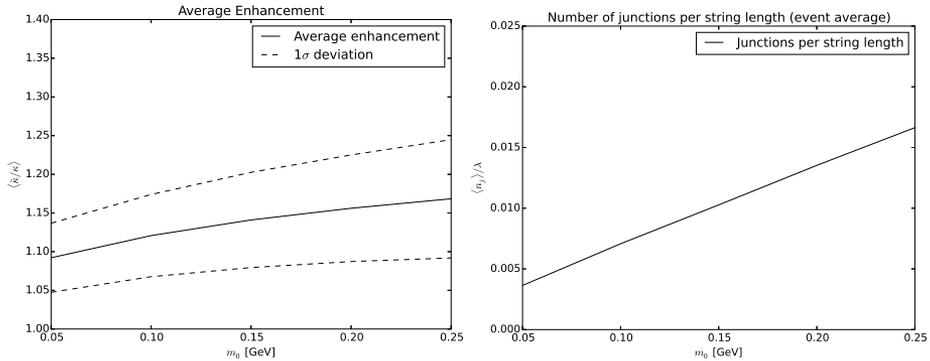
Figure 1.14: Average enhancement (left) $\langle h \rangle = \langle \tilde{\kappa}/\kappa \rangle$ as a function of m_0 at $\sqrt{s} = 900$ GeV in pp collisions. The band indicates one standard deviation. Number of junctions (right) per string length as a function of r_0.

is an encouraging indication that the interesting physics lies in the model itself, and not in a more or less arbitrary choice of how to estimate the numbers m and n denoting the number of interacting strings. We do, however, see that the $\sqrt{s}$-dependence for the pipe based approach is not nearly as good as the dipole based one. For this reason, we believe the dipole approach to bear more physical sense, and in sections 5.1 and 5.2, we have thus only shown the dipole approach.

In a future work we will address the issue of the high-$p_\perp$ tails in ratios. A more sophisticated version of the cut applied to the pipe based approach must be added to ensure that hadronization takes place with local parameters suitable for the actual location of the process, and not just let the dipoles propagate a fixed length.

In figure 1.16 we see the $K^\pm/\pi^\pm$ ratio in bins of $p_\perp$ at $\sqrt{s} = 200$ GeV and 7000 GeV. This ratio does not show the same type of intermediate-$p_\perp$ "bump" (also not present in data, see *e.g.* ref. [81]), but rather a more smooth rise. The rope model (in both dipole and pipe approaches) shows some, but not much, effect, in accordance with our expectations.

6   Conclusions and outlook

It was early observed that string hadronization models, when tuned to e^+e^- annihilation data at LEP, underestimates the production of strange quarks in pp collisions. At the higher LHC energies the experiments show significantly enhanced production of strangeness and baryons, in particular strange baryons are strongly enhanced. In pp collisions the strings or cluster chains are usually assumed to hadronize independently, although the density of strings becomes quite high at LHC energies, and interaction between the strings therefore ought to be expected. Interaction between strings have been discussed by many authors in connection with nucleus collisions, where very high string densities are also expected. Here
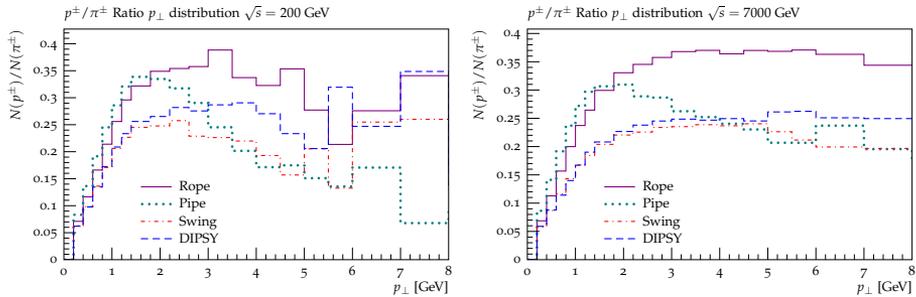
Figure 1.15: Proton ($p + \bar{p}$) to pion ($\pi^+ + \pi^-$) ratio in bins of $p_\perp$ ($|y| < 2.0$) at $\sqrt{s} = 200$ GeV (left) and 7000 GeV (right).

the formation of "ropes" are generally predicted to give higher ratios of strange particles and baryons. Although the geometrical distribution of nucleons within a nucleus can give a good estimate of the density of strings in nucleus collisions, for a quantitative description of string interaction in pp collisions, a description of the parton distribution in impact parameter space must be essential.

In this work we use the DIPSY model, which is a formulation of BFKL evolution in transverse coordinate space, including NLL effects and effects of saturation and confinement, taking also fluctuations and correlations into account. Within this model it is possible to calculate the distribution of strings in the transverse plane, and thus estimate the amount of interaction. For the actual hadronization process we use PYTHIA8.

Following the early work by Biro *et al.* [3], we assume that a set of strings within a limited transverse size can interact coherently, forming a colour rope. If the strings are stretched between random colour charges, the net charge at the end of a rope is obtained by a random walk in colour space. Results from lattice calculations show that the tension in a rope is proportional to the corresponding quadratic Casimir operator. If the rope breaks up in a step-wise manner by the production of $q\bar{q}$ pairs, then the number of such pairs needed to break the rope, is in general smaller than the initial number of strings. More energy will, however, be released in the production of the individual pairs, thus simulating a higher effective string tension. An important point is here that it is the decrease in rope tension following the $q\bar{q}$ pair production, which specifies the "effective string tension", and we note here that this leads to a significantly smaller increase, compared to what is usually assumed.

Besides higher fractions of strange particles and baryons, a higher string tension also implies that the string breaks earlier. Early breakups usually imply lower multiplicity, but we argue here that for rope hadronization this effect is compensated by the fact that shorter string pieces are needed to form a final state hadron.

Special attention is needed for handling colour singlets, which can be formed *e.g.* when a triplet and an antitriplet combines as $3 \otimes \bar{3} = 8 \oplus 1$. We treat this by colour reconnection
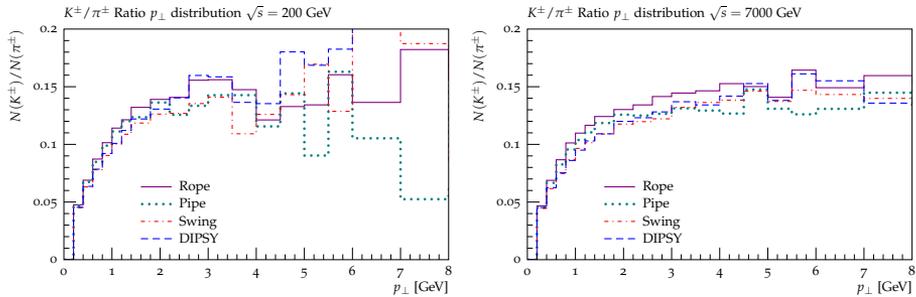
Figure 1.16: Kaon ($K^+ + K^-$) to pion ($\pi^+ + \pi^-$) ratio in bins of $p_\perp$ at $\sqrt{s} = 200$ GeV (left) and 7000 GeV (right).

via a "final state swing", described in section 4.1. This idea could potentially also be used to reconnect parallel strings into the anti-triplet in $3 \otimes 3 = 6 \oplus \bar{3}$ (see eq. (1.24)), as sketched in figure 1.6. As the hadronization model in PYTHIA8 is currently being improved to better handle complicated junction topologies, we expect to be able to implement such a sextet swing mechanism in ARIADNE in the near future.

Naturally the range within which the strings can act coherently cannot be calculated from basic principles. It ought to be of the hadronic scale ∼1 fm, but might be treated as a tunable parameter. Partly overlapping strings also give rise to uncertainties. We have here studied two different schemes for estimating the effects of rope formation, which both attempt to account for the actual overlap of strings in impact parameter space and rapidity. The schemes differ in the level of detail considered; the "pipe-based" scheme is only looking at the average enhancement of the tension in a string, while the "dipole-based" version estimates the increased string tension in each individual string break-up. The dipole scheme also introduces a simple junction model, both formation and breaking. In spite of the differences between the schemes, the results are fairly similar. In both cases observables sensitive to the increased relative abundance of baryons and strange hadrons are much better described by the rope models, compared to conventional string fragmentation.

The fact that the model reproduces the increase both for several collision energies and for several different hadron species, is a strong indication that our picture of the increased string tension in overlapping strings, and its effect on the fragmentation process, is reasonable. Although our model introduces a couple of new parameters, we have shown that these mainly affects the overall strength of the effect, while the influence of the string tension on individual hadron species is fixed by the model and by the tuning of parameters in PYTHIA8 to single-string data from e^+e^--experiments. Also the energy dependence is fairly well constrained by the comparison to data presented in this article, and our implementation in the DIPSY generator can therefore make rather firm predictions, *e.g.* for relevant observables to be measured at Run 2 of the LHC.

A particularly interesting result is that the model reproduces the increase in the ratios p/π

and Λ/K with $p_\perp$ in the range $p_\perp < 2$ GeV, in a way mimicking a hydrodynamic transverse flow. This effect is frequently interpreted as caused by a transition to a quark–gluon plasma. It was also pointed out in ref. [80] that colour reconnection, as implemented in PYTHIA, gives rise to a flow-like effect in pp collisions. Thus the results presented in section 5 originate partly from the increased tension in ropes with high colour multiplets, and partly from colour reconnections in cases where strings combine to colour singlets or other small multiplets.

Our model does, however, not reproduce the drop in the p/π ratio for $p_\perp > 2$ GeV. In analyses based on flow, it is frequently assumed that high-$p_\perp$ particles result from fragmentation of jets not participating in the thermalisation, and hadronizing outside the plasma (see *e.g.* ref. [78]). A similar effect should be expected in our rope model. High-$p_\perp$ hadrons may be predominantly formed outside the overlap regions, and therefore not feel the increased tension in the rope. This effect is not included in the present implementation of the model, giving the results presented in section 5. A crude modification of our pipe-based scheme indicates that the effect may be qualitatively accounted for, but further studies are needed of the formation times and the transverse propagation in space within our rope model. In this context we also need to revisit the description of high-$p_\perp$ gluons, which currently are not well modelled in DIPSY.

We have in our analyses also neglected a possibly increased pressure exerted by the ropes. In the bag model the pressure from a high colour flux tends to expand the transverse size of a flux tube, in a way which also could contribute to flow-like effects. An estimate of this effect also needs a better understanding of the relative time-scales for rope formation and the hadronization process.

We conclude that several mechanisms can contribute to the flow-like behaviour in high energy collisions: besides a phase transition to a plasma, also increased string tension in colour ropes, colour reconnection in low colour multiplets, and transverse expansion due to high pressure inside the ropes. To estimate the relative contributions from these sources, it is important to study different reactions, pp, pA, and AA, and also all possible observables, besides those discussed in this paper also *e.g.* angular flow, fluctuations, and correlations of different kinds. The time-scales for the different processes is here very important. We want to return with results of such studies in forthcoming publications.

Acknowledgments

Associates, LLC operate the Thomas Jefferson National Accelerator Facility.

1.A   The DIPSY model

It has since long been clear that a proper description of the multi-particle final states in high energy hadron collisions requires some kind of multi-parton interaction model. The most successful such model to date is the one developed by Sjöstrand and van Zijl [68], but also other models have been proposed (see *e.g.* [82] and [83]).

For the purpose of our investigations, however, it is important that not only the momentum distribution of the produced partons is described; to estimate the degree to which strings overlap we also need to understand the impact-parameter distribution of partons. For this reason we have used DIPSY event generator [16], which will be described briefly in this appendix.

DIPSY is based on Mueller's dipole cascade model [39, 40, 41], which is a formulation of leading-log BFKL evolution [61, 62] in transverse coordinate space. This model relies on the fact that initial-state radiation from a colour charge (quark or a gluon) in a hadron is screened at large transverse distances by an accompanying anticharge, and that gluon emissions therefore can be described in terms of colour-dipole radiation. Thus the partonic state is described in terms of dipoles in impact-parameter space and rapidity, which is evolved in rapidity when an emitted gluon splits a dipole into two. We here note that the suppression of large dipoles in transverse coordinate space is equivalent to the suppression of small $k_\perp$ in the conventional BFKL evolution in momentum space.

For a dipole with charges at the transverse points x_1 and x_2, the probability to emit a gluon at x_g is given by

$$\frac{d\mathcal{P}_g}{dY} = \frac{\bar{\alpha}}{2\pi} d^2 x_g \frac{(x_1 - x_2)^2}{(x_1 - x_g)^2(x_g - x_2)^2}, \quad \text{with } \bar{\alpha} = \frac{N_c \alpha_s}{\pi}. \tag{1.21}$$

The emission produces two new dipoles, (x_1, x_g) and (x_g, x_2), which can split independently by further gluon emissions. Repeated emissions form a cascade, with dipoles connected in a chain. When two cascades collide, a dipole (x_1, x_2) in a right-moving cascade can interact with a left-moving dipole (x_3, x_4), with probability

$$P = \frac{\alpha_s^2}{4} \left[\ln \left(\frac{(x_1 - x_3)^2(x_2 - x_4)^2}{(x_1 - x_4)^2(x_2 - x_3)^2} \right) \right]^2. \tag{1.22}$$

In a series of papers [15, 59, 60, 16] a generalization of Mueller's model, implemented in the Monte Carlo event generator DIPSY, has been described in detail. Here we will only discuss the main points. The basic idea behind the model is to include important non-leading effects in the BFKL evolution, saturation effects in the evolution, and confinement.

The full next-to-leading logarithmic corrections have been calculated and have been found to be very large [84, 85]. A physical interpretation of these corrections has been presented by Salam [86], and a dominant part is related to energy–momentum conservation. In the DIPSY model this is achieved by equating the emission of a gluon at small transverse distances with high transverse momenta of the emitted and recoiling gluons. In this way the gluons emitted in the evolution are traced in both momentum and coordinate space, allowing us to generate the final-state momentum distribution of gluons. The conservation of energy and momentum implies a dynamic cutoff for very small gluons with correspondingly high transverse momenta. This constraint has also important computational advantages; in the standard Mueller model the number of small gluons diverges which, although the cross section is still finite, gives computational problems.

Other important non-leading effects are the running coupling, $\alpha_s(p_\perp^2)$, and the "energy scale terms" (which correspond to the consistency constraint discussed by Kwiecinski et al. [87]). The latter implies that the emissions are ordered in both the positive and negative light-cone components [88]. Besides these perturbative corrections, confinement effects are included via a small gluon mass, m_g, and non-linear saturation effects through the so-called swing mechanism, described in more detail below.

In a high energy collision, two hadrons are evolved from their respective rest frames to a Lorentz frame in which they collide. In its own rest system a proton is currently modelled by a simple triangle of gluons connected by dipoles, and the gluonic Fock state is built by successive dipole emissions of virtual gluons. (The small-x gluons are rather insensitive to the initial parton configuration, apart from the overall size, and valence quarks are later introduced by hand in the final state). The two evolved systems are then made to collide, allowing some of the dipoles in the left-moving system to interact with some in the right-moving ones. This enables the gluons in these dipoles to come on-shell, together with all parent dipoles, while non-interacting dipoles must be regarded as virtual and thus be reabsorbed.

1.A.1   The initial-state Swing mechanism

The swing mechanism in DIPSY is a saturation effect within the evolution, which is conceptually interesting in connection with the rope formalism in this article. Mueller's dipole evolution is derived in the large N_c limit, where each colour charge is uniquely connected to an anticharge within a dipole. Saturation effects are here included as a result of multiple dipole collisions, in the frame used for the analysis. Such multiple interactions give dipole chains forming loops, and are related to multiple pomeron exchange. Loops formed within

the evolution are, however, not included.[12] Besides missing parts of the saturation, this also makes the result dependent on the frame used for the calculation. As dipole interaction in eq. (1.22) is colour suppressed compared to the dipole splitting, loop formation is related to the possibility that two dipoles have identical colours.

If two dipoles happen to have the same colour, we have actually a colour quadrupole, where a colour charge is effectively screened by the nearest anticolour charge. Thus approximating the field by a sum of two dipoles, one should preferentially combine a colour charge with a nearby anticharge. This interference effect is taken into account in DIPSY in an approximate way, by allowing two dipoles with the same colour to recouple forming the new dipoles, in a way that favours small dipoles.

In the simulation this is handled by assigning all dipoles a colour index running from 1 to N_c^2, not allowing two dipoles connected to the same gluon to have the same index. A pair of two dipoles, (x_1, x_2) and (x_3, x_4), with the same colour may be better approximated by the combination (x_1, x_4) and (x_3, x_2), if these dipoles are smaller. In the evolution the pair is allowed to "swing" back and forth between the two possible configurations as indicated in figure 1.4. The swing mechanism is adjusted to give the relative probabilities

$$\frac{P_{(12)(34)}}{P_{(14)(32)}} = \frac{(x_1 - x_4)^2 (x_3 - x_2)^2}{(x_1 - x_2)^2 (x_3 - x_4)^2}, \tag{1.23}$$

thus favouring the configuration with smallest dipoles. (In the implementation of the cascade evolution, the swing is competing with the gluon emission in eq. (1.21), where a Sudakov-veto algorithm can be used to choose which of the two happens next.)

The dipole interaction in eq. (1.22) is smaller for smaller dipoles, which reproduces the colour transparency effect. As the swing leads to smaller average dipole size, the probability for interactions is reduced, and thus the swing represents a saturation effect within the evolution. This reduced interaction probability is equivalent to the $2 \rightarrow 1$ and $2 \rightarrow 0$ vertices in *e.g.* the BK evolution equation.

1.B   Colour algebra

1.B.1   Calculation of p and q

In this section the recursion relations presented in eq. (1.12) for calculating all possible $\{p, q\}$ multiplets arising from the combination of m triplets and n antitriplets will be presented in detail.

---

[12]This is also the case *e.g.* for the non-linear BK equation [89, 90], which describes the interaction between a relatively dilute cascade and a dense target.

It is worth noting that the combination of any SU(3) multiplets can be carried out using Young tableaux (just as the more familiar case of SU(2)). In the notation of this article, an SU(3) multiplet is denoted by the quantum numbers p and q, which can be directly a Young tableaux, as $\{1,0\} = \square$ and $\{0,1\} = \begin{array}{c}\square\\\square\end{array}$, and so the number of boxes in the top row is $p + q$. and the number of boxes in the bottom row is q.

Now the usual rules of manipulating Young tableaux can be used to review the simple cases of combining a single triplet with an (anti-)triplet:

$$\{1,0\} \otimes \{1,0\} = \square \otimes \square = \square\square \oplus \begin{array}{c}\square\\\square\end{array} = \{2,0\} \oplus \{0,1\}, \tag{1.24}$$

$$\{1,0\} \otimes \{0,1\} = \square \otimes \begin{array}{c}\square\\\square\end{array} = \begin{array}{cc}\square\square\\\square\end{array} \oplus I = \{1,1\} \oplus \{0,0\}, \tag{1.25}$$

where $I = \{0,0\}$ denotes a singlet. Note that symmetry ensures that $\{1,0\} \otimes \{1,0\} = \{0,1\} \otimes \{0,1\}$. Physically eq. (1.24) corresponds to the situation where two colour strings, with colour flow in the same direction, merge to a rope. In the case where the colour pairs are equal, the resulting rope will be a sextet ($\{2,0\}$), and in all other cases an antitriplet ($\{0,1\}$). Eq. (1.25) corresponds to two strings with opposite colour flow merging. This can either result in a gluon-like octet rope ($\{1,1\}$) or no colour flow at all, in the singlet case.

The recursion relations of eq. (1.12) can be derived using a similar procedure. Adding a single triplet to an existing multiplet $\{p, q\}$ gives eq. (1.12) directly, as:

$$\{p,q\} \otimes \{1,0\} = \underbrace{\begin{array}{c}\square\square\end{array}\cdots\begin{array}{c}\square\square\end{array}}_{q}\underbrace{\cdots\square}_{p} \otimes \square = \tag{1.26}$$

$$\{p, q - 1\} \oplus \{p - 1, q + 1\} \oplus \{p + 1, q\}.$$

Combining the general $\{p, q\}$ multiplet with an antitriplet proves directly symmetry is ensured as:

$$\{p,q\} \otimes \{0,1\} = \underbrace{\begin{array}{c}\square\square\end{array}\cdots\begin{array}{c}\square\square\end{array}}_{q}\underbrace{\cdots\square}_{p} \otimes \begin{array}{c}\square\\\square\end{array} \tag{1.27}$$

$$= \{p - 1, q\} \oplus \{p, q + 1\} \oplus \{p + 1, q - 1\}.$$

Using the stated recursion relations, a random walk in colour space is simulated, as in ref. [3] by starting from a singlet $I = \{0,0\}$. The resultant relation between $\langle p + q \rangle$ and $m + n$ is shown in figure 1.3.

In the same way the recursion relation for all multiplets arising from combining the general $\{p, q\}$ multiplet with an octet can be defined. The proof follows in a straightforward way from the same considerations as above, and only the result is stated here:

$$\{p,q\} \otimes \{1,1\} = \{p - 1, q - 1\} \oplus \{p + 1, q + 1\} \oplus 2 \cdot \{p, q\} \oplus \{p - 1, q + 2\} \tag{1.28}$$

$$\oplus \{p + 1, q - 2\} \oplus \{p - 2, q + 1\} \oplus \{p + 2, q - 1\}.$$
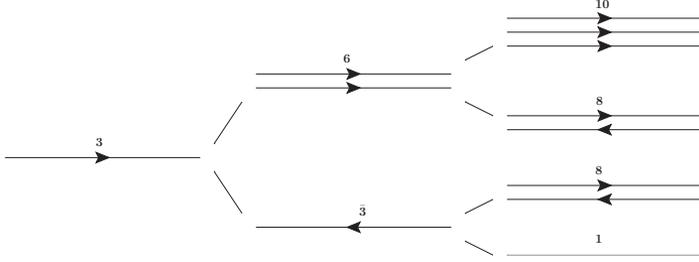
Figure 1.17: Illustration of the addition of triplets to an initial triplets, reads from left to right. By combining the initial 3 in the left column with another 3, one gets either 6 or $\bar{3}$ and so on (see text).

1.B.2 An illustrative example

As a simple illustrative example we can look at a rope spanned between three quarks with random colours in one end, matched by three antiquarks in the other end, illustrated in figure 1.17. The first quark is a triplet, 3, denoted {1,0}, and depicted to the left in figure 1.17. The addition of a second quark can give a 6 ({2,0}) or an $\bar{3}$ ({0,1}), as shown in the central column of figure 1.17, with probabilities 2/3 and 1/3 respectively. Adding the third quark to the sextet can give 10 ({3,0}) or 8 ({1,1}), while adding it to the $\bar{3}$ gives 8 ({1,1}) or a singlet ({0,0}), as shown in the rightmost column in figure 1.17. The result is therefore a decuplet, two octets, and a singlet, with probabilities proportional to their respective multiplicities (*i.e.* 10/27, 8/27, 8/27, and 1/27).

For the fragmentation of the rope, we find first that in the case of the singlet, there is no colour field stretched. For the decuplet and the octets the relative rope tension is 9/2 and 9/4 respectively. The decuplet can fragment in three steps giving successively a sextet and a triplet, before the final breakup. The relative effective string tension, $\tilde{\kappa}/\kappa$, in these steps are $9/2 - 5/2 = 2, 5/2 - 1 = 3/2$, and 1 respectively. Thus the first breakup will give the highest effective string tension, and correspondingly higher s/u-ratio and higher $p_\perp$. An initial octet will similarly break in two steps via a triplet, with $\tilde{\kappa}/\kappa$ equal to $9/4 - 1 = 5/4$, followed by the break of the triplet with the tension κ for a single string. If the $\{p, q\}$ multiplet is in the left end of the rope, the antiquark is pulled to the left when p is reduced, and pulled to the right when q is reduced.

1.C Detailed description of the rope models

The models for rope formation and fragmentation presented in this paper are similar in spirit, but as always when implementing models in a Monte Carlo code, there are a number of choices to be made and different levels of detail that can be chosen. One of our models is fairly crude, using the average overlap for individual strings in an event, while the other

is very detailed in the treatment of the individual string break-ups.

In common for the two models is that, for technical reasons, the fragmentation of a rope is done one individual string at the time, emulating the rope effects by modifying the parameters in the string fragmentation implementation of PYTHIA8, thus taking into account the effective string tension of the rope. We have concentrated on a selection of parameters which should be particularly sensitive to rope effects:

- ρ: the suppression of s quark production relative to u or d type production.

- ξ: the suppression of diquark production relative to quark production, meaning *(all diquarks)/(all quarks)*.

- x: the suppression of diquarks with strange quark content relative to diquarks without strange quarks (in addition to the factor ρ for each extra s-quark).

- y: the suppression of spin 1 diquarks relative to spin 0 diquarks (not counting a factor three due to the number of spin states of spin 1 diquarks).

- σ: the width of the transverse momentum distribution in string break-ups.

Of these we assume that ρ, x and y are directly related to mass effects in the tunneling mechanism in eq. (1.2), such that if the modification of the string tension be given by a simple scaling with an enhancement factor h, such that $\kappa \mapsto \tilde{\kappa} = h\kappa$, we obtain the following rescalings:

$$
\begin{aligned}
\rho &\mapsto \tilde{\rho} = \rho^{1/h}, \\
x &\mapsto \tilde{x} = x^{1/h}, \\
y &\mapsto \tilde{y} = y^{1/h}.
\end{aligned}
\tag{1.29}
$$

Also the scaling of σ is quite straight forward and is simply given by $\sigma \mapsto \tilde{\sigma} = \sigma\sqrt{h}$.

The treatment of the ξ parameter is somewhat more involved as it gives a global probability of having a diquark break-up relative to a simple quark break-up, which means it cannot be simply related to the tunneling mechanism. Looking at the relation between the individual probabilities for different quarks and diquarks, they are determined by the relations: $\mathcal{P}_s = \rho\mathcal{P}_u$, $\mathcal{P}_{ud_1} = 3y\mathcal{P}_{ud_0}$ and $\mathcal{P}_{us_1} = x\rho\mathcal{P}_{ud_1}$, *etc.* The total probability for diquark production relative to quark production, can therefore be expressed in terms of the ratio $\mathcal{P}_{ud_0}/\mathcal{P}_u$.

$$
\xi \equiv \frac{\sum_{qq_s} \mathcal{P}_{qq_s}}{\sum_q \mathcal{P}_q} = \frac{1 + 2x\rho + 9y + 6x\rho y + 3yx^2\rho^2}{2 + \rho} \frac{\mathcal{P}_{ud_0}}{\mathcal{P}_u} \equiv \alpha \frac{\mathcal{P}_{ud_0}}{\mathcal{P}_u},
\tag{1.30}
$$

(where we have assumed that u and d quarks are equivalent).

However, it is not the case that $\mathcal{P}_{ud_0}/\mathcal{P}_u$ is affected by the string tension in the same way as the ρ-parameter. According to the popcorn mechanism described in section 2.3 and figure 1.1, there is a two step procedure where first a $q\bar{q}$ pair is produced as a fluctuation that does not break the string, and then another pair is produced which actually does, allowing a diquark–antidiquark pair to tunnel out. We will therefore assume that the ratio is composed of two factors, one is related to the probability to have a $q\bar{q}$ fluctuation in the first place, and one related to the differences in masses. We will call these β and γ respectively, where we assume that β is independent of the string tension, while γ transforms as ρ.

Hence we have $\xi = \alpha\beta\gamma$ where

$$\alpha \mapsto \tilde{\alpha} = \frac{1 + 2\tilde{x}\tilde{\rho} + 9\tilde{y} + 6\tilde{x}\tilde{\rho}\tilde{y} + 3\tilde{y}\tilde{x}^2\tilde{\rho}^2}{2 + \tilde{\rho}}, \tag{1.31}$$

and

$$\gamma \mapsto \tilde{\gamma} = \gamma^{1/h}, \tag{1.32}$$

and the total effect on ξ from a modified string tension is given by

$$\xi = \alpha\beta\gamma \mapsto \tilde{\xi} = \tilde{\alpha}\beta \left(\frac{\xi}{\alpha\beta} \right)^{1/h}. \tag{1.33}$$

As explained in section 2.4, also the parameters a and b are indirectly affected by a modified string tension. One could also expect other parameters to be affected, but the ones presented here are the the most important ones.

1.C.1 A pipe-based treatment

In the crude, pipe-based approach, we expect all flux tubes to be directed dominantly along the rapidity axis. For a string stretched from parton $(\vec{b}_0, y_0)$, via the gluons $(\vec{b}_i, y_i)$, and ending at $(\vec{b}_k, y_k)$, the volume of the corresponding flux tube in (*transverse coord., rapidity*) space is thus given by

$$V_{string} = \sum_{i=1}^{k} \pi r_0^2 |y_i - y_{i-1}|. \tag{1.34}$$

As the string can go back and forth in rapidity, the separations in rapidity enters with its absolute value. To estimate the amount of overlap between two strings, we must take into account that the string tubes are not parallel to the rapidity axis, but go up and down in transverse space. This is approximated by replacing the winding flux tube by a wider straight pipe, with a correspondingly lower density. The pipe is parallel to the rapidity axis and stretched between the partons with the smallest and the largest rapidity, y_{min} and y_{max}.

Its center is taken at $\vec{b}_{cent} = (\vec{b}_{min} + \vec{b}_{max})/2$, and its radius, r_{pipe}, is increased to enclose the major part of a wiggling string:

$$r_{pipe}^2 = r_0^2 + \frac{1}{k} \sum_{i=0}^{k} (\vec{b}_i - \vec{b}_{cent})^2. \tag{1.35}$$

The volume of the pipe is thus given by $V_{pipe} = \pi r_{pipe}^2 (y_{max} - y_{min})$. Note that since the string can go back and forth, the ratio $d = V_{string}/V_{pipe}$ can be larger than one. This number is the relative field density in the pipe, and in terms of overlap, it represents the string's "self-overlap". It is, however, important to keep track of the direction of the overlap. The relative field density in each pipe is thus assigned both an m and an n component, defined by the sign of its projection on the rapidity axis. For each pipe i, we thus have a relative field density with two components $d_{i,n}$ and $d_{i,m}$. To estimate the total $\{m, n\}$ of each string, we must therefore sum over the two components separately, weighting with the geometrical overlap of the pipes, such that:

$$m = \sum_{i=0}^{N} C_i d_{i,m} \quad \text{and} \quad n = \sum_{i=0}^{N} C_i d_{i,n}, \tag{1.36}$$

where C_i is the geometrical overlap with pipe i, there are N pipes in an event. (Note that the geometrical overlap of an object with itself will always be 1.) These numbers are rounded off to integers m and n corresponding to the number of interfering colour charges and anticharges in the rope. To find the relevant colour multiplet $\{p, q\}$ for the rope, we add m triplets and n antitriplets (parallel and anti-parallel strings) with random colours, as described in section 3.1 and appendix 1.B.1. The $n + m$ strings in the rope should then fragment in a sequential way in $p + q$ steps, with a gradually decreasing effective tension. This is technically difficult to implement using the PYTHIA implementation of the Lund fragmentation model. In this first study we therefore make an approximation, where we use the average value for $\tilde{\kappa}$, given by $\kappa_{\text{rope}}/(p + q)$ with κ_{rope} determined by eq. (1.13). Thus the enhancement factor h becomes:

$$h = \frac{\langle \tilde{\kappa} \rangle}{\kappa} = \frac{p^2 + pq + q^2 + 3p + 3q}{4(p + q)}. \tag{1.37}$$

The averaging described here will not properly take into account the situation where two triplets become an anti-triplet instead of a sextet. (Note that the situation where a triplet and an antitriplet form a singlet is taken care of by the swing described in section 4.1.) To account for this, we throw away strings in a multiplet with probability $1 - \frac{p+q}{m+n}$. A string that is discarded in this way, is simply not hadronized, and will not appear in the final state. Removing strings in this way will have an effect on total multiplicity, which can largely be tuned away, but more seriously, it will break energy–momentum conservation. We have therefore devised a more elaborate scheme in the dipole-based treatment, which will be presented next.

1.C.2 A dipole-based treatment

After the final-state shower in ARIADNE, the string can be seen as a chain of dipoles connected by gluons, and in the string fragmentation in PYTHIA8 the break-ups of the string basically follow these dipoles in momentum space. The dipoles, together with their respective overlaps, are thus the basic structures considered in the more sophisticated dipole-based treatment. We study one dipole at a time in its own rest frame, with its two partons along the z-axis. All other dipoles in the event are boosted to the same frame before calculating their overlap with the dipole under study, using the rapidity span and transverse distance of each of them. As gluons are massless, the rapidity span of a dipole can in principle become infinite, and we therefore use a small gluon mass, $m_0 \propto 1/r_0 \sim 0.2$ GeV, to limit the rapidities. To allow for a finite formation time of the string pieces between the partons in a dipole, we let the partons propagate in space a fixed time before calculating the transverse distances.[13] For a pair of dipoles, we can now make a linear interpolation between the transverse positions of their respective partons, and we can thus calculate their overlap as the region in rapidity where the two string pieces are closer than r_0.

Just as in the pipe-based procedure, the colour charges in the dipoles are assumed to be random, although they have a definite direction. We therefore calculate separately the summed overlap of parallel and antiparallel dipoles as

$$ m_i = \sum_{j_+ \neq i} \frac{\delta y_{i(j_+)}}{\Delta y_i} \qquad \text{and} \qquad n_i = \sum_{j_- \neq i} \frac{\delta y_{i(j_-)}}{\Delta y_i}. \tag{1.38} $$

With these overlaps (rounded to integers) we now perform a random walk in colour space to arrive at a multiplet (p_i, q_i) for the dipole. The random walk is, however, somewhat restricted due to the final-state swing mechanism. If, e.g., we find that $m = 0$ and $n = 1$ and add a triplet, we only allow the step $\{1, 0\} \to \{1, 1\}$ in colour space, since the swing is assumed to have taken care of the step $\{1, 0\} \to \{0, 0\}$ already.

If we had a proper procedure for the junction swing in figure 1.6 we could have limited the random walk further, e.g. with $m = 1$ and $n = 0$ we would only allow $\{1, 0\} \to \{2, 0\}$ and not $\{1, 0\} \to \{0, 1\}$, and we would always end up in the highest possible multiplet $\{m, n\}$. However, since the current version of PYTHIA8 only can handle a limited number of junctions, we have to allow such steps and will end up with dipoles with $p_i < m$ or $q_i < n$, which then corresponds to a partial attenuation of the colour field of the dipole by other nearby dipoles.

If we consider two completely overlapping dipoles which are in the multiplet $\{0, 1\}$ this would correspond to the right hand side of figure 1.6, where we basically only have one

---

[13]The propagation time should be of the order of r_0, and the effect of this propagation turns out to be very similar to simply reducing the transverse thickness of the string pieces.

string piece to be hadronized. To avoid junctions, we therefore break one of the dipoles by replacing the two gluons with a diquark and antidiquark. In this way we should get approximately the right multiplicity from the string piece that is left (although its colour flow is reversed compared to a proper junction treatment) and also get the same number of (anti-)baryons that would otherwise have come from the junctions. However, it should be noted that two connected junctions will not necessarily result in a baryon–anti-baryon pair. As we have seen in section 2.4, the popcorn model for baryon production assumes that $q\bar{q}$ fluctuations that do not break the string occur fairly frequently, allowing additional fluctuations to tunnel out as diquark–antidiquark pairs by locally reversing the colour flow. In the case of a string piece connecting two nearby junctions, these fluctuations may actually again turn the colour flow around, and the $\bar{q}$ (q) from the fluctuation may very well travel along the string and combine with one of the (anti-)quarks in the nearby junction. Note that the probability for this to happen is higher than the probability for the corresponding diquark–antidiquark breakup of a string, since it does not involve the tunneling probability for the heavier diquarks in eq. (1.2). Thus the probability of having a fluctuation, which prevents a baryon–antibaryon pair to result from two connected junctions, should only be governed by the β-parameter in eq. (1.33). Therefore, we will not always break the dipole by introducing diquarks, but with a probability β we will instead use quarks.

This procedure is generalized, so that if a given dipole has overlaps m_i and n_i resulting in a multiplet (p_i, q_i), the dipole is broken up with a probability $(1 + m_i + n_i - p_i - q_i)/(1 + m_i + n_i)$. We note that it may happen that a dipole cannot break up, *e.g.* if the dipole ends are quarks rather than gluons. In this case the probability is modified to increase the probability for the other overlapping dipoles to break by replacing the denominator by $(1 + m'_i + n'_i)$ where m'_i and n'_i are calculated as in eq. (1.38), but only summing over breakable dipoles.

For the dipoles that are left, we can now start the hadronization. To further increase the amount of fluctuations included, we do not average over all breakups, but hadronize each string piece with a local effective string tension

$$\tilde{\kappa} = \tilde{\kappa}(p, q) - \tilde{\kappa}(p - 1, q) = \frac{1}{4}\left(2 + 2p + q\right). \tag{1.39}$$

Note that while the expression in eq. (1.13) is symmetric in p and q, eq. (1.39) is not. Hadronizing one string at a time implies a choice of whether *this* string is in the p or q direction, and here the implicit choice is taken towards the p direction. The choice is of course still arbitrary, with no effect on the result. The strings are then send to be hadronized one at a time by PYTHIA8, utilizing a customization described in appendix 1.C.3. This customization enables PYTHIA8 to change hadronization parameters for each string breakup, according to the calculated value of the effective string tension.

1.C.3 Implementation details

The implementation of the rope production, through estimation of m and n by either an approach based on enclosing cylinders or an approach based on dipoles, followed by a random walk procedure is extensively described in section 4.2, and shall not be repeated. The use of PYTHIA for hadronization, and consequently changing hadronization parameters in a PYTHIA run, is however not part of standard usage of the program, and will be described briefly here. The basic idea is to use PYTHIA to hadronize one string at a time, with the ability to change hadronization parameters while the string is being hadronized, based on the local string tension at that particular point on the string. Since PYTHIA normally sets hadronization parameters once and for all, when the program is initialized, a feature to intercept the hadronization loop was introduced. In PYTHIA such interceptions are done with so-called `UserHooks`, which in turn allows for re-initialization of parameters. The DIPSY program then delivers a single string to PYTHIA, which calls back for new hadronization parameters every time a step is made. Owing to the interpretation of strings as dipoles connected with gluons introduced in section 1.C.2, the callback needs to include information about which dipole PYTHIA has reached, as well as the position in the dipole. This is done by comparing the invariant mass of all hadrons made from each string end so far, to the invariant mass of the dipoles, starting from the same string end. This relies on PYTHIA and DIPSY having identical, fixed string ends when the hadronization procedure begins. This is not the case for gluon loops, as PYTHIA will first cut one dipole at random, with probability proportional to invariant mass squared. As an approximation, gluon loops are hadronized with the average value of the string tension for the whole string. Thus, parameters need to be set only once for gluon loops.

1.D Tuning

To ensure that the observables of main interest for rope formation, such as the rates of baryons and strange hadrons, are not affected by global flavour independent effects on particle spectra, we made a complete tuning of relevant parameters in DIPSY, ARIADNE and PYTHIA8, with and without inclusion of our new rope models. For this we have used a selection of data analyses from the Rivet program [91], and used the Professor framework [92] for the actual tuning.

1.D.1 Tuning final-state shower and hadronization

We followed the standard procedure of first tuning the parameters in the final-state shower (in ARIADNE) and in the hadronization (in PYTHIA8) to e^+e^--observables as measured at
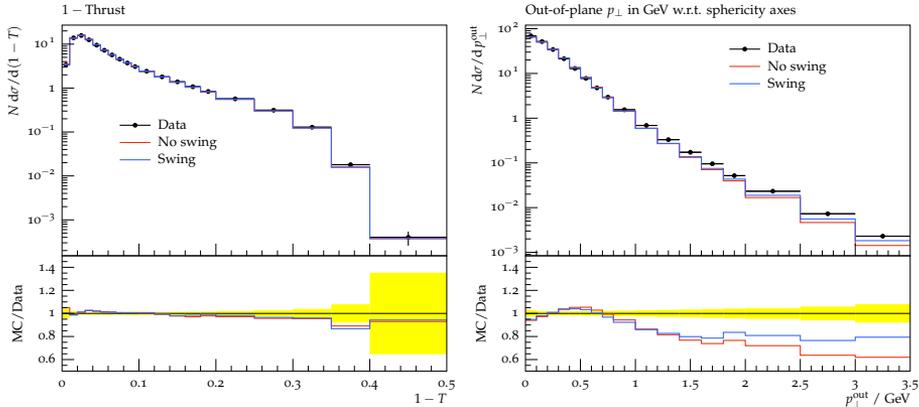
Figure 1.18: Sample plots from tuning of the ARIADNE dipole shower with string fragmentation from PYTHIA8 to DELPHI data [93], with and without final state swing. On the left is shown the distribution in thrust, and on the right the distribution of transverse momenta out of the event plane.

LEP. It can be noted that the old Fortran version of ARIADNE has already been tuned to such data with very good results (see *e.g.* ref. [93]), and since the final-state shower in ARIADNE is basically unchanged in the new version, we obtain equally good results for the default version. When we now add the final-state swing and rope fragmentation we do not expect the results to change very much, as the number of dipoles produced are fairly low, and do not allow for many reconnections. We do expect some changes in parameters, however, since the swing tends to decrease the total string lengths and therefore also the multiplicity. Indeed, we find that *e.g.* the tuned value for the *a* parameter in the fragmentation is somewhat increased when the swing is included.

In figure 1.18 we show two distributions used in the tuning. We find that the thrust distribution is equally well described with and without swing. This is expected since it should be dominated by effects from the hardest gluon emission, and by construction there are no effects of the swing for the first two emissions. For the transverse momentum distribution out of the event plane (defined by the thrust major and minor axes) we do, however, find some differences. Here we should be dominated by the two hardest gluon emissions, and there we can expect larger effects from the swing in subsequent emissions and in the hadronization. We see that the description of data is somewhat improved, and in general the total χ^2/Ndf. is also somewhat improved when the swing is included.

Note that we do not expect any effects of the rope hadronization in $e^+e^- \rightarrow$ hadrons, as we should be dominated by a single string. In high multiplicity events there could be some internal overlaps but we found[14] no change in the tuned observables when including the ropes.

---

[14]In $e^+e^- \rightarrow$ hadrons we use the thrust axis rather than the beam axis to define the rapidity span of strings for the pipe-based treatment.
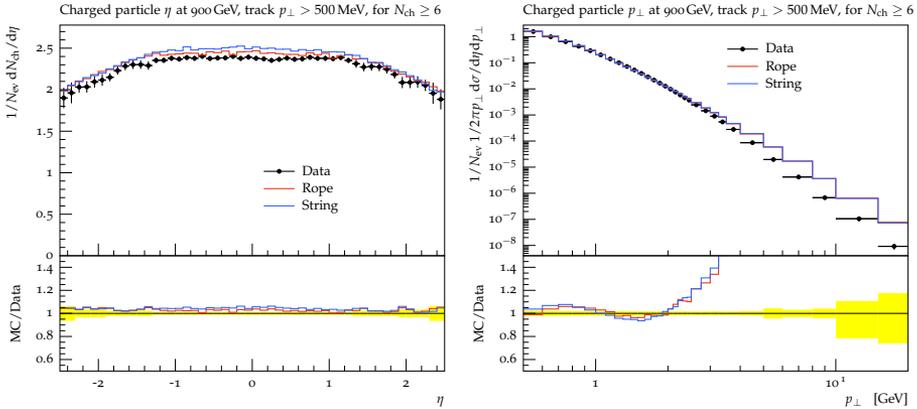
Figure 1.19: Sample plots from the tuning of DIPSY to 900 GeV *pp* minimum-bias data from ATLAS [94]. On the left is shown the pseudo-rapidity distribution of charged particles with transverse momenta larger than 500 MeV in events with at least six charged particles. On the right is given the transverse momentum distribution of charged particles for the same events. In both plots the lines labelled *Rope* is DIPSY with the new (dipole-based) rope model, wile *String* indicates DIPSY with the standard fragmentation. In both cases the final-state swing model is used.

1.D.2   Tuning DIPSY

We then proceed to tune the parameters of the DIPSY model to *pp* collisions. Here we tune both to the total and elastic cross sections as well as to final-state observables in minimum bias events. It should be emphasized that the DIPSY program is not yet ready for precision description of final-state observables. Although the model has improvements beyond the leading logarithmic BFKL accuracy, there are no proper matrix elements included for hard scatterings and there are no quarks included in the evolution. We therefore do not expect it to be able to give a good description of observables involving high transverse momenta, and indeed we find that the particle rates above $p_\perp \sim 5$ GeV are severely overestimated. In addition we have found that, although the energy dependence of the total, elastic, and diffractive cross sections are well reproduced, the energy dependence of the total multiplicity is a bit too flat. We therefore decided to make separate tunes for different collision energies as well as global tunes. As it turned out that the observables in section 5, were insensitive to whether we used separate or global tunes, we there only present results using the latter.

In figures 1.19 and 1.20 we show examples of observables used in the tuning of 900 GeV and 7 TeV respectively. The rapidity distribution of charged particles is well described for both energies and both for the default fragmentation and for the rope model. While above a couple of GeV, the transverse momentum distribution in all cases is too hard, the average transverse momenta are well described as shown in figure 1.21. In a future publication we intend to try to cure these deficiencies, but here we are satisfied that we obtain very similar results with and without ropes.

94
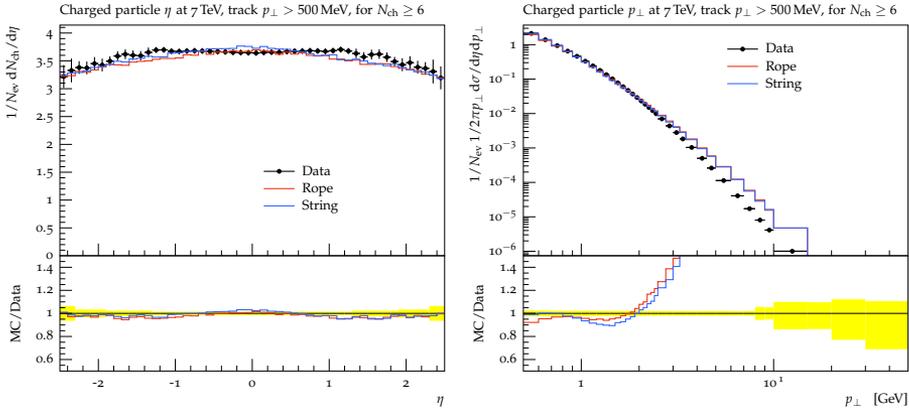
Figure 1.20: Sample plots from the tuning of DIPSY to 7 TeV pp minimum-bias data from ATLAS [94], using the same distributions and models as in figure 1.19.

Since DIPSY in the current version does not describe diffractive final states (see [16]), it is necessary to choose observables for comparison which are not greatly affected by the presence of diffractive events. This is important both for the tuning and for the observables studied in section 5.1. In PYTHIA8 it is possible to turn on and off the diffractive contributions, and such runs can be used to determine which observables should be used for the present analysis. As an example we show in figure 1.22 a comparison between results from PYTHIA8 and data from CMS for the rapidity distribution of Λ (figure 1.22 (left)) and the ratio K_s^0/Λ in figure 1.22 (right). It is clear that the inclusion of diffractive events plays a great role when looking at raw per-event distributions. In PYTHIA8 the diffractive events are hadronizing in the same way as the non-diffractive, and the K_s^0/Λ ratio is therefore not modified by including diffractive events. Even if this is not confirmed by experiments at present, we note that the contribution from diffractive events is relatively small. A moderate difference in particle ratios in diffractive events should therefore not change predictions for particle ratios in a serious way, and such ratios should therefore be better observables in comparisons between our model and data.

Looking at figure 1.22 it is also directly visible that PYTHIA8 has difficulties reproducing these distributions, which is also the case for almost all contemporary generators (see. *e.g.* `mcplots.cern.ch`)
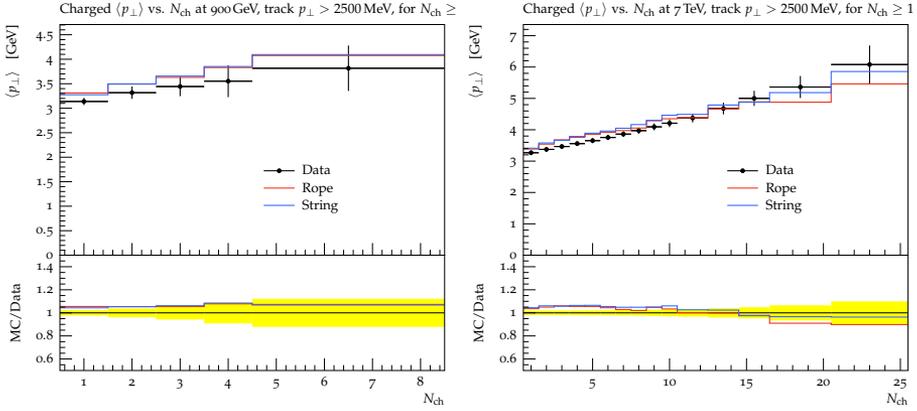
Figure 1.21: Sample plots from the tuning of DIPSY to 900 GeV (left) and 7 TeV (right) pp minimum-bias data from ATLAS [94]. Both plots show the average transverse momenta (above 2.5 GeV) as a function of the number of charged particles per event. The models are the same as in figure 1.19.
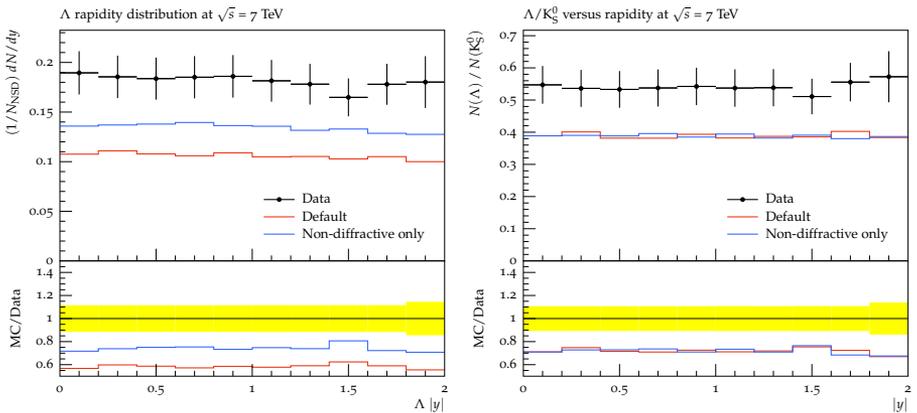

Figure 1.22: Pythia non-diffractive only (blue) and including diffractive (red), compared to 7000 GeV data from CMS for the Λ rapidity distribution (left) and the Λ/K_s^0 ratio (right).

References

[1] T. Sjöstrand, S. Mrenna, and P. Z. Skands, "PYTHIA 6.4 Physics and Manual," *JHEP* **05** (2006) 026, `arXiv:hep-ph/0603175 [hep-ph]`.

[2] M. Bahr *et al.*, "Herwig++ Physics and Manual," *Eur. Phys. J.* **C58** (2008) 639–707, `arXiv:0803.0883 [hep-ph]`.

[3] T. S. Biro, H. B. Nielsen, and J. Knoll, "Color Rope Model for Extreme Relativistic Heavy Ion Collisions," *Nucl. Phys.* **B245** (1984) 449–468.

[4] A. Białas and W. Czyz, "Chromoelectric Flux Tubes and the Transverse Momentum Distribution in High-energy Nucleus-nucleus Collisions," *Phys. Rev.* **D31** (1985) 198.

[5] A. K. Kerman, T. Matsui, and B. Svetitsky, "Particle Production in the Central Rapidity Region of Ultrarelativistic Nuclear Collisions," *Phys. Rev. Lett.* **56** (1986) 219.

[6] M. Gyulassy and A. Iwazaki, "Quark and gluon pair production in SU(N) covariant constant fields," *Phys. Lett.* **B165** (1985) 157–161.

[7] B. Andersson and P. A. Henning, "On the dynamics of a color rope: The Fragmentation of interacting strings and the longitudinal distributions," *Nucl. Phys.* **B355** (1991) 82–105.

[8] M. Braun and C. Pajares, "A Probabilistic model of interacting strings," *Nucl. Phys.* **B390** (1993) 542–558.

[9] M. Braun and C. Pajares, "Cross-sections and multiplicities in hadron nucleus collisions with interacting color strings," *Phys. Rev.* **D47** (1993) 114–122.

[10] N. S. Amelin, M. A. Braun, and C. Pajares, "String fusion and particle production at high-energies: Monte Carlo string fusion model," *Z. Phys.* **C63** (1994) 507–516.

[11] N. Armesto, M. A. Braun, E. G. Ferreiro, and C. Pajares, "Strangeness enhancement and string fusion in nucleus-nucleus collisions," *Phys. Lett.* **B344** (1995) 301–307.

[12] K. Kajantie and T. Matsui, "Decay of Strong Color Electric Field and Thermalization in Ultrarelativistic Nucleus-Nucleus Collisions," *Phys. Lett.* **B164** (1985) 373–378.

[13] G. Gatoff, A. K. Kerman, and T. Matsui, "The Flux Tube Model for Ultrarelativistic Heavy Ion Collisions: Electrohydrodynamics of a Quark Gluon Plasma," *Phys. Rev.* **D36** (1987) 114.

[14] M. A. Braun, C. Pajares, and J. Ranft, "Fusion of strings versus percolation and the transition to the quark gluon plasma," *Int. J. Mod. Phys.* **A14** (1999) 2689–2704, arXiv:hep-ph/9707363 [hep-ph].

[15] E. Avsar, G. Gustafson, and L. Lönnblad, "Energy conservation and saturation in small-x evolution," *JHEP* **07** (2005) 062, arXiv:hep-ph/0503181 [hep-ph].

[16] C. Flensburg, G. Gustafson, and L. Lönnblad, "Inclusive and Exclusive Observables from Dipoles in High Energy Collisions," *JHEP* **08** (2011) 103, arXiv:1103.4321 [hep-ph].

[17] C. Merino, C. Pajares, and J. Ranft, "Effects of interaction of strings in the Dual Parton Model," *Phys. Lett.* **B276** (1992) 168–172.

[18] H. J. Mohring, J. Ranft, C. Merino, and C. Pajares, "String fusion in the dual parton model and the production of anti-hyperons in heavy ion collisions," *Phys. Rev.* **D47** (1993) 4142–4145.

[19] H. Sorge, M. Berenguer, H. Stoecker, and W. Greiner, "Color rope formation and strange baryon production in ultrarelativistic heavy ion collisions," *Phys. Lett.* **B289** (1992) 6–11.

[20] M. Bleicher, W. Greiner, H. Stoecker, and N. Xu, "Strangeness enhancement from strong color fields at RHIC," *Phys. Rev.* **C62** (2000) 061901, arXiv:hep-ph/0007215 [hep-ph].

[21] S. Soff, J. Randrup, H. Stoecker, and N. Xu, "Effects of strong color fields on baryon dynamics," *Phys. Lett.* **B551** (2003) 115–120, arXiv:nucl-th/0209093 [nucl-th].

[22] B. Andersson, G. Gustafson, and B. Söderberg, "A General Model for Jet Fragmentation," *Z. Phys.* **C20** (1983) 317.

[23] B. Andersson and G. Gustafson, "Semiclassical Models for Gluon Jets and Leptoproduction Based on the Massless Relativistic String," *Z. Phys.* **C3** (1980) 223.

[24] B. Andersson, G. Gustafson, G. Ingelman, and T. Sjöstrand, "Parton Fragmentation and String Dynamics," *Phys. Rept.* **97** (1983) 31–145.

[25] A. Buckley *et al.*, "General-purpose event generators for LHC physics," *Phys. Rept.* **504** (2011) 145–233, `arXiv:1101.2599 [hep-ph]`.

[26] **DELPHI** Collaboration, K. Hamacher and M. Weierstall, "The Next round of hadronic generator tuning heavily based on identified particle data," `arXiv:hep-ex/9511011 [hep-ex]`.

[27] T. Sjöstrand, S. Ask, J. R. Christiansen, R. Corke, N. Desai, P. Ilten, S. Mrenna, S. Prestel, C. O. Rasmussen, and P. Z. Skands, "An Introduction to PYTHIA 8.2," *Comput. Phys. Commun.* **191** (2015) 159–177, `arXiv:1410.3012 [hep-ph]`.

[28] A. Casher, H. Neuberger, and S. Nussinov, "Chromoelectric Flux Tube Model of Particle Production," *Phys. Rev.* **D20** (1979) 179–188.

[29] B. Andersson, G. Gustafson, and T. Sjöstrand, "A Three-Dimensional Model for Quark and Gluon Jets," *Z. Phys.* **C6** (1980) 235.

[30] E. G. Gurvich, "The Quark Anti-Quark Pair Production Mechanism in a Quark Jet," *Phys. Lett.* **B87** (1979) 386–388.

[31] N. K. Glendenning and T. Matsui, "Creation of Anti-Q Q Pair in a Chromoelectric Flux Tube," *Phys. Rev.* **D28** (1983) 2890–2891.

[32] J. S. Schwinger, "On gauge invariance and vacuum polarization," *Phys. Rev.* **82** (1951) 664–679.

[33] E. Brezin and C. Itzykson, "Pair production in vacuum by an alternating field," *Phys. Rev.* **D2** (1970) 1191–1199.

[34] **UA5** Collaboration, G. J. Alner *et al.*, "Kaon Production in $\bar{p}p$ Reactions at a Center-of-mass Energy of 540-GeV," *Nucl. Phys.* **B258** (1985) 505–539.

[35] **H1** Collaboration, F. D. Aaron *et al.*, "Strangeness Production at low Q**2 in Deep-Inelastic ep Scattering at HERA," *Eur. Phys. J.* **C61** (2009) 185–205, `arXiv:0810.4036 [hep-ex]`.

[36] **CMS** Collaboration, V. Khachatryan *et al.*, "Strange Particle Production in *pp* Collisions at $\sqrt{s} = 0.9$ and 7 TeV," *JHEP* **05** (2011) 064, `arXiv:1102.4282 [hep-ex]`.

[37] J. Ambjørn, P. Olesen, and C. Peterson, "Stochastic Confinement and Dimensional Reduction. 2. Three-dimensional SU(2) Lattice Gauge Theory," *Nucl. Phys.* **B240** (1984) 533–542.

[38] G. S. Bali, "Casimir scaling of SU(3) static potentials," *Phys. Rev.* **D62** (2000) 114503, `arXiv:hep-lat/0006022 [hep-lat]`.

[39] A. H. Mueller, "Soft gluons in the infinite momentum wave function and the BFKL pomeron," *Nucl. Phys.* **B415** (1994) 373–385.

[40] A. H. Mueller and B. Patel, "Single and double BFKL pomeron exchange and a dipole picture of high-energy hard processes," *Nucl. Phys.* **B425** (1994) 471–488, `arXiv:hep-ph/9403256 [hep-ph]`.

[41] A. H. Mueller, "Unitarity and the BFKL pomeron," *Nucl. Phys.* **B437** (1995) 107–126, `arXiv:hep-ph/9408245 [hep-ph]`.

[42] L. D. McLerran and R. Venugopalan, "Computing quark and gluon distribution functions for very large nuclei," *Phys. Rev.* **D49** (1994) 2233–2241, `arXiv:hep-ph/9309289 [hep-ph]`.

[43] L. D. McLerran and R. Venugopalan, "Gluon distribution functions for very large nuclei at small transverse momentum," *Phys. Rev.* **D49** (1994) 3352–3355, `arXiv:hep-ph/9311205 [hep-ph]`.

[44] C. Flensburg, G. Gustafson, L. Lönnblad, and A. Ster, "Correlations in double parton distributions at small x," *JHEP* **06** (2011) 066, `arXiv:1103.4320 [hep-ph]`.

[45] C. Flensburg and G. Gustafson, "Fluctuations, Saturation, and Diffractive Excitation in High Energy Collisions," *JHEP* **10** (2010) 014, `arXiv:1004.5502 [hep-ph]`.

[46] C. Flensburg, G. Gustafson, and L. Lönnblad, "Exclusive final states in diffractive excitation," *JHEP* **12** (2012) 115, `arXiv:1210.2407 [hep-ph]`.

[47] C. Flensburg, "Correlations and Fluctuations in the Initial State of high energy Heavy Ion Collisions," `arXiv:1108.4862 [nucl-th]`.

[48] C. Flensburg, "Heavy ion inital states from DIPSY," *Prog. Theor. Phys. Suppl.* **193** (2012) 172–175.

[49] K. G. Wilson, "Confinement of Quarks," *Phys. Rev.* **D10** (1974) 2445–2459. [,45(1974)].

[50] B. Andersson and G. Gustafson, "Why are Vector Mesons Suppressed in Jet Fragmentation?," *LU-TP-82-5* (1982) .

[51] B. Andersson, G. Gustafson, and T. Sjöstrand, "A Model for Baryon Production in Quark and Gluon Jets," *Nucl. Phys.* **B197** (1982) 45–54.

[52] B. Andersson, G. Gustafson, and T. Sjöstrand, "Baryon Production in Jet Fragmentation and Υ Decay," *Phys. Scripta* **32** (1985) 574.

[53] S. Jeon and R. Venugopalan, "Random walks of partons in SU(N(c)) and classical representations of color charges in QCD at small x," *Phys. Rev.* **D70** (2004) 105012, `arXiv:hep-ph/0406169 [hep-ph]`.

[54] K. Johnson, "The M.I.T. Bag Model," *Acta Phys. Polon.* **B6** (1975) 865.

[55] K. Johnson and C. B. Thorn, "String-Like Solutions of the Bag Model," *Phys. Rev.* **D13** (1976) 1934.

[56] C. Semay, "About the Casimir scaling hypothesis," *Eur. Phys. J.* **A22** (2004) 353–354, `arXiv:hep-ph/0409105 [hep-ph]`.

[57] M. Cardoso, N. Cardoso, and P. Bicudo, "Lattice QCD computation of the colour fields for the static hybrid quark-gluon-antiquark system, and microscopic study of the Casimir scaling," *Phys. Rev.* **D81** (2010) 034504, `arXiv:0912.3181 [hep-lat]`.

[58] P. Cea, L. Cosmai, F. Cuteri, and A. Papa, "Flux tubes in the SU(3) vacuum: London penetration depth and coherence length," *Phys. Rev.* **D89** no. 9, (2014) 094505, `arXiv:1404.1172 [hep-lat]`.

[59] E. Avsar, G. Gustafson, and L. Lönnblad, "Small-x dipole evolution beyond the large-N(c) imit," *JHEP* **01** (2007) 012, `arXiv:hep-ph/0610157 [hep-ph]`.

[60] E. Avsar, G. Gustafson, and L. Lönnblad, "Diifractive excitation in DIS and *pp* collisions," *JHEP* **12** (2007) 012, `arXiv:0709.1368 [hep-ph]`.

[61] E. A. Kuraev, L. N. Lipatov, and V. S. Fadin, "The Pomeranchuk Singularity in Nonabelian Gauge Theories," *Sov. Phys. JETP* **45** (1977) 199–204. [Zh. Eksp. Teor. Fiz.72,377(1977)].

[62] I. I. Balitsky and L. N. Lipatov, "The Pomeranchuk Singularity in Quantum Chromodynamics," *Sov. J. Nucl. Phys.* **28** (1978) 822–829. [Yad. Fiz.28,1597(1978)].

[63] G. Gustafson, "Dual Description of a Confined Color Field," *Phys. Lett.* **B175** (1986) 453. [,193(1986)].

[64] G. Gustafson and U. Pettersson, "Dipole Formulation of QCD Cascades," *Nucl. Phys.* **B306** (1988) 746–758.

[65] L. Lönnblad, "ARIADNE version 4: A Program for simulation of QCD cascades implementing the color dipole model," *Comput. Phys. Commun.* **71** (1992) 15–31.

[66] T. Sjöstrand, S. Mrenna, and P. Z. Skands, "A Brief Introduction to PYTHIA 8.1," *Comput. Phys. Commun.* **178** (2008) 852–867, `arXiv:0710.3820 [hep-ph]`.

[67] L. Lönnblad, "Reconnecting colored dipoles," *Z. Phys.* **C70** (1996) 107–114.

[68] T. Sjöstrand and M. van Zijl, "A Multiple Interaction Model for the Event Structure in Hadron Collisions," *Phys. Rev.* **D36** (1987) 2019.

[69] G. Gustafson, U. Pettersson, and P. M. Zerwas, "Jet Final States in W W Pair Production and Color Screening in the QCD Vacuum," *Phys. Lett.* **B209** (1988) 90–94.

[70] T. Sjöstrand and V. A. Khoze, "Does the W mass reconstruction survive QCD effects?," *Phys. Rev. Lett.* **72** (1994) 28–31, `arXiv:hep-ph/9310276 [hep-ph]`.

[71] A. Edin, G. Ingelman, and J. Rathsman, "Soft color interactions as the origin of rapidity gaps in DIS," *Phys. Lett.* **B366** (1996) 371–378, `arXiv:hep-ph/9508386 [hep-ph]`.

[72] R. Enberg, G. Ingelman, and N. Timneanu, "Soft color interactions and diffractive hard scattering at the Tevatron," *Phys. Rev.* **D64** (2001) 114015, `arXiv:hep-ph/0106246 [hep-ph]`.

[73] B. Andersson, G. Gustafson, and B. Söderberg, "A Probability Measure on Parton and String States," *Nucl. Phys.* **B264** (1986) 29. [,145(1985)].

[74] B. Andersson, P. Dahlkvist, and G. Gustafson, "An Infrared Stable Multiplicity Measure on QCD Parton States," *Phys. Lett.* **B214** (1988) 604–608.

[75] L. Lönnblad, "ThePEG, Pythia7, herwig++ and Ariadne," *Nucl. Instrum. Meth.* **A559** (2006) 246–248.

[76] A. Karneyeu, L. Mijovic, S. Prestel, and P. Z. Skands, "MCPLOTS: a particle physics resource based on volunteer computing," *Eur. Phys. J.* **C74** (2014) 2714, `arXiv:1306.3436 [hep-ph]`.

[77] **STAR** Collaboration, J. Adams *et al.*, "Identified hadron spectra at large transverse momentum in p+p and d+Au collisions at s(NN)**(1/2) = 200-GeV," *Phys. Lett.* **B637** (2006) 161–169, `arXiv:nucl-ex/0601033 [nucl-ex]`.

[78] K. Werner, B. Guiot, I. Karpenko, and T. Pierog, "A unified description of the reaction dynamics from pp to pA to AA collisions," *Nucl. Phys.* **A931** (2014) 83–91, `arXiv:1411.1048 [nucl-th]`.

[79] N. Armesto, N. Borghini, S. Jeon, U. A. Wiedemann, S. Abreu, V. Akkelin, J. Alam, J. L. Albacete, A. Andronic, D. Antonov, *et al.*, "Heavy Ion Collisions at the LHC - Last Call for Predictions," *J. Phys.* **G35** (2008) 054001, `arXiv:0711.0974 [hep-ph]`.

[80] A. Ortiz Velasquez, P. Christiansen, E. Cuautle Flores, I. Maldonado Cervantes, and G. Paić, "Color Reconnection and Flowlike Patterns in *pp* Collisions," *Phys. Rev. Lett.* **111** no. 4, (2013) 042001, `arXiv:1303.6326 [hep-ph]`.

[81] **ALICE** Collaboration, B. B. Abelev *et al.*, "Production of charged pions, kaons and protons at large transverse momenta in pp and Pb–Pb collisions at $\sqrt{s_{NN}}$ =2.76 TeV," *Phys. Lett.* **B736** (2014) 196–207, `arXiv:1401.1250 [nucl-ex]`.

[82] R. Engel and J. Ranft, "Hadronic photon-photon interactions at high-energies," *Phys. Rev.* **D54** (1996) 4244–4262, `arXiv:hep-ph/9509373 [hep-ph]`.

[83] J. M. Butterworth, J. R. Forshaw, and M. H. Seymour, "Multiparton interactions in photoproduction at HERA," *Z. Phys.* **C72** (1996) 637–646, `arXiv:hep-ph/9601371 [hep-ph]`.

[84] V. S. Fadin and L. N. Lipatov, "BFKL pomeron in the next-to-leading approximation," *Phys. Lett.* **B429** (1998) 127–134, `arXiv:hep-ph/9802290 [hep-ph]`.

[85] M. Ciafaloni and G. Camici, "Energy scale(s) and next-to-leading BFKL equation," *Phys. Lett.* **B430** (1998) 349–354, `arXiv:hep-ph/9803389 [hep-ph]`.

[86] G. P. Salam, "An Introduction to leading and next-to-leading BFKL," *Acta Phys. Polon.* **B30** (1999) 3679–3705, `arXiv:hep-ph/9910492 [hep-ph]`.

[87] J. Kwiecinski, A. D. Martin, and P. J. Sutton, "Constraints on gluon evolution at small x," *Z. Phys.* **C71** (1996) 585–594, `arXiv:hep-ph/9602320 [hep-ph]`.

[88] B. Andersson, G. Gustafson, and J. Samuelsson, "The Linked dipole chain model for DIS," *Nucl. Phys.* **B467** (1996) 443–478.

[89] I. Balitsky, "Operator expansion for high-energy scattering," *Nucl. Phys.* **B463** (1996) 99–160, `arXiv:hep-ph/9509348 [hep-ph]`.

[90] Y. V. Kovchegov, "Small x F(2) structure function of a nucleus including multiple pomeron exchanges," *Phys. Rev.* **D60** (1999) 034008, `arXiv:hep-ph/9901281 [hep-ph]`.

[91] A. Buckley, J. Butterworth, L. Lönnblad, D. Grellscheid, H. Hoeth, J. Monk, H. Schulz, and F. Siegert, "Rivet user manual," *Comput. Phys. Commun.* **184** (2013) 2803–2819, `arXiv:1003.0694 [hep-ph]`.

[92] A. Buckley, H. Hoeth, H. Lacker, H. Schulz, and J. E. von Seggern, "Systematic event generator tuning for the LHC," *Eur. Phys. J.* **C65** (2010) 331–357, `arXiv:0907.2973 [hep-ph]`.

[93] **DELPHI** Collaboration, P. Abreu *et al.*, "Tuning and test of fragmentation models based on identified particles and precision event shape data," *Z. Phys.* **C73** (1996) 11–60.

[94] **ATLAS** Collaboration, G. Aad *et al.*, "Charged-particle multiplicities in pp interactions measured with the ATLAS detector at the LHC," *New J. Phys.* **13** (2011) 053033, `arXiv:1012.5104 [hep-ex]`.

II

Effects of Colour Reconnection on Hadron Flavour Observables

Christian Bierlich[1], and Jesper Roy Christiansen[1].

[1] Dept. of Astronomy and Theoretical Physics, Lund University, Sölvegatan 14A, SE-223 62 Lund, Sweden.

ABSTRACT: We present a series of observables for soft inclusive physics, and utilize them for comparison between two recently developed colour reconnection models; the new colour reconnection model in PYTHIA and the DIPSY rope hadronization model. The observables are ratios of identified hadron yields as a function of the final-state activity, as measured by the charged multiplicity. Since both considered models have a nontrivial dependence on the final-state activity, the above observables serve as excellent probes to test the effect of these models. Both models show a clear baryon enhancement with increasing multiplicity, while only the DIPSY rope model leads to a strangeness enhancement. Flow-like patterns, previously found to be connected to colour reconnection models, are investigated for the new models. Only PYTHIA shows a $p_\perp$-dependent enhancement of the Λ/K ratio as the final-state activity increases, with the enhancement being largest in the mid-$p_\perp$ region.

1   Introduction

The first run of the LHC has provided a large number of measurements probing both soft and hard QCD, and thereby a large number of tests for the Monte Carlo event generators. Even though the overall performance of the event generators have been quite good, there are still some phenomena that are insufficiently understood [1]. One of the more intriguing soft QCD deviations is the observed enhancement of Λ production [2, 3]. No model has been simultaneously able to describe the identified hadron spectra at both LEP and LHC. This has led to the development of several phenomenological models [4, 5, 6], partly aimed to address this problem. With the planned low pile-up runs at the beginning of the second LHC run, it is now an ideal time to test these models further, and thereby probe the physical origin of the Λ enhancement. In this study we consider two of the models: the new colour reconnection (CR) model in the PYTHIA event generator [5, 7] and the colour rope model in the DIPSY event generator [4, 8, 9]. The models have previously been compared to pp data at $\sqrt{s}$ of 200, 900 and 7000 GeV. In this paper new possible observables to test the models are suggested, and predictions are made for collisions at $\sqrt{s} = 13$ TeV. The observables are not model dependent, and can be used for constraining predictions from other models of soft inclusive physics. Both considered colour reconnection models are built upon the Lund model for string hadronization [10]. Nonperturbative differences can therefore be ascribed to differences in the new phenomenological ideas.

One of the key ideas for the two models in question is *jet universality*. Stated in terms of the string model, it essentially means that fragmentation of a string does not depend on how the string is formed. Free strings at both lepton and hadron colliders should thus hadronize in a similar fashion. Fragmentation parameters are therefore tuned in the clean $e^+e^- \rightarrow Z \rightarrow q\bar{q}$ environment, and then directly applied to hadron colliders. Any discrepancy has to be due to physical phenomena not active at lepton colliders. For all the models attempting to describe the Λ enhancement, the enhancement is linked to the increased density of quarks and gluons in the final state at hadron colliders[1]. It would therefore be of natural interest to measure the Λ enhancement as a function of this density. The quark-gluon density is experimentally ill-defined, however, and we suggest to use the number of charged tracks in the forward region as a measure of final-state activity. A similar idea for using the hyperon-to-meson ratio to search for indications of a miniQGP was suggested in ref. [11]. We suggest ratios that allows for separation of strangeness enhancement from baryon enhancement, which both could be present in the hyperon-to-meson ratio.

Another puzzling observation is the indication of collective effects in high-multiplicity pp collisions [12, 13], often interpreted as the presence of flow. These effects were only expected in the dense medium of heavy ion collisions, where the pressure gradients give rise to flow effects. A study of the models for pp collisions showed that CR generated similar effects

---

[1]Sometimes also referred to as string density, colour density, or energy density.

even without the introduction of a thermalized medium [14]. We therefore consider one of the standard observables in heavy ion physics, that of identified particle ratios as a function of $p_\perp$, separated into bins of centrality, and compare the model predictions for pp collisions. Since centrality is not experimentally well defined in pp collisions, the number of charged tracks in the forward region is used as a measure of activity.

The outline of the paper is as follows. In section 2 we will briefly recap the most important features of the two models considered. Comparison to existing e^+e^- data at $\sqrt{s} = 91.2$ GeV, and pp data at $\sqrt{s}$ of 200 GeV and 7 TeV, is shown in section 3. The event selection and tuning for 13 TeV is described in section 4. In section 5, the predictions at $\sqrt{s} = 13$ TeV, for the second run of LHC, are presented. Finally, in section 6, we summarize and present an outlook.

2   The models

Both models for colour reconnection are built upon the Lund string model for hadronization. In this model, outgoing partons are connected with stringlike colour fields, which fragment into hadrons when moving apart. The model contains two main parameters relevant to this study, which determine the suppression of strange quarks and of diquarks (giving baryons) in the break ups. Assuming jet universality, these parameters are tuned to LEP data.

Baryons can in addition be created around string junctions, which can arise as a consequence of colour reconnection. Consider the simple configuration of two $q\bar{q}$ dipoles in figure 2.1, which for example could have originated from a decay of two W-bosons in a LEP environment, as described in ref. [15]. What essentially could be described as a quadrupole configuration is instead described as either the original (on top) or the left configuration in figure 2.1. Without CR only the original configuration is considered. Extending this type of colour reconnection to hadron colliders has been shown [16] to be a necessary condition to describe the rising of $\langle p_\perp \rangle (N_{ch})$ distributions. The QCD ε-tensor gives rise to the rightmost configuration, containing two junction connections, depicted as empty circles. Since such junctions constitute proto-baryons, in the same way string segments constitute proto-mesons, they become an additional source of baryons.

2.1   Colour reconnection in PYTHIA

The new CR model in PYTHIA is situated just prior to the hadronization. It takes the leading-colour ($N_c \to \infty$) strings and transform them to a different colour configuration based on three principles: firstly the SU(3) colour rules from QCD determine if two strings
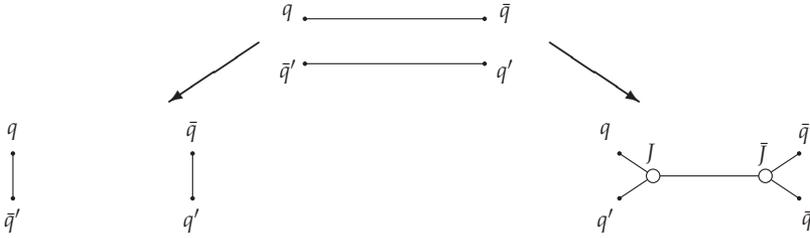
Figure 2.1: Sketch of how two $q\bar{q}$ dipoles (top) can be reconnected to different colour topologies (left and right). The right connection gives rise to a double junction, which in turn will produce baryons. Notice that the placement of the pairs differs in the junction figure.

are colour compatible (*e.g.* there is only a 1/9 probability that the top configuration of figure 2.1 can transform to the left configuration purely from colour considerations). Secondly a simplistic space-time picture to check causal contact between the strings. Finally the λ measure [17] (which is a string-length measure, $\lambda = \sum_i \log(1 + m_i^2/(2m_0^2))$ where the sum goes over all dipoles, m_i is the invariant mass of the dipole and m_0 is a parameter) to decide whether a possible reconnection is actually favoured. Since the model relies purely on the outgoing partons, it is in principle applicable to any type of collision. So far it has only been tested for *pp* [5] and *ee* collisions [18]. The main extension compared to the other CR models in PYTHIA is the introduction of reconnections that form junction structures. From a pure colour consideration the probability to form a junction topology is three times larger than an ordinary reconnection. The junction will introduce additional strings, however, and it is therefore often disfavoured due to a larger λ measure. Given the close connection between junctions and baryons, the new model predicts a baryon enhancement. It was shown to be able to simultaneously describe the Λ production for both LEP and LHC experiments, which neither of the earlier PYTHIA tunes have been able to.

The new CR model essentially contains two new parameters: a parameter that constrains the overall strength of the CR, and a parameter that controls the baryon enhancement. Both of these parameters were tuned to data [3, 19] from the LHC experiments at 7 TeV.

2.2   Rope hadronization in DIPSY

Rope hadronization [20] is a normer for QCD inspired models, which includes interactions between strings. From previous attempts to include this effect in Monte Carlo generators [21], it is well known that strange and baryonic content will rise in very dense events.

A model introducing rope hadronization was recently developed and implemented in the event generator DIPSY [4]. Along with a final-state swing, the model introduces local calculation of string density, and corrects the evolution of the final-state parton shower and hadronization based on this local density.

The model is based upon the idea [20] that when several parton pairs are next to each other in geometric space, they can act together coherently to form a colour rope. Each string is treated as a flux tube with a fixed radius, and the amount of overlap between strings, in impact parameter space and rapidity, can be directly calculated.

If such an overlap is found to exist, it can have different effects, determined by SU(3) colour rules. The overlapping strings can end up in a colour singlet configuration. This is handled by a final-state "swing", that reconnects colour dipoles, in the final-state parton shower as the transformation from the top to the bottom left configuration in figure 2.1. In all other cases, the strings end up forming a "rope". This is hadronized with a higher effective string tension, reflecting the fact that more energy is available for the fragmentation, in accordance with results from lattice QCD [22]. In some cases, the strings forming the rope end up in a junction structure. In such cases the junction pair is handled using a simple approach, where the two junctions collapse to either two diquarks or two quarks, with a probability controlled by a tuneable parameter. The resulting strings are then hadronized with the appropriate effective string tension.

An increased string tension results in more strange quarks and diquarks produced in string breakups. Since the effect increases with the density of quarks and gluons in the final state, the expected outcome is more baryons and strangeness among the resulting hadrons. The model includes two free parameters; the string radius and the probability for a junction to resolve to diquarks. Both are tuned to LHC data [3] at 7 TeV.

3 Comparison to data

The models performs as intended when comparing to existing data. Ratios of baryons to mesons are enhanced for both models, whereas ratios of particles with strange quark content is enhanced only in the DIPSY rope model. Comparisons are done to ratios of integrated yields of identified particles, using the analyses published through the Rivet [23] framework. The raw results from comparing the Monte Carlo to data using Rivet, are integrated to give figures 2.2 and 2.3, using Matplotlib [24]. Error estimates are conservative, as they assume the error of all bins are fully correlated.

In figure 2.2, a comparison to LEP data [25, 26, 27] is seen. Two conclusions can be drawn from this figure. First of all, these are the data the original string model is tuned to. The fact that the Monte Carlo is so well aligned with data is thus not an indication that the string model predicts all these ratios so well, but rather that the parameters of the model are tuned to these data. The exception here is the Ω baryon[2], reflected in the Ω/Ξ ratio,

---

[2]We denote a particle and its antiparticle with just a single letter such that *e.g.p* means both proton and anti-proton. Special cases are π with denotes $\pi^+\pi^-$, K which denotes $K^+K^-K^0_sK^0_L$ and Ξ which denotes
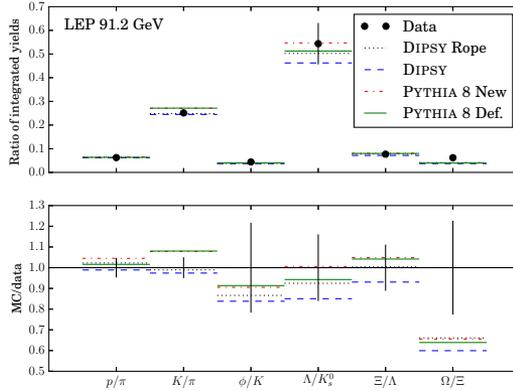
Figure 2.2: Comparison to e^+e^- at 91.2 GeV from ALEPH, SLD and PDG. Color online.

which lies below the observed value. However, the experimental statistical uncertainty is large for this ratio.

The other conclusion, which is the most relevant for this article, is that only small effects at LEP data is observed. The Λ/K ratio increases by about 10 % for both the DIPSY rope model and the new CR model in PYTHIA (over their respective default models), but all models stay within the experimental uncertainty. The overall low variance is exactly what is expected, due to the low final state activity at LEP.

In figure 2.3 comparison to STAR data [28, 29, 30] at 200 GeV indicated that the description of the baryon to meson ratios improves with both models, while the description of the Ξ/Λ ratio only improves with the DIPSY rope model. The change in the $K^\pm/\pi$ ratio is not visible on this scale for this energy.

Comparison to 7 TeV data from ALICE [31, 32] and CMS [3] confirms that the description improves, even for the Ω/Ξ ratio. The description of the p/π ratio is seen to be somewhat worse with the new models. This could either have a mundane explanation originating in the fact that the very low-$p_\perp$ area of the individual distributions (which contains most of the multiplicity) are not fully understood, or have further reaching consequences. We point to the measurements suggested in the next section of this paper to shed light on this issue.

$\Xi^+\Xi^-$.
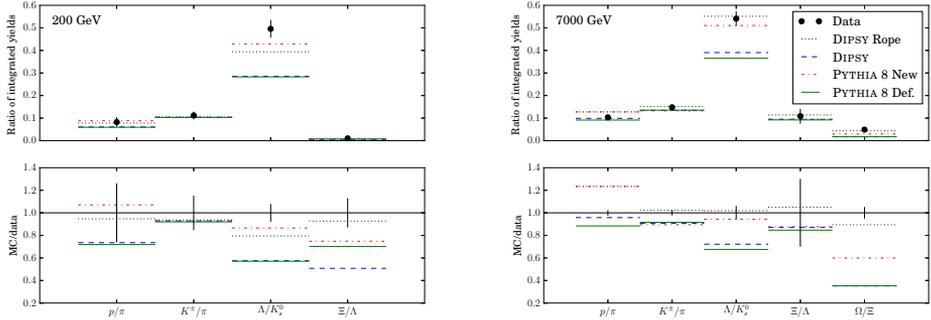
Figure 2.3: Comparison to *pp* data at 200 GeV from STAR (left) and at 7 TeV from ALICE and CMS (right). Color online.

4 Tuning and event selection

Before studying exclusive observables at 13 TeV, it is necessary to verify that the baselines for the two models agree reasonable well. Normally this is achieved by tuning the models to the available data. Data at $\sqrt{s} = 13$ TeV is, however, not yet published in a state where event generators can be tuned to it, so the DIPSY model was instead tuned to the PYTHIA predictions for $dN_{ch}/d\eta$, $\langle p_\perp \rangle (N_{ch})$ and the multiplicity distribution. Both models will eventually have to be retuned, when more data, in a suitable format for tuning, become available. Only small effects are expected from the retuning, firstly due to fragmentation mainly being determined from LEP data, and secondly since the already presented results at 13 TeV show a good agreement between the Monash tune and the data [33, 34]. The full list of all parameters changed from their default values is included in an appendix.

An event and particle selection was implemented to mimic a possible experimental setup. Each particle is required to have $p_\perp > 0.15$ GeV. Two different η regions are used; a forward region ($2 < |\eta| < 5$) to measure the activity, and a central region ($|\eta| < 1$) to measure the identified hadron yields. The reason for the split is to avoid any potential bias, which otherwise happens at low N_{ch}, in particular for ratios involving both charged and non-charged hadrons. Since DIPSY does not have a model for diffraction, only non-diffractive events are considered for both models. To reflect this in the event selection, only events with at least six forward charged particles are considered.

All particles with $c\tau > 10$ mm are treated as stable. In practice this means that $\pi^\pm, K, \Lambda, \Xi$ and Ω are all stable whereas ϕ (which decays strongly) is not. This introduces some double counting in the ϕ/K-ratio, where a ϕ can potentially be counted in the numerator and its decay products in the denominator.
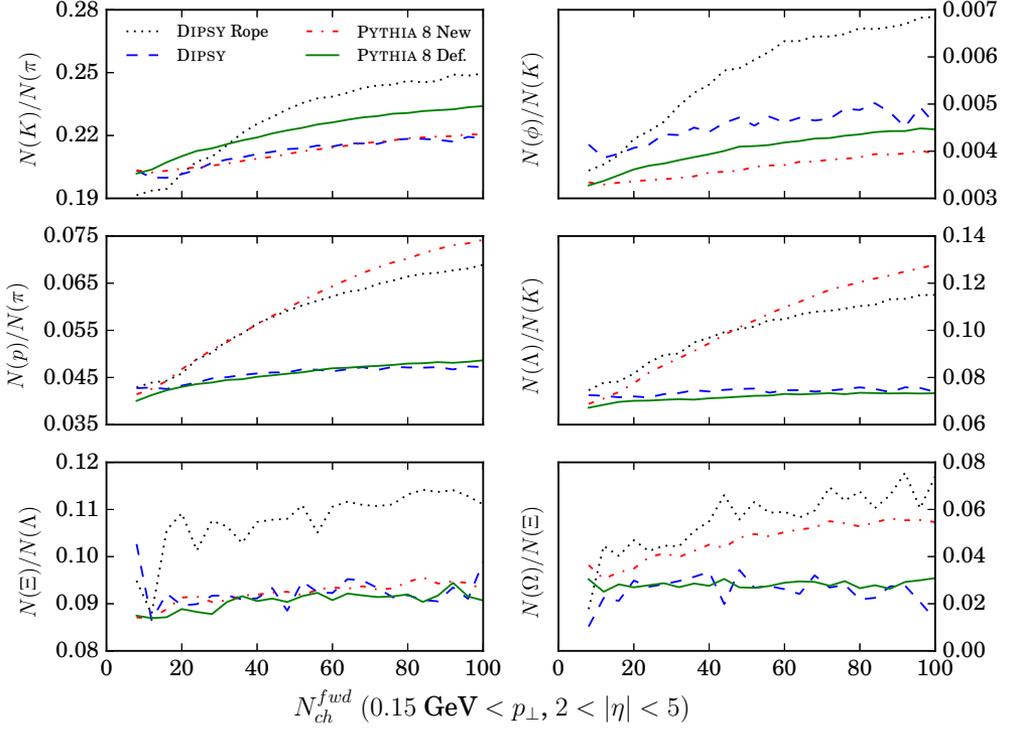
Figure 2.4: Ratios of identified hadrons as functions of N_{ch}^{fwd} at $\sqrt{s} = 13$ TeV. The top row shows meson ratios with the numerator having one more strange quark than the denominator. The middle row shows baryon to meson ratios, with same amount of strange quarks. The bottom row shows baryon ratios with the numerator having one more strange quark than the denominator. Note that the vertical axis differs between the figures and that zero is suppressed.

5 Predictions for 13 TeV

Differences between the colour reconnection models are best determined using observables controlled by hadronization effects. Ratios of identified particles is exactly such an observable, since particle species production is determined by the quark and diquark content in string breaks. In the first part of this section, ratios of identified particles are shown as a function of N_{ch} in the forward region, as a measure of event activity. Then flow-like effects are considered, by showing $(\Lambda/K)\,(p_\perp)$ in four different bins of N_{ch} in the forward region.

5.1 Particle ratios

Ratios of hadrons with different strange and baryon numbers as function of event activity, measured as functions of N_{ch}^{fwd}, are shown in figure 2.4. The strangeness enhancement in meson production is probed by the K/π and ϕ/K ratios, for which the numerator always contains one more strange quark than the denominator. As expected, only the DIPSY rope model shows an enhancement relative to the baseline, since it contains a strangeness enhancement. The new PYTHIA CR model lies slightly below the baseline. This can be explained by phase-space constraints for low invariant-mass strings, which the new model produces more of. It should be recalled that both the new as well as the old models are capable of describing the total K_s^0 yield at 7 TeV. Thus, the limited effects in this ratio is somewhat expected. The ϕ/K ratio shows more promise as a means to distinguish between the two models, since the DIPSY model shows a larger enhancement. It is, however, more experimentally challenging.

The baryon enhancement is tested for both hadrons containing zero or one strange quark, p/π and Λ/K. For both ratios, and both models, clear enhancements are expected and seen. For the Λ/K ratio both models agree quite well, which is not surprising, given that both models are tuned to describe the inclusive Λ/K distributions at 7 TeV. A similar picture is seen for the p/π ratio, indicating similar predictions for the baryon enhancement from both the models.

The multistrange baryon enhancement is tested in the same way as the strange-meson enhancement by considering the ratios Ξ/Λ and Ω/Ξ. The large variations at low multiplicity for both distributions are due to statistical fluctuations. For Ξ/Λ the DIPSY rope model shows a clear enhancement as opposed to the new PYTHIA CR model. The Λ/p ratio is not shown, but the enhancement is similar to the enhancement of Ξ/Λ. An enhancement is seen for both models in the Ω/Ξ, with the enhancement factor being around 2.5 for the DIPSY rope model in the highest multiplicity bins. This is larger than any of the other enhancements seen. The enhancement for the new PYTHIA CR model is somewhat surprising, as the increased junction production should be equal for both Ξ and Ω. The production of Ω in the standard PYTHIA fragmentation is, however, significantly suppressed, as the production of ss-diquarks is disfavoured. This suppression is not present in the junction handling, since it takes two already formed quarks and combine into a diquark. The enhancement in the new PYTHIA model should therefore not be interpreted as a "real" strangeness enhancement, but more as an absence of suppression of ss diquarks. For the DIPSY model the above effect is also present, but there is an additional enhancement of strangeness and diquarks. It should be noted that the Ω baseline from LEP is not that well constrained, due to a large experimental uncertainty, and the model predictions are below the actual measurements. A measurement of $(\Omega/\Xi)(N_{ch})$ would cast light on whether an actual activity-based enhancement takes place.

Increased hyperon production in high activity *pp* events have previously been associated with production of a miniQGP [11]. The hyperon-to-pion ratio is only indirectly shown in figure 2.4, but the rise is similar to the one predicted by miniQGP. The new models therefore provide an alternative explanation, if such an enhancement is observed.

5.2   Flow-like effects

The Λ/K ratio as a function of $p_\perp$ for different N_{ch}^{fwd} ranges is shown in figure 2.5. The two models show different behaviours for the different multiplicity ranges: the DIPSY rope model only gives a small enhancement ($\sim 10\%$ at maximum) between the lowest and highest multiplicity regions. Even though the differential enhancement is generally below 10 %, the enhancement of the ratio of integrated yields is about 20 %, which is in good agreement with figure 2.4. It should be noted that the DIPSY model is inadequate in describing the high $p_\perp$ tails ($p_\perp >\sim 4$ GeV). This was observed for 900 GeV and 7 TeV in ref. [4].

The new PYTHIA CR model shows a clear change in $p_\perp$ with increasing multiplicity. The enhancement is largest in the mid-$p_\perp$ region ($p_\perp \sim 2 - 6$ GeV), leading to a "peak" structure. This structure looks qualitatively similar to what is observed in *PbPb* and *pPb* collisions [35, 36]. The peak also moves towards larger $p_\perp$ with increased multiplicity, an effect normally attributed to radial flow in heavy ion collisions [37]. That the new CR model predicts a qualitatively similar effect in *pp* collisions is quite intriguing and strengthens the hint at a potential connection between flow and CR effects already observed [14].

6   Conclusions

A series of new model-independent observables, well suited for distinguishing between between different physical models for soft inclusive physics is suggested. The observables are ratios of identified hadrons measured as a function of event activity, with the identified hadrons chosen such that a distinction is made between baryon-only, strangeness-only and baryon-and-strangeness enhancement. Measurement of these observables at present and future energies at *pp* colliders is encouraged, as the can serve as constraints on any soft physics model aiming to explain low-multiplicity and minimum bias data simultaneously.

The observables are, in this article, used to separate two new CR models. The new CR model in PYTHIA only contains a baryon enhancement with increasing multiplicity, while the DIPSY rope models contains both a baryon and a strangeness enhancement. The multi-strange hyperon ratios, as well as the ϕ/K ratio, provide clear observables for distinguishing between the two models. It should be mentioned that this is already possible to observe
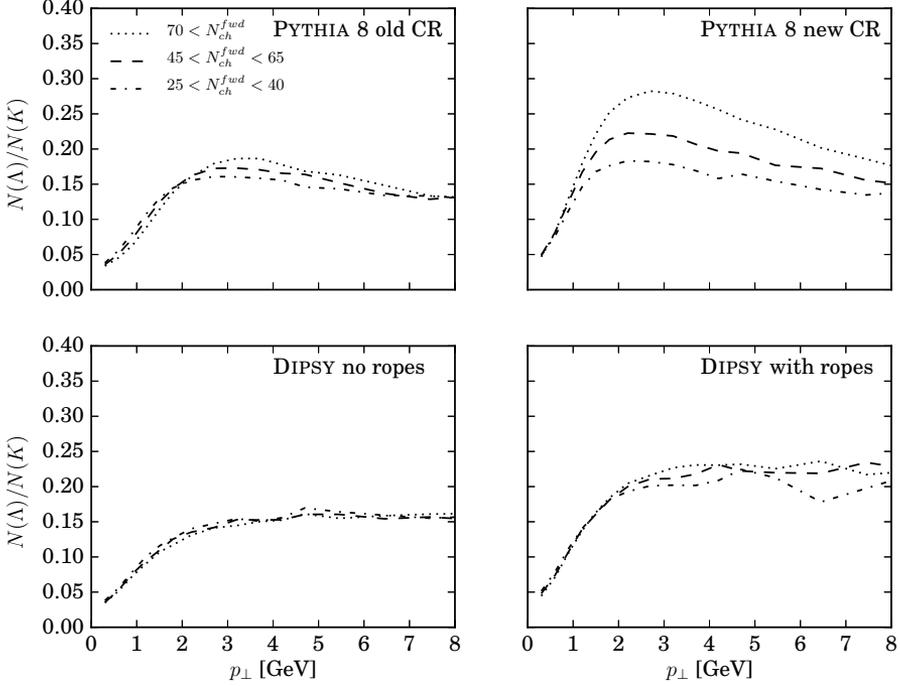
Figure 2.5: Ratio of Λ/K as a function of $p_\perp$ in three bins of N_{ch}^{fwd}. In the right column the new colour reconnection models are shown, and in the left column the old ones.

in inclusive measurements, but the separation into different multiplicity regions highlights the enhancement.

Both new models are based on interactions between strings in the hadronization phase, and confirmation of the common predictions made by the two models is a direct hint that colour reconnections among strings are of physical importance. Both baseline models show almost no dependency on multiplicity for the identified hadron yield ratios. Therefore, any observed dependency would provide a clearer indication that the old models miss a feature, better than an inclusive measurement alone could provide. We therefore strongly suggest that these observables should be measured at the LHC experiments. In this paper we only studied the effects at a center-of-mass energy of 13 TeV, but the effects should also be visible in the already collected data at 7 TeV.

We have also shown that one of the CR models predicts effects similar to those normally attributed to radial flow in heavy ion collisions. This is in agreement with earlier indications that also hint at a connection between the two phenomena. It should however be recalled that neither of the models provide a satisfactory description of the individual $p_\perp$ spectra for the identified hadrons. And before these are fully understood, claims of connections

Table 2.1: Table of parameters of the string hadronization model, which differs from Monash tune [33] default values. The changed parameters have been retuned to LEP and SLD data, cf. figure 2.2

Fragmentation parameter	Pythia def.	Pythia new	DIPSY	DIPSY rope
StringPT:sigma	0.335	0.335	0.32	0.31
StringZ:aLund	0.68	0.36	0.30	0.41
StringZ:bLund	0.98	0.56	0.36	0.37
StringFlav:probQQtoQ	0.081	0.078	0.082	0.073
StringFlav:ProbStoUD	0.217	0.22	0.22	0.21
	0.5	0.0275	–	–
StringFlav:probQQ1toQQ0join	0.7	0.0275	–	–
	0.9	0.0275	–	–
	1.0	0.0275	–	–

between flow and CR may be premature.

7 Acknowledgements

2.A Model parameters

A complete list of all the parameters that differ from their default values for the considered models.

Hadronization model parameters are found in table 2.1, Pythia parameters in table 2.2 and DIPSY parameters in tables 2.3 and 2.4.

Table 2.2: The new Pythia CR model introduces a number of new parameters, and requires retuning of a few old ones, besides hadronization. The details of the retuning can be found in ref. [5].

PYTHIA parameter	Default	New
MultiPartonInteractions:pT0Ref	2.28	2.15
BeamRemnants:remnantMode	0	1
BeamRemnants:saturation	–	5
ColourReconnection:mode	0	1
ColourReconnection:allowDoubleJunRem	on	off
ColourReconnection:m0	–	0.3
ColourReconnection:allowJunctions	–	on
ColourReconnection:junctionCorrection	–	1.2
ColourReconnection:timeDilationMode	–	2
ColourReconnection:timeDilationPar	–	0.18

Table 2.3: The DIPSY rope model introduces three extra parameters, which are fixed using pp data from LHC. See ref. [4] for the meaning of the parameters.

DIPSY parameter	Default	Rope
FragmentationScheme	default	dipole
StringR0	–	0.773
Stringm0	–	0.113
BetaPopcorn	–	0.2

Table 2.4: The DIPSY initial state model needs retuning at each energy to reproduce total charged multiplicity. See ref. [9] for the meaning of the parameters.

Energy	pp 200 GeV		pp 7 TeV		pp 13 TeV	
DIPSY parameter	Default	Rope	Default	Rope	Default	Rope
LambdaQCD	0.29	0.26	0.17	0.25	0.29	0.27
RMax	2.32	3.34	3.23	2.90	1.05	3.39
PMinusOrdering	1.05	0.98	1.24	0.67	0.31	0.75
PTScale	0.70	0.92	1.60	1.65	1.28	1.35

References

[1] A. De Roeck, "Experimental results on quantum chromo dynamics: what is next?," *Phys. Scripta* **T158** (2013) 014001.

[2] **ALICE** Collaboration, K. Aamodt *et al.*, "Strange particle production in proton-proton collisions at sqrt(s) = 0.9 TeV with ALICE at the LHC," *Eur. Phys. J.* **C71** (2011) 1594, arXiv:1012.3257 [hep-ex].

[3] **CMS** Collaboration, V. Khachatryan *et al.*, "Strange Particle Production in pp Collisions at $\sqrt{s} = 0.9$ and 7 TeV," *JHEP* **05** (2011) 064, arXiv:1102.4282 [hep-ex].

[4] C. Bierlich, G. Gustafson, L. Lönnblad, and A. Tarasov, "Effects of Overlapping Strings in pp Collisions," *JHEP* **03** (2015) 148, arXiv:1412.6259 [hep-ph].

[5] J. R. Christiansen and P. Z. Skands, "String Formation Beyond Leading Colour," *JHEP* **08** (2015) 003, arXiv:1505.01681 [hep-ph].

[6] T. Pierog, I. Karpenko, J. M. Katzy, E. Yatsenko, and K. Werner, "EPOS LHC: Test of collective hadronization with data measured at the CERN Large Hadron Collider," *Phys. Rev.* **C92** no. 3, (2015) 034906, arXiv:1306.0121 [hep-ph].

[7] T. Sjöstrand, S. Ask, J. R. Christiansen, R. Corke, N. Desai, P. Ilten, S. Mrenna, S. Prestel, C. O. Rasmussen, and P. Z. Skands, "An Introduction to PYTHIA 8.2," *Comput. Phys. Commun.* **191** (2015) 159–177, arXiv:1410.3012 [hep-ph].

[8] E. Avsar, G. Gustafson, and L. Lönnblad, "Energy conservation and saturation in small-x evolution," *JHEP* **07** (2005) 062, arXiv:hep-ph/0503181 [hep-ph].

[9] C. Flensburg, G. Gustafson, and L. Lönnblad, "Inclusive and Exclusive Observables from Dipoles in High Energy Collisions," *JHEP* **08** (2011) 103, arXiv:1103.4321 [hep-ph].

[10] B. Andersson, G. Gustafson, G. Ingelman, and T. Sjöstrand, "Parton Fragmentation and String Dynamics," *Phys. Rept.* **97** (1983) 31–145.

[11] V. Topor Pop, M. Gyulassy, J. Barrette, C. Gale, and A. Warburton, "Can hyperon/meson ratios in rare high multiplicity pp collisions at Large Hadron Collider energies provide signatures of mini-quark-gluon plasma formation?," *Phys. Rev.* **C86** (2012) 044902, arXiv:1203.6679 [hep-ph].

[12] A. Kisiel, "Signatures of collective flow in high multiplicity pp collisions," *Phys. Rev.* **C84** (2011) 044913, arXiv:1012.1517 [nucl-th].

[13] **CMS** Collaboration, V. Khachatryan *et al.*, "Observation of Long-Range Near-Side Angular Correlations in Proton-Proton Collisions at the LHC," *JHEP* **09** (2010) 091, arXiv:1009.4122 [hep-ex].

[14] A. Ortiz Velasquez, P. Christiansen, E. Cuautle Flores, I. Maldonado Cervantes, and G. Paić, "Color Reconnection and Flowlike Patterns in *pp* Collisions," *Phys. Rev. Lett.* **111** no. 4, (2013) 042001, arXiv:1303.6326 [hep-ph].

[15] T. Sjöstrand and V. A. Khoze, "On Color rearrangement in hadronic W+ W- events," *Z. Phys.* **C62** (1994) 281–310, arXiv:hep-ph/9310242 [hep-ph].

[16] T. Sjöstrand and M. van Zijl, "A Multiple Interaction Model for the Event Structure in Hadron Collisions," *Phys. Rev.* **D36** (1987) 2019.

[17] B. Andersson, "The Lund model," *Camb. Monogr. Part. Phys. Nucl. Phys. Cosmol.* **7** (1997) 1–471.

[18] J. R. Christiansen and T. Sjöstrand, "Color reconnection at future e^+ e^- colliders," *Eur. Phys. J.* **C75** no. 9, (2015) 441, arXiv:1506.09085 [hep-ph].

[19] **ATLAS** Collaboration, G. Aad *et al.*, "Charged-particle multiplicities in pp interactions measured with the ATLAS detector at the LHC," *New J. Phys.* **13** (2011) 053033, arXiv:1012.5104 [hep-ex].

[20] T. S. Biro, H. B. Nielsen, and J. Knoll, "Color Rope Model for Extreme Relativistic Heavy Ion Collisions," *Nucl. Phys.* **B245** (1984) 449–468.

[21] H. Sorge, M. Berenguer, H. Stoecker, and W. Greiner, "Color rope formation and strange baryon production in ultrarelativistic heavy ion collisions," *Phys. Lett.* **B289** (1992) 6–11.

[22] G. S. Bali, "Casimir scaling of SU(3) static potentials," *Phys. Rev.* **D62** (2000) 114503, `arXiv:hep-lat/0006022 [hep-lat]`.

[23] A. Buckley, J. Butterworth, L. Lönnblad, D. Grellscheid, H. Hoeth, J. Monk, H. Schulz, and F. Siegert, "Rivet user manual," *Comput. Phys. Commun.* **184** (2013) 2803–2819, `arXiv:1003.0694 [hep-ph]`.

[24] J. D. Hunter, "Matplotlib: A 2d graphics environment," *Computing In Science & Engineering* **9** no. 3, (2007) 90–95.

[25] **ALEPH** Collaboration, R. Barate *et al.*, "Studies of quantum chromodynamics with the ALEPH detector," *Phys. Rept.* **294** (1998) 1–165.

[26] **SLD** Collaboration, K. Abe *et al.*, "Production of pi+, pi-, K+, K-, p and anti-p in light (uds), c and b jets from Z0 decays," *Phys. Rev.* **D69** (2004) 072003, `arXiv:hep-ex/0310017 [hep-ex]`.

[27] **Particle Data Group** Collaboration, C. Amsler *et al.*, "Review of Particle Physics," *Phys. Lett.* **B667** (2008) 1–1340.

[28] **STAR** Collaboration, B. I. Abelev *et al.*, "Systematic Measurements of Identified Particle Spectra in pp, d^+ Au and Au+Au Collisions from STAR," *Phys. Rev.* **C79** (2009) 034909, `arXiv:0808.2041 [nucl-ex]`.

[29] **STAR** Collaboration, B. I. Abelev *et al.*, "Strange particle production in p+p collisions at s**(1/2) = 200-GeV," *Phys. Rev.* **C75** (2007) 064901, `arXiv:nucl-ex/0607033 [nucl-ex]`.

[30] **STAR** Collaboration, J. Adams *et al.*, "Identified hadron spectra at large transverse momentum in p+p and d+Au collisions at s(NN)**(1/2) = 200-GeV," *Phys. Lett.* **B637** (2006) 161–169, `arXiv:nucl-ex/0601033 [nucl-ex]`.

[31] **ALICE** Collaboration, J. Adam *et al.*, "Measurement of pion, kaon and proton production in proton–proton collisions at $\sqrt{s} = 7$ TeV," *Eur. Phys. J.* **C75** no. 5, (2015) 226, `arXiv:1504.00024 [nucl-ex]`.

[32] **ALICE** Collaboration, B. Abelev *et al.*, "Multi-strange baryon production in pp collisions at $\sqrt{s} = 7$ TeV with ALICE," *Phys. Lett.* **B712** (2012) 309–318, `arXiv:1204.0282 [nucl-ex]`.

[33] T. A. collaboration, "Charged-particle distributions in sqrt(s)=13 TeV p p interactions measured with the ATLAS detector at the LHC," tech. rep., CERN, 2015.

[34] T. A. collaboration, "Leading Track Underlying Event at 13 TeV," Tech. Rep. ATL-PHYS-PUB-2015-019, CERN, Geneva, Jul, 2015. `http://cds.cern.ch/record/2037684`.

[35] **ALICE** Collaboration, B. B. Abelev *et al.*, "K^0_S and Λ production in Pb-Pb collisions at $\sqrt{s_{NN}}$ = 2.76 TeV," *Phys. Rev. Lett.* **111** (2013) 222301, `arXiv:1307.5530` `[nucl-ex]`.

[36] **ALICE** Collaboration, B. B. Abelev *et al.*, "Multiplicity Dependence of Pion, Kaon, Proton and Lambda Production in p-Pb Collisions at $\sqrt{s_{NN}}$ = 5.02 TeV," *Phys. Lett.* **B728** (2014) 25–38, `arXiv:1307.6796` `[nucl-ex]`.

[37] R. J. Fries and B. Muller, "Heavy ions at LHC: Theoretical issues," *Eur. Phys. J.* **C34** (2004) S279–S285, `arXiv:nucl-th/0307043` `[nucl-th]`.

III

Diffractive and non-diffractive wounded nucleons and final states in pA collisions

Christian Bierlich[1], Leif Lönnblad[1], and Gösta Gustafson[1].

[1] Dept. of Astronomy and Theoretical Physics, Lund University, Sölvegatan 14A, SE-223 62 Lund, Sweden.

ABSTRACT: We review the state-of-the-art of Glauber-inspired models or estimating the distribution of the number of participating nucleons in pA and AA collisions. We argue that there is room for improvement in these model when it comes to the treatment of diffractive excitation processes, and present a new simple Glauber-like model where these processes are better taken into account. We also suggest a new way of using the number of participating, or wounded, nucleons to extrapolate event characteristics from pp collisions, and hence get an estimate of basic hadronic final-state properties in pA collisions, which may be used to extract possible nuclear effects. The new method is inspired by the Fritiof model, but based on the full, semi-hard multiparton interaction model of PYTHIA8.

1   Introduction

An important topic in the studies of the strong interaction is the understanding of the features of hot and dense nuclear matter. To correctly interpret signals for collective behaviour in high energy nucleus–nucleus collisions, it is necessary to have a realistic extrapolation of the dynamics in pp collisions. Here experiments on pA collisions have been regarded as an important intermediate step. As an example refs. [1, 2] have discussed the possibility to discriminate between the dynamics of the wounded nucleon model and that of the Color Glass Condensate formalism in pPb collisions at the LHC.

An extrapolation of results from pp to pA and AA collisions is generally performed using the Glauber formalism [3, 4]. This model is based on the eikonal approximation, where the interaction is driven by absorption into inelastic channels. Elastic scattering is then the shadow of absorption, and determined by the optical theorem. The projectile nucleon(s) are assumed to travel along straight lines and undergo multiple sub-collisions with nucleons in the target. The Glauber model has been commonly used in experiments at RHIC and LHC, *e.g.* to estimate the number of participant nucleons, N_{part}, and the number of binary nucleon–nucleon collisions, N_{coll}, as a function of centrality. A basic assumption is then that one can compare a pA or an AA collision, at a certain centrality with, *e.g.*, $N_{\text{part}}/2$ or N_{coll} times the corresponding result in pp collisions (for which $N_{\text{part}} = 2$). A comparison with a fit to pp collision data, folded by the distribution in $N_{\text{part}}/2$ or N_{coll}, can then be used to investigate nuclear effects on various observables.

There are several problems related to such analyses, and in this paper we will concentrate on two of them:

- Since the actual impact parameter is not a physical observable, the experiments typically select an observable, which is expected to be strongly correlated with the impact parameter (such as a forward energy or particle flow). This implies that the definition of centrality becomes detector dependent, which, among other problems, also implies difficulties when comparing experimental results with each other and with theoretical calculations.

- When the interaction is driven by absorption, shadow scattering (meaning diffraction) can contain elastic *as well as single and double diffractive excitation*. This is important since experiments at high energy colliders show, that diffractive excitation is a significant fraction of the total cross section, and not limited to low masses (see *e.g.* [5, 6, 7]). Thus the driving force in Glauber's formalism should be the absorptive, meaning the non-diffractive inelastic cross section, and *not the total inelastic* cross section.

In the following we will argue that the approximations normally used in this procedure

are much too crude, and we will present a number of suggestions for how they can be improved, both in the way N_{part} and N_{coll} are calculated and the way pp event characteristics are extrapolated to get reference distributions. In both cases we will show that diffractive processes play an important role.

In Glauber's original analysis only elastic scattering was taken into account, but it was early pointed out by Gribov [8], that diffractive excitation of the intermediate nucleons gives a significant contribution. However, problems encountered when taking diffractive excitation into account have implied, that this has frequently been neglected, also in recent applications (see *e.g.* the review by Miller *et al.* [4]). Thus the "black disk" approximation, and other simplifying treatments, are still frequently used in analyses of experimental results.[1]

A way to include diffractive excitation in a Glauber analysis, using the Good–Walker formalism, was formulated by Heiselberg *et al.* [10]. It was further developed in several papers (see refs. [11, 12, 13, 14] and further references in there) and is often called the "Glauber–Gribov" (GG) model. In the Good–Walker formalism [15], diffractive excitation is described as the result of fluctuations in the nucleon's partonic substructure. When used in impact parameter space, it has the advantage that saturation effects can easily be taken into account, which makes it particularly suited for applications in collisions with nuclei.

The "Glauber–Gribov" model has been applied both to data from RHIC and in recent analyses of data from the LHC, *e.g.* in refs. [16, 17] However, although this formalism implies a significant improvement of the data analyses, also in this formulation the treatment of diffractive excitation is simplified, as the full structure of single excitation of either the projectile or the target, and of double diffraction, is not taken into account. As we will show in this paper, this simplification causes important problems, and we will here present a very simple model which separates the fluctuations in the projectile and the target nucleons.

To guide us in our investigation of conventional Glauber models we use the DIPSY Monte Carlo program [18, 19, 20], which is based on Mueller's dipole approach to BFKL evolution [21, 22], but also includes important non-leading effects, saturation and confinement. It reproduces fairly well both total, elastic, and diffractive pp cross sections, and has also recently been applied to pA collisions [9]. The DIPSY model gives a very detailed picture of correlations and fluctuations in the initial state of a nucleon, and by combining it with a simple geometrical picture of the distribution of nucleons in a nucleus in its ground state, we can build up an equally detailed picture of the initial states in pA and AA collisions. This allows us to gain new insights into the pros and cons of the approximations made in conventional Glauber Models.

The DIPSY program is also able to produce fully exclusive hadronic final states in pp col-

---

[1]The effects of the black disk approximation have also been discussed in ref. [9].

lisions, giving a reasonable description of minimum bias data from *e.g.* the LHC [20]. It could, in principle also be used to directly model final states in p*A* and *AA*, but due to some shortcomings, we will in this paper instead only use general features of these final states to motivate a revival of the old Fritiof model [23, 24] with great similarities with the original "wounded nucleon" model [25]. (For a more recent update of the wounded nucleon model see ref. [26].)

For energies up to (and including) those at fixed target experiments at CERN, the particle density at mid-rapidity in pp collisions is almost energy independent. For higher energies the density increases, and the $p_\perp$ distribution gets a tail to larger values. However, for minimum bias events with lower $p_\perp$, the wounded nucleon model still works with the multiplicity scaling with the number of participating (wounded) nucleons, both at RHIC [27, 28] and LHC [29]. For higher $p_\perp$ the distributions scale, however, better with the number of binary *NN* collisions, indicating the effect of hard parton-parton sub-collisions [17].

We will here argue that, due to the relatively flat distribution in rapidity of high-mass diffractive processes, absorbed and diffractively excited nucleons will contribute to the p*A* (and in principle also *AA*) final states in very similar ways, as wounded nucleons. We will also present preliminary results where we use our modified GG model to calculate the number distribution of wounded nucleons in p*A*, and from that construct hadronic final states by stacking diffractive excitation events, on top of a primary non-diffractive scattering, using PYTHIA8 with its semi-hard multi-parton interaction picture of hadronic collisions.

Although this remarkably simple picture gives very promising results, we find that there is a need for differentiating between diffractively and non-diffractively wounded nucleons. We will here be helped by the simple model mentioned above, in which fluctuations in the projectile and the target nucleon are treated separately. The model involves treating both the projectile and target as semi-transparent disks, separately fluctuating between two sizes according to a given probability. The radii, the transparency and the fluctuation probability is then adjusted to fit the non-diffractive nucleon–nucleon cross section, as well as the elastic, single diffractive and double diffractive cross sections. Even though this is a rather crude model, it will allow us to investigate effects of the difference between diffractively and non-diffractively wounded nucleons.

We will begin this article by establishing in section 2 the framework we will use to describe high energy nucleon–nucleon scattering, with special emphasis on the Good–Walker formalism for diffractive excitation. In section 3 we will then use this framework to analyse the Glauber formalism in general and define the concept of a *wounded* target cross section. In section 4 we dissect the conventional Glauber models and the Glauber–Gribov model together with the DIPSY model and present some comparisons of the resulting number dis-

tributions of wounded nucleons in pA. In section 5 we then go on to present our proposed model for constructing fully exclusive hadronic final states, and compare the procedure to recent results on particle distributions in pA collisions from the LHC, before we present conclusions and an outlook in section 6.

2 Dynamics of high energy pp scattering

2.1 Multiple sub-collisions and perturbative parton–parton interaction

As mentioned in the introduction, at energies up to those at fixed target experiments and the ISR at CERN, the pp cross sections and particle density, dn/dy are relatively independent of energy. For collisions with nuclei the wounded nucleon model works quite well [25], which formed the basis for the development of the Fritiof model [23]. This model worked very well within that energy range, but at higher energies it could not in a satisfactory way reproduce the development of a high $p_\perp$ tail caused by hard parton-parton interactions. Nevertheless the wounded nucleon model works well for minimum bias events even at LHC energies, if the rising rapidity plateau in pp collisions is taken into account, although the production of high $p_\perp$ particles appear to scale better with the number of NN collisions. These features may be interpreted as signals for dominance of soft interactions, and were the basis for the development of the Fritiof model [23]. This model worked very well within that energy range, but at higher energies, available at $\bar{p}$p colliders at CERN and Fermilab, the effects of (multiple) hard parton–parton sub-collisions became increasingly important, and not so easily incorporated in the Fritiof model.

Today high energy collisions (above $\sqrt{s} \sim 100$ GeV) are more often described as the result of multiple partonic sub-collisions, described by perturbative QCD. This picture was early proposed by Sjöstrand and van Zijl [30], and is implemented in the PYTHIA8 event generator [31]. This picture has also been applied in other generators such as HERWIG [32], SHERPA [33], DIPSY [18, 20], and others. The dominance of perturbative effects can here be understood from the suppression of low-$p_\perp$ partons due to saturation, as expressed *e.g.* in the Color Glass Condensate formalism [34].

2.2 Saturation and the transverse coordinate space

The eikonal approximation

The large cross sections in hadronic collisions imply that unitarity constraints are important, and the elastic amplitude has to satisfy the optical theorem, which with convenient

normalisation reads

$$\text{Im}\, A_{\text{el}} = \frac{1}{2} \left\{ |A_{\text{el}}|^2 + \sum_j |A_j|^2 \right\}. \tag{3.1}$$

Here the sum runs over all inelastic channels j. In high energy pp collisions the real part of the elastic amplitude is small, which indicates that the interaction is dominated by absorption into inelastic channels, with elastic scattering formed as the diffractive shadow of this absorption. This diffractive scattering is dominated by small $p_\perp$, and the scattered proton continues essentially along its initial direction.

At high energies and small transverse momenta, multiple scattering corresponds to a convolution in transverse momentum space, which is represented by a product in transverse coordinate space. This implies that diffraction and rescattering is more easily described in impact parameter space. In a situation where all inelastic channels correspond to absorption (meaning *no diffractive excitation*), the optical theorem in eq. (3.1) implies that the elastic amplitude in impact parameter space is given by

$$A_{\text{el}}(b) = i \left\{ 1 - \sqrt{1 - P_{\text{abs}}(b)} \right\}. \tag{3.2}$$

Here $P_{\text{abs}}(b) = \sum_j |A_j(b)|^2$ represents the probability for absorption into inelastic channels.

If the absorption probability in the Born approximation is given by $2F(b)$, then unitarity is restored by rescattering effects, which exponentiates in **b**-space and give the eikonal approximation:

$$P_{\text{abs}} = d\sigma_{\text{abs}}/d^2 b = 1 - e^{-2F(b)}, \tag{3.3}$$

To simplify the notation we introduce the nearly real amplitude $T = -iA_{\text{el}} = 1 - S$. The relation in eq. (3.2) then gives $S(b) = e^{-F(b)}$ and $T(b) = 1 - e^{-F(b)}$. The optical theorem then gives

$$
\begin{aligned}
T = 1 - \quad S \quad &= 1 - e^{-F} \\
d\sigma_{\text{el}}/d^2 b \quad &= \quad T^2 = (1 - e^{-F})^2 \\
d\sigma_{\text{tot}}/d^2 b \quad &= \quad 2T = 2(1 - e^{-F}).
\end{aligned} \tag{3.4}
$$

We note that the possibility of diffractive excitation is not included here. Therefore the absorptive cross section in eq. (3.3) is the same as the inelastic cross section.

How to include diffractive excitation and its relation to fluctuations will be discussed below in section 2.3. We then also note that diffractive excitation is very sensitive to saturation effects, as the fluctuations go to zero when saturation drives the interaction towards the black limit.

That rescattering exponentiates in transverse coordinate space also makes this formulation suitable for generalisations to collisions with nuclei.
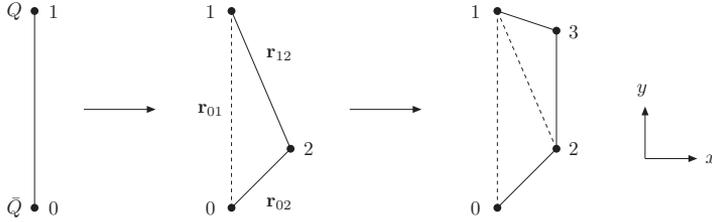
Figure 3.1: A colour dipole cascade in transverse coordinate space. A dipole can radiate a gluon. The gluon carries away colour, which implies that the dipole is split in two dipoles, which in the large N_c limit radiate further gluons independently.

Dipole models in transverse coordinate space

In this paper we will use our implementation of Mueller's dipole model, called DIPSY, in order to have a model which gives a realistic picture of correlations and fluctuations in the colliding nucleons. In this way we can evaluate to what extent Glauber-like models are able to take such effects into account. The DIPSY model has been described in a series of papers [18, 19, 20] and we will here only give a very brief description. Mueller's dipole model [21, 22] is a formulation of LL BFKL evolution in impact parameter space. A colour charge is always screened by an accompanying anti-charge. A charge–anti-charge pair can emit bremsstrahlung gluons in the same way as an electric dipole, with a probability per unit rapidity for a dipole $(\mathbf{r}_0, \mathbf{r}_1)$ to emit a gluon in the point $\mathbf{r}_2$, given by (*c.f.* figure 3.1)

$$\frac{dP}{dy} = \frac{\bar{\alpha}}{2\pi} d^2\mathbf{r}_2 \frac{r_{01}^2}{r_{02}^2 \, r_{12}^2}. \tag{3.5}$$

The important difference from electro-magnetism is that the emitted gluon carries away colour, which implies that the dipole splits in two dipoles. These dipoles can then emit further gluons in a cascade, producing a chain of dipoles as illustrated in figure 3.1.

When two such chains, accelerated in opposite directions, meet, they can interact via gluon exchange. This implies exchange of colour, and thus a reconnection of the chains as shown in figure 3.2.

The elastic scattering amplitude for gluon exchange is in the Born approximation given by

$$f_{ij} = \frac{\alpha_s^2}{2} \ln^2 \left(\frac{r_{13} r_{24}}{r_{14} r_{23}} \right). \tag{3.6}$$

BFKL evolution is a stochastic process, and many sub-collisions may occur independently. Summing over all possible pairs gives the total Born amplitude

$$F = \sum_{ij} f_{ij}. \tag{3.7}$$
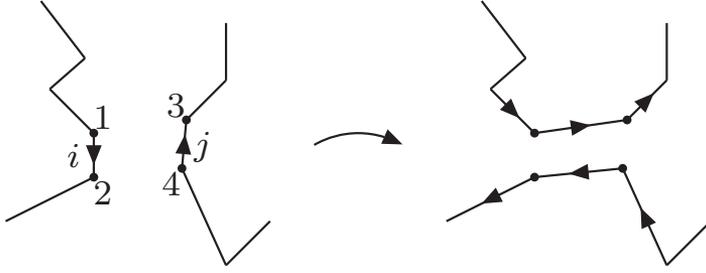
Figure 3.2: In a collision between two dipole cascades, two dipoles can interact via gluon exchange. As the exchanged gluon carries colour, the two dipole chains become recoupled.

The unitarised amplitude then becomes

$$T = 1 - e^{-\sum f_{ij}},\tag{3.8}$$

and the cross sections are given by

$$d\sigma_{\mathrm{el}}/d^2b = T^2, \qquad d\sigma_{\mathrm{tot}}/d^2b = 2T\tag{3.9}$$

The Lund dipole model DIPSY

The DIPSY model [18, 19, 20] is a generalisation of Mueller's cascade, which includes a set of corrections:

- Important non-leading effects in BFKL evolution.
  Most essential are those related to energy conservation and running α_s.

- Saturation from Pomeron loops in the evolution.
  Dipoles with identical colours form colour quadrupoles, which give Pomeron loops in the evolution. These are not included in Mueller's model or in the BK equation.

- Confinement via a gluon mass satisfies t-channel unitarity.

- It can be applied to collisions between electrons, protons, and nuclei.

Some results for pp total and elastic cross sections are shown in refs. [35, 36]. We note that there is no input structure functions in the model; the gluon distributions are generated within the model. We also note that the elastic cross section goes to zero in the dip of the t-distribution, as the real part of the amplitude is neglected.

2.3 Diffractive excitation and the Good–Walker formalism

In his analysis of the Glauber formalism, Gribov considered low mass excitation in the resonance region, but experiments at high energy colliders have shown, that diffractive excitation is not limited to low masses, and that high mass diffraction is a significant fraction of the pp cross section also at high energies (see *e.g.* [5, 6, 7]). Diffractive excitation is often described within the Mueller–Regge formalism [37], where high-mass diffraction is given by a triple-Pomeron diagram. Saturation effects imply, however, that complicated diagrams with Pomeron loops have to be included, which leads to complicated resummation schemes, see *e.g.* refs. [38, 39, 40]. These effects make the application in Glauber calculations quite difficult.

High mass diffraction can also be described, within the Good–Walker formalism [15], as the result of fluctuations in the nucleon's partonic substructure. Diffractive excitation is here obtained when the projectile is a linear combination of states with different absorption probabilities. This formalism was first applied to pp collisions by Miettinen and Pumplin [41], and later within the formalism for QCD cascades by Hatta *et al.* [42] and by Avsar and coworkers [43, 36]. When used in impact parameter space, this formulation has the advantage that saturation effects can easily be taken into account, and this feature makes it particularly suited in applications for collisions with nuclei. (For a BFKL Pomeron, the Good–Walker and the Mueller–Regge formalisms describe the same physics, seen from different sides [44].)

As an illustration of the Good–Walker mechanism, we can study a photon in an optically active medium. For a photon beam passing a black absorber, the waves around the absorber are scattered elastically, within a narrow forward cone. In the optically active medium, right-handed and left-handed photons move with different velocities, meaning that they propagate as particles with different mass. Study a beam of right-handed photons hitting a polarised target, which absorbs photons polarised in the *x*-direction. The diffractively scattered beam is then a mixture of right- and left-handed photons. If the right-handed photons have lower mass, this means that the diffractive beam contains also photons excited to a state with higher mass.

A projectile with substructure colliding with a structureless target

For a projectile with a substructure, the mass eigenstates can differ from the eigenstates of diffraction. Call the diffractive eigenstates Φ_k, with elastic scattering amplitudes T_k. The mass eigenstates Ψ_i are linear combinations of the states Φ_k:

$$\Psi_i = \sum_k c_{ik}\Phi_k \quad (\text{with } \Psi_{in} = \Psi_1). \tag{3.10}$$

The elastic scattering amplitude is given by

$$\langle \Psi_1 | T | \Psi_1 \rangle = \sum c_{1k}^2 T_k = \langle T \rangle, \tag{3.11}$$

and the elastic cross section

$$d\sigma_{\text{el}}/d^2 b = \left(\sum c_{1k}^2 T_k \right)^2 = \langle T \rangle^2. \tag{3.12}$$

The amplitude for diffractive transition to the mass eigenstate Ψ_k is given by

$$\langle \Psi_i | T | \Psi_1 \rangle = \sum_k c_{ik} T_k c_{1k}, \tag{3.13}$$

which gives a total diffractive cross section (including elastic scattering)

$$d\sigma_{\text{diff}}/d^2 b = \sum_i \langle \Psi_1 | T | \Psi_i \rangle \langle \Psi_i | T | \Psi_1 \rangle = \langle T^2 \rangle. \tag{3.14}$$

Consequently the cross section for diffractive excitation is *given by the fluctuations*:

$$d\sigma_{\text{D}}/d^2 b = d\sigma_{\text{diff}} - d\sigma_{\text{el}} = \langle T^2 \rangle - \langle T \rangle^2. \tag{3.15}$$

We note in particular that in this case the *absorptive cross section equals the inelastic non-diffractive cross section*. Averaging over different eigenstates eq. (3.3) gives

$$
\begin{aligned}
d\sigma_{\text{abs}}/d^2 b &= \left\langle 1 - e^{-2F(b)} \right\rangle = \left\langle 1 - (1-T)^2 \right\rangle = 2 \langle T \rangle - \langle T^2 \rangle \\
&= d\sigma_{\text{tot}}/d^2 b - d\sigma_{\text{diff}}/d^2 b.
\end{aligned}
\tag{3.16}
$$

A target with a substructure

If also the target has a substructure, it is possible to have either single excitation of the projectile, of the target, or double diffractive excitation. Let $\Psi_k^{(p)}$ and $\Psi_l^{(t)}$ be the diffractive eigenstates for the projectile and the target respectively, and T_{kl} the corresponding eigenvalue. (We here make the assumption that the set of eigenstates for the projectile are the same, for all possible target states. This assumption is also made in the DIPSY model discussed above.) The total diffractive cross section, including elastic scattering, is then obtained by taking the average of T_{kl}^2 over all possible states for the projectile and the target. Subtracting the elastic scattering then gives the total cross section for diffractive excitation:

$$d\sigma_{\text{D}}/d^2 b = \langle T^2 \rangle_{p,t} - (\langle T \rangle_{p,t})^2. \tag{3.17}$$

Here the subscripts p and t denote averages over the projectile and target respectively.

Taking the average over target states before squaring gives the probability for an elastic interaction for the target. Subtracting single diffraction of the projectile and the target from the total in eq. (3.17) will finally give the double diffraction. Thus we get the following relations:

$$
\begin{aligned}
d\sigma_{\text{tot}}/d^2 b &= 2 \left\langle T \right\rangle_{p,t} \\
d\sigma_{\text{el}}/d^2 b &= \left\langle T \right\rangle^2_{p,t} \\
d\sigma_{\text{Dp}}/d^2 b &= \left\langle \left\langle T \right\rangle^2_t \right\rangle_p - \left\langle T \right\rangle^2_{p,t} \\
d\sigma_{\text{Dt}}/d^2 b &= \left\langle \left\langle T \right\rangle^2_p \right\rangle_t - \left\langle T \right\rangle^2_{p,t} \\
d\sigma_{\text{DD}}/d^2 b &= \left\langle T^2 \right\rangle_{p,t} - \left\langle \left\langle T \right\rangle^2_t \right\rangle_p - \left\langle \left\langle T \right\rangle^2_p \right\rangle_t + \left\langle T \right\rangle^2_{p,t} ,
\end{aligned} \tag{3.18}
$$

where σ_{Dp} and σ_{Dt} is single diffractive excitation of the projectile and target respectively and σ_{DD} is double diffractive excitation. Also here the absorptive cross section, which will be important in the following discussion of the Glauber model, corresponds to the *non-diffractive* inelastic cross section:

$$
d\sigma_{\text{abs}}/d^2 b = 2 \left\langle T \right\rangle_{p,t} - \left\langle T^2 \right\rangle_{p,t} . \tag{3.19}
$$

Diffractive eigenstates at high energies

In the early work by Miettinen and Pumplin [41], the authors suggested that the diffractive eigenstates correspond to different geometrical configurations of the valence quarks, as a result of their relative motion within a hadron. At higher energies the proton's partonic structure is dominated by gluons. The BFKL evolution is a stochastic process, and it is then natural to interpret the perturbative parton cascades as the diffractive eigenstates (which may also depend on the positions of the emitting valence partons). This was the assumption in the work by Hatta *et al.* [42] and in the DIPSY model. Within the DIPSY model, based on BFKL dynamics, it was possible to obtain a fair description of both the experimental cross section [43, 36] and final state properties [45] for diffractive excitation. In the GG model two sources to fluctuations are considered; first fluctuations in the geometric distribution of valence quarks, and secondly fluctuations in the emitted gluon cascades, called colour fluctuations or flickering. In ref. [13] it was concluded that the latter is expected to dominate at high energies.

We here also note that at very high energies, when saturation drives the interaction towards the black limit, the fluctuations go to zero. This implies that diffractive excitation is largest in peripheral collisions, where saturation is less effective. This is true both for pp collisions and collisions with nuclei. (Although diffractive excitation of the projectile is almost zero in central pA collisions, this is not the case for nucleons in the target.)

3 Glauber formalism for collisions with nuclei

3.1 General formalism

High energy nuclear collisions are usually analysed within the Glauber formalism [3] (for a more recent overview see [4]). In this formalism, target nucleons are treated as independent, and any interaction between them is neglected[2]. The projectile nucleon(s) travel along straight lines, and undergo multiple diffractive sub-collisions with small transverse momenta. As mentioned in the introduction, multiple scattering, which in transverse momentum space corresponds to a convolution of the scattering S-matrices, corresponds to a product in transverse coordinate space. Thus the matrices $S^{(\mathrm{p}N_\nu)}$, for the encounters of the proton with the different nucleons in the target nucleus, factorise:

$$S^{(\mathrm{p}A)} = \prod_{\nu=1}^{A} S^{(\mathrm{p}N_\nu)}. \tag{3.20}$$

We denote the impact parameters for the projectile and for the different nucleons in the target nucleus by $\mathbf{b}$ and $\mathbf{b}_\nu$ respectively, and define $\tilde{\mathbf{b}}_\nu \equiv \mathbf{b} - \mathbf{b}_\nu$. Using the notation in eq. (3.4), we then get the following elastic scattering amplitude for a proton hitting a nucleus with A nucleons:

$$T^{(\mathrm{p}A)}(\mathbf{b}) = 1 - \prod_{\nu=1}^{A} S^{(\mathrm{p}N_\nu)}(\tilde{\mathbf{b}}_\nu) = 1 - \prod_{\nu} \left(1 - T^{(\mathrm{p}N_\nu)}(\tilde{\mathbf{b}}_\nu)\right) = 1 - e^{-\sum_\nu F^{(\mathrm{p}N_\nu)}(\tilde{\mathbf{b}}_\nu)}. \tag{3.21}$$

If there are no fluctuations, neither in the pp interaction nor in the distribution of nucleons in the nucleus, a knowledge of the positions $\mathbf{b}_\nu$ and the pp elastic amplitude $T^{(\mathrm{pp})}(\tilde{\mathbf{b}})$ would give the total and elastic pA cross sections via the relations in eq. (3.4):

$$\sigma_{\mathrm{tot}}^{(\mathrm{p}A)} = 2 \int d^2b\, T^{(\mathrm{p}A)}(\mathbf{b}) \tag{3.22}$$

$$\sigma_{\mathrm{el}}^{(\mathrm{p}A)} = \int d^2b\, \left(T^{(\mathrm{p}A)}(\mathbf{b})\right)^2 \tag{3.23}$$

The inelastic cross section (now equal to the absorptive) would be equal to the difference between these two, in accordance with eq. (3.3).

---

[2]In the DIPSY model gluons with the same colour can interfere, also when they come from different nucleons. This so-called inter-nucleon swing mechanism was shown [9] to have noticeable effects in photon–nucleus collisions, but in pA, especially for heavy nuclei, the effects were less that 5%. We have therefore chosen to ignore such effects in this paper, but may return to the issue in a future publication.

Fluctuations in the pp interaction are discussed in the following subsection. Fluctuations and correlations in the nucleon distribution within the nucleus are difficult to treat analytically, and therefore most easily studied by means of a Monte Carlo, as discussed further in sections 3.4, 4 and 5 below. Valuable physical insight can, however, be gained in an approximation where all correlations between target nucleons are neglected. Such an approximation, called the optical limit, is discussed in section 3.5.

3.2 Gribov corrections. Fluctuations in the pp interaction

Gribov pointed out that the original Glauber model gets significant corrections due to possible diffractive excitation. In the literature it is, however, common to take only diffractive excitation of the projectile into account, disregarding possible excitation of the target nucleons. In this section we will develop the formalism to account for excitations of nucleons in both projectile and target. We will then see that in many cases fluctuations in the target nucleons will average out, while in other cases they may give important effects. (Fluctuations in both projectile and target will, however, be even more essential in nucleus–nucleus collisions, which we plan to discuss in a future publication.)

Total and elastic cross sections

When the nucleons can be in different diffractive eigenstates, the amplitudes $T^{(pN_\nu)}$ in eq. (3.21) are matrices $T^{(pN_\nu)}_{k,l_\nu}$, depending on the states k for the projectile and l_ν for the target nucleon ν. The elastic pA amplitude, $\langle T^{(pA)}(\mathbf{b}) \rangle$, can then still be calculated from eq. (3.21), by averaging over all values for k and l_ν, with ν running from 1 to A. Thus

$$d\sigma^{(pA)}_{\text{tot}}/d^2 b = 2\left\langle T^{(pA)}(\mathbf{b})\right\rangle = 2\left\{1 - \left\langle S^{(pA)}(\mathbf{b})\right\rangle\right\}, \qquad (3.24)$$

$$d\sigma^{(pA)}_{\text{el}}/d^2 b = \left\langle T^{(pA)}(\mathbf{b})\right\rangle^2. \qquad (3.25)$$

When evaluating the averages in these equations, it is essential that the projectile proton stays in the same diffractive eigenstate, Φ_k, throughout the whole passage through the target nucleus, while the states, Φ_{l_ν}, for the nucleons in the target nucleus are uncorrelated from each other. This implies that for a *fixed* projectile state k, the average of the S-matrix over different states, l_ν, for the target nucleons factorise in eq. (3.20) or (3.24). Thus we have

$$\left\langle S^{(pA)}(\mathbf{b})\right\rangle = \left\langle \left\langle \prod_\nu \left\langle S^{(pp,\nu)}_{k,l_\nu}(\tilde{\mathbf{b}}_\nu)\right\rangle_{l_\nu}\right\rangle_{\mathbf{b}_\nu}\right\rangle_k. \qquad (3.26)$$

Here $\langle \cdots \rangle_k$ ($\langle \cdots \rangle_{l_\nu}$) denotes average over projectile (target nucleon) substructures k (l_ν), while $\langle \cdots \rangle_{\mathbf{b}_\nu}$ denotes average over the target nucleon positions $\mathbf{b}_\nu$, an as before $\tilde{\mathbf{b}}_\nu \equiv$

$\mathbf{b} - \mathbf{b}_\nu$. We introduce the following notation for the average of the pp amplitude over target states:

$$T_k^{(\mathrm{pp})}(\tilde{\mathbf{b}}_\nu) \equiv \left\langle T_{k,l}^{(\mathrm{pp})}(\tilde{\mathbf{b}}_\nu) \right\rangle_l = \left\langle (1 - S_{k,l}^{(\mathrm{pp})}(\tilde{\mathbf{b}}_\nu)) \right\rangle_l. \qquad (3.27)$$

The pA amplitude can then be written in the form

$$\left\langle T_k^{(\mathrm{p}A)}(\mathbf{b}) \right\rangle_k = \left\langle \left\{ 1 - \prod_\nu S_k^{(\mathrm{pp})}(\tilde{\mathbf{b}}_\nu) \right\} \right\rangle_{\mathbf{b}_\nu,k} = \left\langle \left\{ 1 - \prod_\nu \left(1 - T_k^{(\mathrm{pp})}(\tilde{\mathbf{b}}_\nu) \right) \right\} \right\rangle_{\mathbf{b}_\nu,k},$$
$$(3.28)$$

where the average is taken over the target nucleon positions $\mathbf{b}_\nu$ and the projectile states, k. The total and elastic cross sections in eqs. (3.24) and (3.25) are finally obtained from eq. (3.4). We want here to emphasise that these expressions only contain the first moment with respect to the fluctuations in the target states, l_ν, but also all higher moments of the fluctuations in the projectile states, k.

To evaluate the b-integrated cross sections, we must know both the distribution of the (correlated) nucleon positions, $\mathbf{b}_\nu$, and the b-dependence of the pp amplitude $T_k^{(\mathrm{pp})}(b)$. The distribution of nucleon positions is normally handled by a Monte Carlo, as will be discussed in section 3.4. When fluctuations and diffractive excitation was neglected in section 3.1, the b-dependence of $T^{(\mathrm{pp})}(b)$ could be well approximated by a Gaussian distribution $C\exp\left(-b^2/2B\right)$, corresponding to an exponential elastic cross section $d\sigma/dt \propto \exp\left(Bt\right)$. With fluctuations it is necessary to take the unitarity constraint $T \leq 1$ into account, which implies that a large cross section must be associated with a wider distribution. One should then check that after averaging the differential elastic cross section reproduces the observed slope.[3]

3.3 Interacting nucleons

Specification of "wounded" nucleons

The notion of "wounded" nucleons was introduced by Białas, Bleszyński, and Czyż in 1976 [25], based on the idea that inelastic pA or AA collisions can be described as a sum of independent contributions from the different participating nucleons[4]. In ref. [25] diffractive excitation was neglected, and thus "wounded nucleons" was identical to inelastically interacting nucleons[5].

---

[3]In ref. [12] unitarity is satisfied assuming the slope B to be proportional to the fluctuating total cross section σ_{tot}.

[4]This idea was also the basis for the Fritiof model [23], which has been quite successful for low energies.

[5]It was also pointed out that for pA collisions the number of participant nucleons, w, and the number of NN sub-collisions, v, are related, $v = w + 1$, and a relation between particle multiplicity and the number of

Although the importance of diffractive excitation was pointed out by Gribov already in 1968 [8], it has, as far as we know, never been discussed whether or not diffractively excited nucleons should be regarded as wounded. These nucleons contribute to the inelastic, but not to the absorptive cross section, as defined in eq. (3.19).

Diffractive excitation is usually fitted to a distribution proportional to $dM_X^2/(M_X^2)^{1+\epsilon}$. A bare triple-Pomeron diagram would give $\epsilon = \alpha_{\mathbb{P}}(0) - 1$, where $\alpha_{\mathbb{P}}(0)$ is the intercept of the Pomeron trajectory, estimated to around 1.2 from the HERA structure functions at small x. More complicated diagrams tend, however, to reduce ϵ. (In ref. [40] it is shown that the largest correction is a four-Pomeron diagram, which gives a contribution with $\epsilon = 0$.) Fits to LHC data [6, 7] give $\epsilon \approx 0.1$, but with rather large uncertainties.

If ϵ is small, diffractively excited target nucleons can contribute to particle production both in the forward and in the central region. If ϵ instead is large, diffraction would contribute mainly close to the nucleus fragmentation region. For $\epsilon \approx 0.1$, the experimentally favoured value, the contribution in the central region would be suppressed by a factor $\exp(-0.1 \cdot \Delta\eta) \sim 1/2$ for pPb collisions at LHC. We conclude that the definition of wounded nucleons should depend critically upon both the experimental observable studied in a certain analyses, and upon the still uncertain M_X-dependence of diffractive excitation at LHC energies. (In section 5.1 we will show that a simple model, assuming similar contributions from absorbed and diffractively excited nucleons actually quite successfully describes the final state in pPb collisions at LHC.)

Below we present first results for the absorbed, non-diffractive, nucleons, followed by results when diffractively excited nucleons are included.

Wounded nucleon cross sections

Absorptive cross section

We first assume that wounded nucleons correspond to nucleons absorbed via gluon exchange, which for large values of ϵ would be relevant for observables in the central region, away from the nucleus fragmentation region. Due to the relation $T = 1 - S$, the absorptive cross section in eq. (3.19) can also be written $d\sigma_{\text{abs}}/d^2b = \langle 1 - S^2 \rangle$. We here note that, as the S-matrix factorises in the elastic amplitude in eqs. (3.20) and (3.24), this is also the

---

wounded nucleons, w, is equivalent to a relation to the number of NN sub-collisions, $v = w + 1$. Only in AA collisions is it possible to distinguish a dependence on the number of participating nucleons from a dependence on the number of nucleon–nucleon sub-collisions.

case for S^2. This implies that

$$\left(S^{(\mathrm{p}A)}_{k,\{l_\nu\}} \right)^2 = \prod_{\nu=1}^{A} \left(S^{(\mathrm{p}N_\nu)}_{k,l_\nu} \right)^2. \tag{3.29}$$

In analogy with eq. (3.27) for σ_{tot}, also here, when taking the average over the target states l_ν, the factors in the product depend only on the projectile state k and the positions $\tilde{\mathbf{b}}_\nu$. We here introduce the notation

$$W^{(w_{\mathrm{abs}})}_{k}(\tilde{\mathbf{b}}_\nu) \equiv \left\langle 1 - \left(S^{(\mathrm{pp})}_{k,l}(\tilde{\mathbf{b}}_\nu) \right)^2 \right\rangle_l. \tag{3.30}$$

This quantity represents the *probability that nucleon ν is absorbed by a projectile in state k.* Averaging over all values for k and $\mathbf{b}_\nu$, it gives the total pA absorptive, meaning inelastic non-diffractive, cross section

$$d\sigma^{\mathrm{p}A}_{\mathrm{abs}}(\mathbf{b})/d^2 b = \left\langle \left\langle \left\{ 1 - \prod_\nu \left(1 - W^{(w_{\mathrm{abs}})}_{k}(\tilde{\mathbf{b}}_\nu) \right) \right\} \right\rangle_{\mathbf{b}_\nu} \right\rangle_k. \tag{3.31}$$

This expression equals the probability that at least one target nucleon is absorbed.

Cross section including diffractively excited target nucleons

We now discuss the situation when also diffractively excited target nucleons should be counted as wounded. (The case with an excited projectile proton is discussed below.) The probability for a nucleon, ν, in the nucleus to be diffractively excited is obtained from eq. (3.18) by adding single and double diffraction:

$$\begin{aligned}
P_{\mathrm{D},\nu} &= \left\langle \left(T^{(\mathrm{pp})}(\tilde{\mathbf{b}}_\nu) \right)^2 \right\rangle_{k,l_\nu} - \left\langle \left(\left\langle T^{(\mathrm{pp})}(\tilde{\mathbf{b}}_\nu) \right\rangle_{l_\nu} \right)^2 \right\rangle_k \\
&= \left\langle \left\langle S^2 \right\rangle_{l_\nu} - \left\langle S \right\rangle^2_{l_\nu} \right\rangle_k.
\end{aligned} \tag{3.32}$$

Adding the absorptive cross section in eq. (3.19) we obtain the total probability that a target nucleon, ν, is excited or broken up by either diffraction or absorption,

$$P_{w_{\mathrm{inc}},\nu} = 1 - \left\langle \left\langle S \right\rangle^2_{l_\nu} \right\rangle_k, \tag{3.33}$$

and we will call such nucleons *inclusively wounded* (w_{inc}), as opposed to *absorptively wounded* (w_{abs}).

In analogy with eq. (3.30) we define $W^{(w_{\mathrm{inc}})}_{k}$ by the relation

$$W^{(w_{\mathrm{inc}})}_{k}(\tilde{\mathbf{b}}_\nu) \equiv 1 - \left\langle S^{(\mathrm{pp})}_{k,l}(\tilde{\mathbf{b}}_\nu) \right\rangle^2_{l_\nu} = 1 - \left(1 - T^{(\mathrm{pp})}_{k}(\tilde{\mathbf{b}}_\nu) \right)^2, \tag{3.34}$$

which gives the probability that the target nucleon ν is either absorbed or diffractively excited, by a projectile in state k. Thus, if these target nucleons are counted as wounded, the cross section is also given by eq. (3.31), when $W_k^{(w_{\mathrm{abs}})}$ is replaced by $W_k^{(w_{\mathrm{inc}})}$. We note that the expression for the wounded nucleon cross section resembles the total one in eqs. (3.28) and (3.25), with $T_k^{(\mathrm{pp})}$ replaced by $W_k^{(w_{\mathrm{abs}})}$ or $W_k^{(w_{\mathrm{exc}})}$. Note also that as $W_k^{(w_{\mathrm{inc}})}$ is determined via eq. (3.34), when $T_k^{(\mathrm{pp})}$ is known including its $\mathbf{b}$-dependence. This is not the case for $W_k^{(w_{\mathrm{abs}})}$, which contains the average over target states of the *square* of the amplitude $T_{k,l}^{(\mathrm{pp})}$.

Elastically scattered projectile protons

We should note that the probabilities given above include events, where the projectile is elastically scattered, and thus not regarded as a wounded nucleon. The probability for this to happen in an event with diffractively excited target nucleons, is given by the relation ($\langle \cdots \rangle_p$ and $\langle \cdots \rangle_t$ denote averages over projectile and target states respectively)

$$ \left\langle \langle S \rangle_p^2 \right\rangle_t - \left(\langle S \rangle_{p,t} \right)^2 = \left\langle \left\langle \prod_\nu S_{k,l_\nu} \right\rangle_k^2 \right\rangle_{l_\nu} - \left\{ \left\langle \left\langle \prod_\nu S_{k,l_\nu} \right\rangle_k \right\rangle_{l_\nu} \right\}^2 . \quad (3.35) $$

In case these events do not contribute to the observable under study, this contribution should thus be removed. For a large target nucleus, this is generally a small contribution.

Wounded nucleon multiplicity

In the following we let W_k denote either $W_k^{(w_{\mathrm{inc}})}$ or $W_k^{(w_{\mathrm{abs}})}$, depending upon whether or not diffractively excited target nucleons should be counted as wounded.

Average number of wounded nucleons

As $W_k(\tilde{\mathbf{b}}_\nu)$ denotes the probability that target nucleon ν is wounded, the average number of wounded nucleons in the target is then (for fixed $\mathbf{b}$) given by $\langle \sum_\nu W_k(\tilde{\mathbf{b}}_\nu) \rangle_{k,\mathbf{b}_\nu}$, obtained by summing over target nucleons ν, and averaging also over projectile states k and all target positions $\mathbf{b}_\nu$. Averaging over impact parameters, $\mathbf{b}$, is only meaningful, when we calculate the average number of wounded target nucleons per event with at least one wounded nucleon, which we denote $\langle N_w^t \rangle$. This is obtained by dividing by the probability in eq. (3.31). Integrating over $\mathbf{b}$, weighting by the same absorptive probability, and

normalising by the total absorptive cross section (also integrated over $\mathbf{b}$) we get

$$\langle N_w^t \rangle = \frac{\int d^2 b \sum_\nu \left\langle \left\langle W_k(\tilde{\mathbf{b}}_\nu) \right\rangle_k \right\rangle_{\mathbf{b}_\nu}}{\int d^2 b \left\langle \left\langle 1 - \prod_\nu \left(1 - W_k(\tilde{\mathbf{b}}_\nu)\right) \right\rangle_k \right\rangle_{\mathbf{b}_\nu}}. \tag{3.36}$$

Note that the total number of wounded nucleons is given by $N_w = N_w^t + 1$, as the projectile proton should be added, provided the projectile proton is not elastically scattered (in which case all wounded target nucleons have to be diffractively excited).

Multiplicity distribution for wounded nucleons

It is also possible to calculate the probability distribution in the number of wounded target nucleons N_w^t. For fixed projectile states k and target nucleon positions $\tilde{\mathbf{b}}_\nu$, the probability for target nucleon ν to be wounded, or not wounded, is $W_k(\tilde{\mathbf{b}}_\nu)$ and $1 - W_k(\tilde{\mathbf{b}}_\nu)$ respectively. For *fixed k* the probability distribution in the number of absorbed target nucleons is then given by

$$\frac{dP_k(\mathbf{b})}{dN_w^t} = \sum_{\mathcal{C}_{N_w^t}} \prod_{\nu \in \mathcal{C}_{N_w^t}} W_k(\tilde{\mathbf{b}}_\nu) \prod_{\mu \in \overline{\mathcal{C}}_{N_w^t}} \left\{ 1 - W_k(\tilde{\mathbf{b}}_\mu) \right\}. \tag{3.37}$$

Here the sum goes over all subsets $\mathcal{C}_{N_w^t}$ of $_w^t$ wounded target nucleons, and $\overline{\mathcal{C}}_{N_w^t}$ is the set of the remaining $A - N_w^t$ target nucleons, which thus are not wounded. The states of the target nucleons can be assumed to be uncorrelated, and the averages could therefore be taken separately, as in eq. (3.30). The state k and positions $\mathbf{b}_\nu$ or $\mathbf{b}_\mu$ give, however, correlations between the different factors, and these averages must be taken after the multiplication, which gives the result

$$\frac{dP(\mathbf{b})}{dN_w^t} = \left\langle \left\langle \left\{ \sum_{\mathcal{C}_{N_w^t}} \prod_{\nu \in \mathcal{C}_{N_w^t}} W_k(\tilde{\mathbf{b}}_\nu) \prod_{\mu \in \overline{\mathcal{C}}_{N_w^t}} \left\{ 1 - W_k(\tilde{\mathbf{b}}_\mu) \right\} \right\} \right\rangle_{\mathbf{b}_\nu} \right\rangle_k. \tag{3.38}$$

The distribution in eq. (3.38) includes the possibility for $N_w^t = 0$. As for the average number of wounded nucleons above, to get the normalised multiplicity distribution for events, with $N_w^t \geq 1$, we should divide by the probability in eq. (3.31). The final distribution is then obtained by integrating over $\mathbf{b}$, with a weight given by the same absorption probability. This gives the result

$$\left. \frac{dP}{dN_w^t} \right|_{\text{ev}} = \frac{\int d^2 b \, dP(\mathbf{b})/dN_w^t}{\int d^2 b \, d\sigma_w^{\text{p}A}(\mathbf{b})/d^2 b}, \tag{3.39}$$

where $dP/dN_w^t(\mathbf{b})$ and $d\sigma_w^{\text{p}A}(\mathbf{b})/d^2 b$ are the expressions in eqs. (3.38)) and (3.31).

We want here to emphasise that the quantity $W_k^{(w_{\mathrm{abs}})}$ contains the average of the *square* of the amplitude $T^{(\mathrm{pp})}$, and is therefore not simply determined from the average $\langle T^{(\mathrm{pp})} \rangle_l = \langle 1 - S^{(\mathrm{pp})} \rangle_l$, which appears in the expression for the total and elastic cross sections in eqs. (3.28) and (3.25). This contrasts to the situation for inclusively wounded nucleons, where $W_k^{(w_{\mathrm{inc}})}$ in eq. (3.34) actually is directly determined by $\langle T_{k,l}^{(\mathrm{pp})} \rangle_l$.

3.4 Nucleus geometry and quasi-elastic scattering

In a real nucleus the nucleons are subject to forces with a hard repulsive core, and their different points $\mathbf{r}_\nu$ are therefore not uncorrelated. In Glauber's original papers this correlation was neglected, and this approximation is discussed in the subsequent section.

In addition to the suppression of nucleons at small separations, the geometrical structure will fluctuate from event to event. These fluctuations are not only a computational problem, but have also physical consequences. Just as fluctuations in the nucleon substructure can induce diffractive excitation of the nucleon, fluctuations in the nucleus substructure induces diffractive excitation of the nucleus. If the projectile is elastically scattered these events are called quasi-elastic. The fluctuations in the target nucleon positions are also directly reproduced by the Monte Carlo programs mentioned above, and within the Good–Walker formalism the quasi-elastic cross section, $\sigma_{\mathrm{el*}}$, is given by (*c.f.* eq. (3.18)):

$$d\sigma_{\mathrm{el*}}/d^2 b = \left\langle \langle T \rangle_p^2 \right\rangle_t . \tag{3.40}$$

The average over the target states here includes averaging over all geometric distributions of nucleons in the nucleus, and all partonic states of these nucleons. Note that this expression includes the elastic proton–nucleus scattering (given by $\langle T \rangle_{p,t}^2$). Some results for quasi-elastic pPb collisions are presented in ref. [46, 9].

3.5 Optical limit – uncorrelated nucleons and large nucleus approximations

Even though the averages in eqs. (3.24) and (3.31) factorise, they are still complicated by the fact that all factors $S^{(pN_\nu)}$ are different, due to the different values for the impact parameters. It is interesting to study simplifying approximations, assuming uncorrelated nucleon positions and large nuclei. This is generally called the optical limit. It was used by Glauber in his initial study [3], and is also described in the review by Miller *et al.* [4], for a situation when diffractive excitation is neglected. We here discuss the modifications necessary when diffractive excitation is included, also separating single excitation of projectile and target, and double diffraction.

Uncorrelated nucleons

Neglecting the correlations between the nucleon positions in the target nucleus, the individual nucleons can be described by a smooth density $A \cdot \rho(b_\nu)$ (normalised so that $\int d^2 b \, \rho(b) = 1$). In this approximation all factors $\left\langle S_{k,l_\nu}^{(pN_\nu)} \right\rangle_t = 1 - \left\langle T_{k,l_\nu}^{(pN_\nu)} \right\rangle_t$ in eq. (3.26), which enter the total pA cross section in eq. (3.24), are uncorrelated and give the same result, depending only on projectile state and impact parameter k and $\mathbf{b}$:

$$\left\langle T_{k,l_\nu}^{(pN_\nu)}(\mathbf{b} - \mathbf{b}_\nu) \right\rangle_t = \int d^2 b_\nu \, \rho(\mathbf{b}_\nu) \left\langle T_{k,l}^{(pp)}(\mathbf{b} - \mathbf{b}_\nu) \right\rangle_l. \tag{3.41}$$

In the same way all factors $W_k(\tilde{\mathbf{b}}_\nu)$, entering the wounded nucleon cross sections in eqs. (3.30) and (3.34), give equal contributions:

$$\left\langle W_k^{(w_{\mathrm{abs}})}(\tilde{\mathbf{b}}_\nu) \right\rangle_{\mathbf{b}_\nu} = \int d^2 b_\nu \, \rho(\mathbf{b}_\nu) \left(1 - \left\langle \left(S_{k,l}^{(pp)}(\mathbf{b} - \mathbf{b}_\nu) \right)^2 \right\rangle_l \right);$$

$$\left\langle W_k^{(w_{\mathrm{inc}})}(\tilde{\mathbf{b}}_\nu) \right\rangle_{\mathbf{b}_\nu} = \int d^2 b_\nu \, \rho(\mathbf{b}_\nu) \left(1 - \left\langle S_{k,l}^{(pp)}(\mathbf{b} - \mathbf{b}_\nu) \right\rangle_l^2 \right). \tag{3.42}$$

Large nucleus

If, in addition to the approximations in eqs. (3.41) and (3.42), the width of the nucleus (specified by ρ) is much larger than the extension of the pp interaction (specified by $T^{(pp)}$), further simplifications are possible. For the amplitude in eq. (3.41) we can integrate over $\mathbf{b}_\nu$, and get the approximation

$$\left\langle T_{k,l_\nu}^{(pN_\nu)}(\mathbf{b} - \mathbf{b}_\nu) \right\rangle_t \approx \rho(\mathbf{b}) \int d^2 \tilde{b} \left\langle T_{k,l}^{(pp)}(\tilde{b}) \right\rangle_l = \rho(\mathbf{b}) \, \sigma_{\mathrm{tot},k}^{pp} / 2. \tag{3.43}$$

We have here introduced the notation $\sigma_{\mathrm{tot},k}^{pp}$ for the total cross section for a projectile proton in state k, averaged over all states for a target proton.

In the same way we get

$$\left\langle W_k(\tilde{\mathbf{b}}_\nu) \right\rangle_t \approx \rho(\mathbf{b}) \int d^2 \tilde{b} \, W_k(\tilde{b}) = \rho(\mathbf{b}) \, \sigma_{w,k}^{pp}, \tag{3.44}$$

where W_k is either $W_k^{(w_{\mathrm{abs}})}$ or $W_k^{(w_{\mathrm{inc}})}$, and $\sigma_{w,k}^{pp}$ is the corresponding pp cross section for a projectile in state k.

Total cross section

Inserting eq. (3.43) into eqs. (3.24) - (3.25) gives the total cross section for a projectile in state k hitting a nucleus:

$$d\sigma_{\text{tot},k}^{(\text{p}A)}/d^2b \;\;=\;\; 2\left\langle T_{k,l}^{(\text{p}A)}(\mathbf{b})\right\rangle_t = 2\left\{1 - \left(1 - \rho(\mathbf{b})\,\sigma_{\text{tot},k}^{\text{pp}}/2\right)^A\right\} =$$

$$=\;\; -2\sum_{N=1}^{A}\binom{A}{N}\left(-\rho(b)\,\sigma_{\text{tot},k}^{\text{pp}}/2\right)^N. \qquad (3.45)$$

The total pA cross section is then finally obtained by averaging over projectile states, k, and integrating over impact parameters, $\mathbf{b}$:

$$\sigma_{\text{tot}}^{(\text{p}A)} = \int d^2b\,\left\langle d\sigma_{\text{tot},k}^{(\text{p}A)}/d^2b\right\rangle_k. \qquad (3.46)$$

We note here in particular, that in this approximation the b-dependence of $T_k^{(\text{pp})}(b)$ is unimportant, and the result depends only on its integral $\sigma_{\text{tot},k}^{\text{pp}}/2$. We also note that to calculate the elastic pA cross section $\sim \int d^2b\,(T(b))^2$, which has a steeper b-dependence, a knowledge about this dependence is also needed.

Proton-deuteron cross section

Neglecting fluctuations, eqs. (3.45) and (3.46) would give the simpler result

$$\sigma_{\text{tot}}^{(\text{p}A)} = -2\sum_{N=1}^{A}\binom{A}{N}\left(\left(-\frac{\sigma_{\text{tot}}}{2}\right)^N \int d^2b\,\rho^N(b)\right). \qquad (3.47)$$

For the special case with a deuteron target we then get the result[6]

$$\sigma_{\text{tot}}^{\text{pd}} = 2\sigma_{\text{tot}}^{\text{pp}} - \frac{1}{2}\left(\int d^2b\,\rho^2(b)\right)(\sigma_{\text{tot}}^{\text{pp}})^2, \qquad (3.48)$$

and with the estimate $\int d^2b\,\rho^2(b) = 1/(2\pi\langle b^2\rangle)$ describing the deuteron wavefunction, we recognise Glauber's original result.

For a non-fluctuating amplitude, the optical theorem gives a direct connection between the total and elastic cross sections. As the integral over d^2b gives the Fourier transform at $q = 0$, we have

$$\sigma_{\text{tot}}^{\text{pp}} = 2\int d^2b\,T_{k,l}^{(\text{pp})}(b) = 4\pi\tilde{T}_{k,l}^{(\text{pp})}(q=0) = \sqrt{16\pi\left.\frac{d}{dt}\sigma_{\text{el}}^{\text{pp}}(t)\right|_{t=0}}. \qquad (3.49)$$

---

[6]Although the deuteron has only 2 nucleons, it is very weakly bound, and its wave function is extended out to more than 5 fm. Therefore the large nucleus approximation is meaningful also here.

Here $\tilde{T}(q)$ denotes the Fourier transform of the amplitude $T(b)$. For a Gaussian interaction profile we get

$$(\sigma_{\text{tot}}^{(\text{pp})})^2 \propto \sigma_{\text{el}}^{\text{pp}} \cdot B, \tag{3.50}$$

where the slope B is a measure of the width of the interaction. As σ_{el} is determined by the squared amplitude, the ratio $\sigma_{\text{el}}/\sigma_{\text{tot}}$ will be larger for a strong interaction with a short range, than for a weaker interaction with a wider range.

For the general case with fluctuating amplitudes, we can using the results in eq. (3.18), in an analogous way rewrite $(\sigma_{\text{tot},k}^{(\text{pp})})^2$ in eq. (3.45) in the following form

$$\left(\sigma_{\text{tot},k}^{(\text{pp})}\right)^2 = 16\pi^2 \langle\langle \tilde{T}_{k,l}^{(\text{pp})}(q=0)\rangle_l^2\rangle_k = 16\pi \frac{d}{dt}\left(\sigma_{\text{el}}^{\text{pp}}(t) + \sigma_{\text{Dp}}^{\text{pp}}(t)\right)\Big|_{t=0}. \tag{3.51}$$

Here $\sigma_{\text{Dp}}^{\text{pp}}$ denotes the cross section for single diffractive excitation of the projectile proton (*i.e.* on one side only). For a fluctuating amplitude we then get instead of eq. (3.48)

$$\sigma_{\text{tot}}^{\text{pd}} = 2\,\sigma_{\text{tot}}^{(\text{pp})} - 8\pi\left(\int d^2b\,\rho^2(b)\right)\frac{d}{dt}\left(\sigma_{\text{el}}^{\text{pp}}(t) + \sigma_{\text{Dp}}^{\text{pp}}(t)\right)\Big|_{t=0}. \tag{3.52}$$

The negative term in eq. (3.52) represents a shadowing effect, which for a deuteron target has one contribution from the elastic proton–nucleon cross section, and another from diffractive excitation. Note in particular, that it is only *single* diffraction which enters, with an excited projectile but an elastically scattered target nucleon. (This would be particularly important in case of a photon or a pion projectile.)

Larger target nuclei For a larger target higher moments, $\left\langle\left\langle T^{(\text{pp})}\right\rangle_t^n\right\rangle_p$ $(n = 1, 2, \ldots, A)$, of the pp amplitude, averaged over target states, are needed. These moments cannot be determined from the total cross section and the cross section for diffractive excitation. They can be calculated if we know the full probability distribution, $dP/d\left\langle T^{(\text{pp})}\right\rangle_t$, for the pp amplitude averaged over target states, but for varying projectile states[7]. In addition also higher moments of the nucleus density, $\int d^2b\,\rho^n(b)$, are needed.

We also note here that the factorisation feature in eq. (3.21) is not realised in AA collisions. This implies that also in the optical limit, the AA-results cannot be directly expressed in terms of the moments $\left\langle\left\langle T^{(\text{pp})}\right\rangle_t^n\right\rangle_p$.

Wounded nucleon cross sections

Also for cross sections corresponding to wounded (absorptively or inclusively) nucleons, approximations analogous to eqs. (3.41) and (3.43) are possible. Integrating the expressions

---

[7]The average for $n = 3$ was estimated from diffractive proton-deuteron scattering in ref. [11].

in eq. (3.44) over $\mathbf{b}_\nu$, and averaging also over projectile states k gives, in analogy with eqs. (3.45) and (3.46), the following result

$$d\sigma_w^{pA}/d^2 b = 1 - \left\langle \left(1 - \rho(b)\,\sigma_{w,k}^{pp}\right)^A \right\rangle_k. \qquad (3.53)$$

The average in eq. (3.53) includes averages of all possible powers $\left\langle (\sigma_{w,k}^{pp})^n \right\rangle_k$. For $n = 1$ this is just equal to the pp cross section σ_w^{pp} for (with w denoting either absorptively or inclusively wounded), but for higher moments a knowledge of the full probability distribution for $\sigma_{w,k}^{pp}$ is needed, in analogy with eq. (3.46) for the total pA cross section. Note, however, that a similar relation is not satisfied for the elastic or total inelastic cross sections, σ_{el} and $\sigma_{in} = \sigma_{tot} - \sigma_{el}$, which as seen in eq. (3.18) contain the average over projectile states k before squaring.

Average number of wounded nucleons

In eq. (3.53) $\rho(b)\sigma_{w,k}^{pp}$ represents the probability that a specific target nucleon is wounded, in a collision with a projectile in state k at an impact parameter $\mathbf{b}$. In the optical limit this probability is the same for all A target nucleons. Averaging over projectile states k then gives the average number of wounded target nucleons for an encounter at this b-value. Dividing by the probability for a "wounded" event, we get the average number of wounded target nucleons per wounded event for this b:

$$\left\langle N_w^t(b) \right\rangle = \frac{A\,\rho(b)\,\sigma_w^{pp}}{1 - \left\langle \left(1 - \rho(b)\sigma_{w,k}^{pp}\right)^A \right\rangle_k}. \qquad (3.54)$$

Normalising by the probability for absorption in eq. (3.53), and integrating over b with a weight given by the same probability, then gives

$$\left\langle N_w^t \right\rangle = \frac{\int d^2 b\, A\,\rho(b)\,\sigma_w^{pp}}{\int d^2 b\, d\sigma_w^{pA}/d^2 b}, \qquad (3.55)$$

with $d\sigma_w^{pA}/d^2 b$ given by eq. (3.53). As noted above, this needs knowledge of the full probability distribution for $\sigma_{w,k}^{pp}$.

Multiplicity distribution for wounded nucleons

As in section 3.3, when calculating the full distribution in $N_w^t(b)$, it is important to take the average over projectile states k after multiplication of the different nucleon absorption

probabilities, which gives

$$\frac{dP(b)}{dN_w^t} = \begin{pmatrix} A \\ N_w^t \end{pmatrix} \left\langle \left(\rho(b)\, \sigma_{w,k}^{\mathrm{pp}} \right)^{N_w^t} \cdot \left(1 - \rho(b)\, \sigma_{w,k}^{\mathrm{pp}} \right)^{A - N_w^t} \right\rangle_k . \qquad (3.56)$$

Similar to the general result in eq. (3.38), this expression includes the probability for zero target participants. Normalising by the probability for absorption in eq. (3.53), and integrating over b with a weight given by the same probability, gives finally

$$\frac{dP}{dN_w^t} = \frac{\int d^2 b \; dP(b)/dN_w^t}{\int d^2 b \; d\sigma_w^{\mathrm{p}A}/d^2 b} . \qquad (3.57)$$

Here $dP(b)/dN_w^t$ and $d\sigma_w^{\mathrm{p}A}/d^2 b$ are the expressions in eqs. (3.56) and (3.53).

4 Models for pp scattering used in Glauber calculations

As mentioned in section 3.4, most analyses today use a Monte Carlo simulation to generate a realistic distribution of nucleons within the nucleus, including fluctuations which cause quasi-elastic scattering of the nucleus [46, 9] as well as initial state anisotropies (*e.g.* [47]). In contrast most Glauber Monte Carlos use a rather simple model for the pp interaction. In this section we discuss some models which have been used in analyses of experimental data. We will also comment on the pros and cons, when these models are applied to pA collisions.

In the optical approximation, where the extension of the nucleus is much larger than the range of the pp interaction, the results for pA collisions can be expressed in terms of integrated pp amplitudes, without knowledge of their respective impact parameter dependence (see eq. (3.43)). It is therefore most essential to use a model, where the integrated pp cross sections are well reproduced. Note, however, that although the total pA cross section is most sensitive to the integrated total pp cross section, the b-dependence is very important for the ratio between the elastic and total cross sections (see eq. (3.50)). This feature naturally also affects the ratio between the inelastic and the total cross sections.

As mentioned in the introduction, the problems encountered when taking fluctuations and diffractive excitation of the nucleons properly into account in the Glauber model, have implied that these effects are neglected or severely approximated in many applications, see *e.g.* ref. [4]. However also in models which do include fluctuations, as far as we know no published analysis uses a model which can separate single excitation of the projectile from that of the target, and from double excitation. This is a problem as the various pA cross sections in section 3 contain powers of pp amplitudes averaged in different ways over projectile and target fluctuation.

We first discuss some simple models determined by just a few parameters, and then the more ambitious approach by Strikman and coworkers, using a continuous distribution for the fluctuations.

4.1 Simple approximations

Non-fluctuating models

i) Black disk model

The simplest approximation is the "black disk model" with a fixed radius. Here diffractive excitation is completely neglected, and the target in a nucleon–nucleon collision acts as a black absorber. The projectile nucleon travels along a straight line, and interacts inelastically if the transverse distance to a nucleon in the target is smaller than a distance R, which gives

$$T^{(\mathrm{pp})}(b) = \Theta(R - b) \tag{3.58}$$

This results in the following cross sections:

$$\sigma_{\mathrm{el}} = \sigma_{\mathrm{in}} = \sigma_{\mathrm{tot}}/2 = \pi R^2, \quad \sigma_D = 0. \tag{3.59}$$

Here σ_{D} denotes the cross section for diffractive excitation. (See eq. (3.4) with $F = \infty$.) This is in clear contrast to the experimental result $\sigma_{\mathrm{el}} \approx \sigma_{\mathrm{tot}}/4$ and the total diffractive excitation of the same order of magnitude as σ_{el}. This again illustrates how a short range amplitude gives a large $\sigma_{\mathrm{el}}/\sigma_{\mathrm{tot}}$ ratio. The radius can therefore be adjusted to reproduce the experimental value for one of these three cross sections, at the cost of not reproducing the other two.

As discussed in ref. [9], choosing to reproduce $\sigma_{\mathrm{tot}}^{\mathrm{pp}}$, the simple black-disk result for pPb collisions agrees rather well with the DIPSY model for $\sigma_{\mathrm{tot}}^{\mathrm{pPb}}$, but not so well for $\sigma_{\mathrm{el}}^{\mathrm{pPb}}$ or $\sigma_{\mathrm{in}}^{\mathrm{pPb}}$. Similarly adjusting R to reproduce $\sigma_{\mathrm{in}}^{\mathrm{pp}}$ or $\sigma_{\mathrm{abs}}^{\mathrm{pp}}$ gives results which agree with DIPSY for the corresponding pPb cross section, but not for the other.

The black disk model is implemented in many Monte Carlos, *e.g.* in the PHOBOS Monte Carlo [48, 49]. It is also used in refs. [46, 47] where the authors study fluctuations in the distribution of nucleons within the nucleus, but do not address the fluctuations in the pp interaction.

ii) Grey disk and Gaussian profile

Also other shapes for a non-fluctuating pp interaction have been used in the literature [50, 24, 4]. The simplest example is a fixed semi-transparent "grey disk", with opacity given

by the parameter α:

$$T^{(\mathrm{pp})}(b) = \alpha\Theta(R - b), \qquad (3.60)$$

which gives $\sigma_{\mathrm{el}} : \sigma_{\mathrm{tot}} : \sigma_{\mathrm{in}} = \alpha : 2 : 2 - \alpha$.

Another example is a Gaussian profile

$$T^{(\mathrm{pp})}(b) = \alpha \exp(-b^2/2B) \qquad (3.61)$$

giving $\sigma_{\mathrm{el}} : \sigma_{\mathrm{tot}} : \sigma_{\mathrm{in}} = \alpha : 4 : 4 - \alpha$.

These models contain two parameters (with $\alpha \leq 1$ to satisfy the unitarity constraint $T \leq 1$), and it is therefore possible to fit *e.g.* the total and the elastic cross sections, with the inelastic (non-diffractive) cross section given by the difference between these two. The lower ratio $\sigma_{\mathrm{el}}/\sigma_{\mathrm{tot}}$ is a consequence of the wider interaction range. We note, however, that even if typical events are well reproduced it is often interesting to study rare events in the tail of a distribution. As an example the tail of the pp amplitude out to large b-values may be important for the probability to produce rare events with many pN sub-collisions at large impact separation. The Gaussian profile may *e.g.* thus give a larger tail than the gray disk, also when they give very similar averages.

Models including fluctuations

To account for diffractive excitation, we must allow the pp amplitude to fluctuate. Models used in the literature do, however, not separate fluctuations in the projectile and the target. From eqs. (3.28) and (3.25) we see that if the amplitude is adjusted to reproduce the amplitude averaged over target states, $\langle T^{(\mathrm{pp})}(b)\rangle_t$, then the correct result for the pA total cross section will be obtained. The fluctuations included in the model should then only describe fluctuations in the projectile state, and should thus reproduce the cross section for single excitation of the projectile. Such a model will, however, not reproduce cross sections for absorptively wounded nucleons properly, as will be discussed further below. **iii)**

Fluctuating grey disk

The simplest model accounting for diffractive excitation is the fluctuating "grey disk model". Here it is assumed that within a radius R the projectile is absorbed with probability a, with $0 < a < 1$. This implies that $\langle T(b)^2\rangle = \langle T(b)\rangle$, and the resulting pp cross sections are

here

$$\sigma_{\text{tot}} = 2 \int d^2b \left\langle T^{(\text{pp})}(b) \right\rangle = 2\pi R^2 a$$

$$\sigma_{\text{el}} = \int d^2b \left\langle T^{(\text{pp})}(b) \right\rangle^2 = \pi R^2 a^2$$

$$\sigma_{\text{D}} = \int d^2b \left(\left\langle T^{(\text{pp})}(b)^2 \right\rangle - \left\langle T^{(\text{pp})}(b) \right\rangle^2 \right) = \pi R^2 a(1-a)$$

$$\sigma_{\text{abs}} = \int d^2b \left\langle 1 - \left(1 - T^{(\text{pp})}(b) \right)^2 \right\rangle = \pi R^2 a. \tag{3.62}$$

The two parameters R and a can now be adjusted to reproduce *e.g.* the total and the elastic pp cross sections. At LHC this would give $a \approx 1/2$. The cross section for diffractive excitation should here be interpreted as representing only the single excitation of the projectile, while target excitation is part of the absorptive cross section. With $a = 1/2$ this is quite an overestimate. It corresponds rather to the total diffractive excitation, which implies that the results for $\sigma_{\text{abs}}/\sigma_{\text{tot}}$ is close to the experimental value. The relation between the absorptive and diffractive cross section, which together make up the inelastic cross section, is also fixed in this model.

The agreement of the fluctuating gray disk with DIPSY results for pPb collisions are not superior to those of the black disk model [9].

iv) Fluctuating Gaussian profile

Here the profile in eq. (3.61) gives the probability for absorption. Thus $T = 1$ with probability $\alpha \exp(-b^2/2B)$ while $T = 0$ with probability $1 - \alpha \exp(-b^2/2B)$. As for the fluctuating gray disk this implies that $\langle T(b)^2 \rangle = \langle T(b) \rangle$. This does not change the total and elastic cross sections, but it splits the inelastic one into relative fractions a non-diffractive (absorptive) and a diffractive part, with the result $\sigma_{\text{tot}} : \sigma_{\text{el}} : \sigma_{\text{D}} : \sigma_{\text{abs}} = 4 : \alpha : 2-\alpha : 2$. For $\alpha \approx 1$ this gives the same result as the fluctuating gray disk. (Although this implies that the results will be very similar in the optical limit, it does not mean that the results are identical for a more realistic nucleus. This will be particularly true for the tail at very large numbers of wounded nucleons.)

This model is also an option in the PHENIX Monte Carlo.

v) Fluctuating black disk model

It is possible to let the radius of the black disk fluctuate. As for the two previous model, the fact that $T(b)$ is either 1 or 0 implies that $\langle T(b)^2 \rangle = \langle T(b) \rangle$, which gives $\sigma_{\text{abs}} = \sigma_{\text{tot}}/2$. Such a fluctuating black disk model has sometimes been used in connection with the GG

model described in section 4.2, and will be further described below.

vi) A new simple model allowing for separate projectile and target excitations

The main reason neither of the above models are able to properly take into account the diffractive aspects of nucleon collisions, is that the fluctuations in the cross sections are not treated in terms of fluctuations in the projectile and target separately. Interpreting the amplitude T as the average over target states, which as mentioned above can give a correct total cross section, excitation of target nucleons will not be separated from the absorptive cross section.

To redeem this we have constructed a new model, which in some sense is the minimal possible extension needed to reproduce all relevant semi-inclusive cross sections. The basis of the model is having fluctuating sizes of the colliding nucleons. With some probability, c, a nucleon with radius r_1, can fluctuate into a larger radius r_2. This will then give us the elastic amplitude for a projectile with radius R_p colliding with a target with radius, R_t,

$$T(b) = \alpha \, \Theta(R_p + R_t - b). \tag{3.63}$$

Here α is again an opacity parameter between zero and one, which together with c, r_1 and r_2 gives us four parameters which can be adjusted to reproduce the relevant nucleon–nucleon cross sections σ_{abs}, σ_{el}, $\sigma_{\mathrm{Dp}} = \sigma_{\mathrm{Dt}}$ and σ_{DD}. Below we will refer to this model as 2×2-disk.

4.2 The approach by Strikman and coworkers

An ambitious approach to describe fluctuations in pp scattering, for use in the Glauber model, was presented in refs. [10, 11]. This model has been further extended in several papers by Alvioli, Strikman and coworkers; for a general overview see ref. [12] and further references in there. Recent studies, with applications to the LHC, discuss effects of colour fluctuations (or flickering) [13], and evidence for x-dependent proton colour fluctuations [14]. The model does not take into account the possibility of separate excitations of the projectile and the target, and the fluctuations in the target are not considered. In this section we will also discuss how the model can be modified to take the target fluctuations into account. (Note that our amplitude T is in ref. [12] denoted Γ.)

pp total cross section

The basic feature of the model is a description of the fluctuations in the *NN* total cross section, as a smooth function, which has the form

$$P_{\text{tot}}(\sigma) = \rho \frac{\sigma}{\sigma + \sigma_0} \exp\left\{-\frac{(\sigma/\sigma_0 - 1)^2}{\Omega^2}\right\}, \tag{3.64}$$

$$\sigma_{\text{tot}} = \int d\sigma\, \sigma\, P_{\text{tot}}(\sigma). \tag{3.65}$$

Here σ is regarded as the total pp cross section in a single event, with the probability distribution $P_{\text{tot}}(\sigma)$, while the observed total cross section σ_{tot} is given by the average in eq. (3.65). [8] For the functional form in eq. (3.64), the average and the width of the distribution are related to (but not identical to) the parameters σ_0 and Ω, while ρ is a normalisation constant.

In eqs. (3.25) and (3.28) we see that the total pA cross section contains all possible moments with respect to the fluctuations in the *projectile* state, but only the average (the first moment) with respect to the fluctuations in the *target* state. Thus, although target fluctuations are not considered explicitly, we conclude that if σ is interpreted as the *average over target states*

$$\sigma = 2 \int d^2 b \langle T_{k,l}^{(\text{pp})} \rangle_l, \tag{3.66}$$

and only the average over *projectile states* is described by the distribution in eq. (3.64), then the total pA cross sections will (in the large nucleus approximation) be determined in terms of all possible moments $\langle \sigma^N \rangle$, obtained from the distribution $P_{\text{tot}}(\sigma)$, and the average in eq. (3.65) will correctly give the total pp cross section.

With this interpretation the width of the distribution can also be determined from eq. (3.51), which gives the second moment

$$\langle \sigma^2 \rangle = 16\pi^2 \langle \langle \tilde{T}_{k,l}^{(\text{pp})}(t=0) \rangle_l^2 \rangle_k = 16\pi \left. \frac{d}{dt}\left(\sigma_{\text{el}}^{\text{pp}}(t) + \sigma_{\text{Dp}}^{\text{pp}}(t)\right)\right|_{t=0}. \tag{3.67}$$

Here the first term in the parenthesis would give $\langle \sigma \rangle^2$ corresponding to Glauber's result, while the second, determined by *single* excitation of the projectile, is the result of fluctuations in the projectile state.

Eq. (3.67) has been used by Blaettel *et al.* [11] together with eq. (3.52) to estimate the width from shadowing in pd collisions at fixed target energies. They also estimated the width from diffractive excitation data at the CERN $\bar{\text{p}}$p collider. With data from TOTEM [51, 52, 53]

---

[8]Note, however, that in ref. [12] the notation is changed, such that $\sigma \to \sigma_{\text{tot}}$ and $\sigma_{\text{tot}} \to \sigma_{\text{tot}}^{(\text{pp})}$.

and ALICE [54] for elastic and single diffractive cross sections and elastic forward slope, supplemented by the assumption that the diffractive slope is approximately half the elastic (as is the case at 560 GeV [55]), we get for 7 TeV the estimated width $\sqrt{\langle\sigma^2\rangle - \langle\sigma\rangle^2} \approx 0.4\langle\sigma\rangle$. As mentioned above, the amplitude for larger nuclei the amplitude in eq. (3.45) contains also higher moments of the pp amplitude. Blaettel *et al.* estimated also the third moment, $\langle\sigma^3\rangle$ from data for diffractive excitation in pd scattering, and they also studied other analytic forms. Most recent applications use, however, the form in eq. (3.64), in which the higher moments are fixed by a determination of the width.

Elastic cross section

We use the notation

$$T^{(\mathrm{pp})}(b,\sigma) \equiv \left\langle T^{(\mathrm{pp})}_{k,l}(b) \right\rangle_l \tag{3.68}$$

to describe the *b*-dependence of the fluctuating cross section σ in eq. (3.66). This gives

$$\sigma = \int d^2b\, 2\, T^{(\mathrm{pp})}(b,\sigma)$$

$$d\sigma_{\mathrm{tot}}/d^2b = \int d\sigma\, P_{\mathrm{tot}}(\sigma)\, 2\, T^{(\mathrm{pp})}(b,\sigma),$$

$$d\sigma_{\mathrm{el}}/d^2b = \left| \int d\sigma\, P_{\mathrm{tot}}(\sigma)\, T^{(\mathrm{pp})}(b,\sigma) \right|^2. \tag{3.69}$$

As pointed out earlier, the relation between σ_{el} and σ_{tot} depends on the width of the interaction. Thus, although the elastic and total cross sections for fixed *b* are given by the same average over target fluctuations, the elastic cross section is not determined by the σ-distribution in eq. (3.64), unless it is supplemented by a knowledge of the *b*-dependence (for all values of σ).

We here note that the distribution in eq. (3.64) has a tail out to large cross sections. The unitarity constraint $T(b) < 1$, or $d\sigma_{\mathrm{tot}}/d^2b < 2$, therefore implies that a large value for σ must be associated with a wider *b*-distribution. The effect of different assumptions about the *b*-dependence will be discussed in section 4.2.

This feature implies of course that also the inelastic cross section cannot be directly determined from eq. (3.64).

Wounded nucleon cross section

As discussed in section 3.3, the definition of a wounded nucleon may depend upon the specific observables under consideration. As pointed out earlier, in cases where the *absorptive*

cross section is the most relevant, this is given by

$$d\sigma_{\rm abs}/d^2 b = 2 \langle T(b) \rangle_{p,t} - \langle T(b)^2 \rangle_{p,t}, \qquad (3.70)$$

which cannot be determined without knowing how the separate fluctuations in the projectile and target result in single and double diffractive excitation. We see that in contrast to the expressions entering the total and elastic cross sections in eq. (3.69), this expression contains also the second moment with respect to the target fluctuations.

In ref. [12] Alvioli and Strikman identify the differential wounded nucleon cross section with the total inelastic pp cross section (which includes diffractive excitation). In the hypothetical situation where the target did not fluctuate, after averaging over projectile fluctuations this also gives the absorptive (inelastic non-diffractive) cross section.

However, if T is identified with the amplitude averaged over target states, as in eq. (3.68) (which gives the correct result for the total cross section), then we get instead

$$\left\langle 2T(b) - T(b)^2 \right\rangle_p = \left\langle T_{k,l}^{\rm (pp)}(b) \right\rangle_{l,k} - \left\langle \left(\left\langle T_{k,l}^{\rm (pp)}(b) \right\rangle_l \right)^2 \right\rangle_k = d\sigma_w/d^2 b. \qquad (3.71)$$

From eq. (3.18) we see that this corresponds exactly to the inclusively wounded nucleon cross section $d\sigma_{w_{\rm inc}}/d^2 b$, where $\sigma_{w_{\rm inc}}$ now includes diffractively excited target nucleons:

$$\sigma_{w_{\rm inc}} = \sigma_{\rm abs} + \sigma_{\rm DD} + \sigma_{\rm Dt} = \sigma_{\rm tot} - \sigma_{\rm el} - \sigma_{\rm Dp}. \qquad (3.72)$$

We here note that, although $d\sigma_w/d^2 b$ in eq. (3.71) contains the same average of $T_{k,l}^{\rm (pp)}(b)$ over target states, to integrate this expression over b we also need to know the b-dependence of $T^{\rm (pp)}(b, \sigma)$ for all σ. We also note that the integral $\int d^2 b \int d\sigma P(\sigma) T^2(b, \sigma)$ appearing in σ_w is different from $\int d^2 b [\int d\sigma P(\sigma) T(b, \sigma)]^2$ appearing in $\sigma_{\rm el}$.

The distribution $P_w(\sigma_w)$ is consequently not easily related to the distribution in the total cross section $P_{\rm tot}(\sigma_{\rm tot})$. Lacking a detailed description, Strikman *et al.* use an approximation assuming the proportional distribution which for the absorption probability would mean

$$P_{\rm abs}(\sigma) \propto P_{\rm tot}(\sigma/\lambda_{\rm abs}), \qquad (3.73)$$

where $\lambda_{\rm abs} = \sigma_{\rm abs}/\sigma_{\rm tot}$. This approximation may be less accurate, since for non-peripheral collisions $T(b)$ is rather close to 1, where $dP_{\rm abs}(b)/dT(b) \equiv d(2T(b)-T(b)^2)/dT(b) = 0$, while for peripheral collisions with small T we have $dP_{\rm abs}(b)/dT(b) = 2$. Also, even if the analytic form in eq. (3.64) may give a satisfying result, there is no obvious reason why the same value of the width parameter Ω, should be applicable as the one determined from shadowing or diffractive excitation.

Monte Carlo implementations

The GG model has been implemented in Monte Carlo simulations in many applications to pA collisions, *e.g.* in ref. [12, 13, 14]. In experimental analyses it has been combined with earlier Monte Carlos, where the parameters in one of the simple models described in section 4.1 are allowed to vary according to eq. (3.64) (or using a scaled version as in eq. (3.73), but typically using the total inelastic cross section rather than the absorptive), in a way reproducing the total (or the inelastic) cross section respectively. The PHOBOS Monte Carlo [48] with a black disk with a variable radius, which is also used by *e.g.* ATLAS [16]. Fitting to the inelastic pp cross section here overestimates the number of absorbed nucleons. In ref. [13] it is argued that this is a small effect, as the cross section for diffractive excitation of the projectile proton is small in pA collisions. However, the cross section for target nucleon excitation is not small, and although the cross section for diffractive projectile excitations is small, it may have a significant effect on the tail of the wounded nucleon distribution at high multiplicities. These problems will be further discussed in section 5.

Impact-parameter profile

To investigate further, we need to make assumptions about the impact-parameter dependence, $T^{(\mathrm{pp})}(b, \sigma)$ in eq. (3.69). Strikman *et al.* have suggested a Gaussian profile on the form

$$T^{(\mathrm{pp})}(b, \sigma) = \frac{\sigma}{4\pi B} \exp\left(-b^2/2B\right), \tag{3.74}$$

where B is proportional to σ. The proportionality factor could then be fit together with the σ_0 and Ω parameters of eq. (3.64) to the total and elastic pp cross sections from eq. (3.69) and the inclusively wounded cross section in eqs. (3.71) and (3.72):

$$\sigma_{\mathrm{tot}} = \int d^2b \int d\sigma \, P_{\mathrm{tot}}(\sigma) \, 2 \, T^{(\mathrm{pp})}(b, \sigma),$$

$$\sigma_{\mathrm{el}} = \int d^2b \left| \int d\sigma \, P_{\mathrm{tot}}(\sigma) \, T^{(\mathrm{pp})}(b, \sigma) \right|^2,$$

$$\sigma_{w_{\mathrm{inc}}} = \int d^2b \int d\sigma \, P_{\mathrm{tot}}(\sigma) \left[2 \, T^{(\mathrm{pp})}(b, \sigma) - T^{(\mathrm{pp})}(b, \sigma)^2 \right]. \tag{3.75}$$

In this case we find that the wounded cross section distribution can indeed be written as a simple scaling of the total, $P_{w_{\mathrm{inc}}}(\sigma) = P_{\mathrm{tot}}(\sigma/\lambda_{w_{\mathrm{inc}}})$, however, the same would still not be true for $P_{w_{\mathrm{abs}}}$.

We also find that for the Gaussian profile, the unitarity constraint, $T^{(\mathrm{pp})}(b, \sigma) \leq 1$, gives a hard limit on $\sigma_{\mathrm{tot}} - \sigma_{w_{\mathrm{inc}}} = \sigma_{\mathrm{el}} + \sigma_{\mathrm{Dp}} < \sigma_{\mathrm{tot}}/4$, which is not found experimentally. To proceed we therefore decided to choose a different form of the b distribution. What is used by ATLAS in *e.g.* [16] is a black disk approximation: $T^{(\mathrm{pp})}(b, \sigma) = \Theta(\sqrt{\sigma/2\pi} - b)$.

We will instead use a semi-transparent disk with

$$T^{(\mathrm{pp})}(b, \sigma) = T_0 \Theta \left(\sqrt{\frac{\sigma}{2\pi T_0}} - b \right),$$ (3.76)

(*c.f.* eq. (3.61)) where the unitarity constraint gives us $\sigma_{\mathrm{el}} + \sigma_{\mathrm{Dp}} < \sigma_{\mathrm{tot}}/2$, which can easily accommodate experimental data.

Conclusion on the GG formalism

We conclude that for the pA total cross sections, it is straight forward to use the GG formalism by Strikman *et al.*, interpreting σ as the total cross section averaged over target states. The distribution $P_{\mathrm{tot}}(\sigma)$ then describes the fluctuations in the projectile states. The average and the variance of P_{tot} are given by eqs. (3.65) and (3.67). However, to get the elastic or inclusively wounded nucleon cross section (including target excitation), we also need to know the b-dependence of $d\sigma(b)/d^2b \equiv \langle T^{(\mathrm{pp})}(b) \rangle_t$ for all values of σ. If wounded nucleons are interpreted as absorbed nucleons, we also need to know $\langle (T^{(\mathrm{pp})}(b))^2 \rangle_t$. To estimate these quantities in a way consistent with eq. (3.18), we believe it is better to use a formalism which include individual excitation of both projectile and target.

4.3 Consequences of fluctuating pp cross section

Adding fluctuations to the pp cross section dramatically changes the distributions of the number of wounded nucleons. But since pp data only offers inclusive and semi-inclusive cross sections to compare models to, one is given little guidance to why one model works better than another. Although the DIPSY model is less than perfect in reproducing experimental data, it includes those fluctuations in the nucleon wave function, which we argue are important when considering the number of participating nucleons in pA and AA collisions. Thus although it only works at high energies due to lack of quarks in the proton, the description of high-$p_\perp$ particles is poor, and generation of exclusive diffractive final states is difficult, we believe these deficiencies are less important when describing the fluctuations.

Comparison with DIPSY

When comparing the GG results in eq. (3.75) with results from DIPSY, we first look at the total cross section. As descussed above, we interpret the GG fluctuating total cross section σ in eq. (3.75) as describing fluctuations in the projectile, averaged over target states:

$$\sigma \equiv 2 \int d^2b \, \langle T(b) \rangle_t.$$ (3.77)

Table 3.1: GG parameters values obtained by fit to inclusive and semi-inclusive cross sections from DIPSY.

	Ω	σ_0	λ
Original parametrisation	0.37	85.25	0.716
Log-normal parametrisation	0.25	85	0.716

The parameters in the GG distribution $P_{\text{tot}}(\sigma)$ can then be tuned to reproduce the corresponding distribution in DIPSY, which is obtained by generating a large ensemble of targets for each projectile, and for each target calculate T at a large number of impact parameters.

To get the corresponding results for the elastic and the "wounded" cross sections $\sigma_{\text{el}} = \int d^2b \, \langle T(b) \rangle_t^2$ and $\sigma_{w_{\text{inc}}} = \int d^2b \left(2 \langle T \rangle_t - \langle T \rangle_t^2 \right)$, we have to make an assumption about the b-distribution of the amplitude $\langle T(b) \rangle_t = T^{(pp)}(b, \sigma)$, appearing in eq. (3.75). We here make the simple approximation in eq. (3.76), and calculate the cross section $\sigma_{w_{\text{inc}}}$ from eq. (3.75).

Tuning the parameters in $P_{\text{tot}}(\sigma)$ to the DIPSY results is now done fitting the cross sections σ_{tot}, σ_{el}, and σw_{inc} using a χ^2 fit. The values obtained with DIPSY are here assigned weights corresponding to the relative error one would expect from experiment (taken from the analysis in ref. [56]). The result of the fit is shown in the first line of table 3.1. The result of the fit is compared with the DIPSY results for the distributions $P_{\text{tot}}(\sigma)$ and $P_{w_{\text{inc}}}(\sigma)$ in figure 3.3. We note here that the b-dependence assumed in eq. (3.76) implies that the distribution $P(\sigma_{w_{\text{inc}}})$ is given by a scaled P_{tot}-distribution $P_{w_{\text{inc}}}(\sigma) \propto P_{\text{tot}}(\sigma/\lambda)$, where $\lambda = \sigma_{w_{\text{inc}}}/\sigma_{\text{tot}}$.

It is clearly seen, that the high-σ tails of the DIPSY distributions are not reproduced by the functional form for P_{tot} in eq. (3.64). Since DIPSY provides a picture of the fluctuations built upon a full dynamical model, it is reasonable to believe that the shape of the DIPSY distributions are closer to reality than eq. (3.64). We therefore try a new parametrisation which makes it easier to obtain a large high-σ tail, namely a log-normal distribution:

$$P_{tot}(\ln \sigma) = \frac{1}{\Omega\sqrt{2\pi}} \exp\left(-\frac{\ln^2(\sigma/\sigma_0)}{2\Omega^2} \right). \qquad (3.78)$$

The fit to the DIPSY cross sections with the log-normal distribution is also shown in table 3.1. The corresponding distributions are shown in figure 3.3 for two different width parameters, labeled $\Omega = 0.25$ and $\Omega = 0.33$. We see that the larger value matches the DIPSY distribution perfectly, while the lower value is close to the GG curve below the maximum but has a higher tail for larger σ.
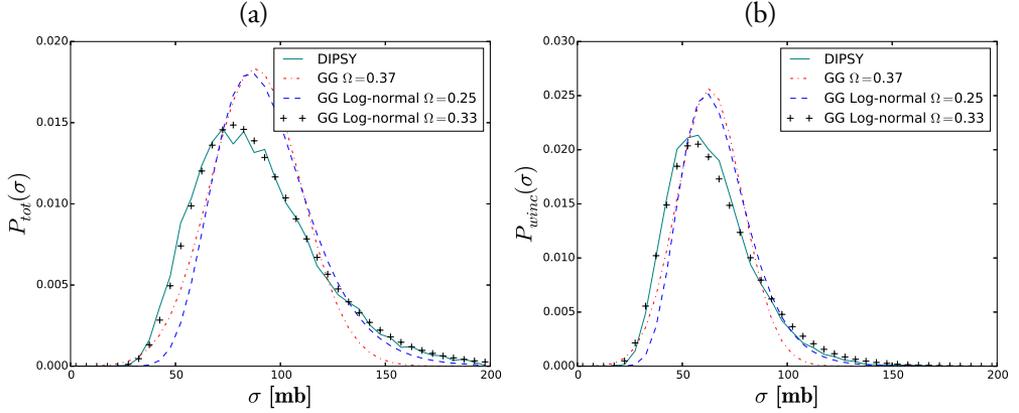
Figure 3.3: Fluctuations in the total (a) and inclusively wounded (b) cross section by DIPSY and the Glauber–Gribov model with different parametrisations of the cross section fluctuations.

We note, however, that for technical reasons the diffractive cross section in DIPSY is calculated demanding a central rapidity gap, restricting the masses to $M_X^2 \leq \sqrt{s} \cdot (1\,\text{GeV})$. This implies that the fluctuations are somewhat underestimated. We therefore believe that the functional form is quite realistic, while the width is underestimated. Results obtained when tuning instead to the experimental cross sections are presented in the folliong subsection.

Comparison to data

We now repeat the same procedure as in the previous section, but with experimental results for the relevant cross sections. There is no experimental access to the distributions in cross section, but the integrated inclusive and semi-inclusive cross sections are measured, and we here use values from ref. [56], extrapolated to $\sqrt{s_{NN}} = 5$ TeV:

$$\sigma_{\text{tot}} = 93.2 \pm 2.3 \text{ mb}, \ \sigma_{\text{el}} = 23.2 \pm 1.2 \text{ mb and } \sigma_{w_{\text{inc}}} = 63.0 \pm 1.8 \text{ mb}. \qquad (3.79)$$

Note that the diffractive cross sections here have been extrapolated into unmeasured M_X regions to the full $0 < M_X < \sqrt{S}$ interval. As mentioned above this was not done in for the DIPSY diffractive cross sections in section 4.3, where by construction a rapidity gap is required at mid rapidity. Hence we expect that the fluctuations for DIPSY are underestimated as compared to data. The parameter values obtained by minimising the χ^2 are listed in table 3.2. In figure 3.4 we compare the fits of the two parametrisations of $P_{w_{\text{inc}}}(\sigma)$ shown above. We see that the new parametrisation provides larger fluctuations in the high-σ tail, as expected. It should be noted that both fits reproduce the experimental cross sections well within the experimental errors. For comparison we also show log-normal distribution

Table 3.2: GG parameter values obtained by fit to inclusive and semi-inclusive cross-section from data.

	Ω	σ_0	λ
Original parametrisation	0.82	77.75	0.677
Log-normal parametrisation	0.43	85	0.677

$P_{w_{\text{inc}}}(\sigma)$, when it's width and mean are fitted to DIPSY by eye (denoted $\Omega = 0.33$), which is significantly more narrow.

We suspect that while the log-normal parametrisation probably gives a more realistic description of the high-σ fluctuations in the GG formalism, it is far from the whole story. The GG results presented here are obtained assuming that all fluctuations are ascribed to fluctuations in projectile *size*, as described in section 4.2. In DIPSY, however, the cross section fluctuations arise from a combination of fluctuations in size and fluctuations in gluon density. We believe that updating the profile functions from simple disks or Gaussian distributions to more realistic ones, could provide a better handle on the parametrisations of the cross section from pp data, this will be investigated in a future publication. So far we have described a prescription which seems to both catch the necessary physics to calculate the inclusive wounded cross section, with all parameters being obtainable from pp data. We will now apply this to pA collisions.

4.4   Distributions of wounded nucleons

Using the considerations about fluctuations in the wounded cross section, we will now turn to generation of distributions of wounded nucleons. Normally, in inelastic, non-diffractive pA collisions, the number of wounded nucleons is always one plus the number of inelastic, non-diffractive NN interactions. In the following we will make the distinction between diffractively and absorptively wounded nucleons. In order to avoid situations where the projectile should sometimes be counted twice as a wounded nucleon, we will solely talk about the number of wounded nucleons in the target, which we denote N_w^t. We note also that since the number of sub-collisions and the number of wounded nucleons are trivially connected, the question whether a specific observable scales better with wounded nucleons or with NN sub-collisions, is much more relevant for nucleus–nucleus collisions.
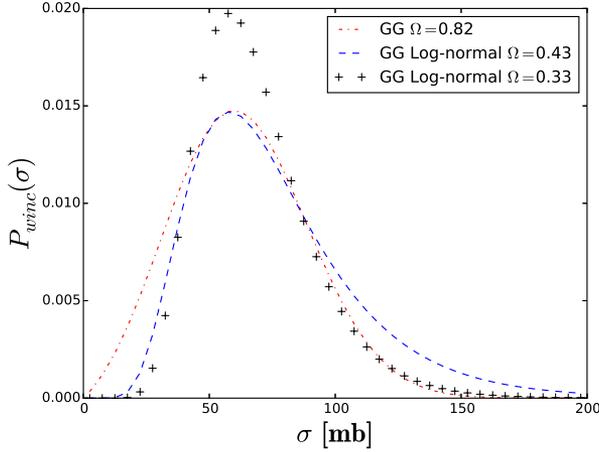
Figure 3.4: Fluctuations in the inclusively wounded cross section by the Glauber–Gribov model with two parametrisations of the cross section fluctuations, fitted to data.

Inclusively wounded nucleons

We will describe the nucleus' transverse structure using a Woods–Saxon distribution in the GLISSANDO parameterisation [57, 58], where the density is given by:

$$\rho(r) = \frac{\rho_0(1 + wr^2/R^2)}{1 + \exp((r - R)/a)}, \qquad (3.80)$$

where R is the nuclear radius, a is "skin width", and ρ_0 is the central density. The parameter w describes a possible non-constant density, but is zero for lead. The nucleons are generated with a hard core, which thus introduces short range correlations among the nucleons. As shown by Rybczynski and Broniowski [59], the correct two-particle correlation can be obtained if the nucleons are generated with a minimum distance equal to $2r_{\text{core}}$. Using $r_{\text{core}} = 0.45$ fm and a skin width of $a = 0.459$, the radius of the Lead nucleus becomes $R^{\text{Pb}} = 6.406$ according to the parameterisation in [58].

For each nucleus state we generate a random impact parameter wrt. the projectile proton and proceed to determine which nucleons will be wounded, following the previously outlined models.

In figure 3.5, we show the distribution in the number of inclusively wounded nucleons (using $\sigma_{w_{\text{inc}}}^{\text{pp}} = 63.0$ mb) for: a black disk model without any pp cross section fluctuations; GG with parameters fitted to data in section 4.3; GG with $P_{tot}(\sigma)$ given by eq. (3.78), also fitted to data; and the new simplified model outlined in section 4.1 (here called 2×2-disk) Fitting the latter to the cross sections in eq. (3.79) as well as to the double diffractive cross section $\sigma_{DD} = 3.2$ mb, we obtain the parameters listed in table 3.3.

Table 3.3: Table of parameters of the 2×2-disk model fitted to pp data.

r_1	r_2	α	c
0.15 fm	1.07 fm	0.97	0.42

Looking at the individual distributions in figure 3.5, we see that all three inclusions of additional fluctuations in the cross section, significantly increases the tail of the distribution compared to the black disk. The 2×2-disk model has fewer fluctuations to very large $N_{w_{\mathrm{inc}}}^t$ numbers, and the dip in the distribution around $N_{w_{\mathrm{inc}}}^t = 10$, also indicates that the fluctuations are too crude. The difference between GG with the original parametrisation and the log-normal distribution is visible in the tail above $N_{w_{\mathrm{inc}}}^t \approx 35$, as expected. One would therefore expect only an effect in the central events.

Distinguishing between absorptively and diffractively wounded nucleons

In our interpretation of the GG model in section 4.2, it can be used to calculate the sum of absorptively and diffractively wounded nucleons. In the Monte Carlo one would, however, like to have an impact parameter dependent recipe for each sub-collision to decide whether or not a target nucleon is diffractively or absorptively wounded, when hit by a projectile in a definite state p. This amounts to calculating the ratio of the absorptive to the inclusively wounded cross sections for a given sub-collision, and compare it to a random number

$$\frac{P_{w_{\mathrm{abs}},p}}{P_{w_{\mathrm{inc}},p}} = \frac{2\left\langle T_{p,t}(b)\right\rangle_t - \left\langle T_{p,t}(b)\right\rangle_t^2}{2\left\langle T_{p,t}(b)\right\rangle_t - \left\langle T_{p,t}^2(b)\right\rangle_t}. \tag{3.81}$$

For the 2×2-disk model this is done easily, as the above ratio reduces to:

$$\frac{P_{w_{\mathrm{abs}},p}}{P_{w_{\mathrm{inc}},p}} = \frac{2 - \alpha}{2 - \alpha\left\langle T_{p,t}^2(b)\right\rangle_t}. \tag{3.82}$$

The GG model on the other hand, implies averaging over target nucleon states, and provides thus no distinction. Instead we follow the 2×2-disk model to calculate the the conditional probability to be diffractively wounded, if a nucleon is already inclusively wounded in the GG model. This is:

$$P(\mathrm{diff}|w_{\mathrm{inc}}) = \Theta\left(\sqrt{\sigma_{GG}/\pi} - (r_1 - r_2) - b\right)\frac{2 - \alpha}{2 - \alpha c}, \tag{3.83}$$
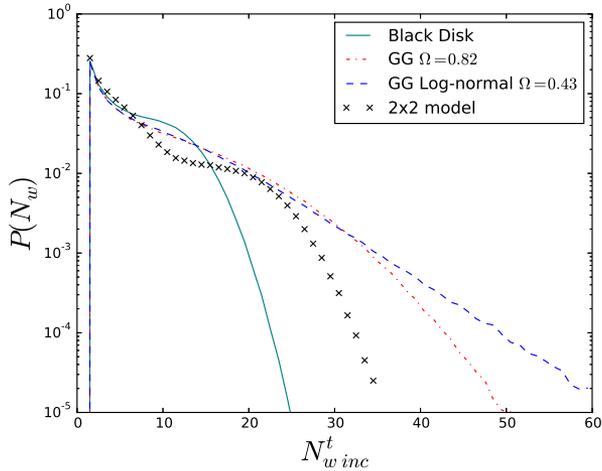
Figure 3.5: Distribution in the number of inclusively wounded nucleons, $N_{w_{\mathrm{inc}}}^t$, in pPb events at $\sqrt{s_{NN}} = 5$ TeV, for a Glauber black disk, the GG model with two parametrisations of $P_{tot}(\sigma)$ and the 2×2-disk model. All models have been fitted to reproduce relevant measured (semi-) inclusive cross sections.

where the first term is a requirement that the two nucleons are separated by an amount such that a fluctuation in size is necessary to be wounded. In figure 3.6 we show distributions of $N_{w_{\mathrm{abs}}}^t$ for the 2×2-disk model and for the corrected GG model, using both parametrisations of $P(\sigma)$.

5 Modelling final states in p*A* collisions

In this section we will take the knowledge about distributions of wounded nucleons and investigate the consequences for final states in p*A* collisions. We will discuss a few views on modelling particle production in such collisions, all assuming that a full final state of a p*A* collision can be adequately modelled by stacking pp events on top of each other, here modelled using PYTHIA8. Following the introduction of the models, we will compare to data, both multiplicity as function of centrality, and inclusive $p_\perp$ spectra. Finally we will give an estimate of the theoretical uncertainties present at this early stage of the model.

5.1 Generating final states with PYTHIA8

The general methodology for generating final states, which will be pursued here, will have the following ingredients:

- For each collision, a Glauber calculation is performed as outlined in section 4.4,
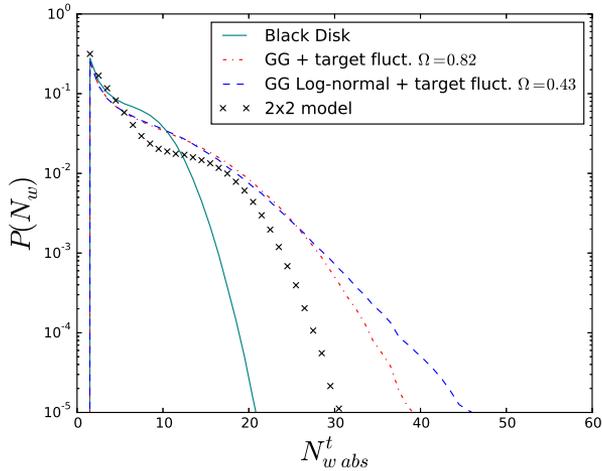
Figure 3.6: Distribution in the number of absorptively wounded nucleons, $N^t_{w\,\mathrm{abs}}$, in pPb events at $\sqrt{s_{NN}} = 5$ TeV, for a Glauber black disk, the GG model with two parametrisation of $P(\sigma)$, corrected using the 2×2-disk model, along with the 2×2-disk model itself. All models have been fitted to reproduce relevant measured (semi-) inclusive cross sections.

setting up the nuclear geometry.

- The total number of inclusively wounded target nucleons is calculated, as well as the number of absorptively wounded targets, if the two differ in the considered approach.

- Sub-collisions are generated as pp collisions, according to two separate approaches, which will be outlined in the following.

- Each sub-collision is treated separately in terms of colour reconnection and hadronisation. Efforts to include cross talk between sub-collisions will be the subject of a future publication.

Cross talk between sub-collisions is, however, included in one respect by accounting for energy-momentum conservation in all approaches. As before, we will concentrate on pPb collisions at $\sqrt{s_{NN}} = 5$ TeV. The methodology is, however, not limited to this, and generalisation to AA collisions will be the subject of a future publication.

5.2   Wounded nucleons and multi-parton interactions

In ref. [25] Białas *et al.* noticed that the central particle density in pA collisions scales approximately with the number of "wounded" or "participating" nucleons, $dN^{(\mathrm{p}A)}/d\eta \approx (N_{wounded}/2)\,dN^{(\mathrm{pp})}/d\eta$. The projectile proton was here included as one of the wounded nucleons, and the distribution in rapidity could be described if each wounded target nucleon gives a contribution proportional to $(\eta - \eta_t)/(\eta_p - \eta_t)$ where $\eta_{t,p}$ are the rapidities

of the target and projectile respectively. The wounded projectile proton gives a similar contribution with p exchanged for t.

The wounded nucleon model worked well for minimum bias events and low $p_\perp$ particles, while high $p_\perp$ particles scale better with the number of NN collisions, which can be understood if the high-$p_\perp$ particles originate from independent partonic subcollisions. (See *e.g.* ref. [26].) A model with this feature, called G-Pythia, has been used in analyses by ALICE [17].

These results can be given a heuristic interpretation in terms of the Landau-Pomeranchuk formation time. The formation time for a hadron is, in a frame where $p_L = 0$:

$$\tau \geq \frac{1}{\sqrt{p_\perp^2 + m^2}}. \tag{3.84}$$

This implies that a produced pion will resolve the nucleus at a length scale given roughly by $1/p_\perp$. For $p_\perp < 1$ GeV the resolution scale is larger than that of the individual nuclei, while for $p_\perp$ larger than ~ 1 GeV, constituents of individual nucleons can be resolved.

Below we will compare two models, generated with the help of PYTHIA 8. The model denoted "Absorptive" is similar to G-Pythia. Here each NN subcollision is treated as a pp collision[9]. The second model, explained in the next subsection, is called FritiofP8 and is more similar to the wounded nucleon model. We note that the models should not be compared on equal footing. From the above arguments, the "Absorptive" model is expected to describe the high-$p_\perp$ part of the spectrum better, while FritiofP8, being similar to the wounded nucleon model, is expected to describe the low-$p_\perp$ part, and thus also the total multiplicity, best.

Technically, the subcollisions are in both models generated with PYTHIA8. This means that for each sub-collision, multiple partonic interactions are created in decreasing order of $p_\perp$ with the probability:

$$\frac{d\mathcal{P}}{dp_{\perp i}} = \frac{1}{\sigma_{\text{abs}}} \frac{d\sigma_{2 \to 2}}{dp_{\perp i}} \exp\left[-\int_{p_{\perp i}}^{p_{\perp i-1}} \frac{1}{\sigma_{\text{abs}}} \frac{d\sigma_{2 \to 2}}{dp'_\perp} dp'_\perp \right], \tag{3.85}$$

starting from a maximum scale related to the impact parameter of the sub-collision. The cross section is obtained by treating everything as perturbative QCD $2 \to 2$ scatterings,

---

[9]Note that the G-Pythia approach really uses a black disk Glauber calculation with $\sigma_{NN} = \sigma_{\text{in}} = \sigma_{\text{abs}} + \sigma_{\text{Dp}} + \sigma_{\text{Dt}} + \sigma_{\text{DD}}$, and lets the collisions be a mixture of the four corresponding processes, while we we consider only absorptive collisions, as we believe this is more in line with the original model by Glauber. There is, however, no notable difference for observables in the near central rapidity range, taken with a minimum bias trigger.

but since the cross section diverges at low $p_\perp$, it is regulated at low $p_\perp$ using:

$$\frac{d\sigma_{2\to2}}{dp_\perp^2} \propto \frac{\alpha_s^2(p_\perp^2)}{p_\perp^4} \to \frac{\alpha_s^2(p_\perp^2 + p_{\perp0}^2)}{(p_\perp^2 + p_{\perp0}^2)^2}. \tag{3.86}$$

Here $p_{\perp0}$ is a tunable parameter.

Aside from momentum conservation, PYTHIA8 also rescales the PDF every time a quark has been used in an MPI. When using this MPI model for generating pA collisions we maintain momentum conservation, but do not maintain the rescaling of the PDF between separate NN collisions.

5.3   The revived Fritiof model

A very different approach was used in the Fritiof model [23]. Where the PYTHIA8 MPI model assumes everything can be described by perturbative scatterings, Fritiof imposed a soft model for everything, specifically limiting it's range of validity to low-$p_\perp$ processes.[10]

In the Fritiof model it is assumed that a soft min-bias interaction causes a momentum exchange, which in light-cone variables has the form

$$P(Q_+, Q_-) \propto \frac{dQ_+}{Q_+}\frac{dQ_-}{Q_-}. \tag{3.87}$$

This produces two excited states assumed to decay like strings stretching the rapidity range between the initial beam rapidities and a point distributed evenly within the kinematically allowed region The result is approximately reproducing the original wounded nucleon model [25], but it is in the Fritiof model also assumed that a secondary encounter with another nucleon will increase the excitation, thus leading to a logarithmic scale breaking.

In ref. [60] it was suggested to extend the Fritiof model to include the possibility for a hard scattering and associated bremsstrahlung when the energy is high enough. At LHC collision energies, the necessity for including the possibility for at least one such interaction is apparent.

In figure 3.7 we show a schematic picture of a projectile proton wounding a number of nucleons. The picture is strongly oversimplified, showing only the main gluon propagators, *i.e.* no initial/final-state radiation (ISR/FSR) or multi-parton interactions (MPI) in the individual sub-collision. Nucleons $\nu_1, \ldots \nu_4$ are wounded absorptively with ν_4 being the

---

[10]A motivation for the development of the Fritiof model, was to get a realistic extrapolation from pp collisions to collisions with nuclei. This could then form a background in searches for possible collective effects. Unfortunately it worked too well (at the energies available in the eighties), basically leaving no evidence for plasma formation.
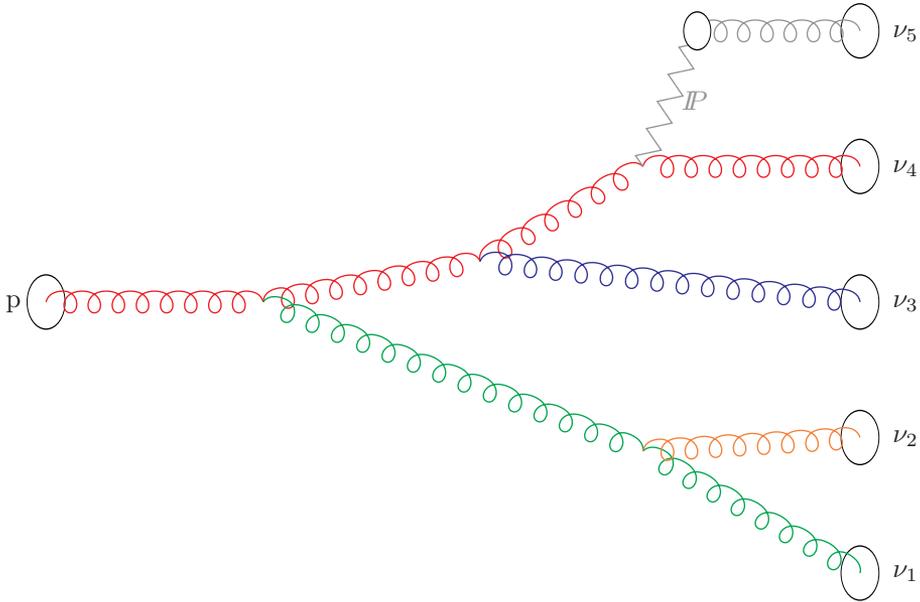
Figure 3.7: Cartoon in rapidity–impact-parameter space, showing the evolution of exchanged gluons between a projectile proton and a number of wounded nucleons in the target nucleus. Nucleons $\nu_1, \ldots, \nu_4$ are wounded absorptively, while ν_5 is wounded diffractively. ν_4 is considered to be the primary wounded nucleon.

hardest or "primary" wounded nucleon, which contributes to the hadronic multiplicity the full rapidity region. The other absorptively wounded nucleons, $\nu_1 \ldots \nu_3$, contributes only to the parts of the rapidity range in the nucleus direction. As indicated by the exchanged Pomeron, P, ν_5 is only diffractively excited, and will also only contribute in the nucleus direction.

Thinking in terms of cut Pomeron diagrams à la AGK [61] we show in figure 3.8 the similarity between the diagram describing diffractive excitation in proton–proton scattering and a fully absorptive proton–deuteron scattering. It is not far fetched to assume that the triple-Pomeron vertex in both cases are distributed in approximately the same way in rapidity, *i.e.*, that the gap size in the single diffractive excitation in pp would be distributed in the same way as the the size of the region of rapidity populated by hadrons from both wounded nucleons in a pd collision.

As discussed in section 3.3 the distribution in diffractive masses indicates a fairly flat distribution in rapidity of the triple-Pomeron vertex as ϵ is close to zero[11]. We will therefore assume as a first approximation, that the secondary absorptive collisions in a pA collision can be approximated by single diffractive collisions.

---

[11]The default in PYTHIA8 is actually to have $\epsilon = 0$ for high-mass diffraction, which corresponds to the distribution used in Fritiof in eq. (3.87).
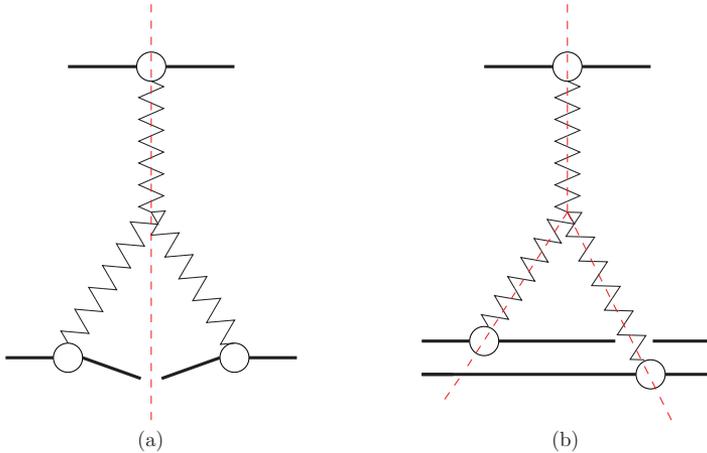
Figure 3.8: Pomeron diagrams with cuts indicated for (a) single diffractive excitation in proton–proton and (b) doubly absorptive proton–deuteron scattering.

Treating secondary absorptive collisions as single diffractive excitation has an additional added benefit. In the PYTHIA8 implementation, one can model high mass soft excitation using a perturbative approach where the exited proton can undergo multiple partonic interactions, as in eq. (3.85), and ISR is included. It is thus possible to treat absorptively wounded nucleons differently, depending on whether the mass of the excited system is larger or smaller than a pre-set threshold mass scale.

Finally, in figure 3.7, we also have ν_5, which is an standard diffractively excited nucleon, and will be modelled as such.

5.4 Comparison to data

We now compare the two methods for particle production, which were introduced above. Stacking absorptive events on top of each other is labelled "Absorptive", we use a black disk Glauber model with $\sigma_{abs} = 67.9$ mb to calculate the number of absorptive sub-collisions event by event. The model including both diffractive excitation and the Fritiof-inspired absorptive sub-collisions is labelled "FritiofP8". To calculate the amount of wounded nucleons we use the modified GG model with cross section fluctuations described by the log-normal distribution in eq. (3.78) and including the modifications introduced in section 4.2, as well as distinguishing between absorptive and diffractive events using the 2×2-disk modification, introduced in section 4.4. All parameters are fitted to pp data.
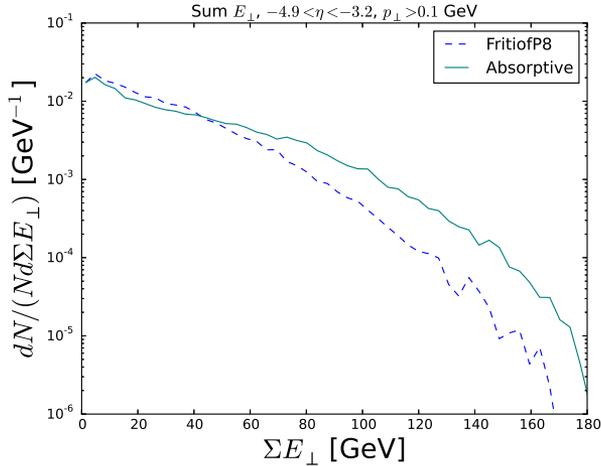
Figure 3.9: Distribution in $\sum E_\perp$ for a sum of full absorptive events and the new FritiofP8 model, for pPb collisions at $\sqrt{s_{NN}} = 5$ TeV.

Centrality estimation and multiplicity

The primary observable we wish to discuss, is the charged particle pseudo-rapidity distribution at different centralities, as measured by ATLAS [16]. When comparing Monte Carlo predictions to data in pp, the work flow has matured greatly over the past years, with the advent of automated frameworks for performing such tasks, such as Rivet [62]. In this framework, equal treatment of theory and unfolded data is ensured by publishing measurements along with an implementation of the analysis. This is not yet tradition in the heavy ion community, and the data comparisons shown here, is the result of our own Rivet implementation on the analysis, based on the paper, with data obtained from HepData [63].

In the experimental analysis by ATLAS, event centrality is calculated by taking fractiles of the distribution in $\sum E_\perp$ of charged particles in the interval[12] $3.1 < \eta < 4.9$. For this particular observable, unfolded data has not been published, but we will still compare theoretical curves for the two previously outlined particle production models. In figure 3.9 we show the model stacking $N^t_{w_{\text{abs}}}$ absorptive events spanning the whole rapidity region (denoted "Absorptive") reaches a much higher $\sum E_\perp$ than the Fritiof inspired model (denoted "FritiofP8") With one absorptive event spanning the whole rapidity region, $N^t_{w_{\text{abs}}} - 1$ absorptive events modelled as diffractive excitation, and $N^t_{w_{\text{inc}}} - N^t_{w_{\text{abs}}}$ events from diffractive excitation. We note that the "FritiofP8" results agree almost perfectly with the data from ATLAS, while the Absorptive model reaches significantly higher $\sum E_\perp$ values.

---

[12]Notice that our definition of η is opposite to the one used in ref. [16], but follows the HepMC published data.
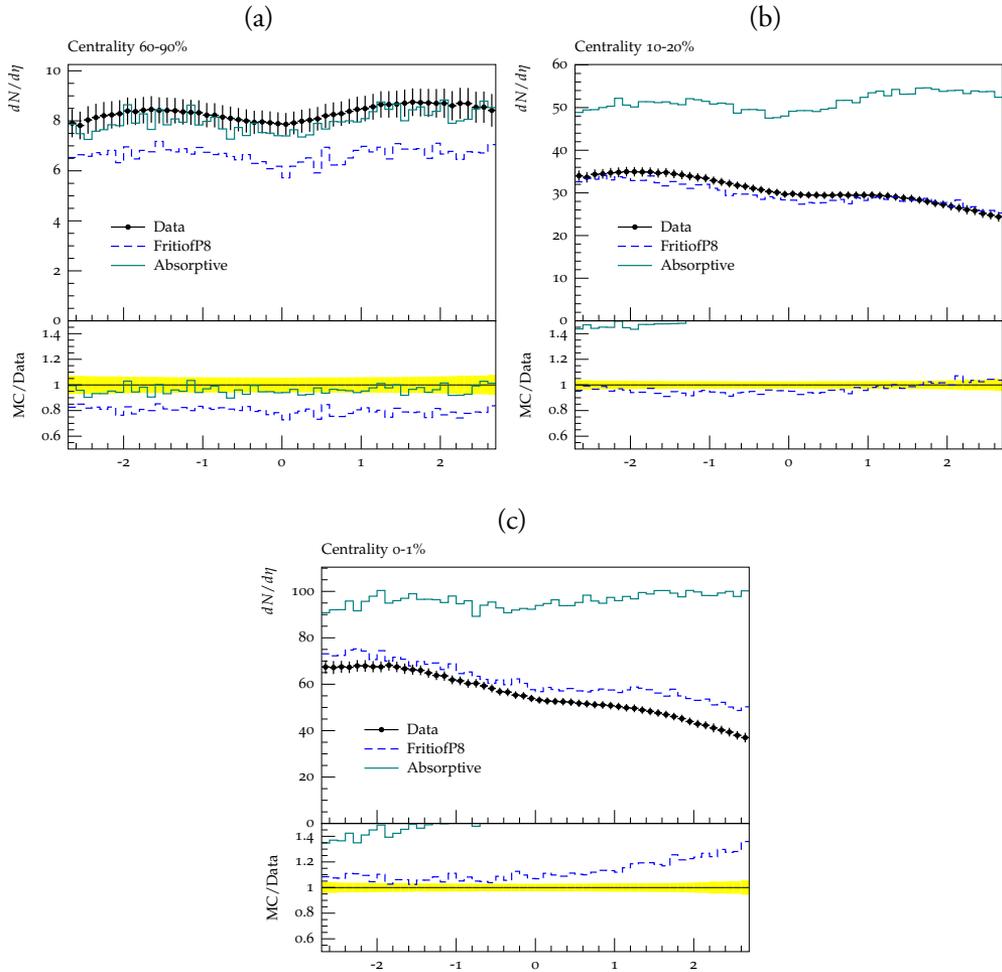
Figure 3.10: Pseudo-rapidity distribution of charged particle multiplicity for centralities $60 - 90\%$ (a), $20 - 30\%$ (b), and $0 - 1\%$ (c), compared to "Absorptive" and "FritiofP8" particle production models.

In figure 3.10 we show pseudorapidity distributions for different centralities, where we have used the same cuts as ATLAS, but reconstructed fractiles from our own distribution. [13] We see that while both models describe the peripheral events reasonably well (which is expected), the new FritiofP8 model based on diffractive excitation does a much better job describing both average multiplicity and the forward–backward asymmetry, as expected.

---

[13]Further centralities are shown on `http://home.thep.lu.se/DIPSY/FritiofP8`, but omitted here for brevity.
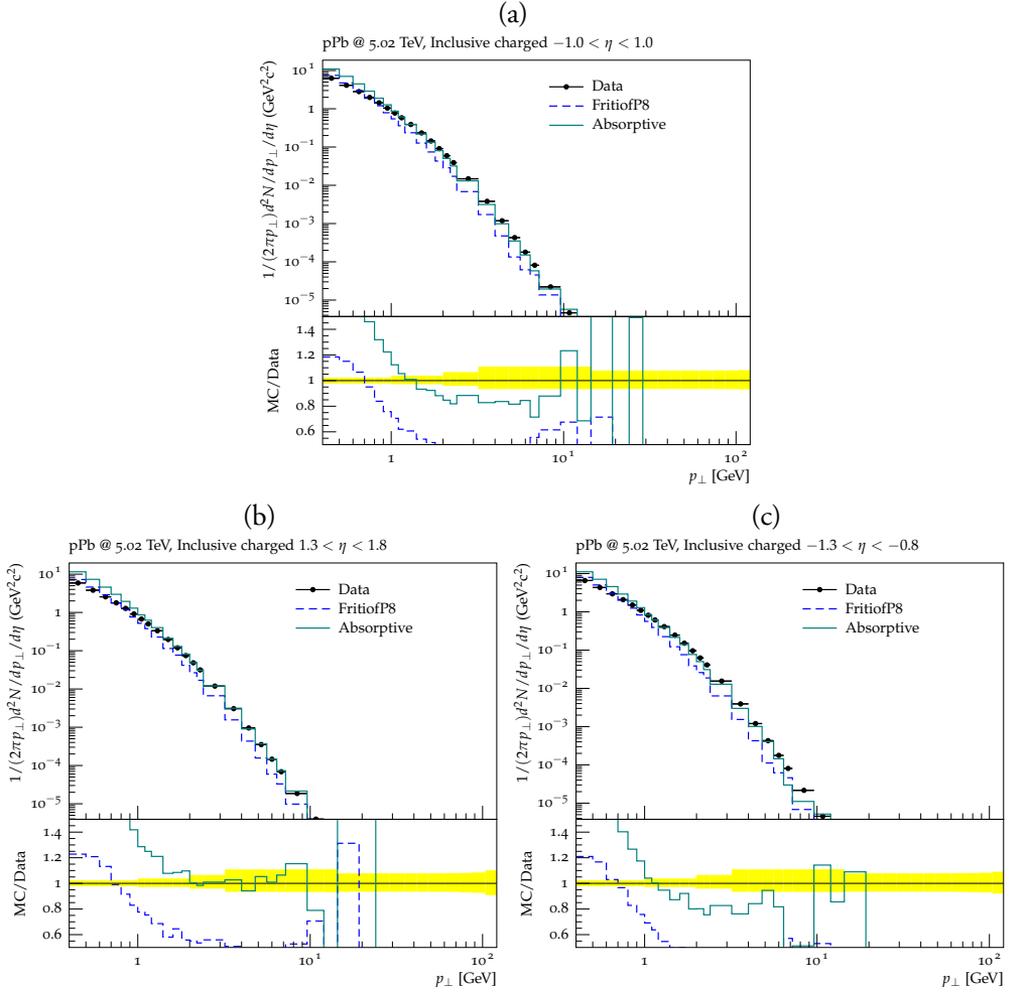
Figure 3.11: Distribution in $p_\perp$, centrality inclusive, for charged particles in (a) the central region, $-1.0 < \eta < 1.0$; (b) the proton direction, $1.3 < \eta < 1.8$; and (c) the nucleus direction $-1.3 < \eta < 0.8$.

Inclusive transverse momentum

We now compare to centrality-inclusive charged particle $p_\perp$ spectra in different ranges of η as measured by CMS [64]. In figure 3.11a we show the transverse momentum distribution for $-1.0 < \eta < 1.0$. We see that the FritiofP8 model performs well at low $p_\perp$, while Absorptive performs well at high $p_\perp$, as expected.

The same picture is seen when going to large negative η (figure 3.11c), but performance of the FritiofP8 model improves slightly when going to large positive η shown in figure 3.11b for $1.3 < \eta < 1.8$ (the proton side). The "absorptive" model performs as before, but it is rather

surprising that the FritiofP8 model performs poorly at high $p_\perp$ here. One explanation could be that the parton distribution function used for for secondary absorptive events is a Pomeron PDF and not a proton PDF, due to the fact that secondary absorptive events are modelled as single diffractive events. This is also a possible explanation for the poor performance at high $p_\perp$ in figure 3.11a and figure 3.11c.

5.5 Uncertainties

The method presented here for generating final states in pA is interesting, as it gives qualitatively correct description of the multiplicity in both the proton and the nucleus direction. It is still mostly a proof-of-principle since, as we will demonstrate here, using the PYTHIA8 default settings introduces several hidden assumptions. We will discuss these assumptions by giving a rough estimate of the uncertainty associated with each of them. That uncertainty will decrease, or vanish entirely, when the assumptions are dealt with more carefully, one by one, which will be done in one or more future publications.

PDFs and MPI activity

In the previous section we described how the secondary absorptive sub-collisions are approximated as single diffractive excitation events. The perturbative handling of single diffractive events at high masses in PYTHIA8 relies on a factorised Pomeron approach, where the diffractive state is modelled by a Pomeron–proton collision, including MPI, and we will study two important uncertainties here.

- The Pomeron PDFs used in the MPI machinery are not really appropriate in our model of the secondary absorptive sub-collisions, since it is still really the parton density in the proton which should drive the MPI. To see possible effects, we have tried to make the Pomeron more proton-like, by modifying the PDF used in PYTHIA8 to have much more small-x gluons[14]. This will increase MPI activity.

- Another way of modifying the MPI activity is to change the Pomeron–proton cross section used in PYTHIA8. This is not a physical cross section, but rather a free parameter in the program which only affects MPI activity, and is adjusted to fit data. The default value of this parameter is 10 mb. We here increase it to it's maximal allowed value, 40 mb, to better reflect a pp absorptive cross section.

---

[14]The default Pomeron PDF in PYTHIA8 is H1 2006 Fit B LO[65], we here use instead a simple Q^2-independent distribution on the form $xf(x) \propto x^a(1-x)^b$, with $a = -0.5$ and $b = 6.0$ for gluons and $a = -0.05$ and $b = 0.05$ for quarks.
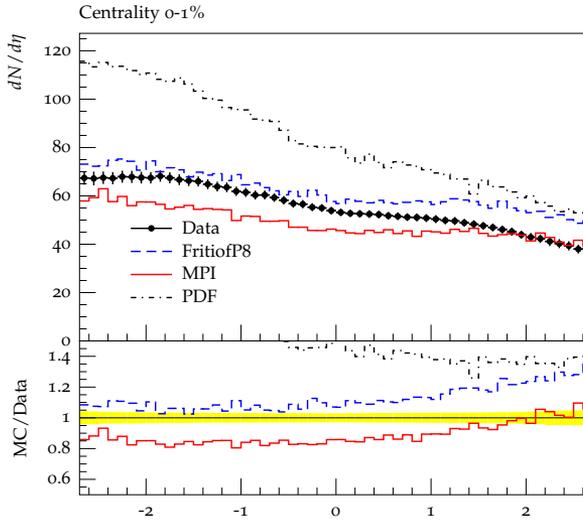
Figure 3.12: Pseudo-rapidity distribution of charged particle multiplicity for centrality $0 - 1\%$ compared to three different ways of estimating the number of MPIs, giving an estimate of the method uncertainty.

In figure 3.12 we show the pseudo-rapidity distribution of charged particles for the highest centrality bin. The two variations above are labelled "PDF" and "MPI" respectively while FritiofP8 is the same as before.

In total, the envelope of the three lines gives what we believe to be a reasonable, albeit conservative, estimate of the uncertainty so far associated with the approximations regarding the parton densities and the amount of MPIs.

GG uncertainty

In section 4.3 we described how the Glauber–Gribov cross section fluctuations could be parameterised with a log-normal distribution. This new parameterisation was used in all the previous data comparison plots, here we show how the traditional parameterisation (also fitted to pp data) compared to the new one. Since distributions of wounded nucleons for the two models differs most in the tail, we are most sensitive in central collisions, In figure 3.13 we show the uncertainty in central particle production arising from changing the parametrisation of cross section fluctuations. We see that the uncertainty covers data well, but is smaller than the uncertainties in the handling of secondary absorptive events above.
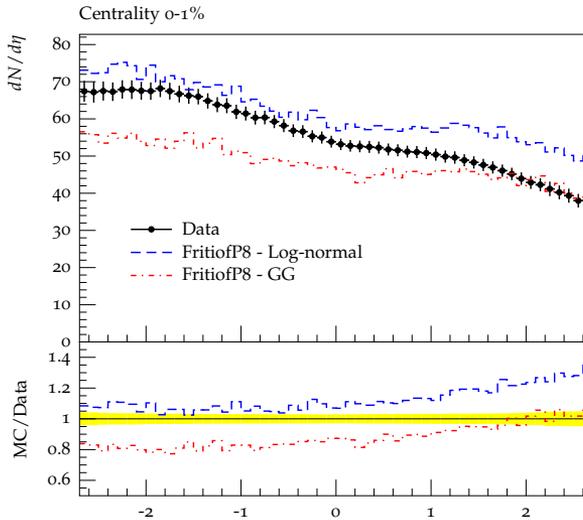
Centrality 0-1%

Figure 3.13: Pseudo-rapidity distribution of charged particle multiplicity for centrality $0-1\%$ compared to two parameterisations for the GG model.

6 Conclusions and outlook

Collisions of heavy nuclei with protons or each other, are often understood in terms of their deviation from minimum bias pp collisions, which after many years of work on models for multiple partonic interactions, are fairly well understood. The extrapolation from pp to pA or AA, which is usually based on Glauber models, is therefore a crucial step toward understanding the deviations, and thus crucial for understanding how and if a de-confined plasma of quarks and gluons are created in heavy ion collisions, and what kind of impact it has on final state observables. In this article we have discussed Glauber models, their extensions including fluctuations and the impact these extensions on the number of wounded nucleons, followed by a possible way of using that knowledge to generate full, exclusive final states as a sum of pp collisions. We will conclude on these two parts separately, followed by an outlook primarily focused on extending the model for full final states, to also include microscopic models for collective effects.

6.1 Fluctuations in the Glauber formalism

Following Good and Walker, we have discussed diffractive excitation as a manifestation of fluctuations in the substructure of the nucleons. As a result of this discussion we identified the *inclusively wounded cross section* to be the relevant pp cross section for calculations of the number of wounded nucleons. The wounded cross section has contributions from

absorptive processes plus diffractively excited target nucleons, in brief form we have for the semi-inclusive pp cross sections:

$$\sigma_{w_{\text{inc}}} = \sigma_{\text{abs}} + \sigma_{\text{DD}} + \sigma_{\text{Dt}} = \sigma_{\text{tot}} - \sigma_{\text{el}} - \sigma_{\text{Dp}}. \tag{3.88}$$

We have discussed the developments in calculating the number distribution of inclusively wounded nucleons in the so-called Glauber–Gribov approach by Strikman and co-workers. By comparing distributions of the cross section to ones calculated with the DIPSY model and measurements, we find that the parametrisation of the cross section suggested in the Glauber–Gribov approach does not fully include all fluctuations necessary to describe the ones in DIPSY.

The simplest Glauber calculations using a fixed black disk, can clearly not describe any fluctuations, and we want to emphasize that just setting $\sigma_{NN} = \sigma_{w_{\text{inc}}}$ in such a calculation, is not enough if one wants to calculate the contribution from the wounded nucleons to a centrality defining observable.

We have shown that a Glauber–Gribov calculation with a black disk fluctuating in size, can be used to predict the distribution of inclusively wounded nucleons, if the fluctuating black disk is attributed to fluctuations in the projectile, while averaging over fluctuations in the target nucleon. However, if one wants to separate absorptively wounded nucleons from diffractively wounded ones, it is necessary to also consider fluctuations in the individual target nucleons.

We have suggested a new functional form for the fluctuations in the pp interaction, with a higher tail to a larger cross section. Instead of the parametrization introduced by Strikman *et al.*, and used in several experimental analyses, we suggest a log-normal distribution, which is believed to give a somewhat better description of the inclusive distribution, though not necessarily a more realistic picture of the cross section fluctuations. We have also included fluctuations in the target nucleons by introducing a crude Glauber-like model, where the radii of the projectile and target are allowed to fluctuate independently between two values. The model includes four parameters, and can be fitted to describe four independent semi-inclusive pp cross sections, including the inclusive wounded one. By using this model to include projectile fluctuations in the Glauber–Gribov approach, we separate the inclusively wounded nucleon into absorptively and diffractively wounded ones.

The parametrisations and toy-models studied are built on the assumption that distributions of wounded nucleons can be described solely by fluctuations in the proton size; projectile size for the inclusive distributions, and target nucleon size for distinguishing between absorptively and diffractively wounded nucleons. Thinking about the dynamics of more involved calculations, like the DIPSY model used in this paper, it is clear that size fluctuations cannot account for all the relevant physics. In the DIPSY model, fluctuations in cross

section will also arise when *e.g.* a small projectile is very dense, and therefore gives rise to a larger cross section. Similarly, a large projectile can be dilute, giving rise to a smaller cross section. In the language of this article, such effects would need to be accounted for by a fluctuating, *b*-dependent opacity, resulting in a profile function which would go beyond the simple Gaussian, grey -or black disks, but still not be as calculationally involved as the full, dynamical models. This will be the subject of a future publication.

6.2 Full final states

We have given a proof-of-principle for an approach to model exclusive final states in p*A* collisions as a sum of several pp collisions. The approach uses PYTHIA8 to calculate the hardest absorptive sub-collision as a normal non-diffractive pp collision, while the subsequent absorptive collisions are modelled as single diffractive events. This was inspired by the old Fritiof model, which is valid at lower energies, but adds another dimension, as high-mass single diffractive exchanges can now be treated perturbatively and allows for multiple parton–parton scatterings.

We have shown that this approach, in a quite crude implementation, is able to give a reasonable description of some recently published final-state measurements of pPb collisions at the LHC, but the uncertainties in our approach are quite large. In future studies we will try to eliminate these uncertainties, in the hope to get a theoretically well motivated and more accurate description of data.

To do this it is helpful to have data published in a usable form for comparison with event generators. The LHC pp community has come a long way in this respect by publishing many of their results in the form of Rivet routines. In this way the measurements are presented in a clearly reproducible form, including all relevant kinematical cuts and unfolding of detector effects but free from dependence of theoretical models. In order to allow for the development of better event generators for heavy ion collisions, it is imperative that the experimental heavy ion community adapts a similar way of presenting their results.

6.3 Outlook: modelling collective effects

In both the theoretical and experimental communities around heavy ion collisions, much attention is given to observables thought to convey information about a possible plasma state created in the collision. A direct application of the work presented in this article, is to use the final state extrapolation as a baseline for calculations of collective effects using microscopic, QCD based models. In the pp community, much attention have been given to models of final state interactions including colour reconnections, rope hadronisation and junction formation [66, 67, 68]. These models have, in pp been shown to reproduce:

the enhancement of strange hadrons to non-strange hadrons in dense environments [69]; flow-like effects in hadron ratios as function of $p_\perp$; and preliminary studies have shown that interactions between strings can produce a ridge [70].

To implement such models in a framework like the one presented here, a necessary component is a good understanding of the sub-collisions in transverse space. Such a picture is not included in *e.g.* the PYTHIA8 MPI model, and must therefore be added *a posteriori*. Guidance can then be had from the DIPSY model, which includes detailed information about the transverse space structure, but does not produce final states describing data as well as PYTHIA8.

Finally, the final state model introduced here should be developed further to model fully exclusive hadronic final states also in *AA* collisions. Since every projectile here also becomes a target, we suspect that the model cannot be transferred one-to-one, but that some modifications may be needed. Here modelling collective effects using microscopic models is also highly desirable.

Acknowledgments

References

[1] A. Bzdak and V. Skokov, "Decisive test of color coherence in proton-nucleus collisions at the LHC," *Phys. Rev. Lett.* **111** (2013) 182301, `arXiv:1307.6168 [hep-ph]`.

[2] L. McLerran and M. Praszalowicz, "Fluctuations and the rapidity dependence of charged particles spectra in fixed centrality bins in p*A* collisions," *Annals Phys.* **372** (2016) 215–225, `arXiv:1507.05976 [hep-ph]`.

[3] R. J. Glauber, "Cross-sections in deuterium at high-energies," *Phys. Rev.* **100** (1955) 242–248.

[4] M. L. Miller, K. Reygers, S. J. Sanders, and P. Steinberg, "Glauber modeling in high energy nuclear collisions," *Ann. Rev. Nucl. Part. Sci.* **57** (2007) 205–243, `arXiv:nucl-ex/0701025 [nucl-ex]`.

[5] **CDF** Collaboration, F. Abe *et al.*, "Measurement of $\bar{p}p$ single diffraction dissociation at $\sqrt{s} = 546$ GeV and 1800 GeV," *Phys. Rev.* **D50** (1994) 5535–5549.

[6] **ATLAS** Collaboration, G. Aad *et al.*, "Rapidity gap cross sections measured with the ATLAS detector in *pp* collisions at $\sqrt{s} = 7$ TeV," *Eur. Phys. J.* **C72** (2012) 1926, `arXiv:1201.2808 [hep-ex]`.

[7] **CMS** Collaboration, V. Khachatryan *et al.*, "Measurement of diffraction dissociation cross sections in pp collisions at $\sqrt{s} = 7$ TeV," *Phys. Rev.* **D92** no. 1, (2015) 012003, `arXiv:1503.08689 [hep-ex]`.

[8] V. N. Gribov, "Glauber corrections and the interaction between high-energy hadrons and nuclei," *Sov. Phys. JETP* **29** (1969) 483–487. [Zh. Eksp. Teor. Fiz.56,892(1969)].

[9] G. Gustafson, L. Lönnblad, A. Ster, and T. Csörgő, "Total, inelastic and (quasi-)elastic cross sections of high energy pA and ☒ A reactions with the dipole formalism," *JHEP* **10** (2015) 022, arXiv:1506.09095 [hep-ph].

[10] H. Heiselberg, G. Baym, B. Blaettel, L. L. Frankfurt, and M. Strikman, "Color transparency, color opacity, and fluctuations in nuclear collisions," *Phys. Rev. Lett.* **67** (1991) 2946–2949.

[11] B. Blaettel, G. Baym, L. L. Frankfurt, H. Heiselberg, and M. Strikman, "Hadronic cross-section fluctuations," *Phys. Rev.* **D47** (1993) 2761–2772.

[12] M. Alvioli and M. Strikman, "Color fluctuation effects in proton-nucleus collisions," *Phys. Lett.* **B722** (2013) 347–354, arXiv:1301.0728 [hep-ph].

[13] M. Alvioli, L. Frankfurt, V. Guzey, and M. Strikman, "Revealing "flickering" of the interaction strength in pA collisions at the CERN LHC," *Phys. Rev.* **C90** (2014) 034914, arXiv:1402.2868 [hep-ph].

[14] M. Alvioli, B. A. Cole, L. Frankfurt, D. V. Perepelitsa, and M. Strikman, "Evidence for *x*-dependent proton color fluctuations in pA collisions at the CERN Large Hadron Collider," *Phys. Rev.* **C93** no. 1, (2016) 011902, arXiv:1409.7381 [hep-ph].

[15] M. L. Good and W. D. Walker, "Diffraction disssociation of beam particles," *Phys. Rev.* **120** (1960) 1857–1860.

[16] **ATLAS** Collaboration, G. Aad *et al.*, "Measurement of the centrality dependence of the charged-particle pseudorapidity distribution in proton–lead collisions at $\sqrt{s_{\mathrm{NN}}} = 5.02$ TeV with the ATLAS detector," *Eur. Phys. J.* **C76** no. 4, (2016) 199, arXiv:1508.00848 [hep-ex].

[17] **ALICE** Collaboration, J. Adam *et al.*, "Centrality dependence of particle production in p-Pb collisions at $\sqrt{s_{\mathrm{NN}}} = 5.02$ TeV," *Phys. Rev.* **C91** no. 6, (2015) 064905, arXiv:1412.6828 [nucl-ex].

[18] E. Avsar, G. Gustafson, and L. Lönnblad, "Energy conservation and saturation in small-x evolution," *JHEP* **07** (2005) 062, arXiv:hep-ph/0503181 [hep-ph].

[19] E. Avsar, G. Gustafson, and L. Lönnblad, "Small-x dipole evolution beyond the large-N(c) imit," *JHEP* **01** (2007) 012, arXiv:hep-ph/0610157 [hep-ph].

[20] C. Flensburg, G. Gustafson, and L. Lönnblad, "Inclusive and Exclusive Observables from Dipoles in High Energy Collisions," *JHEP* **08** (2011) 103, arXiv:1103.4321 [hep-ph].

[21] A. H. Mueller, "Soft gluons in the infinite momentum wave function and the BFKL pomeron," *Nucl. Phys.* **B415** (1994) 373–385.

[22] A. H. Mueller and B. Patel, "Single and double BFKL pomeron exchange and a dipole picture of high-energy hard processes," *Nucl. Phys.* **B425** (1994) 471–488, `arXiv:hep-ph/9403256 [hep-ph]`.

[23] B. Andersson, G. Gustafson, and B. Nilsson-Almqvist, "A Model for Low p(t) Hadronic Reactions, with Generalizations to Hadron - Nucleus and Nucleus-Nucleus Collisions," *Nucl. Phys.* **B281** (1987) 289–309.

[24] H. Pi, "An Event generator for interactions between hadrons and nuclei: FRITIOF version 7.0," *Comput. Phys. Commun.* **71** (1992) 173–192.

[25] A. Białas, M. Bleszynski, and W. Czyz, "Multiplicity Distributions in Nucleus-Nucleus Collisions at High-Energies," *Nucl. Phys.* **B111** (1976) 461–476.

[26] A. Białas, "Wounded nucleons, wounded quarks: An update," *J. Phys.* **G35** (2008) 044053.

[27] **PHOBOS** Collaboration, B. B. Back *et al.*, "Scaling of charged particle production in d + Au collisions at s(NN)**(1/2) = 200-GeV," *Phys. Rev.* **C72** (2005) 031901, `arXiv:nucl-ex/0409021 [nucl-ex]`.

[28] **PHENIX** Collaboration, A. Adare *et al.*, "Centrality categorization for $R_{p(d)+A}$ in high-energy collisions," *Phys. Rev.* **C90** no. 3, (2014) 034902, `arXiv:1310.4793 [nucl-ex]`.

[29] **ALICE** Collaboration, B. Abelev *et al.*, "Pseudorapidity density of charged particles in p + Pb collisions at $\sqrt{s_{NN}} = 5.02$ TeV," *Phys. Rev. Lett.* **110** no. 3, (2013) 032301, `arXiv:1210.3615 [nucl-ex]`.

[30] T. Sjöstrand and M. van Zijl, "A Multiple Interaction Model for the Event Structure in Hadron Collisions," *Phys. Rev.* **D36** (1987) 2019.

[31] T. Sjöstrand, S. Ask, J. R. Christiansen, R. Corke, N. Desai, P. Ilten, S. Mrenna, S. Prestel, C. O. Rasmussen, and P. Z. Skands, "An Introduction to PYTHIA 8.2," *Comput. Phys. Commun.* **191** (2015) 159–177, `arXiv:1410.3012 [hep-ph]`.

[32] M. Bahr *et al.*, "Herwig++ Physics and Manual," *Eur. Phys. J.* **C58** (2008) 639–707, `arXiv:0803.0883 [hep-ph]`.

[33] T. Gleisberg, S. Hoeche, F. Krauss, M. Schonherr, S. Schumann, F. Siegert, and J. Winter, "Event generation with SHERPA 1.1," *JHEP* **02** (2009) 007, `arXiv:0811.4622 [hep-ph]`.

[34] L. D. McLerran and R. Venugopalan, "Computing quark and gluon distribution functions for very large nuclei," *Phys. Rev.* **D49** (1994) 2233–2241, `arXiv:hep-ph/9309289 [hep-ph]`.

[35] C. Flensburg, G. Gustafson, and L. Lönnblad, "Elastic and quasi-elastic pp and γ^*p scattering in the Dipole Model," *Eur. Phys. J.* **C60** (2009) 233–247, `arXiv:0807.0325 [hep-ph]`.

[36] C. Flensburg and G. Gustafson, "Fluctuations, Saturation, and Diffractive Excitation in High Energy Collisions," *JHEP* **10** (2010) 014, `arXiv:1004.5502 [hep-ph]`.

[37] A. H. Mueller, "O(2,1) Analysis of Single Particle Spectra at High-energy," *Phys. Rev.* **D2** (1970) 2963–2968.

[38] E. Gotsman, E. Levin, and U. Maor, "A comprehensive model of soft interactions in the LHC era," *Int. J. Mod. Phys.* **A30** no. 08, (2015) 1542005, `arXiv:1403.4531 [hep-ph]`.

[39] V. A. Khoze, A. D. Martin, and M. G. Ryskin, "Elastic scattering and Diffractive dissociation in the light of LHC data," *Int. J. Mod. Phys.* **A30** no. 08, (2015) 1542004, `arXiv:1402.2778 [hep-ph]`.

[40] S. Ostapchenko, "Monte Carlo treatment of hadronic interactions in enhanced Pomeron scheme: I. QGSJET-II model," *Phys. Rev.* **D83** (2011) 014018, `arXiv:1010.1869 [hep-ph]`.

[41] H. I. Miettinen and J. Pumplin, "Diffraction Scattering and the Parton Structure of Hadrons," *Phys. Rev.* **D18** (1978) 1696.

[42] Y. Hatta, E. Iancu, C. Marquet, G. Soyez, and D. N. Triantafyllopoulos, "Diffusive scaling and the high-energy limit of deep inelastic scattering in QCD at large N(c)," *Nucl. Phys.* **A773** (2006) 95–155, `arXiv:hep-ph/0601150 [hep-ph]`.

[43] E. Avsar, G. Gustafson, and L. Lönnblad, "Diifractive excitation in DIS and pp collisions," *JHEP* **12** (2007) 012, `arXiv:0709.1368 [hep-ph]`.

[44] G. Gustafson, "The Relation between the Good-Walker and Triple-Regge Formalisms for Diffractive Excitation," *Phys. Lett.* **B718** (2013) 1054–1057, `arXiv:1206.1733 [hep-ph]`.

[45] C. Flensburg, G. Gustafson, and L. Lönnblad, "Exclusive final states in diffractive excitation," *JHEP* **12** (2012) 115, `arXiv:1210.2407 [hep-ph]`.

[46] M. Alvioli, H. J. Drescher, and M. Strikman, "A Monte Carlo generator of nucleon configurations in complex nuclei including Nucleon-Nucleon correlations," *Phys. Lett.* **B680** (2009) 225–230, `arXiv:0905.2670 [nucl-th]`.

[47] M. Alvioli, H. Holopainen, K. J. Eskola, and M. Strikman, "Initial state anisotropies and their uncertainties in ultrarelativistic heavy-ion collisions from the Monte Carlo Glauber model," *Phys. Rev.* **C85** (2012) 034902, `arXiv:1112.5306 [hep-ph]`.

[48] B. Alver, M. Baker, C. Loizides, and P. Steinberg, "The PHOBOS Glauber Monte Carlo," `arXiv:0805.4411 [nucl-ex]`.

[49] C. Loizides, J. Nagle, and P. Steinberg, "Improved version of the PHOBOS Glauber Monte Carlo," *SoftwareX* **1-2** (2015) 13–18, `arXiv:1408.2549 [nucl-ex]`.

[50] L.-K. Ding and E. Stenlund, "A Monte Carlo for Nuclear Collision Geometry," *Comput. Phys. Commun.* **59** (1990) 313–318.

[51] G. Antchev *et al.*, "First measurement of the total proton-proton cross section at the LHC energy of $\sqrt{s}$ =7 TeV," *Europhys. Lett.* **96** (2011) 21002, `arXiv:1110.1395 [hep-ex]`.

[52] **TOTEM** Collaboration, G. Antchev *et al.*, "Measurement of proton-proton elastic scattering and total cross-section at S**(1/2) = 7-TeV," *Europhys. Lett.* **101** (2013) 21002.

[53] **TOTEM** Collaboration, G. Antchev *et al.*, "Proton-proton elastic scattering at the LHC energy of s** (1/2) = 7-TeV," *Europhys. Lett.* **95** (2011) 41001, `arXiv:1110.1385 [hep-ex]`.

[54] **ALICE** Collaboration, B. Abelev *et al.*, "Measurement of inelastic, single- and double-diffraction cross sections in proton–proton collisions at the LHC with ALICE," *Eur. Phys. J.* **C73** no. 6, (2013) 2456, `arXiv:1208.4968 [hep-ex]`.

[55] **UA4** Collaboration, D. Bernard *et al.*, "The Cross-section of Diffraction Dissociation at the CERN SPS Collider," *Phys. Lett.* **B186** (1987) 227–232.

[56] P. Lipari and M. Lusignoli, "Interpretation of the measurements of total, elastic and diffractive cross sections at LHC," *Eur. Phys. J.* **C73** no. 11, (2013) 2630, `arXiv:1305.7216 [hep-ph]`.

[57] W. Broniowski, M. Rybczynski, and P. Bozek, "GLISSANDO: Glauber initial-state simulation and more..," *Comput. Phys. Commun.* **180** (2009) 69–83, `arXiv:0710.5731 [nucl-th]`.

[58] M. Rybczynski, G. Stefanek, W. Broniowski, and P. Bozek, "GLISSANDO 2 : GLauber Initial-State Simulation AND mOre…, ver. 2," *Comput. Phys. Commun.* **185** (2014) 1759–1772, `arXiv:1310.5475 [nucl-th]`.

[59] M. Rybczynski and W. Broniowski, "Two-body nucleon-nucleon correlations in Glauber-like models," *Phys. Part. Nucl. Lett.* **8** (2011) 992–994, `arXiv:1012.5607 [nucl-th]`.

[60] B. Andersson, G. Gustafson, and H. Pi, "The FRITIOF model for very high-energy hadronic collisions," *Z. Phys.* **C57** (1993) 485–494.

[61] V. A. Abramovsky, V. N. Gribov, and O. V. Kancheli, "Character of Inclusive Spectra and Fluctuations Produced in Inelastic Processes by Multi - Pomeron Exchange," *Yad. Fiz.* **18** (1973) 595–616. [Sov. J. Nucl. Phys.18,308(1974)].

[62] A. Buckley, J. Butterworth, L. Lönnblad, D. Grellscheid, H. Hoeth, J. Monk, H. Schulz, and F. Siegert, "Rivet user manual," *Comput. Phys. Commun.* **184** (2013) 2803–2819, `arXiv:1003.0694 [hep-ph]`.

[63] A. Buckley, W. J. Stirling, M. R. Whalley, J. M. Butterworth, J. Monk, E. Nurse, and B. Waugh, "HepData and JetWeb: HEP data archiving and model validation," in *15th International Conference on Computing in High Energy and Nuclear Physics (CHEP 2006) Mumbai, Maharashtra, India, February 13-17, 2006.* 2006. `arXiv:hep-ph/0605048 [hep-ph]`.

[64] **CMS** Collaboration, V. Khachatryan *et al.*, "Nuclear Effects on the Transverse Momentum Spectra of Charged Particles in pPb Collisions at $\sqrt{s_{\mathrm{NN}}} = 5.02$ TeV," *Eur. Phys. J.* **C75** no. 5, (2015) 237, `arXiv:1502.05387 [nucl-ex]`.

[65] **H1** Collaboration, A. Aktas *et al.*, "Measurement and QCD analysis of the diffractive deep-inelastic scattering cross-section at HERA," *Eur. Phys. J.* **C48** (2006) 715–748, `arXiv:hep-ex/0606004 [hep-ex]`.

[66] C. Bierlich, G. Gustafson, L. Lönnblad, and A. Tarasov, "Effects of Overlapping Strings in pp Collisions," *JHEP* **03** (2015) 148, `arXiv:1412.6259 [hep-ph]`.

[67] C. Bierlich and J. R. Christiansen, "Effects of color reconnection on hadron flavor observables," *Phys. Rev.* **D92** no. 9, (2015) 094010, `arXiv:1507.02091 [hep-ph]`.

[68] J. R. Christiansen and P. Z. Skands, "String Formation Beyond Leading Colour," *JHEP* **08** (2015) 003, `arXiv:1505.01681 [hep-ph]`.

[69] **ALICE** Collaboration, J. Adam *et al.*, "Multiplicity-dependent enhancement of strange and multi-strange hadron production in proton-proton collisions at $\sqrt{s} = 7$ TeV," `arXiv:1606.07424 [nucl-ex]`.

[70] I. Altsybeev, "Mean transverse momenta correlations in hadron-hadron collisions in MC toy model with repulsing strings," *AIP Conf. Proc.* **1701** (2016) 100002, `arXiv:1502.03608 [hep-ph]`.

IV

A shoving model for collectivity in hadronic collisions

Christian Bierlich[1], Leif Lönnblad[1] and Gösta Gustafson[1].

[1] Dept. of Astronomy and Theoretical Physics, Lund University, Sölvegatan 14A, SE-223 62 Lund, Sweden.

ABSTRACT: An extension of the rope hadronization model, which has previously provided good descriptions of hadrochemistry in high multiplicity pp collisions, is presented. The extension includes a dynamically generated transverse pressure, produced by the excess energy from overlapping strings. We find that this model can qualitatively reproduce soft features of Quark Gluon Plasma in small systems, such as higher $\langle p_\perp \rangle$ for heavier particles and long range azimuthal correlations forming a ridge. The effects are similar to those obtained from a hydrodynamic expansion, but without assuming a thermalized medium.

Recent precise measurements of pp and pA collisions at the LHC show flow-like effects [1, 2, 3] similar to those found in high energy nucleus collisions. Examples are ridge like structures, quantified in different flow coefficients, and measurements of strangeness enhancement with increasing event activity [4]. These are regarded as two important characteristics of the soft features of the Quark Gluon Plasma, and are often described in a hydrodynamical framework assuming thermal equilibrium.

Dynamical models based on string [5, 6] or cluster [7] hadronization models, *e.g.* PYTHIA8 [8, 9] and HERWIG7 [10], are able to describe the general soft features of pp collisions in a very satisfactory way. The need for imposing new dynamics at a macroscopic level, only present at soft scales, is complicated, as it breaks the principle of jet universality by introducing a scale below which new dynamics should be "switched on". A quite successful model based on this principle, is the core–corona model [11], implemented in the EPOS generator [12], where events are subdivided into a "core" and a "corona", based on event activity. Recently, attempts has been made to incorporate a "thermal" exponential $m_\perp$-spectrum for the string break-ups in the Lund hadronization model [13] with promising results, but it is still unclear whether such a "microscopization" can capture the essential features of hydrodynamics, and if so, if this picture can correctly describe both hadrochemistry and flow.

To provide a description of the hadrochemistry in the underlying event of pp collisions, we recently suggested a "rope hadronization" model [14], based on work by Biro, Knoll and Nielsen [15]. This model provides corrections to the string hadronization model, by allowing strings overlapping in transverse space to act coherently as a "rope". The model is implemented in the DIPSY event generator [16], which provides a dynamical picture of the event structure in impact parameter space, allowing for a calculation of the colour field strength in each small rope segment[1]. This formalism also includes all fluctuations. The colour field is characterized by two quantum numbers $\{p, q\}$, which together signifies its SU(3) multiplet structure. Lattice calculations have shown [18], that the string tension – energy per unit length – scales with the quadratic Casimir operator of the multiplet, such that the ratio of the enhanced rope tension ($\tilde{\kappa}$) to the triplet string tension in vacuum (κ) is:

$$\frac{\tilde{\kappa}}{\kappa} = \frac{1}{4}\left(p^2 + q^2 + pq + 3(p + q)\right). \tag{4.1}$$

The enhancement of string tension was shown [19] to greatly influence the ratio of strange to non–strange hadrons, and to give the correct dependence on event activity as measured by ALICE [4].

---

[1]A Lund string is in its simplest form, a straight piece stretched between a quark and an anti-quark, or a colour triplet and anti-triplet. As gluons are added to the string, they act as point-like "kinks" on the string, carrying energy and momentum [17]. We will denote all straight pieces between gluons or (anti)quarks string segments. A $q - g - \bar{q}$ string thus has two segments.
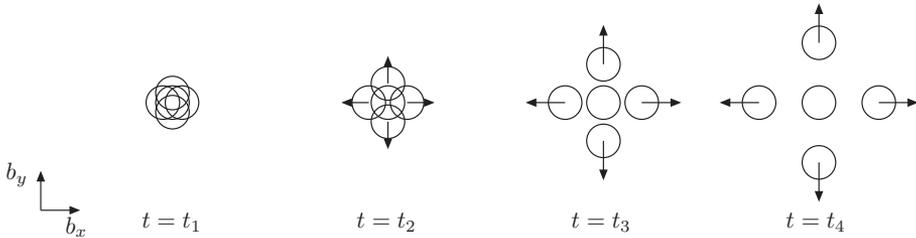
Figure 4.1: Cartoon in impact parameter space showing strings overlapping at time $t = t_1$, and as time progresses ($t_1 < t_2 < t_3 < t_4$), they move apart, picking up $p_\perp$ as indicated with arrows.

In this letter we show how this enhanced string tension can also be employed to generate a flow–like effect. Since the energy density in the overlap region is higher than outside, a pressure will be dynamically generated, pushing strings outwards. In figure 4.1 this principle is illustrated; we sketch several overlapping strings in impact parameter space at some initial time t_1. The density is larger towards center, giving a pressure gradient. We start a spatio-temporal evolution and let the strings pick up transverse momentum from the excess energy in the overlap regions. As the strings move further apart, the excess energy will decrease, and so will the transverse pressure. From time t_1 to t_2 the strings pick up some transverse momentum, as indicated with arrows, and move a little bit. From t_2 to t_3 the strings move, but picks up less transverse momentum, as the overlap is now smaller. From t_3 to t_4 the strings only move, and picks up no transverse momentum, as there is no overlap. The strings should of course hadronize at some point along the way, and we interrupt the evolution at some given time, where strings are no longer allowed to pick up $p_\perp$ or propagate.

The partonic state obtained from the DIPSY MC is formulated in rapidity (y) and transverse coordinate space ($\mathbf{b}_\perp$). Colour-connected partons separated by a distance $\Delta\mathbf{b}_\perp$ are also given opposite transverse momenta $\mathbf{p}_\perp \approx \Delta\mathbf{b}_\perp/(\Delta\mathbf{b}_\perp)^2$. The initial state is two Lorentz contracted pancakes colliding at $z = 0$, and the string segments are then stretched out mainly along the z direction. The distribution of gluons is approximately boost invariant, and to visualize the effect of the transverse repulsion, it is most easy to study a string segment stretched between two gluons in a system where they have rapidities $\pm\Delta y/2$. The endpoints of this string segment will then move out with longitudinal velocities $v_L = \pm\tanh(\Delta y/2)$, and the length of the segment in coordinate space, at time t, is consequently $t\cdot\tanh(\Delta y)$. The repulsive transverse force between two strings is proportional to the length of the overlapping region, and is therefore proportional to $f\cdot t \cdot\Delta y$, where f is the force per unit string length.

The cartoon in figure 4.1 represents in a schematic way a "slice" in rapidity[2]. The result of the repulsion will be a transverse velocity for the string, which might be represented by very

---

[2]In reality the strings are, of course, not distributed symmetrically, instead there are large fluctuations in the transverse positions of the strings.

many very soft gluons. The breakup of such a string state cannot be handled current implementations of string hadronization, as in *e.g.* Pythia8. As the DIPSY generator interfaces to the Pythia8 hadronization implementation, this must be remedied. A transverse gluon will give momentum to hadrons within one unit of rapidity on either side of the gluon. It is therefore possible to simulate the effect of the continuous distribution of infinitely soft gluons by finite gluons separated by at most one rapidity unit. In our calculations we cut the event into many rapidity slices, and in each slice we let the strings "shove" each other apart. The mechanism for shoving is to add a small excitation (*i.e.* a gluon) to each string in each slice. In each time–step δt a string within a slice δy (and thus length $\delta l = t\delta y$) will get a kick in the transverse direction $\delta p_\perp = f t \delta y \delta t$. As the mass of the string piece is $\approx \kappa \delta l = \kappa t \delta y$ also is proportional to the time t, we note that the factors t drop out in the result for the transverse velocity boost. When the strings no longer overlap, the many small kicks are added to a set of gluons, which can be handled by Pythia8. The $p_\perp$ of these gluons are chosen sufficiently small, so that they have lost their energy before the string hadronizes. This implies that their transverse momenta do not produce a jet, but just some extra $p_\perp$ within a rapidity range ± 1 unit. The result is then not sensitive to the exact number of gluons within such an interval, as long as their transverse $p_\perp$ add up to the same value.

In our current implementation, the shoving is implemented as the sum of many small kicks between all pairs of string segments in different rapidity intervals spread out evenly in the available phase space. This is done in several time steps, and in each such kick, the momentum is conserved as the inserted gluons will get equal and opposite transverse kicks, while the longitudinal recoils are absorbed by the original partons in the end of the string segments.

If the string is similar to a flux tube in a type I superconductor, the field is approximately constant within a cylindrical tube. Such a picture was used in analytic studies by Abramovsky and coworkers as early as 1988 [20]. At that time there was no experimental evidence for long range azimuthal correlations, but the model was recently revived in ref. [21], and implemented as a Monte Carlo toy model. In this model the increased energy per unit string length, $\frac{\delta E}{\delta l}$, scales with the overlap area in transverse space. This gives (in our notation):

$$\frac{\delta E}{\delta l} = \Theta(R - d) \sqrt{\left(\kappa + \tilde{\kappa} \frac{A(R, d_\perp)}{\pi R^2} \right)^2 - \kappa^2}, \tag{4.2}$$

where R is a characteristic transverse radius of the cylinder, and $A(R, d_\perp)$ is the overlap area between two circles of radius R, sitting at a distance $d_\perp$ apart in the transverse plane. Due to the repulsion, this energy is transferred to kinetic energy, giving a transverse velocity boost to the strings.

For a type II superconductor the field strength falls off more smoothly away from a central

core. Lattice calculations favour a QCD string with properties on the border between type I and II [22]. In our implementation we have assumed a smooth Gaussian form, similar to the lattice result, and furthermore added a temporal part to the evolution, as described above:

$$\frac{dp_\perp}{dt\,dl} = \frac{g\kappa}{R\sqrt{2\pi}} \exp\left(-\frac{d_\perp^2(t)}{2R^2}\right). \tag{4.3}$$

Here g is a free parameter controlling the strength of the shoving, which should be of order unity. The transverse distance between the strings has acquired explicit time dependence. As discussed above, such a repulsion gives a transverse boost to the string segments, and thus extra $p_\perp$ to heavier hadrons. The $\langle p_\perp \rangle$ dependence on the hadronic mass, is an observable which is often connected to hydrodynamics, as a thermodynamic pressure would provide the same physical effect.

In figure 4.2 we show the $\langle p_\perp \rangle$ for several hadron species, divided by $\langle p_\perp \rangle$ for pions, in pp collisions at $\sqrt{s} = 7$ TeV. We show results for DIPSY without ropes, with ropes but no shoving, and with both ropes and shoving. By choosing a ratio, rather than the raw $\langle p_\perp \rangle$, we minimize effects from small differences in the tuning of the three models. Even DIPSY without ropes shows a rise. This is expected, as lighter hadrons are more likely to be decay products – consequently with lower $\langle p_\perp \rangle$ – than heavy particles originating directly from the string breaking. When ropes are switched on, the $\langle p_\perp \rangle$ rises slightly. This is an effect of the enhanced string tension. When the string breaks, the emerging hadron obtains a $p_\perp$ taken from a Gaussian distribution. The width of this distribution rises with the effective string tension as [14]:

$$\tilde{\sigma}_\perp = \sigma_\perp \sqrt{\frac{\tilde{\kappa}}{\kappa}}. \tag{4.4}$$

The rise in $\langle p_\perp \rangle$ from ropes is, however, not directly mass dependant, while the expected mass dependence in the effect from shoving is clearly seen in figure 4.2.

Di-hadron correlations, which in data show a ridge effect, are of particular interest. We know that the DIPSY generator has problems reproducing the high-$p_\perp$ end of charged particle spectra; it generates too many hard partons. This introduces a potential problem for our string shoving model, which assumes parallel strings. To study the correlation effects on pairs of soft hadrons, we have therefore biased the generated events (pp at $\sqrt{s} = 7$ TeV) by only considering strings that span a rapidity range larger than $\Delta y = 8$, and with no partons above $p_\perp = 3$ GeV. Thus we get events with long strings, almost parallel in rapidity.[3]

To calculate the correlations, we employ an analysis similar to the one chosen by experiments [1, 2], where a signal distribution $S(\Delta\phi, \Delta\eta)$ is divided by a random background distribution, $B(\Delta\phi, \Delta\eta)$, constructed by combining particles from two different events in

---

[3]Note that the results on the mass dependence of $\langle p_\perp \rangle$ are fairly insensitive to this bias, and in figure 4.2 the bias was not applied.
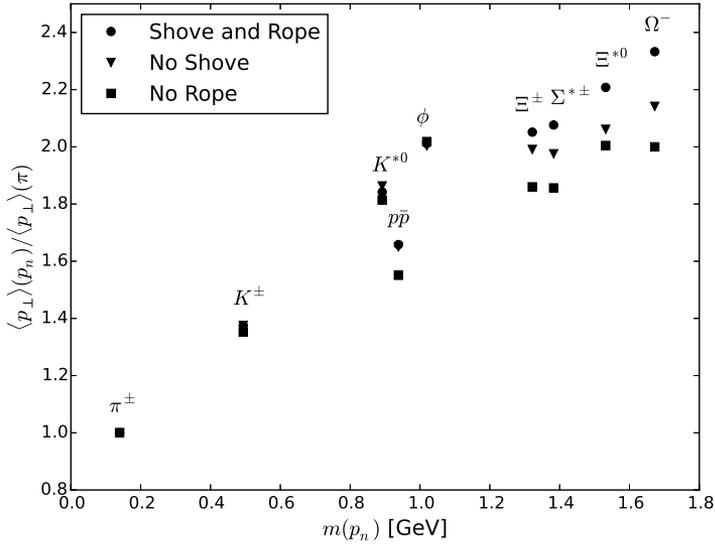
Figure 4.2: Average $p_\perp$ as a function of hadronic mass, for several species. Results are presented for DIPSY without ropes, DIPSY with ropes and DIPSY with ropes and shoving.

the same centrality class. In figure 4.3 we show results for $2 < \Delta\eta < 4$, for particles with transverse momentum between 0.5 and 3 GeV, using the rope model in DIPSY without (left) and with (right) shoving effects. We see the emergence of a clear "ridge" around $\Delta\eta = 0$. Although the emerging ridge is roughly of the same relative size as the one recently measured by ATLAS [1] in high multiplicity pp events at $\sqrt{s} = 13$ TeV, we stress that the results presented here can only be taken as a qualitative proof-of-concept, due to the event bias we have introduced.

In this letter we have demonstrated that by introducing shoving in the rope hadronization mechanism implemented in DIPSY, we are able to qualitatively describe collective phenomena in pp collisions, in addition to the quantitatively correct description of hadrochemistry already provided by the ropes. We remark that the mechanism does not require any medium or thermalization, but is composed solely of microscopic interactions.

To get a better quantitative description of collective phenomena, further studies are needed. High $p_\perp$ jets are expected to rapidly leave the dense system of strings, and more work is needed for a realistic description of the interplay beteen the jet and the rope. Also, as it stands, the model introduces a number of parameters, *e.g.*, the strength of the shoving, the number of rapidity intervals, and the number and size of the time steps. Although all of them have physically motivated values, their influence on the results must be studied in more detail and, in the end, they need to be tuned to data.
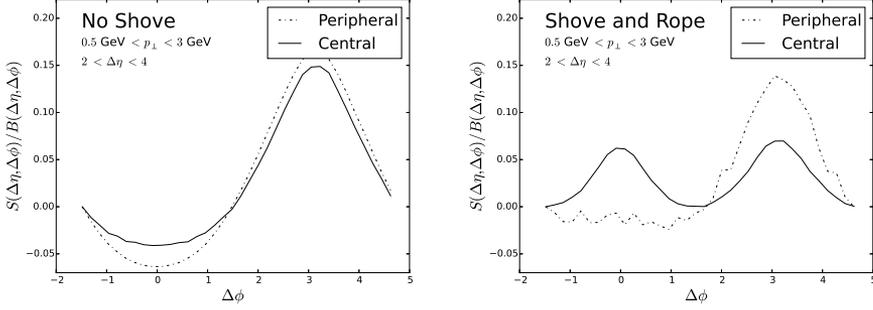
Figure 4.3: Two particle correlations without (left) and with (right) shoving effects, for central and peripheral pp events at $\sqrt{s} = 7$ TeV.

Finally we note that, if successfully tuned to pp data, the model can be directly applied to collisions involving heavy ions in DIPSY, and in that way provide a complementary picture to the conventional hydrodynamical description of pA and AA collisions. In addition we plan to implement the model to our developing heavy ion event generator based on Pythia8 presented in ref. [23].

References

[1] **ATLAS** Collaboration, M. Aaboud *et al.*, "Measurements of long-range azimuthal anisotropies and associated Fourier coefficients for *pp* collisions at $\sqrt{s} = 5.02$ and 13 TeV and *p*+Pb collisions at $\sqrt{s_{\mathrm{NN}}} = 5.02$ TeV with the ATLAS detector," *arXiv:1609.06213* (2016) , `arXiv:1609.06213 [nucl-ex]`.

[2] **CMS** Collaboration, V. Khachatryan *et al.*, "Evidence for collectivity in pp collisions at the LHC," *arXiv:1606.06198* (2016) , `arXiv:1606.06198 [nucl-ex]`.

[3] **ALICE** Collaboration, B. Abelev *et al.*, "Long-range angular correlations on the near and away side in *p*-Pb collisions at $\sqrt{s_{NN}} = 5.02$ TeV," *Phys. Lett.* **B719** (2013) 29–41, `arXiv:1212.2001 [nucl-ex]`.

[4] **ALICE** Collaboration, J. Adam *et al.*, "Multiplicity-dependent enhancement of strange and multi-strange hadron production in proton-proton collisions at $\sqrt{s} = 7$ TeV," *arXiv:1606.07424* (2016) , `arXiv:1606.07424 [nucl-ex]`.

[5] B. Andersson, G. Gustafson, and B. Söderberg, "A General Model for Jet Fragmentation," *Z. Phys.* **C20** (1983) 317.

[6] B. Andersson, G. Gustafson, G. Ingelman, and T. Sjöstrand, "Parton Fragmentation and String Dynamics," *Phys. Rept.* **97** (1983) 31–145.

[7] G. Marchesini and B. R. Webber, "Simulation of QCD Jets Including Soft Gluon Interference," *Nucl. Phys.* **B238** (1984) 1–29.

[8] T. Sjöstrand, S. Mrenna, and P. Z. Skands, "PYTHIA 6.4 Physics and Manual," *JHEP* **05** (2006) 026, `arXiv:hep-ph/0603175 [hep-ph]`.

[9] T. Sjöstrand, S. Ask, J. R. Christiansen, R. Corke, N. Desai, P. Ilten, S. Mrenna, S. Prestel, C. O. Rasmussen, and P. Z. Skands, "An Introduction to PYTHIA 8.2," *Comput. Phys. Commun.* **191** (2015) 159–177, `arXiv:1410.3012 [hep-ph]`.

[10] J. Bellm *et al.*, "Herwig 7.0/Herwig++ 3.0 release note," *Eur. Phys. J.* **C76** no. 4, (2016) 196, `arXiv:1512.01178 [hep-ph]`.

[11] K. Werner, "Core-corona separation in ultra-relativistic heavy ion collisions," *Phys. Rev. Lett.* **98** (2007) 152301, `arXiv:0704.1270 [nucl-th]`.

[12] T. Pierog, I. Karpenko, J. M. Katzy, E. Yatsenko, and K. Werner, "EPOS LHC: Test of collective hadronization with data measured at the CERN Large Hadron Collider," *Phys. Rev.* **C92** no. 3, (2015) 034906, `arXiv:1306.0121 [hep-ph]`.

[13] N. Fischer and T. Sjöstrand, "Thermodynamical String Fragmentation," *arXiv:1610.09818* (2016) , `arXiv:1610.09818 [hep-ph]`.

[14] C. Bierlich, G. Gustafson, L. Lönnblad, and A. Tarasov, "Effects of Overlapping Strings in pp Collisions," *JHEP* **03** (2015) 148, `arXiv:1412.6259 [hep-ph]`.

[15] T. S. Biro, H. B. Nielsen, and J. Knoll, "Color Rope Model for Extreme Relativistic Heavy Ion Collisions," *Nucl. Phys.* **B245** (1984) 449–468.

[16] C. Flensburg, G. Gustafson, and L. Lönnblad, "Inclusive and Exclusive Observables from Dipoles in High Energy Collisions," *JHEP* **08** (2011) 103, `arXiv:1103.4321 [hep-ph]`.

[17] B. Andersson and G. Gustafson, "Semiclassical Models for Gluon Jets and Leptoproduction Based on the Massless Relativistic String," *Z. Phys.* **C3** (1980) 223.

[18] G. S. Bali, "Casimir scaling of SU(3) static potentials," *Phys. Rev.* **D62** (2000) 114503, `arXiv:hep-lat/0006022 [hep-lat]`.

[19] C. Bierlich and J. R. Christiansen, "Effects of color reconnection on hadron flavor observables," *Phys. Rev.* **D92** no. 9, (2015) 094010, `arXiv:1507.02091 [hep-ph]`.

[20] V. A. Abramovsky, E. V. Gedalin, E. G. Gurvich, and O. V. Kancheli, "Long Range Azimuthal Correlations in Multiple Production Processes at High-energies," *JETP Lett.* **47** (1988) 337–339. [Pisma Zh. Eksp. Teor. Fiz.47,281(1988)].

[21] I. Altsybeev, "Mean transverse momenta correlations in hadron-hadron collisions in MC toy model with repulsing strings," *AIP Conf. Proc.* **1701** (2016) 100002, `arXiv:1502.03608 [hep-ph]`.

[22] P. Cea, L. Cosmai, F. Cuteri, and A. Papa, "Flux tubes in the SU(3) vacuum: London penetration depth and coherence length," *Phys. Rev.* **D89** no. 9, (2014) 094505, `arXiv:1404.1172 [hep-lat]`.

[23] C. Bierlich, G. Gustafson, and L. Lönnblad, "Diffractive and non-diffractive wounded nucleons and final states in pA collisions," *JHEP* **10** (2016) 139, `arXiv:1607.04434 [hep-ph]`.

List of Figures